

AN ABSTRACT OF THE THESIS OF

Ying Ouyang for the degree of Doctor of Philosophy  
in Soil Science presented on September 27, 1990  
Title: Dynamic Mathematical Model of Oxygen and Carbon  
Dioxide Exchange Between Soil and Atmosphere

Abstract approved: **Redacted for Privacy**  
Larry Boersma

Gaseous transport through soil in the presence of soil microorganisms has been investigated. More recently, modeling of gaseous transport in the unsaturated zone has been investigated. However, the problem of mathematical model of oxygen and carbon dioxide transport through soil, as affected by the climatic conditions, the transport of soil water, and the biological activities, has not been studied.

The problem of time-dependent diffusion of oxygen and carbon dioxide through plant canopy and soil system, as affected by the infiltration and evaporation of soil water and the rate of consumption of oxygen and production of carbon dioxide by plant leaves and roots and soil microorganisms was studied, using a one-dimensional mathematical model. This model consists of four sets of non-linear partial differential field equations, which describe the time-dependent simultaneous transport of water, heat, oxygen, and carbon dioxide through the soils.

Finite difference methods were used to find the approximate solutions for the four sets of non-linear partial differential field equations. The field equations for the transport of water and heat were approximated by using the implicit scheme. The field equations for the transport of oxygen and carbon dioxide were approximated by using the explicit scheme. A computer program was written in Fortran code to conduct the simulations of the mathematical model.

Simultaneous transport of water, heat, oxygen, and carbon dioxide through the unsaturated Indio loam soil, through the compacted and the non-compacted soil during infiltration, redistribution, and evaporation of soil water was evaluated. Diffusion of oxygen and carbon dioxide within the canopy and soil system was examined. Several different functions for the root elongation and the root oxygen consumption rates were used. Root elongation rate was chosen to depend on oxygen or carbon dioxide concentrations, in addition to being a function of time. Root oxygen consumption rate was assumed to be a function of root age, in addition to being a function of oxygen or carbon dioxide concentrations. Results illustrate that the behaviors of the simultaneous transport of water, heat, oxygen, and carbon dioxide were well predicted by the model.

Dynamic Mathematical Model of Oxygen and Carbon Dioxide  
Exchange between Soil and Atmosphere

by  
Ying Ouyang

A THESIS  
submitted to  
Oregon State University

in partial fulfillment of  
the requirements for the  
degree of  
Doctor of Philosophy

Completed September 27, 1986

Commencement June 1991

APPROVED:

Redacted for Privacy

\_\_\_\_\_  
Professor of Crop and Soil Science in charge of major

Redacted for Privacy

\_\_\_\_\_  
Head of Department of Crop and Soil Science

Redacted for Privacy

\_\_\_\_\_  
Dean of Graduate School

Date thesis is presented:

September 27, 1990

Typed by Ying Ouyang for:

Ying Ouyang

## ACKNOWLEDGEMENTS

I would like to express my deep appreciation to Dr. Larry Boersma for the support, counseling, and encouragement that has been given to me throughout my graduate program.

I am also grateful to the members of my graduate committee, Dr. R. B. Guenther, Dr. G. F. Kling, Dr. J. Baham, and Dr. T. G. Lewis for their careful review of this thesis. In addition, I wish to thank Dr. Tom Lindstrom and Mr. D. Cawlfild for frequent insight and help in mathematics and computer program.

Appreciation is extended to the Agricultural Experiment Station at Oregon State University for financial support of this research.

Finally, for her love, patience, and encouragement, my wife, Min Li, deserves all my love and appreciation.

TABLE OF CONTENTS

DESCRIPTION OF SOIL AIR AND SOIL AERATION . . . . . 1

    Composition and Properties of Soil Air . . . . . 1

    Soil Aeration and Problems in the Field. . . . . 3

    Characterization of Soil Aeration. . . . . 5

        Oxygen Content in the Soil . . . . . 5

        Oxygen Diffusion Rate (ODR). . . . . 6

        Oxidation-Reduction Potential (Eh) . . . . . 6

TRANSPORT OF OXYGEN AND CARBON DIOXIDE THROUGH SOILS. . . . . 8

    Transport Processes. . . . . 8

    Factors Affecting the Transport Processes. . . . . 10

        Soil Water Content . . . . . 10

        Soil Temperature . . . . . 11

        Irrigation, Rainfall, and Drainage . . . . . 11

        Soil Depth . . . . . 12

        Time . . . . . 12

OBJECTIVE . . . . . 13

SCOPE OF RESEARCH . . . . . 14

DEVELOPMENT OF FIELD EQUATIONS. . . . . 17

    Basic Assumption. . . . . 17

        Assumptions Pertaining to the Atmosphere. . . . . 17

        Assumptions Pertaining to the Soil Slab . . . . . 19

    Field Equations for Water and Heat Transport in the Soil. . . . . 20

    Derivation of Oxygen and Carbon Dioxide Field Equations . . . . . 23

Boundary Conditions . . . . .	33
Boundary Between the Atmosphere and the Soil Slab . . . . .	34
Water. . . . .	34
Heat . . . . .	38
Oxygen. . . . .	43
Carbon Dioxide. . . . .	43
Boundary Between Soil Slab and Impervious Layer . . . . .	43
Summary of Field Equations and Their Boundary Conditions . . . . .	46
SOLUTION METHOD FOR THE FOUR FIELD EQUATIONS . . . . .	51
Solution of the Water Field Equation . . . . .	51
Solution of the Heat Field Equation . . . . .	57
Solution of the Oxygen Field Equation . . . . .	62
Solution of the Carbon Dioxide Field Equation . . . . .	64
Solution of the Boundary Conditions . . . . .	66
Stability Consideration . . . . .	70
Iteration Solution Algorithm for the Four Field Equations . . . . .	73
DESCRIPTION OF EXAMPLES TO BE SOLVED AND DISCUSSION	
OF SIMULATION RESULTS . . . . .	77
Example 1 . . . . .	77
Statement of the Problem . . . . .	77
Input Parameters . . . . .	78
Simulation Soil Depth and Simulation Time. . . . .	78
Weather Conditions. . . . .	79
Soil Properties. . . . .	88
Biological Activities. . . . .	95

Initial Distribution of Water Content, Temperature, Oxygen and Carbon Dioxide Concentrations in the Soil Profile. . . . .	100
Activity Coefficients of Oxygen and Carbon Dioxide. . .	101
Other Coefficients of Oxygen and Carbon Dioxide . . .	105
Adsorption and Solubility . . . . .	107
Discussion of Simulation Results . . . . .	107
Soil Water Content. . . . .	107
Surface Evaporation . . . . .	108
Soil Temperature. . . . .	109
Concentrations of Oxygen and Carbon Dioxide . . . . .	111
Rates of Oxygen Consumption by Roots and Microorganisms. . . . .	112
Conclusions . . . . .	113
Example 2a. . . . .	134
Statement of the Problem. . . . .	134
Input Parameters. . . . .	134
Root Elongation . . . . .	134
Rate of Oxygen Consumption by Roots . . . . .	136
Rate of Oxygen Consumption by Soil Microorganisms . .	137
Discussion of Simulation Results. . . . .	138
Concentrations of Oxygen and Carbon Dioxide . . . . .	138
Rates of Oxygen Consumption by Roots and Microorganisms. . . . .	140
Comparison of Root Length . . . . .	141
Conclusions . . . . .	142

Example 2b. . . . .	157
Statement of the Problem. . . . .	157
Input Parameters. . . . .	157
Root Elongation . . . . .	157
Rate of Oxygen Consumption by Roots . . . . .	158
Discussion of Simulation Results. . . . .	159
Concentrations of Oxygen and Carbon Dioxide . . . . .	159
Rates of Oxygen Consumption by Roots and Microorganisms. . . . .	160
Comparison of Root Length . . . . .	161
Conclusions . . . . .	162
Example 3 . . . . .	172
Statement of the Problem. . . . .	172
Input Parameters. . . . .	172
Discussion of Simulation Results. . . . .	173
Conclusions . . . . .	173
Example 4 . . . . .	177
Statement of the Problem. . . . .	177
Input Parameters. . . . .	177
Hydraulic Conductivity and Water Potential. . . . .	177
Initial Root Length . . . . .	178
Initial Soil Water Content. . . . .	178
Simulation Time . . . . .	178
Discussion of Simulation Results. . . . .	178
Soil Water Content. . . . .	178
Concentration of Oxygen . . . . .	179

Concentration of Carbon Dioxide . . . . .	181
Rates of Oxygen Consumption by Roots and Microorganisms. . . . .	182
Comparison of Root Length . . . . .	183
Conclusions . . . . .	183
Example 5a. . . . .	194
Statement of the Problem. . . . .	194
Assumptions . . . . .	194
Field Equations . . . . .	196
Input Parameters. . . . .	197
(1) Solar Radiation . . . . .	197
(2) Rainfall. . . . .	197
(3) Air Temperature . . . . .	197
(4) Relative Humidity of the Air. . . . .	198
(5) Wind Speed. . . . .	198
(6) Height of Plant and Length of Canopy. . . . .	198
(7) Initial Oxygen Concentration. . . . .	198
(8) Initial Carbon Dioxide Concentration. . . . .	198
(9) Initial Soil Water Content. . . . .	198
(10) Initial Root Length. . . . .	198
(11) Rate of Carbon Dioxide Fixation and Oxygen Evolution by the Photosynthesis Processes . . . . .	198
(12) Rate of Oxygen Consumption and Carbon Dioxide Production by Respiration. . . . .	200
(13) Diffusion Coefficient of Oxygen and Carbon Dioxide. . . . .	202

Discussion of Simulation Results. . . . .	202
Concentrations of Oxygen and Carbon Dioxide Within the Plant Canopy. . . . .	202
Concentration of Oxygen in Soil Profile . . . . .	203
Concentration of Carbon Dioxide in Soil Profile . . . . .	204
Oxygen and Carbon Dioxide Concentration at the Soil Surface. . . . .	205
Comparison of Root Length . . . . .	206
Conclusions . . . . .	207
Example 5b. . . . .	221
Statement of the Problem. . . . .	221
Input Parameters. . . . .	221
Root Elongation Rate. . . . .	221
Rate of Oxygen Consumption by Roots . . . . .	222
Discussion of Simulation Results. . . . .	223
Concentrations of Oxygen and Carbon Dioxide Within the Plant Canopy . . . . .	223
Concentration of Oxygen and Carbon Dioxide in the Soil Profile . . . . .	224
Oxygen and Carbon Dioxide Concentration at the Soil Surface. . . . .	225
Comparison of Root Length . . . . .	225
Conclusions . . . . .	226
SUMMARY AND CONCLUSIONS . . . . .	236
Results of the Study. . . . .	236
Applications. . . . .	238

Advantages, Disadvantages, and Further Development of the Model . . . . .	239
REFERENCES . . . . .	242
APPENDIX I . . . . .	246
Definitions of Mathematical Symbols and Units For Equations (61) Through (70) . . . . .	246
APPENDIX II . . . . .	249
Finite Difference Formulations for Approximating the Four Field Equations . . . . .	249
APPENDIX III. . . . .	251
Conversion of Units . . . . .	251
Conversion of Unit for the Rate of Oxygen Consumption by Root (Srt) . . . . .	251
Conversion of Unit for the Rate of Oxygen Consumption by Microorganisms (Smo) . . . . .	252
APPENDIX IV . . . . .	254
Computer Program Information Flow and Program Listing . . .	254
Program Listing . . . . .	257

## LIST OF FIGURES

<u>Figure</u>	<u>Page</u>
1. Schematic diagram of processes of the transport of oxygen and carbon dioxide in the soil environment.	15
2. Schematic diagram of a soil profile for which a model of water, heat, oxygen, and carbon dioxide transport will be developed.	18
3. Interface between the atmosphere and the soil surface. $z$ is soil depth (cm). $\Delta z_1$ is the depth interval of the first soil layer (cm).	35
4. Gaussian Pill Box concept for water flow at the atmosphere-soil interface.	36
5. Gaussian Pill Box concept for heat flux at the interface between the atmosphere and the soil surface.	39
6. Interface between soil slab and impervious layer. $z$ is the soil depth (cm). $N$ is the number of the last node of soil at the interface. $z_{N-1}$ is the soil depth one layer thick above the interface (cm). $z_N$ is the soil depth at the interface (cm).	44
7. Closure of space-time cylinder with lattice of nodal points superimposed on it.	54
8. Schematic diagram of space positions of all the field nodal points. $\theta$ is the water content ( $\text{cm}^3 \text{cm}^{-3}$ ). $T$ is the temperature ( $^{\circ}\text{C}$ ). $C$ is the concentration of oxygen or carbon dioxide ( $\mu\text{g cm}^{-3}$ air).	55
9. Intensity of solar radiation as a function of time. Data shown are the hourly average intensities of solar radiation during October for the period from 1975 to 1986 in Western Oregon (Solar Monitoring Lab., 1987).	80
10. Air temperature as a function of time. Data shown are the hourly average air temperatures during October for the period from 1975 to 1986 in Western Oregon (Redmond, 1988).	81
11. Relative humidity as a function of time. Data shown are the hourly average relative humidities during October for the period from 1975 to 1986 in Western Oregon (Redmond, 1988).	84

12. Hydraulic conductivity as a function of soil water content for Indio loam soil. Data taken from McCoy et al. (1984). 89
13. The water potential as a function of soil water content for Indio loam soil. Data taken from McCoy et al. (1984). 92
14. Water content as a function of soil depth at 0, 6, and 12 hours. Rain fell during this period at the rate of  $0.5 \text{ cm hr}^{-1}$ . The rainfall started at 0 hours and stopped at 12 hours. The initial soil water content was  $0.15 \text{ cm}^3 \text{ cm}^{-3}$ . 115
15. Water content as a function of soil depth at 24, 48, and 72 hours since start. Evaporation and redistribution processes occurred during this period. 116
16. Water content as a function of soil depth at 76, 88, 96, and 120 hours since start. Rainfall started at 76 hours and stopped at 88 hours. The rainfall rate was  $0.5 \text{ cm hr}^{-1}$ . During the period from 88 hours to 120 hours, redistribution and evaporation occurred. 117
17. Rate of surface evaporation (-) or condensation (+) of water as a function of time from 0 to 24 hours. Rainfall started at 0 hours and stopped at 12 hours. 118
18. Rate of surface evaporation (-) or condensation (+) of water as a function of time during the period from 24 to 48 hours. 119
19. Rate of surface evaporation (-) or condensation (+) of water as a function of time during the period from 48 to 72 hours. 120
20. Rate of surface evaporation (-) or condensation (+) of water as a function of time during the period from 72 to 96 hours. Rainfall started at 76 hour and stopped at 88 hours. 121
21. Rate of surface evaporation (-) or condensation (+) of water as a function of time during the period from 96 to 120 hours. 122
22. Soil temperature as a function of time at the soil depths of 0, 5, 10, 20, and 50 cm. Initial soil temperature was  $8.7 \text{ }^\circ\text{C}$ . Rainfall started at 0 hours and stopped at 12 hours. Rain water temperature was  $4 \text{ }^\circ\text{C}$ . During the rainy period, the air temperature was assumed to be reduced by 50 percent and solar radiation was assumed to be reduced by 85 percent compared to conditions without rain. 123

23.	Soil temperature as a function of time at soil depths of 0, 5, 10, 20, and 50 cm during the period of 24 to 48 hours.	124
24.	Soil temperature as a function of time at the soil depths of 0, 5, 10, 20, and 50 cm during the period of 48 to 72 hours.	125
25.	Soil temperature as a function of time at the soil depths of 0, 5, 10, 20, and 50 cm during the period of 72 to 96 hours. Rainfall started at 76 and ended at 88 hours. Conditions were the same as during the first rain shown in Figure 22.	126
26.	Soil temperature as a function of time at the soil depths of 0, 5, 10, 20, and 50 cm during the period from 96 to 120 hours.	127
27.	Oxygen and carbon dioxide concentrations as a function of soil depth at 0, 6, and 12 hours since start. The rainfall started at 0 hours and stopped at 12 hours.	128
28.	Oxygen and carbon dioxide concentrations as a function of soil depth at 24, 48, and 72 hours since start.	129
29.	Oxygen and carbon dioxide concentrations as a function of soil depth at 76, 88, 96, and 120 hours since start. Rainfall, evaporation, and redistribution occurred during the period. The rainfall started at 76 hours and stopped at 88 hours.	130
30.	Oxygen consumption rates by plant roots and soil microorganisms as a function of soil depth at times of 6 and 12 hours. The rate of oxygen consumption in $\mu\text{g cm}^{-3}$ fresh roots $\text{hr}^{-1}$ was converted to $\mu\text{g cm}^{-3}$ air $\text{hr}^{-1}$ as shown on the Figure.	131
31.	Oxygen consumption rates by plant roots and soil microorganisms as a function of soil depth at times of 24, 48, and 72 hours. The rate of oxygen consumption in $\mu\text{g cm}^{-3}$ fresh roots $\text{hr}^{-1}$ was converted to $\mu\text{g cm}^{-1}$ air $\text{hr}^{-1}$ as shown on the Figure.	132
32.	Oxygen consumption rates by plant roots and soil microorganisms as a function of soil depth at times of 76, 88, 96, and 120 hours. The rate of oxygen consumption in $\mu\text{g cm}^{-3}$ fresh roots $\text{hr}^{-1}$ was converted to $\mu\text{g cm}^{-3}$ air $\text{hr}^{-1}$ as was shown on the Figure.	133
33.	Root length as a function of time calculated from equation (145).	143

34.	Correction factor for the root elongation rate as a function of soil oxygen concentration, calculated from equation (146).	144
35.	Oxygen consumption rate of roots as a function of soil oxygen concentration calculated from equation (148).	145
36.	Correction factor for the oxygen consumption rate of roots as a function of root length starting from the root tip, calculated from equation (149).	146
37.	Oxygen and carbon dioxide concentrations as a function of soil depth at 0, 6, and 12 hours since start. The rainfall started at 0 hours and stopped at 12 hours.	147
38.	Oxygen and carbon dioxide concentrations as a function of soil depth at 24, 48, and 72 hours.	148
39.	Oxygen and carbon dioxide concentrations as a function of soil depth at 76, 88, 96, and 120 hours since start. Rain, evaporation, and redistribution occurred during the period. The rainfall started at 76 hours and stopped at 88 hours.	149
40.	Soil depth where the minimum oxygen concentration occurred as a function of time from 0 to 120 hours.	150
41.	Oxygen concentration as a function of time at the soil depths of 5, 20, and 40 cm.	151
42.	Carbon dioxide concentration as a function of time at the soil depths of 5, 20, and 40 cm.	152
43.	Oxygen consumption rates by plant roots and soil microorganisms as a function of soil depth at times of 6 and 12 hours. The rate of oxygen consumption in $\mu\text{g cm}^{-3}$ fresh roots $\text{hr}^{-1}$ was converted to $\mu\text{g cm}^{-3}$ air $\text{hr}^{-1}$ as shown on the Figure.	153
44.	Oxygen consumption rates by plant roots and soil microorganisms as a function of soil depth at times of 24, 48, and 72 hours. The rate of oxygen consumption in $\mu\text{g cm}^{-3}$ fresh roots $\text{hr}^{-1}$ was converted to $\mu\text{g cm}^{-3}$ air $\text{hr}^{-1}$ as shown on the Figure.	154
45.	Oxygen consumption rates by plant roots and soil microorganisms as a function of soil depth at times of 76, 88, 96, and 120 hours. The rate of oxygen consumption in $\mu\text{g cm}^{-3}$ fresh roots $\text{hr}^{-1}$ was converted to $\mu\text{g cm}^{-3}$ air $\text{hr}^{-1}$ as shown on the Figure.	155

46.	Root length in soil profile as a function of time in Example 1 and Example 2a since the start of the simulation.	156
47.	Correction factor for the root elongation rate as a function of soil carbon dioxide concentration, calculated from equation (151).	163
48.	Oxygen consumption rate of roots as a function of soil carbon dioxide concentration, calculated from equation (153).	164
49.	Oxygen and carbon dioxide concentrations as a function of soil depth at 0, 6, and 12 hours since start. The rainfall started at 0 hour and stopped at 12 hours.	165
50.	Oxygen and carbon dioxide concentrations as a function of soil depth at 24, 48, and 72 hours.	166
51.	Oxygen and carbon dioxide concentrations as a function of soil depth at 76, 88, 96, and 120 hours since start. Rain, evaporation, and redistribution occurred during the period. The rainfall started at 76 hours and stopped at 88 hours.	167
52.	Oxygen consumption rates by plant roots and soil microorganisms as a function of soil depth at times of 6 and 12 hours. The rate of oxygen consumption in $\mu\text{g cm}^{-3}$ fresh roots $\text{hr}^{-1}$ was converted to $\mu\text{g cm}^{-3}$ air $\text{hr}^{-1}$ as shown on the figure.	168
53.	Oxygen consumption rates by plant roots and soil microorganisms as a function of soil depth at times of 24, 48, and 72 hours. The rate of oxygen consumption in $\mu\text{g cm}^{-3}$ fresh roots $\text{hr}^{-1}$ was converted to $\mu\text{g cm}^{-3}$ air $\text{hr}^{-1}$ as shown on the figure.	169
54.	Oxygen consumption rates by plant roots and soil microorganisms as a function of soil depth at times of 76, 88, 96, and 120 hours. The rate of oxygen consumption in $\mu\text{g cm}^{-3}$ fresh roots $\text{hr}^{-1}$ was converted to $\mu\text{g cm}^{-3}$ air $\text{hr}^{-1}$ as shown on the figure.	170
55.	Root length in soil profile as a function of time in Example 2a and Example 2b since the start of the simulation.	171
56.	Initial oxygen concentration as a function of soil depth.	174
57.	Initial carbon dioxide concentration as a function of soil depth.	175

58.	Difference of carbon dioxide concentrations between non-ideal and ideal diffusion as a function of soil depth at 76 hours. $CO_2^{ND}$ and $CO_2^{ID}$ are the concentrations of carbon dioxide in non-ideal and ideal diffusion, respectively.	176
59.	Hydraulic conductivity as a function of soil water content at the soil depth of 17.5 cm.	185
60.	Water potential as a function of soil water content at the soil depth of 17.5 cm.	186
61.	Water content as a function of soil depth in compacted and non-compacted soil at 0, 12, 48, and 72 hours. Rainfall started at 0 hours and stopped at 12 hours with a constant rate of 0.5 cm hr <sup>-1</sup> .	187
62.	Oxygen concentration as a function of soil depth in the compacted and non-compacted soil at 0, 12, 48, and 72 hours since start. The rainfall started from 0 hours and stopped at 12 hours.	188
63.	Oxygen concentration as a function of time at the soil depth of 35 cm in compacted and non-compacted soil.	189
64.	Carbon dioxide concentration as a function of soil depth in the compacted and non-compacted soil at 0, 12, 48, and 72 hours since start.	190
65.	Oxygen consumption rates by plant roots as a function of soil depth in the compacted and non-compacted soil at times of 0, 12, 48 and 72 hours. The rate of oxygen consumption in $\mu\text{g cm}^{-3}$ fresh roots hr <sup>-1</sup> was converted to $\mu\text{g cm}^{-1}$ air hr <sup>-1</sup> as shown on the Figure.	191
66.	Oxygen consumption rates by microorganisms as a function of soil depth in the compacted and non-compacted soil at times of 12, 48 and 72 hours.	192
67.	Root length in soil profile as a function of time in the compacted and the non-compacted soil since the start of the simulation.	193
68.	Schematic diagram of a plant and soil profile for which the diffusion of oxygen and carbon dioxide within the plant canopy and through the soil was simulated.	195
69.	Air temperature as a function of time for conditions with and without the plant canopy.	209
70.	Relative humidity as a function of time for conditions with and without the plant canopy.	210

71.	Rates of photosynthesis and respiration as a function of time. Data adapted from Nobel (1983).	211
72.	Correction factor for photosynthesis as a function of carbon dioxide concentration within the plant canopy (Devlin and Barker, 1971).	212
73.	Correction factor for photorespiration and respiration as a function of oxygen concentration within the plant canopy (Devlin and Barker, 1971).	213
74.	Oxygen and carbon dioxide concentrations as a function of plant height at the three midnights. Initial oxygen and carbon dioxide concentrations are 300 and 0.6134 $\mu\text{g cm}^{-3}$ air, respectively.	214
75.	Oxygen and carbon dioxide concentrations as a function of plant height at the three noons. Initial oxygen and carbon dioxide concentrations are 300 and 0.6134 $\mu\text{g cm}^{-3}$ air, respectively.	215
76.	Oxygen concentration as a function of soil depth at times of 0, 24, 48 and 72 hours for conditions with and without the plant canopy.	216
77.	Carbon dioxide concentration as a function of soil depth at times of 0, 24, 48, and 72 hours for conditions with and without the plant canopy.	217
78.	Oxygen concentration as a function of time at the soil surface from 0 to 72 hours for conditions with the plant canopy.	218
79.	Carbon dioxide concentration as a function of time at the soil surface from 0 to 72 hours for conditions with the plant canopy.	219
80.	Root length as a function of time in soil profile from 0 to 72 hours for conditions with and without the plant canopy.	220
81.	Correction factor for root elongation as a function of carbon dioxide concentration, calculated from equation (165).	228
82.	Oxygen consumption rate of roots as a function of soil carbon dioxide concentration, calculated from equation (168).	229
83.	Oxygen and carbon dioxide concentrations as a function of plant height at the three midnights. Initial oxygen and carbon dioxide concentrations are 300 and 0.6134 $\mu\text{g cm}^{-3}$ air, respectively.	230

84.	Oxygen and carbon dioxide concentrations as a function of plant height at the three noons. Initial oxygen and carbon dioxide concentrations are 300 and $0.6134 \mu\text{g cm}^{-3}$ air, respectively.	231
85.	Oxygen and carbon dioxide concentrations as a function of soil depth at times of 0, 24, 48 and 72 hours. Initial oxygen and carbon dioxide concentrations are 300 and $0.6134 \mu\text{g cm}^{-3}$ air, respectively.	232
86.	Oxygen concentration as a function of time at the soil surface from 0 to 72 hours.	233
87.	Carbon dioxide concentration as a function of time at the soil surface from 0 to 72 hours.	234
88.	Root length as a function of time in the soil profile from 0 to 72 hours.	235
89.	Basic computer program flow structures.	256

## LIST OF TABLES

<u>Table</u>	<u>Page</u>
1. Composition of air in the atmosphere and in the soil surface layer under well aerated soil conditions (Childyal and Tripathi, 1987).	2
2. Field equations for water, heat, oxygen, and carbon dioxide transport in unsaturated soil.	47
3. Boundary conditions at: (1) the interface between the atmosphere and the soil surface and (2) at impervious layers.	48
4. The hourly averages of air temperatures, relative humidities, and solar radiation during October for the period of 1975 to 1986 (Solar Monitoring Lab., 1987; Redmond, 1988).	83
5. Time schedule for rain on and rain off, and for light on and light off during the five day simulation period. Hours are counted consecutively, starting with 0 at the beginning of the first day and ending at the midnight of the fifth day, for a total simulation time of 120 hours.	87
6. Soil hydraulic conductivity and water potential at different water contents. Data taken from McCoy et al. (1984).	90
7. Values of the soil parameters used for the Indio loam soil that remain constant throughout the simulation.	94
8. Parameters of microbial kinetics for solving equation (130) in the simulation. Data are adopted from Molz et al. (1986) and Widdowson et al. (1988).	100
9. Some parameters used to calculate the hydraulic conductivity and water potential in a compacted soil layer by equations (123) and (124).	178

DYNAMIC MATHEMATICAL MODEL OF OXYGEN AND CARBON DIOXIDE  
EXCHANGE BETWEEN SOIL AND ATMOSPHERE

DESCRIPTION OF SOIL AIR AND SOIL AERATION

Composition and Properties of Soil Air

Soils are composed of solid, liquid, and gaseous constituents in various proportions. Soil solids are so arranged that a considerable portion of the soil volume is available for water and gaseous constituents. The portion of the soil which is not occupied by solids is referred to as a pore space or a void. These spaces are filled with water and gases in reciprocally varying amounts. The principal components of soil air are nitrogen, oxygen, carbon dioxide, water vapor, hydrogen, methane, and other gases. The proportion of nitrogen in the soil is usually found to be equal to that of the atmosphere and is about 79 percent by volume. Oxygen, carbon dioxide, and other gases vary in complementary proportions to make up the remaining 21 percent by volume.

A typical composition of soil air at the surface layers of soil under well aerated conditions is given in Table 1 (Ghildyal and Tripathi, 1987). As is indicated in Table 1, the proportion of soil air at the soil surface layer is different from that of the atmosphere as a consequence of the biological activities of soil flora and fauna. The major difference is the carbon dioxide content. The carbon dioxide content in the atmosphere is 0.034 percent by volume, while it varies from 0.2 to 1 percent by volume in the air

extracted from the soil pores of the surface layer of soil with adequate aeration. However, under anaerobic conditions, the carbon dioxide content in the soil can be as much as 10 percent by volume, which is about 300 times as much as that in the atmosphere (Brady, 1984). The oxygen content of soil air is usually slightly lower than that of the atmosphere at the soil surface layer under well aerated conditions. Under anaerobic conditions, the oxygen content in the soil can drop to 5 percent by volume or even to zero when the soil is waterlogged.

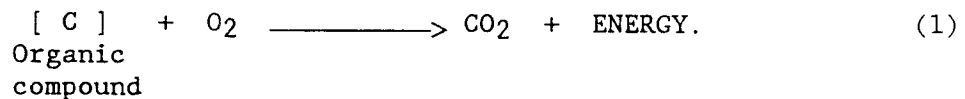
Table 1. Composition of air in the atmosphere and in the soil surface layer under well aerated soil conditions (Ghildyal and Tripathi, 1987).

Gases	Atmosphere air	Soil air
	% by volume	% by volume
Nitrogen	79.000	79.200
Oxygen	20.966	20.600
Carbon dioxide	0.034	0.200
Other gases	Traces	Traces

Soil air exhibits all the characteristics of gases. It is compressible and has low density and low viscosity. The specific heat of soil air is intermediate between that of solid and water components. The thermal conductivity of the soil air is also quite low and varies with soil temperature and soil water content.

Soil Aeration and Problems in the Field

Plant roots and aerobic soil microorganisms use oxygen and release carbon dioxide during the processes of their biological respiratory activities. The generalized reaction for these processes may be expressed as follows (Brady, 1984):



If there were no mechanisms to replenish the oxygen in the soil and permit the escape of carbon dioxide out of the soil, the processes would be curtailed due to the deficiency of oxygen and the accumulation of carbon dioxide in the soil, and plant growth would suffer. Soil aeration is the mechanism by which oxygen and carbon dioxide are exchanged between the soil and the atmosphere, thereby preventing oxygen deficiency and carbon dioxide toxicity and permitting normal growth of plant roots and aerobic microorganisms.

Although some plant species (e.g., wetland rice) may have sufficient internal diffusion of oxygen from leaves to roots to supply the respiration requirements of roots, in most plant species this internal transfer is either unimportant or at least insufficient to meet the respiration requirements of large root systems (Marschner, 1986; De Willigen and Van Noordwijk, 1989). Therefore, root respiration requires that the soil itself be aerated. A soil in which aeration is considered satisfactory must have at least two characteristics. First, sufficient spaces free of solids and water should be present. Second, there must be ample opportunity for the ready movement of oxygen into, and carbon dioxide out of, these spaces.

Oxygen, a gas used in biological reactions, must be continually supplied from the atmosphere. The activities of many plant roots are hampered when the content of oxygen in soil air is less than 10 percent by volume (Brady, 1984). At the same time, the content of carbon dioxide, a gas released in biological reactions, must not be allowed to build up excessively in the soil. The activities of many roots, such as maize (Zea mays) and cotton (Gossypium spp.), may be inhibited if the carbon dioxide content is above 5 percent by volume (Nobel and Palta, 1989).

Under actual field conditions, there are generally two situations that may result in poor aeration in soils, namely: (1) when the water content is excessively high, leaving little or no pore space for the gases, and (2) when the exchange of oxygen and carbon dioxide with the atmosphere is not sufficiently rapid to keep the concentration of oxygen and carbon dioxide at desirable levels.

The first case usually exists in a waterlogged condition. Waterlogging is frequently found in poorly drained, fine-textured soils having a minimum of macropores through which water can move rapidly. It also occurs in soil that is normally well-drained if the rate of water supply to the soil surface is sufficiently faster than the rate of water infiltrating from the soil surface layer to the subsoil layer. Such complete saturation of the soil can be disastrous for certain plants in a short time. Prevention of this type of poor aeration requires the rapid removal of excess water either by land drainage or by controlled runoff.

The seriousness of an inadequate exchange of oxygen and carbon dioxide between the soil and the atmosphere is dependent primarily on

two factors: (1) the rates of oxygen consumption and carbon dioxide production by roots and soil microorganisms during their respiration, and (2) the actual rate at which each gas is moved into or out of the soil. Obviously, the more rapid the consumption of oxygen and the corresponding production of carbon dioxide, the greater the necessity for the exchange of oxygen and carbon dioxide between the soil and the atmosphere. Rate of exchange is limited by low pore space due to excess water or due to soil compaction.

### Characterization of Soil Aeration

Soil aeration can be characterized conveniently in three ways: (1) the content of oxygen and other gases in the soil; (2) the oxygen diffusion rate (ODR); and (3) the oxidation-reduction potential. Each of these will be briefly discussed.

#### Oxygen Content in the Soil

The amount of oxygen in the soil can be expressed as a percentage of volume, or concentration. It is determined by the quantity of air-filled pore space, the proportion of that space that is filled with oxygen, and the rate of use of oxygen by plant roots and soil microorganisms. The oxygen content may be slightly below 20 percent by volume in the upper layer of a well aerated soil. It may drop to less than 5 percent by volume, or even to zero, in poorly drained soils with few macropores (Brady, 1984).

### Oxygen Diffusion Rate (ODR)

The oxygen diffusion rate is the amount of oxygen that diffuses through the soil per unit area of soil per unit time. This is used as an index of oxygen availability to plant roots. Researchers have found that the ODR is of critical importance to growing plants. Stolzy and Letey (1964) stated that roots of many plant species cannot grow in an environment with an ODR of less than  $12 \mu\text{g oxygen cm}^{-2} \text{ wet soil hr}^{-1}$ . An insufficient ODR also causes the accumulation of carbon dioxide, ethanol, and other toxic gases that can damage the plant roots. The description of the ODR measurement technique has been published by Birkle et al., (1964) and McIntyre (1970).

### Oxidation-Reduction Potential (Eh)

One important chemical characteristic of soils, related to soil aeration, is the reduction and oxidation states of chemical elements in soils. If a soil is well aerated, oxidized states such as that of ferric iron ( $\text{Fe}^{+3}$ ), manganic manganese ( $\text{Mn}^{+4}$ ), nitrate ( $\text{NO}_3^-$ ), and sulfate ( $\text{SO}_4^{-2}$ ) dominate. The reduced forms of elements such as ferrous iron ( $\text{Fe}^{+2}$ ), manganous manganese ( $\text{Mn}^{+2}$ ), ammonium ( $\text{NH}_4^+$ ), and sulfides ( $\text{S}^{-2}$ ) are found in poorly drained and poorly aerated soils. The presence of these reduced forms is an indication of restricted drainage and poor aeration.

An indication of a system in oxidation and reduction states is given by the oxidation-reduction or redox potential (Eh). This variable provides a measure of the tendency of an environment to

reduce or oxidize chemicals, and is usually measured in volts or millivolts. If it is positive or high, strong oxidation conditions exist. If it is low or even negative, elements are found in reduced forms. In a well-drained soil, the Eh is in the range of 0.4-0.7 volts. The Eh declines to a level of about 0.3-0.35 volts when gaseous oxygen is depleted. Under water-logged conditions, the Eh may be lowered to an extreme of -0.4 volts (Brady, 1984).

## TRANSPORT OF OXYGEN AND CARBON DIOXIDE THROUGH SOILS

Transport Processes

When the concentration of oxygen decreases in the soil, the concentration of carbon dioxide generally increases. This is mainly due to the fact that plant roots and soil microorganisms use oxygen and produce carbon dioxide during their respiratory activities. The use of oxygen by roots and microorganisms in the soil causes a concentration gradient between the atmosphere and the soil profile. The concentration of oxygen in the atmosphere is higher than it is in the soil. This leads to the diffusion of oxygen from the atmosphere to the soil. Carbon dioxide, on the other hand, is produced by roots and microorganisms in the soil. This also causes a concentration gradient between the atmosphere and the soil profile. The concentration of carbon dioxide in the atmosphere is lower than it is in the soil. This leads to the diffusion of carbon dioxide from the soil to the atmosphere. Thus, the coupled transport of oxygen and carbon dioxide through soil is a problem of counter transport. Therefore, when modeling the transport of oxygen and carbon dioxide through soil, a simultaneous transport system should be considered.

The transport of oxygen and carbon dioxide through a porous media, such as soil, is mainly facilitated by the following several mechanisms and processes:

- (1) Mass flow, which is caused by the gradient of total gas pressure of oxygen and carbon dioxide. It results in the entire mass of oxygen and carbon dioxide streaming from a zone of higher pressure

to one of lower pressure.

(2) Diffusion, which is due to the gradient of concentration (or partial pressure) of oxygen and carbon dioxide. It causes the molecules of unevenly distributed oxygen and carbon dioxide to migrate from a zone of higher concentration to lower concentration.

(3) Dissolution of oxygen and carbon dioxide in the soil water, which will create a concentration gradient of oxygen and carbon dioxide between soil air-filled pore space and soil water.

(4) Consumption of oxygen by the respiration activities of plant roots and soil microorganisms, creating an oxygen concentration gradient between the surface of the roots and the microorganisms, and their surrounding soil. This will cause the oxygen to diffuse more rapidly from surrounding soil to the surfaces of the roots and the microorganisms.

(5) Production of carbon dioxide by the respiration activities of plant roots and soil microorganisms, creating a carbon dioxide concentration gradient between the surface of the roots and the microorganisms, and their surrounding soil. This will cause the carbon dioxide to diffuse more rapidly from the surfaces of the roots and the microorganisms to the surrounding soil.

(6) Physical adsorption of oxygen and carbon dioxide by the colloidal surfaces of soil particles. This is due to the force operating between the colloidal surfaces and the molecules of oxygen and carbon dioxide, which is similar to the Van der Waals force between molecules (Moore, 1983). The adsorption of oxygen by the colloidal surfaces of soil particles reduces the concentration of oxygen in the soil air-filled pore space. This results in an oxygen

concentration gradient between the soil and the atmosphere, thereby causing the oxygen to diffuse more rapidly from the atmosphere to the soil. The adsorption of carbon dioxide by the colloidal surfaces of soil particles reduces the concentration of carbon dioxide in the soil air-filled pore space.

(7) Replacement of soil air by water when the soil is wetting and replacement of soil water by air when the soil is drying. These processes either bring the oxygen and carbon dioxide out of, or into, the soil.

### Factors Affecting the Transport Processes

Soil factors that are important in affecting the transport of oxygen and carbon dioxide through soil include soil water content, soil temperature, irrigation, rainfall, drainage, soil depth, and time.

#### Soil Water Content

Soil water content governs the soil air content and the distribution and arrangement of air spaces in the soil, thereby affecting the rates of transport of oxygen and carbon dioxide in the soil. The effect of soil water content on the rates of respiration activities of plant roots and soil microorganisms has an indirect effect on the transport of oxygen and carbon dioxide through soil, since oxygen is consumed and carbon dioxide is produced by the respiration activities of plant roots and soil microorganisms.

### Soil Temperature

It is well known that the specific volume of a gas is temperature-dependent. Whenever a temperature gradient between the atmosphere and the soil is created, the resulting density and pressure gradient causes oxygen and carbon dioxide to flow. Temperature differences also exist within different soil layers. These differences may cause mass flow within the soil air-filled pore space and, also, between the soil air-filled pore space and the atmosphere.

The effects of soil temperature on the exchange of oxygen and carbon dioxide between the soil and the atmosphere also plays an important role, through its effects on the rate of consumption of oxygen and the rate of production of carbon dioxide in the biological activities, as well as on the transport velocities of oxygen and carbon dioxide. For example, increasing soil temperature from 15°C to 30°C raises the rate of oxygen consumption from 450 to 1350 cm<sup>3</sup> kg<sup>-1</sup> (fresh root) hr<sup>-1</sup>, with the initial soil water content at 0.1 cm<sup>3</sup> cm<sup>-3</sup> by onion (Allium cepa) roots (Glinski and Stepniewski, 1985). The change of soil temperature affects the transport velocities of oxygen and carbon dioxide through its effects on the thermodynamic energy of molecules of oxygen and carbon dioxide (Moore, 1983). Therefore, an increase of soil temperature raises the rate of transport of oxygen and carbon dioxide through soil.

### Irrigation, Rainfall, and Drainage

Irrigation and rainfall may also cause oxygen and carbon dioxide

exchange. This may take place in two ways. First, by water displacement of air in the soil pores and second, by carrying dissolved oxygen and carbon dioxide via water. The downward penetration of the saturation zone during the infiltration following rain or irrigation may cause flushing or displacement of soil air, leading to gas interchange. Similarly, water is replaced by air as water is removed by drainage or evaporation. Due to the downward displacement of air from the surface soil, oxygen levels at lower soil depths have been found to increase immediately after irrigation (Ghildyal and Tripathi, 1987).

#### Soil Depth

Soil is a heterogeneous system whose properties change with soil depth. At different soil layers, soil properties such as soil porosity, hydraulic conductivity and thermal conductivity, are different. Therefore, the transport of oxygen and carbon dioxide through soil, which is subjected to the soil properties, will change with soil depth.

#### Time

The transport of oxygen and carbon dioxide through soil changes over time. In addition, soil water, temperature, and biological activities, which are important factors controlling the transport of oxygen and carbon dioxide, also change over time. This makes the transport of oxygen and carbon dioxide strongly dependent on time.

## OBJECTIVE

An important objective of modeling gaseous transport through agricultural soil is the investigation of the problem of soil aeration, especially the exchange of oxygen and carbon dioxide between the soil and the atmosphere. Although the processes of transport of gases through soils have been investigated by many soil scientists (Van Noordwijk and De Willigen, 1984; Glinski and Stepniewski, 1985; Skopp, 1985; Molz, et al., 1986; Thorstenson and Pollock, 1989; Mendoza and Frind, 1990), their work mainly considered the gaseous transport at a constant soil water content and soil temperature. The climatic and biological effects on the transport of gases are not included in their studies. The purpose of this study is: (1) to develop a one-dimensional mathematical model for the simultaneous transport of water, heat, oxygen, and carbon dioxide through unsaturated soils with the effects of climatic conditions, soil physical conditions, and biological activities of plant roots and soil microorganisms; and (2) to apply the model to examine the transport of oxygen and carbon dioxide through soils as well as conditions under which the deficiency of oxygen and the toxicity of carbon dioxide occur in the root zone.

## SCOPE OF RESEARCH

A schematic presentation of the processes of transport of oxygen and carbon dioxide through soil, which are of interest in this research, are shown in Figure 1. The processes include: (1) diffusion of oxygen and carbon dioxide through air-filled pore spaces of soil; (2) consumption of oxygen and production of carbon dioxide by plant roots and soil microorganisms during their respiratory activities; (3) dissolution of oxygen and carbon dioxide in soil water; (4) physical adsorption of oxygen and carbon dioxide onto the colloidal surfaces of soil particles; (5) replacement of air by water due to soil wetting, and replacement of water by air due to soil drying, which will cause the flow of oxygen and carbon dioxide out of or into the soil (not shown in Figure 1). The studies of transport of oxygen and carbon dioxide through soils are based on the above considerations.

In this research, the following factors, which affect the transport of oxygen and carbon dioxide through soil, are of major concern:

- (1) Rate of solar radiation, which changes over time;
- (2) Rate and duration of rainfall as a function of time;
- (3) Air temperature and its changes over time as affected by solar radiation, relative humidity, and rain;
- (4) Relative humidity and its changes over time as influenced by air temperature, air moisture content, and rain;
- (5) Soil water content and its changes over time and soil depth as affected by soil temperature;

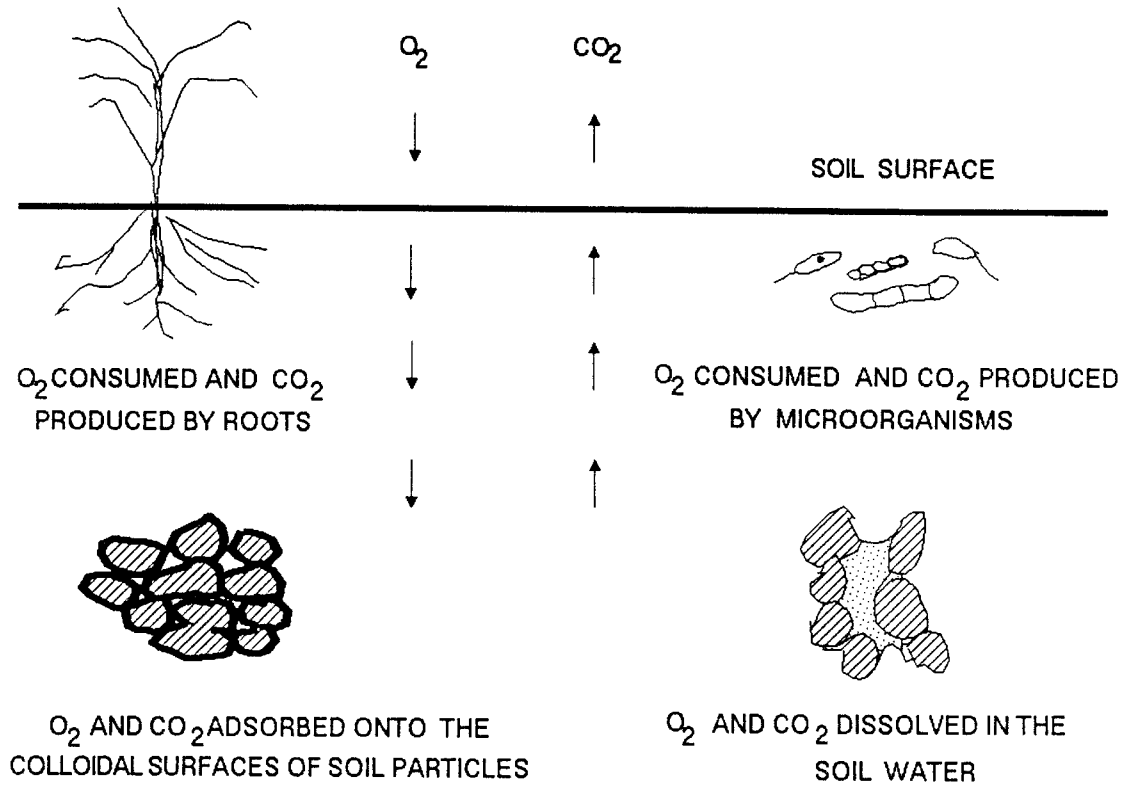


Figure 1. Schematic diagram of processes of the transport of oxygen and carbon dioxide in the soil environment.

- (6) Soil temperature and its changes over time and soil depth as affected by soil water content;
- (7) The transport of oxygen and carbon dioxide changes over time and soil depth, and is affected by both soil water content and soil temperature.

## DEVELOPMENT OF FIELD EQUATIONS

Basic Assumption

Figure 2 shows a schematic diagram of a soil profile. Development of field equations for the simultaneous transport of water, heat, oxygen, and carbon dioxide will be stated for this simple soil profile. The simple soil profile is defined as a soil slab, which may be up to 170 cm thick and of nonhomogenous soil properties. The slab is bound below by an impervious layer and above by the atmosphere. Assumptions pertaining to the atmosphere and the soil slab will be discussed in the following sections.

Assumptions Pertaining to the Atmosphere

The assumptions used in the development of field equations pertaining to the atmosphere are:

- (1) Diurnal changes in air temperature and relative humidity can be characterized by Fourier Series;
- (2) Diurnal changes in solar intensity can be characterized by a Gaussian normal distribution function;
- (3) The initial distributions of water, temperature, oxygen, and carbon dioxide in the atmosphere are known;
- (4) The rate and duration of rainfall is prescribed.

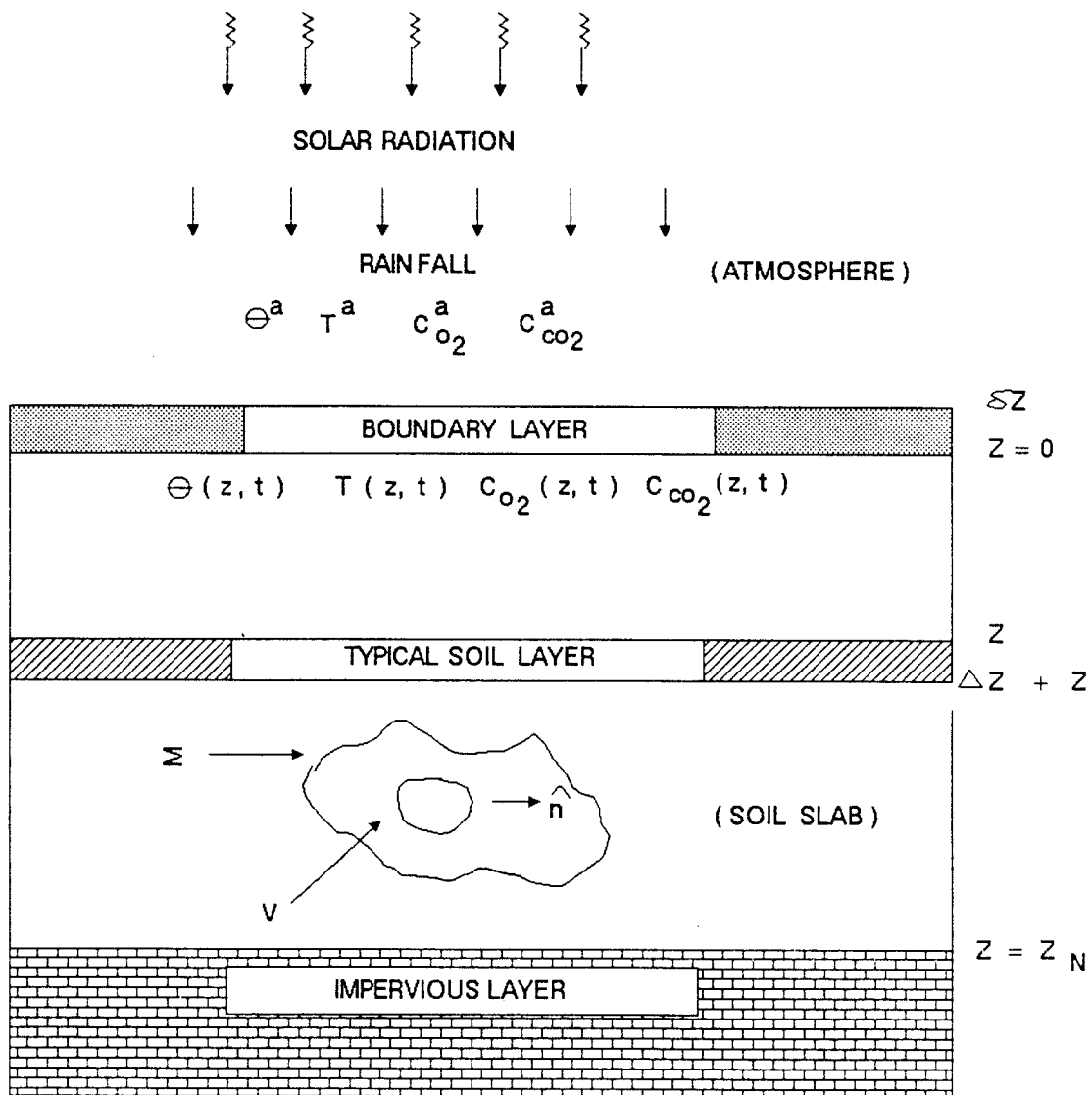


Figure 2. Schematic diagram of a soil profile for which a model of water, heat, oxygen, and carbon dioxide transport will be developed.

Assumptions Pertaining to the Soil Slab

The assumptions used in the development of field equations pertaining to the soil slab are:

- (1) The soil can be characterized by known parameters such as: the soil porosity; the specific heats of solids, water, and air; the thermal conductivities of solids, water, and air; the latent heat of vaporization; the water potential function; the hydraulic conductivity function; and the densities of solids, water, air, and water vapor;
- (2) The atmosphere and soil surface are coupled for the water, heat, oxygen, and carbon dioxide fields by heat and mass transport rules operating in the boundary layer at the atmosphere-soil interface;
- (3) The initial distributions of water content, temperature, oxygen, and carbon dioxide in the soil slab are prescribed;
- (4) Entrapped air is assumed to be negligible. This is in part justified by choosing a stable soil structure (i.e., no swelling and shrinking) and a lower rate of soil infiltration.

The oxygen and carbon dioxide fields are assumed to depend upon the water and heat fields, but the water and heat fields operate independently of the oxygen and carbon dioxide fields.

Field Equations for Water and Heat Transport in the Soil

Water and heat field equations derived by Lindstrom and Piver (1985) for conditions similar to this thesis are given as:

$$\frac{\partial}{\partial t} [\rho_w \theta + \rho_{wv}^{sat}(T)h(\epsilon - \theta)] = -\nabla \cdot [\rho_w \theta \vec{V}_l + \rho_{wv}(\epsilon - \theta)\vec{V}_v] \quad (1)$$

for water transport, and:

$$\begin{aligned} \frac{\partial}{\partial t} [(1 - \epsilon)c_{solid} \rho_{solid} T + (\epsilon - \theta)c_{air} \rho_{air} T + \theta c_w \rho_w T] \\ = -\nabla \cdot [(1 - \epsilon)\vec{H}_{SS} + \theta\vec{H}_{Sl} + (\epsilon - \theta)\vec{H}_{Sv}] \end{aligned} \quad (2)$$

for heat transport, where  $t$  is the time (hr),  $\rho_w$  is the density of water ( $\text{g cm}^{-3}$ ),  $\theta$  is the volumetric water content ( $\text{cm}^3 \text{ cm}^{-3}$ ),  $\rho_{wv}^{sat}(T)$  is the density of water vapor at saturation at temperature  $T$  ( $\text{g vapor cm}^{-3} \text{ air}$ ),  $h$  is the relative humidity (dimensionless),  $\epsilon$  is the soil porosity ( $\text{cm}^3 \text{ soil voids cm}^{-3} \text{ soil}$ ),  $\vec{V}_l$  and  $\vec{V}_v$  are the velocity vectors of water in the liquid and vapor phases ( $\text{cm hr}^{-1}$ ), respectively,  $\rho_{wv}$  is the density of water vapor ( $\text{g vapor cm}^{-3} \text{ air}$ ),  $c_{solid}$  is the specific heat of soil particles ( $\text{cal soil}^{-1} \text{ particle } ^\circ\text{C}^{-1}$ ),  $\rho_{solid}$  is the density of soil particles ( $\text{g cm}^{-3} \text{ solids}$ ),  $T$  is the temperature ( $^\circ\text{C}$ ),  $c_{air}$  and  $c_w$  are specific heats of air and water ( $\text{cal g}^{-1} \text{ } ^\circ\text{C}^{-1}$ ), respectively,  $\rho_{air}$  is the density of air ( $\text{g cm}^{-3} \text{ air}$ ),  $\vec{H}_{SS}$  is the vector of the heat conduction through the soil particles ( $\text{cal cm}^{-2} \text{ hr}^{-1}$ ),  $\vec{H}_{Sl}$  is the vector of the heat conduction and convection in the liquid phase ( $\text{cal cm}^{-2} \text{ hr}^{-1}$ ),  $\vec{H}_{Sv}$  is the vector of the heat conduction in the vapor phase and the transport of latent heat ( $\text{cal cm}^{-2} \text{ hr}^{-1}$ ).

The velocity vectors,  $\vec{V}_1$  and  $\vec{V}_v$ , in equations (1) and (2) are defined as:

$$\vec{V}_1 = -D_{\leftrightarrow\theta 1} \cdot \nabla\theta - D_{\leftrightarrow T 1} \cdot \nabla T + K_{\leftrightarrow} \cdot (\hat{z} - \frac{\partial\psi}{\partial z}), \quad (3)$$

and

$$\vec{V}_v = -D_{\leftrightarrow\theta v} \cdot \nabla\theta - D_{\leftrightarrow T v} \cdot \nabla T + D_{\leftrightarrow\psi} \cdot (-\frac{\partial\psi}{\partial z}), \quad (4)$$

with

$$D_{\leftrightarrow\theta 1} = (\frac{\partial\psi}{\partial z}) K_{\leftrightarrow}, \quad (5)$$

$$D_{\leftrightarrow T 1} = (\frac{\partial\psi}{\partial T}) K_{\leftrightarrow}, \quad (6)$$

$$D_{\leftrightarrow\theta v} = D_{\text{atm}} \alpha_{\text{tort}} (\frac{g}{RT}) (\frac{\partial\psi}{\partial z}) E_{\leftrightarrow}, \quad (7)$$

$$D_{\leftrightarrow T v} = D_{\text{atm}} \alpha_{\text{tort}} \left[ \begin{array}{l} 1 \\ (\frac{\rho^{\text{sat}}}{\rho_{\text{wv}}^{\text{sat}}(T)}) (\frac{d\rho_{\text{wv}}^{\text{sat}}(T)}{dT}) \\ + (\frac{g}{RT}) [(\frac{\partial\psi}{\partial z}) - (\frac{\psi}{T})] \end{array} \right] E_{\leftrightarrow}, \quad (8)$$

$$D_{\leftrightarrow\psi} = D_{\text{atm}} \alpha_{\text{tort}} (\frac{g}{RT}) E_{\leftrightarrow}, \quad (9)$$

where  $D_{\leftrightarrow\theta 1}$  is the second rank tensor describing the diffusion coefficient of water in the liquid phase ( $\text{cm}^2 \text{hr}^{-1}$ ),  $D_{\leftrightarrow T 1}$  is the second tensor describing the thermal diffusivity in the liquid phase ( $\text{cm}^2 \text{hr}^{-1}$ ),  $K_{\leftrightarrow}$  is the second rank tensor describing the water conductivity ( $\text{cm hr}^{-1}$ ),  $\hat{z}$  is the unit vector normal to plane  $z = 0$  with positive orientation vertically downward,  $z$  is the soil depth (cm),  $\psi$  is the water potential (cm),  $D_{\leftrightarrow\theta v}$  is the second rank tensor describing the

diffusion coefficient of water in the vapor phase ( $\text{cm}^2 \text{hr}^{-1}$ ),  $D_{\leftrightarrow T_V}$  is the second rank tensor describing the thermal diffusivity in the vapor phase ( $\text{cm}^2 \text{hr}^{-1}$ ),  $D_{\leftrightarrow \psi}$  is the second rank tensor describing the diffusion coefficient of water affected by the water potential ( $\text{cm}^2 \text{hr}^{-1}$ ),  $D_{\text{atm}}$  is the water vapor molecular diffusion coefficient in air ( $\text{cm}^2 \text{hr}^{-1}$ ),  $\alpha_{\text{tort}}$  is the tortuosity factor of the soil,  $g$  is the gravitational constant ( $\text{cm hr}^{-1}$ ),  $R$  is the gas constant ( $\text{cm}^2 \text{hr}^{-2} \text{ } ^\circ\text{C}^{-1}$ ),  $\underline{\underline{E}}$  is the second rank identity tensor (dimensionless),  $\rho_{\text{wv}}^{\text{sat}}(T)$  is the density of water vapor at saturation at temperature  $T$  ( $\text{g vapor cm}^{-3} \text{ air}$ ).

The vectors  $\vec{H}_{\text{ss}}$ ,  $\vec{H}_{\text{s1}}$ , and  $\vec{H}_{\text{sv}}$  in equations (1) and (2) are defined as:

$$\vec{H}_{\text{ss}} = -\lambda_{\text{solid}} \nabla T, \quad (10)$$

$$\vec{H}_{\text{s1}} = -\lambda_{\text{w}} \nabla T + c_{\text{w}} \rho_{\text{w}} \vec{V}_1 T, \quad (11)$$

and

$$\vec{H}_{\text{sv}} = -\xi D_{\text{atm}} \alpha_{\text{tort}} \nabla \rho_{\text{wv}} - \lambda_{\text{air}} \nabla T, \quad (12)$$

where  $\lambda_{\text{solid}}$  is the thermal conductivity of the solids ( $\text{cal cm}^{-1} \text{hr}^{-1} \text{ } ^\circ\text{C}^{-1}$ ),  $\lambda_{\text{w}}$  is the thermal conductivity of water ( $\text{cal cm}^{-1} \text{hr}^{-1} \text{ } ^\circ\text{C}^{-1}$ ),  $\xi$  is the latent heat of evaporation ( $\text{cal g}^{-1}$ ), and  $\lambda_{\text{air}}$  is the thermal conductivity of the air ( $\text{cal cm}^{-1} \text{hr}^{-1} \text{ } ^\circ\text{C}^{-1}$ ).

The variables  $\rho_{\text{wv}}^{\text{sat}}(T)$ ,  $\rho_{\text{wv}}$ ,  $h$ , and  $\xi$  in equations (1), (2), and (12), which are functions of temperature and water content, are given as (Weast, 1986):

$$\rho_{\text{wv}}^{\text{sat}}(T) = 0.004928 + 0.0002581 T + 0.0000183 T^2, \quad (13)$$

for  $0 < T \leq 22.5^\circ\text{C}$ , and

$$\rho_{\text{wv}}^{\text{sat}}(T) = 0.004928 + 0.0002581 T + 0.0000183 T^2 + 0.0000213 T^3, \quad (14)$$

for  $T > 22.5^\circ\text{C}$ ,

$$\rho_{\text{wv}} = \rho_{\text{wv}}^{\text{sat}}(T) h, \quad (15)$$

$$h = \exp(\psi g/RT), \quad (16)$$

and

$$\xi = 598.88 - 0.547 T. \quad (17)$$

#### Derivation of Oxygen and Carbon Dioxide Field Equations

Following the sketch of the soil slab shown in Figure 2, consider the representative volume element  $v$  surrounded by the simple closed surface  $\Sigma$ . Let  $\bar{n}$  be the unit vector outward going normal to  $\Sigma$ . We now develop the field equations for the total amount of oxygen and carbon dioxide in the arbitrary volume element embedded in the soil slab.

The total fluxes of oxygen and carbon dioxide can be expressed as:

$$\vec{q}_{\text{o}_2} = \theta \vec{q}_{\text{o}_2\text{liq}} + (\epsilon - \theta) \vec{q}_{\text{o}_2\text{air}} \quad (18)$$

for the oxygen, and:

$$\vec{q}_{\text{co}_2} = \theta \vec{q}_{\text{co}_2\text{liq}} + (\epsilon - \theta) \vec{q}_{\text{co}_2\text{air}} \quad (19)$$

for the carbon dioxide, where  $\vec{q}_{\text{o}_2}$  and  $\vec{q}_{\text{co}_2}$  are the total fluxes of

volumetric water content of the soil ( $\text{cm}^3 \text{ cm}^{-3}$ ),  $\vec{q}_{\text{o}_2\text{liq}}$  and  $\vec{q}_{\text{co}_2\text{liq}}$  are the fluxes of oxygen and carbon dioxide in liquid phase of soil water, respectively ( $\mu\text{g cm}^{-2} \text{ hr}^{-1}$ ),  $\epsilon$  is the porosity of the soil ( $\text{cm}^3 \text{ soil voids cm}^{-3} \text{ soil}$ ),  $\vec{q}_{\text{o}_2\text{air}}$  and  $\vec{q}_{\text{co}_2\text{air}}$  are the fluxes of oxygen and carbon dioxide in the air-filled pore spaces of the soil, respectively ( $\mu\text{g cm}^{-2} \text{ hr}^{-1}$ ).

Since the fluxes of oxygen and carbon dioxide in the soil water are much smaller than they are in the air-filled pore spaces of the soil (Glinski and Stepniewski, 1985), the fluxes of oxygen and carbon dioxide in the liquid phase of soil water are ignored. Therefore, equations (18) and (19) reduce to:

$$\vec{q}_{\text{o}_2} = (\epsilon - \theta) \vec{q}_{\text{o}_2\text{air}}, \quad (20)$$

$$\vec{q}_{\text{co}_2} = (\epsilon - \theta) \vec{q}_{\text{co}_2\text{air}}. \quad (21)$$

The fluxes of oxygen and carbon dioxide in the air-filled pore spaces of the soil in equations (20) and (21) can be expressed as:

$$\vec{q}_{\text{o}_2\text{air}} = \vec{q}_{\text{o}_2\text{diff}} + \vec{V}_{\text{air}} C_{\text{o}_2}, \quad (22)$$

and

$$\vec{q}_{\text{co}_2\text{air}} = \vec{q}_{\text{co}_2\text{diff}} + \vec{V}_{\text{air}} C_{\text{co}_2}, \quad (23)$$

respectively, where  $\vec{q}_{\text{o}_2\text{diff}}$  and  $\vec{q}_{\text{co}_2\text{diff}}$  are the diffusional fluxes of oxygen and carbon dioxide in the air-filled pore space of the soil, respectively ( $\mu\text{g cm}^{-2} \text{ hr}^{-1}$ ),  $\vec{V}_{\text{air}} C_{\text{o}_2}$  and  $\vec{V}_{\text{air}} C_{\text{co}_2}$  are the mass flow of oxygen and carbon dioxide through the air-filled pore spaces of the soil, respectively ( $\mu\text{g cm}^{-2} \text{ hr}^{-1}$ ),  $\vec{V}_{\text{air}}$  is the velocity vector

of air ( $\text{cm hr}^{-1}$ ),  $C_{\text{o}_2}$  and  $C_{\text{co}_2}$  are the concentrations of oxygen and carbon dioxide, respectively ( $\mu\text{g cm}^{-3}$  air). For a counter diffusion of oxygen and carbon dioxide, the diffusional fluxes of  $\vec{q}_{\text{o}_2\text{diff}}$  and  $\vec{q}_{\text{co}_2\text{diff}}$  can be expressed as:

$$\vec{q}_{\text{o}_2\text{diff}} = - \delta_{\text{o}_2} \frac{\partial \mu_{\text{o}_2}}{\partial z} C_{\text{o}_2} , \quad (24)$$

$$\vec{q}_{\text{co}_2\text{diff}} = - \delta_{\text{co}_2} \frac{\partial \mu_{\text{co}_2}}{\partial z} C_{\text{co}_2} , \quad (25)$$

and

$$\mu_{\text{o}_2} = \mu_{\text{o}_2}^0 + RT \ln(a_{\text{o}_2}) , \quad (26)$$

$$\mu_{\text{co}_2} = \mu_{\text{co}_2}^0 + RT \ln(a_{\text{co}_2}) , \quad (27)$$

with

$$a_{\text{o}_2} = \gamma_{\text{o}_2} C_{\text{o}_2} , \quad (28)$$

$$a_{\text{co}_2} = \gamma_{\text{co}_2} C_{\text{co}_2} , \quad (29)$$

where  $\delta_{\text{o}_2}$  and  $\delta_{\text{co}_2}$  are the coefficients characterizing the mobility of oxygen and carbon dioxide in the soil, respectively ( $\text{mol cm}^2 \text{ cal}^{-1} \text{ hr}^{-1}$ ),  $\mu_{\text{o}_2}$  and  $\mu_{\text{co}_2}$  are the chemical potentials of oxygen and carbon dioxide, respectively ( $\text{cal mol}^{-1}$ ),  $C_{\text{o}_2}$  and  $C_{\text{co}_2}$  are the concentrations of oxygen and carbon dioxide, respectively ( $\mu\text{g cm}^{-3}$  air),  $\mu_{\text{o}_2}^0$  and  $\mu_{\text{co}_2}^0$  are the chemical potentials of oxygen and carbon dioxide at standard state, respectively ( $\text{cal mol}^{-1}$ ),  $R$  is the gas constant ( $\text{cal mol}^{-1} \text{ K}^{-1}$ ),  $T$  is the temperature ( $^{\circ}\text{C}$ ),  $a_{\text{o}_2}$  and  $a_{\text{co}_2}$  are the activities of oxygen and carbon dioxide, respectively (dimension-

less), and  $\gamma_{o_2}$  and  $\gamma_{co_2}$  are the activity coefficients of oxygen and carbon dioxide, respectively ( $\mu\text{g cm}^{-3}$  air).

Substitution of equations (26) and (28) into equation (24) yields:

$$\vec{q}_{o_2 \text{ diff}_2} = -\delta_{o_2} RT \left[ C_{o_2} \frac{\partial \ln \gamma_{o_2}}{\partial C_{o_2}} + 1 \right] \frac{\partial C_{o_2}}{\partial z} . \quad (30)$$

By comparing equation (30) with Fick's first law (Nobel, 1983), we have:

$$D_{o_2} = \delta_{o_2} RT , \quad (31)$$

where  $D_{o_2}$  is the diffusion coefficient of oxygen ( $\text{cm}^2 \text{hr}^{-1}$ ). Therefore equation (30) becomes:

$$\vec{q}_{o_2 \text{ diff}_2} = -D_{o_2} \left[ C_{o_2} \frac{\partial \ln \gamma_{o_2}}{\partial C_{o_2}} + 1 \right] \frac{\partial C_{o_2}}{\partial z} . \quad (32)$$

Similarly, by substituting equations (27) and (29) into equation (25) yields:

$$\vec{q}_{co_2 \text{ diff}} = -\delta_{co_2} RT \left[ C_{co_2} \frac{\partial \ln \gamma_{co_2}}{\partial C_{co_2}} + 1 \right] \frac{\partial C_{co_2}}{\partial z} . \quad (33)$$

Again, by comparing with Fick's first law, we have:

$$D_{co_2} = \delta_{co_2} RT , \quad (34)$$

where  $D_{co_2}$  is the diffusion coefficient of carbon dioxide ( $\text{cm}^2 \text{hr}^{-1}$ ).

Therefore, equation (33) becomes:

$$\vec{q}_{co \text{ diff}_2} = -D_{co_2} \left[ C_{co_2} \frac{\partial \ln \gamma_{co_2}}{\partial C_{co_2}} + 1 \right] \frac{\partial C_{co_2}}{\partial z} . \quad (35)$$

Since the diffusion of gases is the main mechanism for gaseous transport through soil (Wilson, et al., 1985), the mass flow will be ignored in this study. Therefore, equations (22) and (23) without mass flow become:

$$\vec{q}_{o_2air} = \vec{q}_{o_2diff} = -D_{o_2} \left[ C_{o_2} \frac{\partial \ln \gamma_{o_2}}{\partial C_{o_2}} + 1 \right] \frac{\partial C_{o_2}}{\partial z}, \quad (36)$$

and

$$\vec{q}_{co_2air} = \vec{q}_{co_2diff} = -D_{co_2} \left[ C_{co_2} \frac{\partial \ln \gamma_{co_2}}{\partial C_{co_2}} + 1 \right] \frac{\partial C_{co_2}}{\partial z}. \quad (37)$$

Substituting equations (36) and (37), respectively into equations (20) and (21) yields:

$$\vec{q}_{o_2} = -(\epsilon - \theta) D_{o_2} \left[ C_{o_2} \frac{\partial \ln \gamma_{o_2}}{\partial C_{o_2}} + 1 \right] \frac{\partial C_{o_2}}{\partial z}, \quad (38)$$

and

$$\vec{q}_{co_2} = -(\epsilon - \theta) D_{co_2} \left[ C_{co_2} \frac{\partial \ln \gamma_{co_2}}{\partial C_{co_2}} + 1 \right] \frac{\partial C_{co_2}}{\partial z}. \quad (39)$$

According to the law of conservation of mass, the oxygen and carbon dioxide field equations in this study can be written as:

$$\begin{aligned} & \int_V \frac{\partial}{\partial t} [(\epsilon - \theta) C_{o_2} + \theta C_{o_2}^l + (1 - \epsilon) C_{o_2}^{sl}] dv \\ &= \int_{\Sigma} -\vec{q}_{o_2} \cdot \vec{n} ds + \int_V (\text{source of oxygen}) dv \\ & - \int_V (\text{sink of oxygen}) dv \pm \int_V (\text{Re } C_{o_2}) dv, \end{aligned} \quad (40)$$

for oxygen transport, and:

$$\begin{aligned}
 & \int_v \frac{\partial}{\partial t} [(\epsilon - \theta) C_{\text{CO}_2} + \theta C_{\text{CO}_2}^{\ell} + (1 - \epsilon) C_{\text{CO}_2}^{\text{sl}}] dv \\
 &= \int_{\Sigma} - \vec{q}_{\text{CO}_2} \cdot \vec{n} ds + \int_v (\text{source of carbon dioxide}) dv \\
 & - \int_v (\text{sink of oxygen}) dv \pm \int_v (\text{Re } C_{\text{O}_2}) dv, \quad (41)
 \end{aligned}$$

for carbon dioxide transport, where  $t$  is the time (hr),  $\epsilon$  is the soil porosity ( $\text{cm}^3$  voids  $\text{cm}^{-3}$  soil),  $\theta$  is the soil water content ( $\text{cm}^3$   $\text{cm}^{-3}$ ),  $C_{\text{O}_2}$  and  $C_{\text{CO}_2}$  are the concentrations of oxygen and carbon dioxide in the air-filled pore spaces, respectively ( $\mu\text{g cm}^{-3}$  air),  $C_{\text{O}_2}^{\ell}$  and  $C_{\text{CO}_2}^{\ell}$  are the concentrations of oxygen and carbon dioxide in liquid phase water, respectively ( $\mu\text{g cm}^{-3}$  water),  $C_{\text{O}_2}^{\text{sl}}$  and  $C_{\text{CO}_2}^{\text{sl}}$  are the concentrations of oxygen and carbon dioxide absorbed onto the colloidal surfaces of soil particles, respectively ( $\mu\text{g cm}^{-3}$  solid),  $\vec{q}_{\text{O}_2}$  and  $\vec{q}_{\text{CO}_2}$  are the total fluxes of oxygen and carbon dioxide through the soil, respectively ( $\mu\text{g cm}^{-2} \text{hr}^{-1}$ ),  $\vec{n}$  is the unit vector outward going normal to the simple closed surface  $\Sigma$ ,  $v$  and  $s$  are the arbitrary volume element ( $\text{cm}^3$ ) and area element ( $\text{cm}^2$ ), respectively,  $\text{Re}$  is the replacement of air by soil water due to soil wetting (-) and the replacement of soil water by air due to soil drying (+) ( $\text{cm}^3$  air  $\text{cm}^{-3}$  soil  $\text{hr}^{-1}$ ).

The  $C_{\text{O}_2}^{\ell}$  and  $C_{\text{CO}_2}^{\ell}$  in the left hand side of equations (40) and (41) can be expressed by Henry's Law as:

$$C_{\text{O}_2}^{\ell} = H_{\text{O}_2} C_{\text{O}_2}, \quad (42)$$

and

$$C_{\text{CO}_2}^{\ell} = H_{\text{CO}_2} C_{\text{CO}_2} , \quad (43)$$

where  $H_{\text{O}_2}$  and  $H_{\text{CO}_2}$  are the inverse Henry's Law constants, respectively ( $\text{cm}^3 \text{ air cm}^{-3} \text{ water}$ ). The  $C_{\text{O}_2}^{\text{sl}}$  and  $C_{\text{CO}_2}^{\text{sl}}$  in the left-hand side of equations (40) and (41) can be expressed by using the Freundlich equation (Hiemenz, 1986) as:

$$C_{\text{O}_2}^{\text{sl}} = \omega_{\text{O}_2} C_{\text{O}_2} , \quad (44)$$

and

$$C_{\text{CO}_2}^{\text{sl}} = \omega_{\text{CO}_2} C_{\text{CO}_2} , \quad (45)$$

where  $\omega_{\text{O}_2}$  and  $\omega_{\text{CO}_2}$  are the oxygen and carbon dioxide absorption coefficients, respectively ( $\text{cm}^3 \text{ air cm}^{-3} \text{ solid}$ ).

Assuming that there are no sources of oxygen and no sinks of carbon dioxide in the soil, equations (40) and (41) reduce to:

$$\begin{aligned} & \int_{\text{v}} \frac{\partial}{\partial t} [(\epsilon - \theta) C_{\text{O}_2} + \theta C_{\text{O}_2}^{\ell} + (1 - \epsilon) C_{\text{O}_2}^{\text{sl}}] dv \\ &= \int_{\Sigma} - \vec{q}_{\text{O}_2} \cdot \vec{n} ds + \int_{\text{v}} (\text{sink of oxygen}) dv \\ & \pm \int_{\text{v}} (\text{Re } C_{\text{O}_2}) dv, \end{aligned} \quad (46)$$

and

$$\begin{aligned}
& \int_{\mathbf{v}} \frac{\partial}{\partial t} [ (\epsilon - \theta) C_{\text{co}_2} + \theta C_{\text{co}_2}^{\ell} + (1 - \epsilon) C_{\text{co}_2}^{\text{sl}} ] dv \\
&= \int_{\Sigma} - \vec{q}_{\text{co}_2} \cdot \vec{n} ds + \int_{\mathbf{v}} (\text{source of carbon dioxide}) dv \\
&\pm \int_{\mathbf{v}} (\text{Re } C_{\text{co}_2}) dv. \tag{47}
\end{aligned}$$

In the soil environment, oxygen is consumed and carbon dioxide is produced as follows:

- a. Oxygen consumption rate by roots

$$S_{\text{o}_2}^{\text{rt}} \quad (\mu\text{g O}_2 \text{ cm}^{-3} \text{ air hr}^{-1})$$

- b. Oxygen consumption rate by microorganisms

$$S_{\text{o}_2}^{\text{mo}} \quad (\mu\text{g O}_2 \text{ cm}^{-3} \text{ air hr}^{-1})$$

- c. Carbon dioxide production rate by roots

$$S_{\text{o}_2}^{\text{rt}} \quad (\mu\text{g CO}_2 \text{ cm}^{-3} \text{ air hr}^{-1})$$

- d. Carbon dioxide production rate by microorganisms

$$S_{\text{co}_2}^{\text{mo}} \quad (\mu\text{g CO}_2 \text{ cm}^{-3} \text{ air hr}^{-1}).$$

Therefore, the equations (46) and (47) become:

$$\begin{aligned}
& \int_{\mathbf{v}} \frac{\partial}{\partial t} [ (\epsilon - \theta) C_{\text{o}_2} + \theta C_{\text{o}_2}^{\ell} + (1 - \epsilon) C_{\text{o}_2}^{\text{sl}} ] dv \\
&= \int_{\Sigma} - \vec{q}_{\text{o}_2} \cdot \vec{n} ds + \int_{\mathbf{v}} (S_{\text{o}_2}^{\text{rt}} + S_{\text{o}_2}^{\text{mo}}) dv \\
&\pm \int_{\mathbf{v}} (\text{Re } C_{\text{o}_2}) dv, \tag{48}
\end{aligned}$$

and

$$\begin{aligned}
& \int_{\mathbf{v}} \frac{\partial}{\partial t} [(\epsilon - \theta) C_{\text{co}_2} + \theta C_{\text{co}_2}^{\ell} + (1 - \epsilon) C_{\text{co}_2}^{\text{sl}}] dv \\
&= \int_{\Sigma} - \vec{q}_{\text{co}_2} \cdot \vec{n} ds + \int_{\mathbf{v}} (S_{\text{co}_2}^{\text{rt}} + S_{\text{co}_2}^{\text{mo}}) dv \\
&\pm \int_{\mathbf{v}} (\text{Re } C_{\text{co}_2}) dv. \tag{49}
\end{aligned}$$

Using the Gaussian Theorem to convert the surface integrals to volume integrals, multiplying both sides of equations (48) and (49), respectively, by  $1/v$ , and letting  $v \rightarrow 0 +$ , yields limits to the oxygen and carbon dioxide field equations in the differential form:

$$\begin{aligned}
& \frac{\partial}{\partial t} [(\epsilon - \theta) C_{\text{o}_2} + \theta C_{\text{o}_2}^{\ell} + (1 - \epsilon) C_{\text{o}_2}^{\text{sl}}] \\
&= - \nabla \cdot \vec{q}_{\text{o}_2} - (S_{\text{o}_2}^{\text{rt}} + S_{\text{o}_2}^{\text{mo}}) \pm R_e C_{\text{o}_2}, \tag{50}
\end{aligned}$$

and

$$\begin{aligned}
& \frac{\partial}{\partial t} [(\epsilon - \theta) C_{\text{co}_2} + \theta C_{\text{co}_2}^{\ell} + (1 - \epsilon) C_{\text{co}_2}^{\text{sl}}] \\
&= - \nabla \cdot \vec{q}_{\text{co}_2} - (S_{\text{co}_2}^{\text{rt}} + S_{\text{co}_2}^{\text{mo}}) \pm R_e C_{\text{co}_2}. \tag{51}
\end{aligned}$$

Substitution of equations (38), (42), and (44) into equation (50) and of equations (39), (43), and (45) into equation (51), respectively, yields a coupled field equation for the simultaneous transport of oxygen and carbon dioxide through soil air-filled pore spaces, namely:

$$\begin{aligned}
& \frac{\partial}{\partial t} [ \{ (\epsilon - \theta) + \theta H_{O_2} + (1 - \epsilon) \omega_{O_2} \} C_{O_2} ] \\
& = \nabla \cdot \left[ (\epsilon - \theta) D_{O_2} \left\{ C_{O_2} \frac{\partial \ln \gamma_{O_2}}{\partial C_{O_2}} + 1 \right\} \frac{\partial C_{O_2}}{\partial z} \right] \\
& \quad - (S_{O_2}^{rt} + S_{O_2}^{mo}) \pm R_e C_{O_2}
\end{aligned} \tag{52}$$

for the oxygen transport, and:

$$\begin{aligned}
& \frac{\partial}{\partial t} [ \{ (\epsilon - \theta) + \theta H_{CO_2} + (1 - \epsilon) \omega_{CO_2} \} C_{CO_2} ] \\
& = \nabla \cdot \left[ (\epsilon - \theta) D_{CO_2} \left\{ C_{CO_2} \frac{\partial \ln \gamma_{CO_2}}{\partial C_{CO_2}} + 1 \right\} \frac{\partial C_{CO_2}}{\partial z} \right] \\
& \quad + S_{CO_2}^{rt} + S_{CO_2}^{mo} \pm R_e C_{CO_2}
\end{aligned} \tag{53}$$

for the carbon dioxide transport, where  $t$  is the time (hr),  $\epsilon$  is the soil porosity ( $\text{cm}^3$  voids  $\text{cm}^{-3}$  soil),  $\theta$  is the soil water content ( $\text{cm}^3 \text{cm}^{-3}$ ),  $H_{O_2}$  and  $H_{CO_2}$  are the inverse Henry's Law constants for oxygen and carbon dioxide, respectively ( $\text{cm}^3$  air  $\text{cm}^{-3}$  water),  $\omega_{O_2}$  and  $\omega_{CO_2}$  are the adsorption coefficients of oxygen and carbon dioxide, respectively ( $\text{cm}^{-1}$ ),  $C_{O_2}$  and  $C_{CO_2}$  are the concentrations of oxygen and carbon dioxide in the air-filled pore spaces of the soil, respectively ( $\mu\text{g cm}^{-3}$  air),  $D_{O_2}$  and  $D_{CO_2}$  are the diffusion coefficients of oxygen and carbon dioxide, respectively ( $\text{cm}^2 \text{hr}^{-1}$ ),  $\gamma_{O_2}$  and  $\gamma_{CO_2}$  are the activity coefficients of oxygen and carbon dioxide, respectively ( $\mu\text{g cm}^{-3}$  air),  $z$  is the soil depth (cm),  $S_{O_2}^{rt}$  and  $S_{O_2}^{mo}$  are the rates of consumption of oxygen by roots and by microorganisms, respectively ( $\mu\text{g cm}^{-3}$  air  $\text{hr}^{-1}$ ),  $S_{CO_2}^{rt}$  and  $S_{CO_2}^{mo}$  are the rates of production of

carbon dioxide by plant roots and by soil microorganisms, respectively ( $\mu\text{g cm}^{-3} \text{ air hr}^{-1}$ ),  $R_e$  is the replacement of air by water due to soil wetting (-) or the replacement of water by air due to soil drying (+), which will either bring oxygen and carbon dioxide out of, or into, the soil ( $\text{cm}^3 \text{ cm}^{-3} \text{ hr}^{-1}$ ).

Equations (52) and (53) are the equations which will be solved by the finite difference method and used for developing the computer program.

The activity coefficients ( $\gamma_{\text{o}_2}$  and  $\gamma_{\text{co}_2}$ ) in equations (52) and (53) need to be further explained. In the case of ideal behaviors of oxygen and carbon dioxide, the activity coefficients are unity, i.e.,  $\gamma_{\text{o}_2} = \gamma_{\text{co}_2} = 1$  (Moore, 1983). When this is so, the transport of oxygen and carbon dioxide through soil pores is independent of each other. In the case of non-ideal behaviors of oxygen and carbon dioxide, the activity coefficients ( $\gamma_{\text{o}_2}$  and  $\gamma_{\text{co}_2}$ ) are functions of oxygen and carbon dioxide concentrations. When this is so, the transport of oxygen and carbon dioxide through soil pores is, therefore, coupled together.

#### Boundary Conditions

Equations (1), (2), (52), and (53) define the coupled fields of water, heat, oxygen, and carbon dioxide, respectively. Boundary conditions must be defined in order to solve these equations.

Boundary Between the Atmosphere and the Soil Slab

Figure 3 shows the interface between the atmosphere and the soil surface. Development of upper boundary conditions for water, heat, oxygen, and carbon dioxide fields is based on the concept shown in the diagram.

Water. By using the "Gaussian Pill Box" concept (Figure 4), the conservation of mass law requires that:

$$\vec{q}_w \cdot (\vec{n} = \hat{z}) + \vec{q}_{\text{rain}} \cdot (\vec{n} = \hat{z}) + \vec{q}_{\text{evap}} \cdot (\vec{n} = -\hat{z}) = 0, \quad (54)$$

where  $\vec{q}_w$  is a vector describing the total water flux at the soil surface (g water cm<sup>-2</sup> hr<sup>-1</sup>),  $\vec{n}$  is the unit vector outward going normal to the simple closed surface,  $\vec{z}$  is the unit vector normal to plane  $z = 0$ , with positive orientation vertically downward,  $\vec{q}_{\text{rain}}$  is a vector describing rainwater flux into the soil (g water cm<sup>-2</sup> hr<sup>-1</sup>), and  $\vec{q}_{\text{evap}}$  is a vector describing evaporation flux or condensation flux of water out of, or into, the soil (g water cm<sup>-2</sup> hr<sup>-1</sup>).

The total water flux vector  $\vec{q}_w$  at the soil surface ( $z = 0$ ) can be defined as:

$$\vec{q}_w \Big|_{z=0} = [\theta_o^* \rho_w \vec{V}_1 + (\epsilon_o - \theta_o^*) \rho_{wv} \vec{V}_v] \Big|_{z=0}, \quad (55)$$

the rainwater flux vector  $\vec{q}_{\text{rain}}$  is written as:

$$\vec{q}_{\text{rain}} = \rho_w \vec{\Phi}_{\text{rain}}, \quad (56)$$

and the evaporation or condensation flux vector  $q_{\text{evap}}$  is given as:

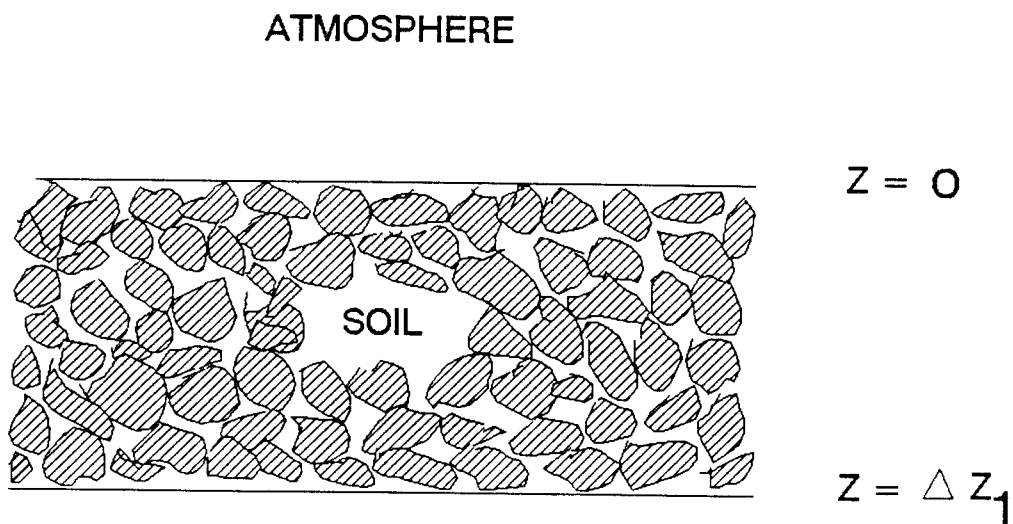


Figure 3. Interface between the atmosphere and the soil surface.

$z$  is soil depth (cm).  $\Delta z_1$  is the depth interval of the first soil layer (cm).

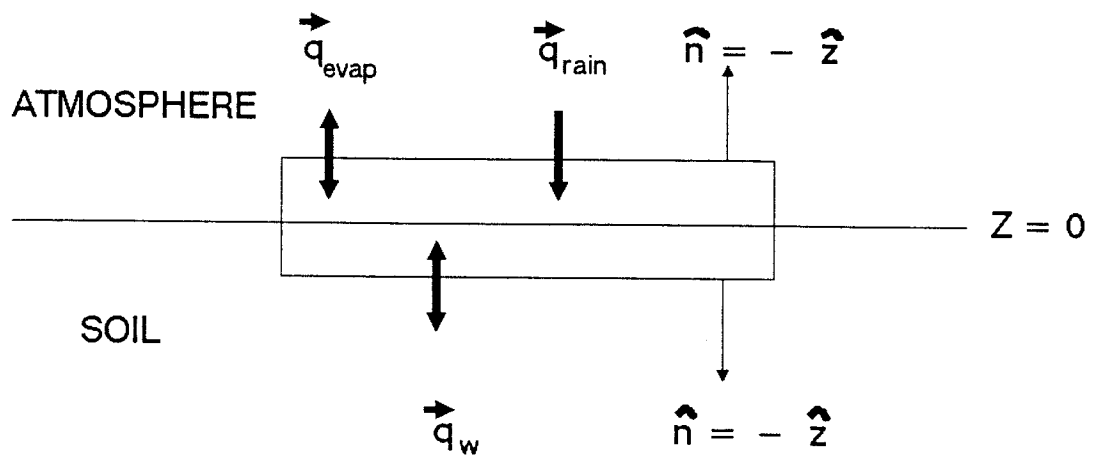


Figure 4. Gaussian Pill Box concept for water flow at the atmosphere-soil interface.

$$\begin{aligned} \vec{q}_{\text{evap}} = & D_{\text{atm}}^* \left[ \frac{d\rho_{\text{wv}}^{\text{sat}}(T_a)}{dT_a} \theta_a \left( \frac{T_o^* - T_a}{\delta z} \right) \right. \\ & \left. + \rho_{\text{wv}}^{\text{sat}}(T_a) \left( \frac{h(\theta_o^*, T_o^*) - \theta_a}{\delta z} \right) \right], \end{aligned} \quad (57)$$

where  $\theta_o^*$  is the water content at the atmosphere-soil interface ( $\text{cm}^3 \text{cm}^{-3}$ ),  $\rho_w$  is the density of water ( $\text{g cm}^{-3}$ ),  $\vec{V}_l$  is the velocity vector of liquid water ( $\text{cm hr}^{-1}$ ),  $\epsilon_o$  is the soil porosity at the atmosphere-soil interface ( $\text{cm}^3 \text{ soil voids cm}^{-3} \text{ soil}$ ),  $\rho_{\text{wv}}$  is the density of water vapor ( $\text{g cm}^{-3}$ ),  $\vec{V}_v$  is the velocity vector of water vapor ( $\text{cm hr}^{-1}$ ),  $\vec{\Phi}_{\text{rain}}$  is the vector describing the rainfall rate ( $\text{cm hr}^{-1}$ ),  $D_{\text{atm}}^*$  is the logistic representation of the boundary layer wind speed dependent coefficient of dispersion of water vapor ( $\text{cm}^2 \text{ hr}^{-1}$ ),  $\rho_{\text{wv}}^{\text{sat}}(T_a)$  is the density of water vapor at saturation at temperature  $T_a$  ( $\text{g vapor cm}^{-3}$ ),  $T_a$  is the temperature in the atmosphere ( $^{\circ}\text{C}$ ),  $\theta_a^*$  is the relative humidity in the atmosphere (dimensionless),  $T_o$  is the temperature at the atmosphere-soil interface ( $^{\circ}\text{C}$ ),  $\delta z$  is the thickness of the boundary layer at the atmosphere-soil interface ( $\text{cm}$ ),  $h(\theta_o^*, T_o^*)$  is the relative humidity at the atmosphere-soil interface (dimensionless).

Substituting equations (55), (56) and (57) into equation (54) yields:

$$\begin{aligned} & \left[ \theta_o^* \rho_w \vec{V}_l + (\epsilon_o - \theta_o^*) \rho_{\text{wv}} \vec{V}_v \right] \Big|_{z=0} \cdot \vec{n} \\ & = (\rho_w \Phi_{\text{rain}}) - D_{\text{atm}}^* \left[ \frac{d\rho_{\text{wv}}^{\text{sat}}(T_a)}{dT_a} \theta_a \left( \frac{T_o^* - T_a}{\delta z} \right) \right. \\ & \quad \left. + \rho_{\text{wv}}^{\text{sat}}(T_a) \left( \frac{h(\theta_o^*, T_o^*) - \theta_a}{\delta z} \right) \right]. \end{aligned} \quad (58)$$

Recall that equations (3) and (4) are written as:

$$\vec{V}_1 = -D_{\leftrightarrow\theta 1} \cdot \nabla\theta - D_{\leftrightarrow T 1} \cdot \nabla T + K_{\leftrightarrow} \cdot \left( \hat{z} - \frac{\partial\psi}{\partial z} \right),$$

$$\vec{V}_v = -D_{\leftrightarrow\theta v} \cdot \nabla\theta - D_{\leftrightarrow T v} \cdot \nabla T + D_{\leftrightarrow\psi} \cdot \left( -\frac{\partial\psi}{\partial z} \right),$$

and  $\hat{n} = \hat{z}$ , substituting  $\vec{V}_1$  and  $\vec{V}_v$  into equation (58) leads to:

$$\begin{aligned} & (\theta_o^* \rho_w D_{\theta 1} + (\epsilon_o - \theta_o^*) \rho_{wv} D_{\theta v}) \left( -\frac{\partial\theta}{\partial z} \right) \Big|_{z=0} \\ & + (\theta_o^* \rho_w D_{T 1} + (\epsilon_o - \theta_o^*) \rho_{wv} D_{T v}) \left( -\frac{\partial T}{\partial z} \right) \Big|_{z=0} \\ & + (\theta_o^* \rho_w K \left( 1 - \frac{\partial\psi}{\partial z} \right) \Big|_{z=0} + (\epsilon_o - \theta_o^*) \rho_{wv} D_{\psi}) \left( -\frac{\partial\psi}{\partial z_1} \right) \Big|_{z=0} \\ & = (\rho_w \Phi_{rain}) - D_{atm}^* \left[ \frac{d\rho_{wv}^{sat}(T_a)}{dT_a} \theta_a \left( \frac{T_o^* - T_a}{\delta z} \right) \right. \\ & \left. + \rho_{wv}^{sat}(T_a) \left( \frac{h(\theta_o^*, T_o^*) - \theta_a}{\delta z} \right) \right], \end{aligned} \quad (59)$$

which is the coupling upper boundary condition for the water field.

Heat. Analogous to the water field, again using the Gaussian Pill Box concept (Figure 5), the conservation of heat requires that:

$$\begin{aligned} & \vec{q}_{heatin} \cdot (\hat{n} = \hat{z}) + \vec{q}_{htevp} \cdot (\hat{n} = -\hat{z}) + \vec{q}_{htswr} \cdot (\hat{n} = \hat{z}) \\ & + \vec{q}_{htssl} \cdot (\hat{n} = \hat{z}) + \vec{q}_{htlwra} \cdot (\hat{n} = \hat{z}) + \vec{q}_{htlwrs} \cdot (\hat{n} = \hat{z}) \\ & + \vec{q}_{hs} \cdot (\hat{n} = \hat{z}) = 0, \end{aligned} \quad (60)$$

where  $\vec{q}_{heatin}$  is a vector describing heat flux into the soil surface via rainwater ( $\text{cal cm}^{-2} \text{hr}^{-1}$ ),  $\vec{q}_{htevp}$  is a vector describing heat flux out of the soil surface due to evaporation or heat flux into the

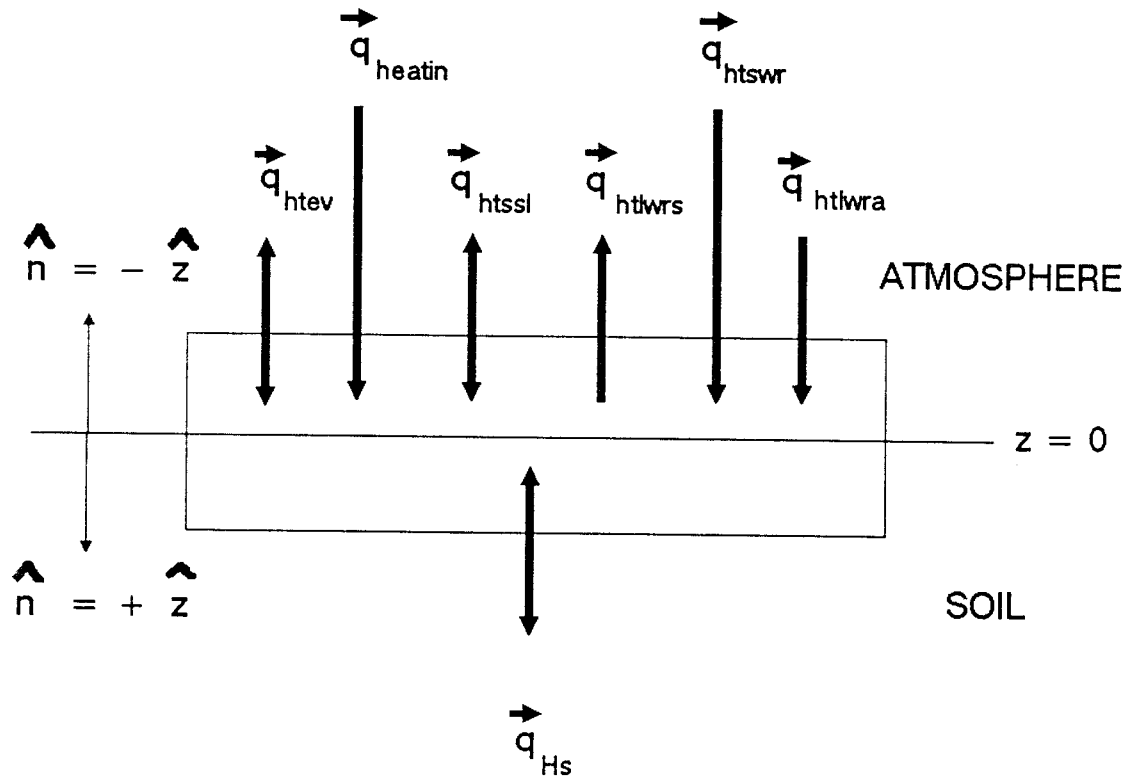


Figure 5. Gaussian Pill Box concept for heat flux at the interface between the atmosphere and the soil surface.

soil surface due to condensation ( $\text{cal cm}^{-2} \text{hr}^{-1}$ ),  $\vec{q}_{htswr}$  is a vector describing heat flux into the soil surface via short wave radiation ( $\text{cal cm}^{-1} \text{hr}^{-1}$ ),  $\vec{q}_{htssl}$  is a vector describing heat flux through the soil surface via sensible heat ( $\text{cal cm}^{-2} \text{hr}^{-1}$ ),  $\vec{q}_{htlwra}$  is a vector describing heat flux into the soil surface via long wave radiation ( $\text{cal cm}^{-2} \text{hr}^{-1}$ ),  $\vec{q}_{htlwrs}$  is a vector describing heat flux out of the soil surface via long wave radiation ( $\text{cal cm}^{-2} \text{hr}^{-1}$ ), and  $\vec{q}_{hs}$  is a vector describing total heat flux into, or out of, the soil surface ( $\text{cal cm}^{-2} \text{hr}^{-1}$ ).

The vectors in equation (60) are defined by (Lindstrom and Piver, 1985):

$$\vec{q}_{heatin} = \rho_w c_w T_{rw} \vec{\Phi}_{rain}, \quad (61)$$

$$\begin{aligned} \vec{q}_{htevp} = D_{atm}^* & \left[ \frac{d\rho_{wv}^{sat}(T_a)}{dT_a} \theta_a \left( \frac{T_o^* - T_a}{\delta z} \right) \right. \\ & \left. + \rho_{wv}^{sat}(T_a) \left( \frac{h(\theta_o^*, T_o^*) - \theta_a}{\delta z} \right) \right] \xi, \end{aligned} \quad (62)$$

$$\begin{aligned} \vec{q}_{htswr} = & [(1 - \epsilon_o)(1 - \alpha_{soil}) + \theta_o^*(1 - \alpha_{water}) \\ & + (\epsilon_o - \theta_o^*)(1 - \alpha_{air})] q_{swr}, \end{aligned} \quad (63)$$

$$\vec{q}_{htssl} = \lambda_{air}^* \frac{(T_o^* - T_a)}{\delta z}, \quad (64)$$

$$\vec{q}_{htlwra} = \epsilon_{air} \sigma T_a^4 \left[ 0.605 + 0.048 \sqrt{e_{H_2O}^{air}(T_a)} \right], \quad (65)$$

$$\begin{aligned} \vec{q}_{htlwrs} = & \sigma (T_o^*)^4 [\epsilon_{soil} (1 - \epsilon_o) \\ & + \epsilon_{water} \theta_o^* + \epsilon_{air} (\epsilon_o - \theta_o^*)] , \end{aligned} \quad (66)$$

$$\vec{q}h_s = (1 - \epsilon_o) \vec{H}_{ss} + \theta_o^* \vec{H}_{sl} + (\epsilon_o - \theta_o^*) \vec{H}_{sv}, \quad (67)$$

with

$$D_{atm}^* = \frac{D_{atm} D_{wvmax}}{D_{atm} + (D_{wvmax} - D_{atm}) \exp(-\beta_{evp} WS)}, \quad (68)$$

$$\lambda_{atm}^* = \frac{\lambda_{air} \lambda_{amax}}{\lambda_{air} + (\lambda_{amax} - \lambda_{air}) \exp(-\beta_{ht} WS)}, \quad (69)$$

and

$$e_{H_2O}^{air}(T_a) = \begin{cases} 4.66894 + 0.24594 T_a \\ \quad + 0.02764 T_a^2 \\ \quad \text{for } T_a \leq 22.5^\circ\text{C} \\ \text{and} \\ 4.66894 + 0.24594 T_a \\ \quad + 0.02764 T_a^2 \\ \quad + 0.02018 T_a^2 \\ \quad \text{for } T_a \geq 22.5^\circ\text{C} . \end{cases} \quad (70)$$

Definitions of variables in equations (61) through (70) are in Appendix I.

Substituting equations (61) through (70) into equation (60) with subsequent combination of variables leads to:

$$\begin{aligned}
& (\theta_o^* c_w \rho_w D_{\theta_1} T_o^* + (\epsilon_o - \theta_o^*) \xi \rho_{wv} D_{\theta_v}) \left(- \frac{\partial \theta}{\partial z}\right) \Big|_{z=0} \\
& + \theta_o^* c_w \rho_w K \left(1 - \frac{\partial \psi}{\partial z}\right) \Big|_{z=0} T_o^* \\
& + (\epsilon_o - \theta_o^*) \xi \rho_{wv} D_{\psi_1} \left(- \frac{\partial \psi}{\partial z}\right) \Big|_{z=0} \\
& + [(1 - \epsilon_o) \lambda_{soil} + \theta_o^* (\lambda_w + c_w \rho_w D_{T_1} T_o^*) \\
& + (\epsilon_o - \theta_o^*) (\lambda_{air} + \xi \rho_{wv} D_{T_v})] \left(- \frac{\partial T}{\partial z}\right) \Big|_{z=0} \\
& = \rho_w c_w T_{rw} \Phi_{rain} \\
& - \xi D_{atm}^* \left[ \frac{d \rho_{wv}^{sat}(T_a)}{dT_a} \theta_a \left(\frac{T_o^* - T_a}{\delta z}\right) \right. \\
& \left. + \rho_{wv}^{sat}(T_a) \left(\frac{h(\theta_o^*, T_o^*) - \theta_a}{\delta z}\right) \right] \\
& - \lambda_{air}^* \frac{(T_o^* - T_a)}{\delta z} \\
& + \epsilon_{air} \sigma T_a^4 [0.605 + 0.048 \sqrt{e_{H_2O}^{air}(T_a)}] \\
& + [(1 - \epsilon_o)(1 - \alpha_{soil}) + \theta_o^*(1 - \alpha_{water}) \\
& + (\epsilon_o - \theta_o^*)(1 - \alpha_{air})] q_{swr} \\
& + \sigma (T_o^*)^4 [\epsilon_{soil} (1 - \epsilon_o) \\
& + \epsilon_{water} \theta_o^* + \epsilon_{air} (\epsilon_o - \theta_o^*)], \tag{71}
\end{aligned}$$

which is the coupling upper boundary conditions for heat field.

Oxygen. For the oxygen field, assume that the concentration of oxygen in the atmosphere-soil interface ( $z = 0$ ) is equal to the concentration of oxygen in the atmosphere. That is:

$$C_{O_2}^* = \text{concentration of oxygen at the atmosphere.} \quad (72)$$

Carbon Dioxide. Analogous to the oxygen field, assume that the concentration of carbon dioxide in the atmosphere-soil interface ( $z = 0$ ) equals the concentration of carbon dioxide in the atmosphere.

That is:

$$C_o^* = \text{concentration of carbon dioxide at the atmosphere.} \quad (73)$$

#### Boundary Between Soil Slab and Impervious Layer

Geologically speaking, the lower boundary conditions existing in soil are commonly: (a) the soil water-table boundary and (b) the soil-impermeable (bed rock) boundary. Mathematically speaking, there are three types of boundary conditions that can be specified for water, heat, oxygen, and carbon dioxide. These are: (a) Dirichlet, which specifies a constant concentration; (b) Neumann, which specifies a concentration gradient; and (c) Cauchy, which is some combination of (a) and (b) and is a mixed condition.

In this dissertation we chose the soil-impermeable lower boundary condition for water, heat, oxygen, and carbon dioxide (Figure 6). The reason for not choosing the soil water-table lower boundary condition is that the position of the water table changes over time in the lower boundary. This means that the position of the lower boundary is not fixed in the soil. In addition, the vertical

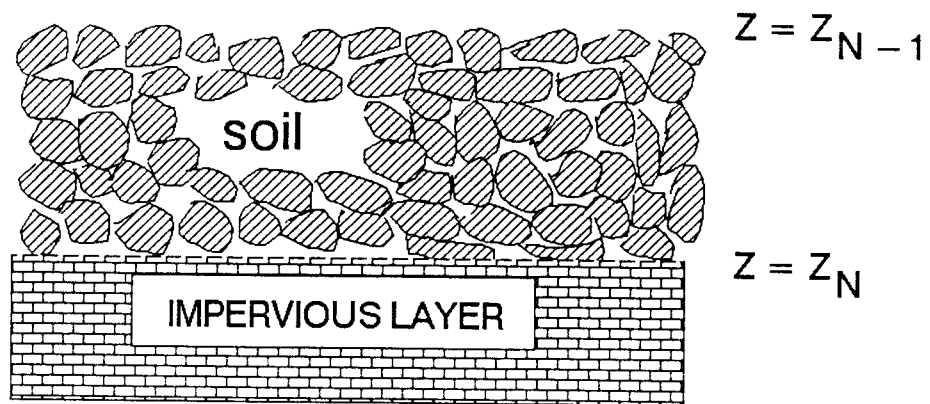


Figure 6. Interface between soil slab and impervious layer.

$z$  is the soil depth (cm).  $N$  is the number of the last node of soil at the interface.  $z_{N-1}$  is the soil depth one layer thick above the interface (cm).  $z_N$  is the soil depth at the interface (cm).

increase (or decrease) of the position of the water table in the soil will cause movement of soil air out of (or into) the soil, which could bring oxygen and carbon dioxide out of (or into) the soil. The changes in the position of the water table will also affect the soil water content and soil temperature at the soil depth close to the water table. Mathematically speaking, this is a mixed lower boundary condition which is difficult to specify. Therefore, we ignore the soil water-table lower boundary in this research. By choosing the soil-impermeable lower boundary condition, there is no change in the position of the lower boundary. The advantage of the choice of this lower boundary condition is that it is easier to specify.

From the mathematical point of view, the lower boundary chosen for oxygen and carbon dioxide here is the no flow boundary (Nuemann boundary condition). In other words, the concentration gradient is specified. That is  $\partial C_{o_2}/\partial z = 0$  and  $\partial C_{co_2}/\partial z = 0$  at  $z = z_n$ , where  $z_n$  is the soil depth at the lower boundary. However, for water and heat field equation, we cannot choose  $\partial \theta/\partial z = 0$  and  $\partial T/\partial z = 0$ . This is because the water and heat field equations include the mass flow or convection. For any transport processes, no flow boundary means the flux equal to zero, i.e.,  $q = 0$  with  $q$  represent the flux. For example, the heat flux through liquid phase of soil in equation equation (11) is:  $\vec{H}_{s1} = -\lambda_w \nabla T + c_w \rho_w \vec{V}_1 T$ . The first part of right hand side is the conduction of heat through liquid phase. The second part of right hand side is the convection of heat through liquid phase. For a no flow boundary condition, this means  $\vec{H}_{s1} = 0$  or  $-\lambda_w \nabla T + c_w \rho_w \vec{V}_1 T = 0$  and is not  $\partial T/\partial z = 0$ . The  $\partial T/\partial z = 0$  can only be true when convection term is neglected from equation (11), i.e.,

$\vec{H}_{s1} = -\lambda_w \nabla T$ . In this case, the no flow boundary is  $\vec{H}_{s1} = -\lambda_w \nabla T = 0$ , which can be simplified to  $\partial T / \partial z = 0$ . Since the water and heat field equations include the mass flow or convection, therefore  $\partial \theta / \partial z = 0$  and  $\partial T / \partial z = 0$  cannot be used. But the oxygen and carbon dioxide field equations do not include the mass flow, the no flow boundary condition can be used, i.e.,  $\partial C_{o_2} / \partial z = 0$  and  $\partial C_{co_2} / \partial z = 0$ . In this simulation, the soil slab was chosen to 150 cm long vertically. In most of the case, changes of soil water content and soil temperature at 150 cm at impervious layer are quite small for a short term simulation (Ghildyal and Tripathi, 1987) and were assumed to be constant, i.e.,  $\theta = \text{constant}$  and  $T = \text{constant}$ . Although the no flow boundary and a mix boundary conditions can be specified, the reason for not choosing these boundary conditions are to avoid the complications for the lower boundary.

#### Summary of Field Equations and Their Boundary Conditions

The water, heat, oxygen, and carbon dioxide field equations and their boundary conditions, discussed above, are summarized in Tables 2 and 3. These field equations, and their respective boundary conditions, will be used to examine the simultaneous transport of water, heat, oxygen, and carbon dioxide in unsaturated soils.

Table 2. Field equations for water, heat, oxygen, and carbon dioxide transport in unsaturated soil.

Water

$$\frac{\partial}{\partial t} [\rho_w \theta + \rho_{wv}^{sat} (T)h(\epsilon - \theta)] = -\nabla \cdot [\rho_w \theta \vec{V}_w + \rho_{wv} (\epsilon - \theta) \vec{V}_v] .$$

Heat

$$\begin{aligned} \frac{\partial}{\partial t} [(1 - \epsilon)c_{solid} \rho_{solid} T + (\epsilon - \theta)c_{air} \rho_{air} T + \theta c_w \rho_w T] \\ = -\nabla \cdot [(1 - \epsilon)H_{ss} + \theta H_{sl} + (\epsilon - \theta)H_{sv}] . \end{aligned}$$

Oxygen

$$\begin{aligned} \frac{\partial}{\partial t} [ \{ (\epsilon - \theta) + \theta H_{o_2} + (1 - \epsilon)\omega_{o_2} \} C_{o_2} ] \\ = \nabla \cdot \left[ (\epsilon - \theta) D_{o_2} \left\{ C_{o_2} \frac{\partial \ln \gamma_{o_2}}{\partial C_{o_2}} + 1 \right\} \frac{\partial C_{o_2}}{\partial z} \right] \\ - (S_{o_2}^{rt} + S_{o_2}^{mo}) \pm R_e C_{o_2} . \end{aligned}$$

Carbon Dioxide

$$\begin{aligned} \frac{\partial}{\partial t} [ \{ (\epsilon - \theta) + \theta H_{co_2} + (1 - \epsilon)\omega_{co_2} \} C_{co_2} ] \\ = \nabla \cdot \left[ (\epsilon - \theta) D_{co_2} \left\{ C_{co_2} \frac{\partial \ln \gamma_{co_2}}{\partial C_{co_2}} + 1 \right\} \frac{\partial C_{co_2}}{\partial z} \right] \\ + S_{co_2}^{rt} + S_{co_2}^{mo} \pm R_e C_{co_2} . \end{aligned}$$

Table 3. Boundary conditions at: (1) the interface between the atmosphere and the soil surface and (2) at impervious layer.

---

Interface Between the Atmosphere and Soil Surface

Water

$$\begin{aligned}
 & (\theta_o^* \rho_w D_{\theta_1} + (\epsilon_o - \theta_o^*) \rho_{wv} D_{\theta_v}) \left( - \frac{\partial \theta}{\partial z} \right) \Big|_{z=0} \\
 & + (\theta_o^* \rho_w D_{T_1} + (\epsilon_o - \theta_o^*) \rho_{wv} D_{T_v}) \left( - \frac{\partial T}{\partial z} \right) \Big|_{z=0} \\
 & + (\theta_o^* \rho_w K \left( 1 - \frac{\partial \psi}{\partial z} \right) \Big|_{z=0} + (\epsilon_o - \theta_o^*) \rho_{wv} D_{\psi_1}) \left( - \frac{\partial \psi}{\partial z} \right) \Big|_{z=0} \\
 & = (\rho_w \Phi_{\text{rain}}) - D_{\text{atm}}^* \left[ \frac{d\rho_{wv}^{\text{sat}}(T_a)}{dT_a} \theta_a \left( \frac{T_o^* - T_a}{\delta z} \right) \right. \\
 & \left. + \rho_{wv}^{\text{sat}}(T_a) \left( \frac{h(\theta_o^*, T_o^*) - \theta_a}{\delta z} \right) \right] .
 \end{aligned}$$

Heat

$$\begin{aligned}
 & (\theta_o^* c_w \rho_w D_{\theta_1} T_o^* + (\epsilon_o - \theta_o^*) \xi \rho_{wv} D_{\theta_v}) \left( - \frac{\partial \theta}{\partial z} \right) \Big|_{z=0} \\
 & + \theta_o^* c_w \rho_w K \left( 1 - \frac{\partial \psi}{\partial z} \right) \Big|_{z=0} T_o^* \\
 & + (\epsilon_o - \theta_o^*) \xi \rho_{wv} D_{\psi_1} \left( - \frac{\partial \psi}{\partial z} \right) \Big|_{z=0} \\
 & + [(1 - \epsilon_o) \lambda_{\text{solid}} + \theta_o^* (\lambda_w + c_w \rho_w D_{T_1} T_o^*) \\
 & + (\epsilon_o - \theta_o^*) (\lambda_{\text{air}} + \xi \rho_{wv} D_{T_v})] \left( - \frac{\partial T}{\partial z} \right) \Big|_{z=0} \\
 & = \rho_w c_w T_{rw} \Phi_{\text{rain}}
 \end{aligned}$$

Table 3. Continued.

$$\begin{aligned}
& - \xi D_{\text{atm}}^* \left[ \frac{d\rho_{\text{wv}}^{\text{sat}}(T_a)}{dT_a} \theta_a \left( \frac{T_o^* - T_a}{\delta z} \right) \right. \\
& \left. + \rho_{\text{wv}}^{\text{sat}}(T_a) \left( \frac{h(\theta_o^*, T_o^*) - \theta_a}{\delta z} \right) \right] \\
& - \lambda_{\text{air}}^* \frac{(T_o - T_a^*)}{\delta z} \\
& + \epsilon_{\text{air}} \sigma T_a^4 \left[ 0.605 + 0.048 \sqrt{e_{\text{H}_2\text{O}}^{\text{air}}(T_a)} \right] \\
& + [(1 - \epsilon_o)(1 - \alpha_{\text{soil}}) + \theta_o(1 - \alpha_{\text{water}}^*)] \\
& + (\epsilon_o - \theta_o^*)(1 - \alpha_{\text{air}})] q_{\text{swr}} \\
& + \sigma (T_o^*)^4 [\epsilon_{\text{soil}}(1 - \epsilon_o) \\
& + \epsilon_{\text{water}} \theta_o^* + \epsilon_{\text{air}} (\epsilon_o - \theta_o^*)] .
\end{aligned}$$

Oxygen

$C_{\text{O}_2}^*$  = concentration of oxygen at the atmosphere.

Carbon dioxide

$C_{\text{CO}_2}^*$  = concentration of carbon dioxide at the atmosphere.

Table 3. Continued.

---

Boundary at Impervious LayerWater

$$\left. \frac{\partial \theta}{\partial z} \right|_{z=z_n} = 0 .$$

Heat

$$\left. \frac{\partial T}{\partial z} \right|_{z=z_n} = 0 .$$

Oxygen

$$\left. \frac{\partial C_{O_2}}{\partial z} \right|_{z=z_n} = 0 .$$

Carbon dioxide

$$\left. \frac{\partial C_{CO_2}}{\partial z} \right|_{z=z_n} = 0 .$$

---

## SOLUTION METHOD FOR THE FOUR FIELD EQUATIONS

Since the solution of the oxygen and carbon dioxide field equations [equations (52) and (53)] requires a point wise, in space and time, knowledge of the water and heat distributions, the water and heat field equations [equations (1) and (2)] must be solved prior to solving the oxygen and carbon dioxide field equations. The finite difference method is used to solve these field equations. The water and heat field equations are solved by using the implicit method, while the oxygen and carbon dioxide field equations are solved by using the explicit method.

Solution of the Water Field Equation

Substitution of equations (3) and (4) into the water field equation (1) obtains:

$$\begin{aligned}
 & \frac{\partial}{\partial t} [\rho_w \theta + \rho_{wv}^{sat}(T) h(\theta, T) (\epsilon - \theta)] \\
 & = \nabla \cdot \left[ \left\{ \theta \rho_w D_{w\theta_1} + (\epsilon - \theta) \rho_{wv} D_{w\theta_v} \right\} \frac{\partial \theta}{\partial z} \right. \\
 & \quad \left. + \left\{ \theta \rho_w D_{wT_1} + (\epsilon - \theta) \rho_{wv} D_{wT_v} \right\} \frac{\partial T}{\partial z} \right. \\
 & \quad \left. - \theta \rho_w \left( 1 - \frac{\partial \psi}{\partial z} \right) K + (\epsilon - \theta) \rho_{wv} D_{w\psi_z} \frac{\partial \psi}{\partial z} \right] . \tag{74}
 \end{aligned}$$

Before approximating equation (74), the diffusivity and conductivity functions are defined as:

$$D_{\theta}^w = \theta \rho_w D_{\theta_1} + (\epsilon - \theta) \rho_{wv} D_{\theta_v}, \quad (75)$$

$$D_T^w = \theta \rho_w D_{T_1} + (\epsilon - \theta) \rho_{wv} D_{T_v}, \quad (76)$$

$$\begin{aligned} \kappa &= \theta \rho_w \left(1 - \frac{\partial \psi}{\partial z}\right) K - (\epsilon - \theta) \rho_{wv} D_{\psi_z} \frac{\partial \psi}{\partial z} \\ &= \rho_w \theta \left[ \left( K - \left( K - \frac{\rho_{wv}}{\rho_w} D_{\psi_z} \right) \frac{\partial \psi}{\partial z} \right) - \rho_{wv} \epsilon D_{\psi_z} \frac{\partial \psi}{\partial z} \right]. \end{aligned} \quad (77)$$

Putting equations (75), (76), and (77) into equation (74)

yields:

$$\begin{aligned} \frac{\partial}{\partial t} \left[ \rho_w \theta + \rho_{wv}^{\text{sat}}(T) h(\theta, T) (\epsilon - \theta) \right] \\ = \nabla \cdot \left[ D_{\theta}^w \frac{\partial \theta}{\partial z} + D_T^w \frac{\partial T}{\partial z} - \kappa \right]. \end{aligned} \quad (78)$$

Following Varga's (1962) method of approximation, integration of both sides of equation (78) over the rectangular subregion of space and time  $\left[ [z_{i-1/2}, z_{i+1/2}] \times [t_n, t_{n+1}] \right]$  yields:

$$\begin{aligned} \int_{z_{i-1/2}}^{z_{i+1/2}} \left[ \rho_w \theta + \rho_{wv}^{\text{sat}}(T) h(\theta, T) (\epsilon - \theta) \right]_{t_{n+1}} dz \\ - \int_{z_{i-1/2}}^{z_{i+1/2}} \left[ \rho_w \theta + \rho_{wv}^{\text{sat}}(T) h(\theta, T) (\epsilon - \theta) \right]_{t_n} dz \\ = \int_{t_n}^{t_{n+1}} \left[ D_{\theta}^w \frac{\partial \theta}{\partial z} + D_T^w \frac{\partial T}{\partial z} - \kappa \right]_{z_{i+1/2}} dt \\ - \int_{t_n}^{t_{n+1}} \left[ D_{\theta}^w \frac{\partial \theta}{\partial z} + D_T^w \frac{\partial T}{\partial z} - \kappa \right]_{z_{i-1/2}} dt. \end{aligned} \quad (79)$$

The space derivatives of equation (79) are approximated by standard space centered three point different quotients. Figure 7 shows the closure of the common space-time cylinder on which the mesh of model points has been superimposed. Figure 8 shows the space positions of all the field nodal points. The time integral of equation (79) is approximated by choosing a classic backward Euler method of quadrature. The finite difference formulations over the sub-internal  $[z_{i-1/2}, z_{i+1/2}]$  for  $i = 1, 2, \dots, N_z - 1$ , which are used for solving the equation (79) are listed in Appendix II. Applying these formulations to equation (79) obtains:

$$\begin{aligned}
& \left[ \frac{\Delta z_i + \Delta z_{i+1}}{2} \right] \left[ (\rho_w \theta + \rho_{wv}^{\text{sat}}(T) h(\theta, T) (\epsilon - \theta))_i^{n+1} \right. \\
& \quad \left. - (\rho_w \theta + \rho_{wv}^{\text{sat}}(T) h(\theta, T) (\epsilon - \theta))_i^n \right] \\
& = \Delta t \left[ D_{\theta}^{w(n+1)} \frac{\theta_{i+1}^{n+1} - \theta_i^{n+1}}{\Delta z_{i+1}} + D_T^{w(n+1)} \frac{T_{i+1}^{n+1} - T_i^{n+1}}{\Delta z_{i+1}} - \kappa_{i+1/2}^{n+1} \right] \\
& \quad - \Delta t \left[ D_{\theta}^{w(n+1)} \frac{\theta_i^{n+1} - \theta_{i-1}^{n+1}}{\Delta z_i} + D_T^{w(n+1)} \frac{T_i^{n+1} - T_{i-1}^{n+1}}{\Delta z_i} - \kappa_{i-1/2}^{n+1} \right] . \quad (80)
\end{aligned}$$

Substitution of  $D_{\theta}^w$ ,  $D_T^w$ , and  $\kappa$  from equations (75), (76), and (77), respectively, into equation (80), and multiplication of both sides of equation (80) by  $2/(\Delta z_i + \Delta z_{i+1})$ , and rearrangement of terms into a common coefficient yields:

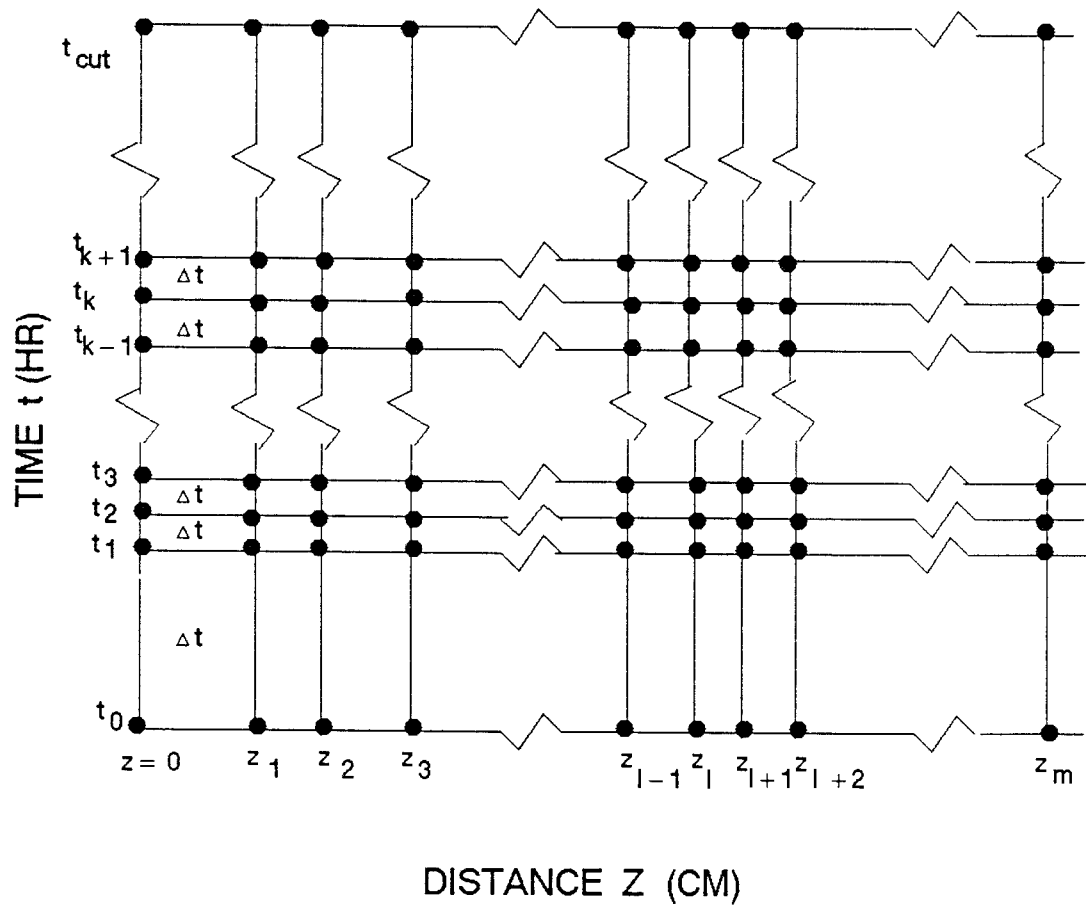


Figure 7. Closure of the space-time cylinder with lattice of nodal points superimposed on it.

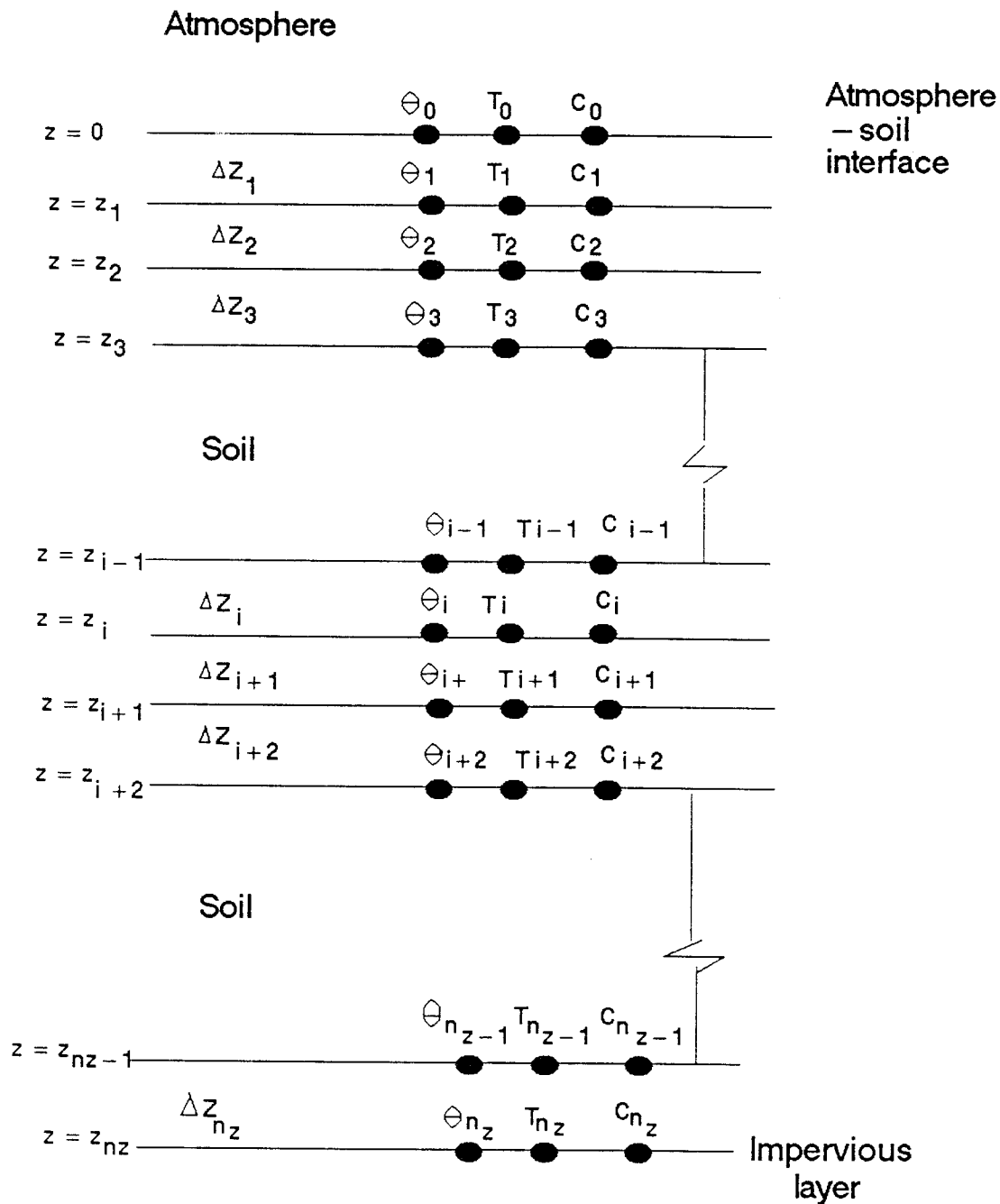


Figure 8. Schematic diagram of space positions of all the field nodal points.  $\theta$  is the water content ( $\text{cm}^3 \text{cm}^{-3}$ ).  $T$  is the temperature ( $^{\circ}\text{C}$ ).  $C$  is the concentration of oxygen or carbon dioxide ( $\mu\text{g cm}^{-3}$  air).

$$\begin{aligned}
& - \frac{2\Delta t}{\Delta z_i + \Delta z_{i+1}} \left[ \frac{[\theta \rho_w D_{\theta 1} + \epsilon - \theta) \rho_{wv} D_{\theta v}]_{i-1/2}^{n+1}}{\Delta z_i} \right. \\
& \quad \left. + \frac{[\rho_w K(1 - \frac{\partial \psi}{\partial z}) + \rho_{wv} D_{\psi z} \frac{\partial \psi}{\partial z}]_{i-1/2}^{n+1}}{2} \right] \theta_{i-1}^{n+1} \\
& + \left[ \frac{2\Delta t}{\Delta z_i + \Delta z_{i+1}} \left\{ \frac{[\theta \rho_w D_{\theta 1} + (\epsilon - \theta) \rho_{wv} D_{\theta v}]_{i+1/2}^{n+1}}{\Delta z_{i+1}} \right. \right. \\
& \quad + \frac{[\rho_w K(1 - \frac{\partial \psi}{\partial z}) + \rho_{wv} D_{\psi z} \frac{\partial \psi}{\partial z}]_{i+1/2}^{n+1}}{2} \\
& \quad + \frac{[\theta \rho_w D_{\theta 1} + (\epsilon - \theta) \rho_{wv} D_{\theta v}]_{i-1/2}^{n+1}}{\Delta z_i} \\
& \quad \left. - \frac{[\rho_w K(1 - \frac{\partial \psi}{\partial z}) + \rho_{wv} D_{\psi z} \frac{\partial \psi}{\partial z}]_{i-1/2}^{n+1}}{2} \right\} \\
& \quad \left. + [\rho_w + \frac{(\epsilon - \theta) \rho_{wv}^{sat} h(\theta, T)}{\theta}]_i^{n+1} \right] \theta_i^{n+1} \\
& - \frac{2\Delta t}{\Delta z_i + \Delta z_{i+1}} \left[ \frac{[\theta \rho_w D_{\theta 1} + (\epsilon - \theta) \rho_{wv} D_{\theta v}]_{i+1/2}^{n+1}}{\Delta z_{i+1}} \right. \\
& \quad \left. - \frac{[\rho_w K(1 - \frac{\partial \psi}{\partial z}) + \rho_{wv} D_{\psi z} \frac{\partial \psi}{\partial z}]_{i+1/2}^{n+1}}{2} \right] \theta_{i+1}^{n+1}
\end{aligned}$$

$$\begin{aligned}
& - \frac{2\Delta t}{\Delta z_i + \Delta z_{i+1}} \left[ \frac{[\theta \rho_w D_{T_1} + (\epsilon - \theta)\rho_{wv} D_{T_v}]_{i-1/2}^{n+1}}{\Delta z_i} T_{i-1}^{n+1} \right. \\
& \quad - \left. \left\{ \frac{[\theta \rho_w D_{T_1} + (\epsilon - \theta)\rho_{wv} D_{T_v}]_{i+1/2}^{n+1}}{\Delta z_{i+1}} \right. \right. \\
& \quad \quad \left. \left. + \frac{[\theta \rho_w D_{T_1} + (\epsilon - \theta)\rho_{wv} D_{T_v}]_{i-1/2}^{n+1}}{\Delta z_i} \right\} T_i^{n+1} \right. \\
& \quad \left. + \frac{[\theta \rho_w D_{T_1} + (\epsilon - \theta)\rho_{wv} D_{T_v}]_{i+1/2}^{n+1}}{\Delta z_{i+1}} T_{i+1}^{n+1} \right] \\
& = - \frac{2\Delta t}{\Delta z_i + \Delta z_{i+1}} \left[ - (\rho_{wv} \epsilon D_{\psi_z})_{i+1/2}^{n+1} \frac{\partial \psi}{\partial z} + (\rho_{wv} \epsilon D_{\psi_z})_{i-1/2}^{n+1} \frac{\partial \psi}{\partial z} \right] \\
& \quad + \left[ \left[ \rho_w + \frac{(\epsilon - \theta) \rho_{wv}^{sat} h(\theta, T)}{\theta} \right]_i^n \right] \theta_i^n . \tag{81}
\end{aligned}$$

Equation (81) is the form used setting up the computer program for solving the water field problem.

### Solution of the Heat Field Equation

Substitution of equations (10), (11), and (12) into the heat field equation (2) yields:

$$\begin{aligned}
& \frac{\partial}{\partial t} \left[ (1 - \epsilon) c_{solid} \rho_{solid} T + (\epsilon - \theta) c_{air} \rho_{air} T + \theta c_w \rho_w T \right] \\
& = \frac{\partial}{\partial z} \left[ \left\{ (1 - \epsilon) \lambda_{solid} + \theta (\lambda_w + c_w \rho_w T D_{T_1}) \right. \right.
\end{aligned}$$

$$\begin{aligned}
& + (\epsilon - \theta)(\xi \rho_{wv} D_{T_v} + \lambda_{air}) \left\} \left( \frac{\partial T}{\partial z} \right) \right. \\
& + \left\{ \theta c_w \rho_w^T D_{\theta_1} + (\epsilon - \theta) \xi \rho_{wv} D_{\theta_v} \right\} \left( \frac{\partial \theta}{\partial z} \right) \\
& - \left. \left\{ \theta c_w \rho_w^T K \left( 1 - \frac{\partial \psi}{\partial z} \right) - (\epsilon - \theta) \xi \rho_{wv} D_{\psi_z} \left( \frac{\partial \psi}{\partial z} \right) \right\} \right] . \quad (82)
\end{aligned}$$

Analogous to the water field, define the following heat diffusivity and conductivity functions:

$$D_{\theta}^H = \theta c_w \rho_w^T D_{\theta_1} + (\epsilon - \theta) \xi \rho_{wv} D_{\theta_v} , \quad (83)$$

$$\begin{aligned}
D_T^H &= (1 - \epsilon) \lambda_{solid} + \theta (\lambda_w + c_w \rho_w^T D_{T_1}) \\
&+ (\epsilon - \theta)(\xi \rho_{wv} D_{T_v} + \lambda_{air}) , \quad (84)
\end{aligned}$$

and

$$\dot{n} = \theta c_w \rho_w^T K \left( 1 - \frac{\partial \psi}{\partial z} \right) - (\epsilon - \theta) \xi \rho_{wv} D_{\psi_z} \left( \frac{\partial \psi}{\partial z} \right) . \quad (85)$$

Putting equations (83), (84), and (85) into equation (82) yields:

$$\begin{aligned}
& \frac{\partial}{\partial \tau} \left[ (1 - \epsilon) c_{solid} \rho_{solid}^T + (\epsilon - \theta) c_{air} \rho_{air}^T + \theta c_w \rho_w^T \right] \\
& = \frac{\partial}{\partial z} \left[ D_{\theta}^H \left( \frac{\partial \theta}{\partial z} \right) + D_T^H \left( \frac{\partial T}{\partial z} \right) - \dot{n} \right] . \quad (86)
\end{aligned}$$

Following again Varga's (1962) method of approximation, integrating both sides of equation (86) over the rectangular subregion of space and time  $\left[ [z_{i-1/2}, z_{i+1/2}] \times [t_n, t_{n+1}] \right]$  yields:

$$\begin{aligned}
& \int_{z_{i-1/2}}^{z_{i+1/2}} \left[ (1 - \epsilon) c_{\text{solid}} \rho_{\text{solid}} T \right. \\
& \quad \left. + (\epsilon - \theta) c_{\text{air}} \rho_{\text{air}} T + \theta c_w \rho_w T \right]_{t_{n+1}} dz \\
& - \int_{z_{i-1/2}}^{z_{i+1/2}} \left[ (1 - \epsilon) c_{\text{solid}} \rho_{\text{solid}} T \right. \\
& \quad \left. + (\epsilon - \theta) c_{\text{air}} \rho_{\text{air}} T + \theta c_w \rho_w T \right]_{t_n} dz \\
& = \int_{t_n}^{t_{n+1}} \left[ D_{\theta}^H \left( \frac{\partial \theta}{\partial z} \right) + D_T^H \left( \frac{\partial T}{\partial z} \right) - \dot{h} \right]_{z_{i+1/2}} dt \\
& - \int_{t_n}^{t_{n+1}} \left[ D_{\theta}^H \left( \frac{\partial \theta}{\partial z} \right) + D_T^H \left( \frac{\partial T}{\partial z} \right) - \dot{h} \right]_{z_{i-1/2}} dt \tag{87}
\end{aligned}$$

Applying the formulations in Appendix II to equation (87)

obtains:

$$\begin{aligned}
& \left( \frac{\Delta z_i + \Delta z_{i+1}}{2} \right) \left[ \left\{ (1 - \epsilon) c_{\text{solid}} \rho_{\text{solid}} T + (\epsilon - \theta) c_{\text{air}} \rho_{\text{air}} T \right. \right. \\
& \quad \left. \left. + \theta c_w \rho_w T \right\}_i^{n+1} \right. \\
& - \left. \left\{ (1 - \epsilon) c_{\text{solid}} \rho_{\text{solid}} T + (\epsilon - \theta) c_{\text{air}} \rho_{\text{air}} T \right. \right. \\
& \quad \left. \left. + \theta c_w \rho_w T \right\}_i^n \right] \\
& = \Delta t \left[ D_{\theta}^{H(n+1)} \frac{\theta_{i+1}^{n+1} - \theta_i^{n+1}}{\Delta z_{i+1}} + D_T^{H(n+1)} \frac{T_{i+1}^{n+1} - T_i^{n+1}}{\Delta z_{i+1}} + \dot{h}_{i+1/2}^{n+1} \right] \\
& - \Delta t \left[ D_{\theta}^{H(n+1)} \frac{\theta_{i+1}^{n+1} - \theta_i^{n+1}}{\Delta z_i} + D_T^{H(n+1)} \frac{T_{i+1}^{n+1} - T_i^{n+1}}{\Delta z_i} + \dot{h}_{i-1/2}^{n+1} \right] \tag{88}
\end{aligned}$$

Substitution of  $D_{\theta}^H$ ,  $D_T^H$ , and  $\kappa$  from equations (83), (84), and (85), respectively, into equation (88), and multiplication of both sides of equation (85) by  $2/(\Delta z_i + \Delta z_{i+1})$ , and rearrangement of terms into common coefficients yields:

$$\begin{aligned}
& - \frac{2\Delta t}{\Delta z_i + \Delta z_{i+1}} \left[ \frac{[\theta c_w \rho_w^T D_{\theta 1} + (\epsilon - \theta)(\xi \rho_{wv} D_{\theta v})]_{i-1/2}^{n+1}}{\Delta z_i} \theta_{i-1}^{n+1} \right. \\
& \quad - \left\{ \frac{[\theta c_w^c \rho_w^T D_{\theta 1} + (\epsilon - \theta)(\xi \rho_{wv} D_{\theta v})]_{i+1/2}^{n+1}}{\Delta z_{i+1}} \right. \\
& \quad \left. + \frac{[\theta c_w \rho_w^T D_{\theta 1} + (\epsilon - \theta)(\xi \rho_{wv} D_{\theta v})]_{i-1/2}^{n+1}}{\Delta z_i} \right\} \theta_i^{n+1} \\
& \quad \left. + \frac{[\theta c_w \rho_w^T D_{\theta 1} + (\epsilon - \theta)(\xi \rho_{wv} D_{\theta v})]_{i+1/2}^{n+1}}{\Delta z_{i+1}} \theta_{i+1}^{n+1} \right] \\
& - \frac{2\Delta t}{\Delta z_i + \Delta z_{i+1}} \left[ \frac{[(1 - \epsilon)\lambda_{\text{solid}} + \theta(\lambda_w + c_w \rho_w^T D_{T1})]_{i-1/2}^{n+1}}{\Delta z_i} \right. \\
& \quad + \frac{[(\epsilon - \theta)(\xi \rho_{wv} D_{Tv} + \lambda_{\text{air}})]_{i-1/2}^{n+1}}{\Delta z_i} \\
& \quad \left. + \frac{(\theta c_w \rho_w K (1 - \frac{\partial \psi}{\partial z}))_{i-1/2}^{n+1}}{2} \right] T_{i-1}^{n+1} \\
& + \left[ \left\{ (1 - \epsilon) c_{\text{solid}} \rho_{\text{solid}} + (\epsilon - \theta) c_{\text{air}} \rho_{\text{air}} + \theta \rho_w c_w \right\}_i^{n+1} \right. \\
& \quad \left. + \frac{2\Delta t}{\Delta z_i + \Delta z_{i+1}} \left\{ \frac{[(1 - \epsilon)\lambda_{\text{solid}} + \theta(\lambda_w + c_w \rho_w^T D_{T1})]_{i+1/2}^{n+1}}{\Delta z_{i+1}} \right. \right.
\end{aligned}$$

$$\begin{aligned}
& + \frac{[(\epsilon - \theta)(\xi \rho_{wv} D_{Tv} + \lambda_{air})]_{l+1/2}^{n+1}}{\Delta z_{i+1}} \\
& + \frac{[(1 - \epsilon)\lambda_{solid} + \theta(\lambda_w + c_w \rho_w T D_{T1})]_{i-1/2}^{n+1}}{\Delta z_i} \\
& + \frac{[(\epsilon - \theta)(\xi \rho_{wv} D_{Tv} + \lambda_{air})]_{l-1/2}^{n+1}}{\Delta z_i} \\
& + \frac{[\theta c_w \rho_w K (1 - \frac{\partial \psi}{\partial z})]_{i+1/2}^{n+1}}{2} \\
& - \left. \frac{[\theta c_w \rho_w K (1 - \frac{\partial \psi}{\partial z})]_{i-1/2}^{n+1}}{2} \right\} T_i^{n+1} \\
& - \frac{2\Delta t}{\Delta z_i + \Delta z_{i+1}} \left[ \frac{[(1 - \epsilon)\lambda_{solid} + \theta(\lambda_w + c_w \rho_w T D_{T1})]_{i+1/2}^{n+1}}{\Delta z_{i+1}} \right. \\
& \quad + \frac{[(\epsilon - \theta)(\xi \rho_{wv} D_{Tv} + \lambda_{air})]_{l+1/2}^{n+1}}{\Delta z_{i+1}} \\
& \quad \left. - \frac{[\theta c_w \rho_w K (1 - \frac{\partial \psi}{\partial z})]_{i+1/2}^{n+1}}{2} \right] T_{i+1}^{n+1} \\
& = \left[ (1 - \epsilon) c_{solid} \rho_{solid} + (\epsilon - \theta) c_{air} \rho_{air} + \theta \rho_w c_w \right]_i T_i^n \\
& \quad + \frac{2 \Delta t}{\Delta z_i + \Delta z_{i+1}} \left[ [(\epsilon - \theta) \xi \rho_{wv} D_{\psi_z} (\frac{\partial \psi}{\partial z})]_{i+1/2}^{n+1} \right. \\
& \quad \quad \left. - [(\epsilon - \theta) \xi \rho_{wv} D_{\psi_z} (\frac{\partial \psi}{\partial z})]_{i-1/2}^{n+1} \right] . \tag{89}
\end{aligned}$$

Equation (89) is the form used for setting up the computer program for solving the heat field equation.

Solution of the Oxygen Field Equation

The Euler Finite Difference Method was used to solve the oxygen field equation (52) by an explicit approximation scheme. Integrating equation (52) over time obtains:

$$\begin{aligned}
 & \left[ \left\{ (\epsilon - \theta) + \theta H_{O_2} + (1 - \epsilon) \omega_{O_2} \right\} C_{O_2} \right]_i^{n+1} \\
 & - \left[ \left\{ (\epsilon - \theta) + \theta H_{O_2} + (1 - \epsilon) \omega_{O_2} \right\} C_{O_2} \right]_i^n \\
 & = \int_{t_n}^{t_{n+1}} \frac{\partial}{\partial z} \left[ (\epsilon - \theta) D_{O_2} \left( C_{O_2} \frac{\partial \ln \gamma_{O_2}}{\partial C_{O_2}} + 1 \right) \frac{\partial C_{O_2}}{\partial z} \right]_i^n dt \\
 & - \int_{t_n}^{t_{n+1}} [S_{O_2}^{rt} + S_{CO_2}^{mo}]_i^n dt \\
 & \pm \int_{t_n}^{t_{n+1}} [R_e C_{O_2}]_i^n dt . \tag{90}
 \end{aligned}$$

Using the finite difference approximations shown in Appendix II gives:

$$\begin{aligned}
 & \frac{\partial}{\partial z} \left[ (\epsilon - \theta) D_{O_2} \left( C_{O_2} \frac{\partial \ln \gamma_{O_2}}{\partial C_{O_2}} + 1 \right) \frac{\partial C_{O_2}}{\partial z} \right] \\
 & = \frac{2}{\Delta z_{i-1} + \Delta z_i} \left[ \left\{ (\epsilon - \theta) D_{O_2} \left( C_{O_2} \frac{\partial \ln \gamma_{O_2}}{\partial C_{O_2}} + 1 \right) \frac{\partial C_{O_2}}{\partial z} \right\}_{i+1/2}^n \right. \\
 & \quad \left. - \left\{ (\epsilon - \theta) D_{O_2} \left( C_{O_2} \frac{\partial \ln \gamma_{O_2}}{\partial C_{O_2}} + 1 \right) \frac{\partial C_{O_2}}{\partial z} \right\}_{i-1/2}^n \right] . \tag{91}
 \end{aligned}$$

Substituting equation (91) into equation (90) and simplifying the result yields:

$$\begin{aligned}
 C_{o_2 i}^{n+1} = & \frac{1}{[(\epsilon - \theta) + \theta H_{o_2} + (1 - \epsilon)\omega_{o_2}]_i^{n+1}} \\
 & \left[ \left\{ (\epsilon - \theta) + \theta H_{o_2} + (1 - \epsilon)\omega_{o_2} \right\}_i^n C_{o_2 i}^n \right. \\
 & + \frac{2\Delta t}{\Delta z_{i-1} + \Delta z_i} \left[ \left[ \left( \frac{(\epsilon - \theta)_{i+1}^n + (\epsilon - \theta)_i^n}{2} \right) \left( \frac{D_{o_2 i+1}^n + D_{o_2 i}^n}{2} \right) \right. \right. \\
 & \left. \left\{ \left( \frac{C_{o_2 i+1}^n + C_{o_2 i}^n}{2} \right) \left( \frac{\ln \gamma_{o_2 i+1}^n - \ln \gamma_{o_2 i}^n}{C_{o_2 i+1}^n - C_{o_2 i}^n} \right) + 1 \right\} \right. \\
 & \left. \left. \left( \frac{C_{o_2 i+1}^n - C_{o_2 i}^n}{\Delta z_i} \right) \right] \right. \\
 & - \left[ \left( \frac{(\epsilon - \theta)_i^n + (\epsilon - \theta)_{i-1}^n}{2} \right) \left( \frac{D_{o_2 i}^n + D_{o_2 i-1}^n}{2} \right) \right. \\
 & \left. \left\{ \left( \frac{C_{o_2 i}^n + C_{o_2 i-1}^n}{2} \right) \left( \frac{\ln \gamma_{o_2 i}^n - \ln \gamma_{o_2 i-1}^n}{C_{o_2 i}^n - C_{o_2 i-1}^n} \right) + 1 \right\} \right. \\
 & \left. \left. \left( \frac{C_{o_2 i}^n - C_{o_2 i-1}^n}{\Delta z_{i-1}} \right) \right] \right] \pm \Delta t R_{e_i}^n C_{o_2 i}^n - \Delta t (S_{o_2}^{rt} + S_{co_2}^{mo})_i^n . \quad (92)
 \end{aligned}$$

Equation (92) is the form used for setting up computer program for solving the oxygen field equation.

### Solution of the Carbon Dioxide Field Equation

Analogous to the solution of oxygen field equation, Euler's Finite Difference Method was used to solve the carbon dioxide field equation (53) by the explicit approximation scheme. Integrating equation (53) over time obtains:

$$\begin{aligned}
 & \left[ \left\{ (\epsilon - \theta) + \theta H_{\text{CO}_2} + (1 - \epsilon) \omega_{\text{CO}_2} \right\} C_{\text{CO}_2} \right]_i^{n+1} \\
 & - \left[ \left\{ (\epsilon - \theta) + \theta H_{\text{CO}_2} + (1 - \epsilon) \omega_{\text{CO}_2} \right\} C_{\text{CO}_2} \right]_i^n \\
 = & \int_{t_n}^{t_{n+1}} \frac{\partial}{\partial z} \left[ (\epsilon - \theta) D_{\text{CO}_2} \left( C_{\text{CO}_2} \frac{\partial \ln \gamma_{\text{CO}_2}}{\partial C_{\text{CO}_2}} + 1 \right) \frac{\partial C_{\text{CO}_2}}{\partial z} \right]_i^n dt \\
 & - \int_{t_n}^{t_{n+1}} [S_{\text{CO}_2}^{\text{rt}} + S_{\text{CO}_2}^{\text{mo}}]_i^n dt \\
 & \pm \int_{t_n}^{t_{n+1}} [R_{\text{CO}_2} C_{\text{CO}_2}]_i^n dt. \tag{93}
 \end{aligned}$$

Using the finite difference approximations shown in Appendix II yields,

$$\begin{aligned}
& \frac{\partial}{\partial z} \left[ (\epsilon - \theta) D_{\text{CO}_2} \left( C_{\text{CO}_2} \frac{\partial \ln \gamma_{\text{CO}_2}}{\partial C_{\text{CO}_2}} + 1 \right) \frac{\partial C_{\text{CO}_2}}{\partial z} \right] \\
&= \frac{2}{\Delta z_{i-1} + \Delta z_i} \left[ \left\{ (\epsilon - \theta) D_{\text{CO}_2} \left( C_{\text{CO}_2} \frac{\partial \ln \gamma_{\text{CO}_2}}{\partial C_{\text{CO}_2}} + 1 \right) \frac{\partial C_{\text{CO}_2}}{\partial z} \right\}_{i+1/2}^n \right. \\
&\quad \left. - \left\{ (\epsilon - \theta) D_{\text{CO}_2} \left( C_{\text{CO}_2} \frac{\partial \ln \gamma_{\text{CO}_2}}{\partial C_{\text{CO}_2}} + 1 \right) \frac{\partial C_{\text{CO}_2}}{\partial z} \right\}_{i-1/2}^n \right]. \quad (94)
\end{aligned}$$

Substituting equation (94) into equation (93) and simplifying the result yields:

$$\begin{aligned}
C_{\text{CO}_2 i}^{n+1} &= \frac{1}{[(\epsilon - \theta) + \theta H^{\text{CO}_2} + (1 - \epsilon) \omega^{\text{CO}_2}]_i^{n+1}} \\
&\quad \left[ \left\{ (\epsilon - \theta) + \theta H^{\text{CO}_2} + (1 - \epsilon) \omega^{\text{CO}_2} \right\}_i^n C_{\text{CO}_2 i}^n \right. \\
&+ \frac{2\Delta t}{\Delta z_{i-1} + \Delta z_i} \left[ \left( \frac{(\epsilon - \theta)_{i+1}^n + (\epsilon - \theta)_i^n}{2} \right) \left( \frac{D_{\text{CO}_2 i+1}^n + D_{\text{CO}_2 i}^n}{2} \right) \right. \\
&\quad \left. \left\{ \left( \frac{C_{\text{CO}_2 i+1}^n + C_{\text{CO}_2 i}^n}{2} \right) \left( \frac{\ln \gamma_{\text{CO}_2 i+1}^n - \ln \gamma_{\text{CO}_2 i}^n}{C_{\text{CO}_2 i+1}^n - C_{\text{CO}_2 i}^n} \right) + 1 \right\} \right. \\
&\quad \left. \left. \left( \frac{C_{\text{CO}_2 i+1}^n - C_{\text{CO}_2 i}^n}{\Delta z_i} \right) \right] \right]
\end{aligned}$$

$$\begin{aligned}
& - \left[ \left( \frac{(\epsilon - \theta)_i^n + (\epsilon - \theta)_{i-1}^n}{2} \right) \left( \frac{D_{\text{co}_2 i}^n + D_{\text{co}_2 i-1}^n}{2} \right) \right. \\
& \left. \left\{ \left( \frac{C_{\text{co}_2 i}^n + C_{\text{co}_2 i-1}^n}{2} \right) \left( \frac{\ln \gamma_{\text{co}_2 i}^n - \ln \gamma_{\text{co}_2 i-1}^n}{C_{\text{co}_2 i}^n - C_{\text{co}_2 i-1}^n} \right) + 1 \right\} \right. \\
& \left. \left. \left( \frac{C_{\text{co}_2 i}^n - C_{\text{co}_2 i-1}^n}{\Delta z_{i-1}} \right) \right\} \right] \pm \Delta t R_e^n C_{\text{co}_2 i}^n - \Delta t (S_{\text{co}_2}^{\text{rt}} + S_{\text{co}_2}^{\text{mo}})^n \quad (95)
\end{aligned}$$

Equation (95) is the form used for setting up the computer program for solving the carbon dioxide field equation.

### Solution of the Boundary Conditions

The boundary conditions for water, heat, oxygen and carbon dioxide at the soil-impervious interface,  $z = z_n$ , were the zero flux boundary (Table 3). The boundary conditions for oxygen and carbon dioxide at the atmosphere-soil interface were prescribed.

However, the boundary conditions for water and heat at the atmosphere-soil interface are fully dynamically coupled to the environmental driving variables by the mixed type boundary conditions given by equations (59) and (71). The two boundary conditions are nonlinear and tightly coupled that we cannot explicitly solve for  $\theta(0, t)$ ,  $\left. \frac{\partial \theta}{\partial z} \right|_{z=0}$ ,  $T(0, t)$ , and  $\left. \frac{\partial T}{\partial z} \right|_{z=0}$ . The water and heat field

values as functions of time must be found by solving, iteratively, an implicit system of equations (Lindstrom and Piver 1985). By moving the right hand side of equations (59) and (71) to the left hand side, respectively, and setting them equal to the functions of  $g_1(\theta_o^*, T_o^*)$  and  $g_2(\theta_o^*, T_o^*)$ , respectively, we have:

$$\begin{aligned}
g_1(\theta_o^*, T_o^*) = & (\theta_o^* \rho_w D_{\theta_1} + (\epsilon_o - \theta_o^*) \rho_{wv} D_{\theta_v}) \left( - \frac{\partial \theta}{\partial z} \right) \Big|_{z=0} \\
& + (\theta_o^* \rho_w D_{T_1} + (\epsilon_o - \theta_o^*) \rho_{wv} D_{T_v}) \left( - \frac{\partial T}{\partial z} \right) \Big|_{z=0} \\
& + (\theta_o^* \rho_w K (1 - \frac{\partial \psi}{\partial z}) \Big|_{z=0} + (\epsilon_o - \theta_o^*) \rho_{wv} D_{\psi}) \left( - \frac{\partial \psi}{\partial z} \right) \Big|_{z=0} \\
& - (\rho_w \Phi_{rain}) - D_{atm}^* \left[ \frac{d\rho_{wv}^{sat}(T_a)}{dT_a} \theta_a \frac{(T_o^* - T_a)}{\delta z} \right. \\
& \left. + \rho_{wv}^{sat}(T_a) \left( \frac{h(\theta_o^*, T_o^*) - \theta_a}{\delta z} \right) \right] = 0, \tag{96}
\end{aligned}$$

and

$$\begin{aligned}
g_2(\theta_o^*, T_o^*) = & (\theta_o^* c_w \rho_w D_{\theta_1} T_o^* + (\epsilon_o - \theta_o^*) \xi \rho_{wv} D_{\theta_v}) \left( - \frac{\partial \theta}{\partial z} \right) \Big|_{z=0} \\
& + [\theta_o^* c_w \rho_w K (1 - \frac{\partial \psi}{\partial z})] \Big|_{z=0} T_o^* \\
& + (\epsilon_o - \theta_o^*) \xi \rho_{wv} D_{\psi_1} \left( - \frac{\partial \psi}{\partial z} \right) \Big|_{z=0} \\
& + [(1 - \epsilon_o) \lambda_{solid} + \theta_o^* (\lambda_w + c_w \rho_w D_{T_1} T_o^*) \\
& + (\epsilon_o - \theta_o^*) (\lambda_{air} + \xi \rho_{wv} D_{T_v})] \left( - \frac{\partial T}{\partial z} \right) \Big|_{z=0} \\
& - \rho_w c_w T_{rw} \Phi_{rain}
\end{aligned}$$

$$\begin{aligned}
& + \xi D_{\text{atm}}^* \left[ \frac{d\rho_{\text{wv}}^{\text{sat}}(T_a)}{dT_a} \theta_a \frac{(T_o^* - T_a)}{\delta z} \right. \\
& \left. - \rho_{\text{wv}}^{\text{sat}}(T_a) \left( \frac{h(\theta_o^*, T_o^*) - \theta_a}{\delta z} \right) \right] \\
& + \lambda_{\text{air}}^* \frac{(T_o^* - T_a)}{\delta z} \\
& - \epsilon_{\text{air}} \sigma T_a^4 \left[ 0.605 + 0.048 \sqrt{e_{\text{H}_2\text{O}}^{\text{air}}(T_a)} \right] \\
& - [(1 - \epsilon_o)(1 - \alpha_{\text{soil}}) + \theta_o^*(1 - \alpha_{\text{water}})] \\
& + (\epsilon_o - \theta_o^*)(1 - \alpha_{\text{air}})] q_{\text{swr}} \\
& - \sigma (T_o^*)^4 [\epsilon_{\text{soil}} (1 - \epsilon_o) \\
& + \epsilon_{\text{water}} \theta_p^* + \epsilon_{\text{air}} (\epsilon_o - \theta_o^*)] = 0 . \tag{97}
\end{aligned}$$

By setting up a Newton-Raphson Iterative scheme, both  $\theta_o^*$  and  $T_o^*$  in equations (96) and (97) can be found by iteration. Applying the multivariate form of the Taylor Series to equations (96) and (97) and retaining the linear terms obtains:

$$g_1^{[u]} + (\theta_o^{*[u+1]} - \theta_o^{*[u]}) \left( \frac{\partial g_1}{\partial \theta_o} \right) \Big|_u + (T_o^{*[u+1]} - T_o^{*[u]}) \left( \frac{\partial g_1}{\partial T_o} \right) \Big|_u \doteq 0, \tag{98}$$

$$g_2^{[u]} + (\theta_o^{*[u+1]} - \theta_o^{*[u]}) \left( \frac{\partial g_2}{\partial \theta_o} \right) \Big|_u + (T_o^{*[u+1]} - T_o^{*[u]}) \left( \frac{\partial g_2}{\partial T_o} \right) \Big|_u \doteq 0, \tag{99}$$

where  $u$  is the iteration index, i.e.,  $u = 0, 1, 2, \dots$ . Solving for  $\theta_o^{*[u+1]}$  and  $T_o^{*[u+1]}$  from equations (97) and (98) obtains:

$$\theta_o^{*[u+1]} = \theta_o^{*[u]} + \frac{g_2^{[u]} \frac{\partial g_1}{\partial T_o^*} \Big|_u - g_1^{[u]} \frac{\partial g_2}{\partial T_o^*} \Big|_u}{\frac{\partial g_1}{\partial \theta_o^*} \Big|_u - \frac{\partial g_2}{\partial T_o^*} \Big|_u - \frac{\partial g_1}{\partial T_o^*} \Big|_u - \frac{\partial g_2}{\partial \theta_o^*} \Big|_u}, \quad (100)$$

$$T_o^{*[u+1]} = T_o^{*[u]} + \frac{g_1^{[u]} \frac{\partial g_2}{\partial \theta_o^*} \Big|_u - g_2^{[u]} \frac{\partial g_1}{\partial \theta_o^*} \Big|_u}{\frac{\partial g_1}{\partial T_o^*} \Big|_u - \frac{\partial g_2}{\partial \theta_o^*} \Big|_u - \frac{\partial g_1}{\partial \theta_o^*} \Big|_u - \frac{\partial g_2}{\partial T_o^*} \Big|_u}. \quad (101)$$

These two equations are placed into equations (112) and (113) for the atmosphere-soil slab boundary in the "Iteration Solution Algorithm for Four Field Equations" section. Unfortunately, at this time we cannot establish how broad a range of the  $(\theta_o^*, T_o^*)$  ordered pair is available (Lindstrom and Piver, 1985). Numerical experiment has shown that we may run into divergence if  $\theta_o^*$  is allowed to go much below 0.1. The range of  $T_o^*$  seems to be quite broad.

Applying difference quotients to the first partial derivatives of  $g_1$  and  $g_2$  in equations (100) and (101) yields:

$$\frac{\partial g_1}{\partial \theta_o^*} = \frac{g_1(\theta_o^* + \delta\theta_o^*, T_o^*) - g_1(\theta_o^*, T_o^*)}{\delta\theta_o^*}, \quad (102)$$

$$\frac{\partial g_1}{\partial T_o^*} = \frac{g_1(\theta_o^*, T_o^* + \delta T_o^*) - g_1(\theta_o^*, T_o^*)}{\delta T_o^*}, \quad (103)$$

$$\frac{\partial g_2}{\partial \theta_o^*} = \frac{g_2(\theta_o^* + \delta\theta_o^*, T_o^*) - g_2(\theta_o^*, T_o^*)}{\delta\theta_o^*}, \quad (104)$$

$$\frac{\partial g_2}{\partial T_o^*} = \frac{g_2 (\theta_o^*, T_o^* + \delta T_o^*) - g_2 (\theta_o^*, T_o^*)}{\delta T_o^*}, \quad (105)$$

where numerical experimentation has shown that  $\delta\theta_o^* = 0.0001$  and  $\delta T_o^* = 0.001$  seem to work well (Lindstrom and Piver, 1985). For approximating the gradients  $\partial\theta/\partial z$  and  $\partial T/\partial z$  at the soil surface ( $z = 0$ ), use:

$$-\frac{\partial\theta}{\partial z} \Big|_{z=0} = \frac{\theta_o^* - \theta_1^*}{\Delta z_1}, \quad (106)$$

and

$$-\frac{\partial T}{\partial z} \Big|_{z=0} = \frac{T_o^* - T_1^*}{\Delta z_1} \quad (107)$$

where  $\Delta z_1$ , the "thickness" of the first soil layer, which is the interval between surface node 0 and the first interior node 1, is kept small for accuracy purposes.

#### Stability Consideration

Water and heat field equations (81) and (89) can be written as a coupled system of nonlinear equations as follows:

$$(B_M - \Delta t \Sigma_1) \vec{\theta}^{n+1} - \Delta t \Sigma_2 \vec{T}^{n+1} = B_M \vec{\theta}^n + \Omega_M^{\rightarrow *n+1} \quad (108)$$

$$-\Delta t \Sigma_3 \vec{\theta}^{n+1} + (B_H - \Delta t \Sigma_4) \vec{T}^{n+1} = B_H \vec{T}^n + \Omega_H^{\rightarrow *n+1} \quad (109)$$

where the  $N_{z-1} \times N_{z-1}$  tridiagonal arrays  $B_M - \Delta t \Sigma_1$ ,  $-\Delta t \Sigma_2$ ,  $B_M$ ,

-  $\Delta t \Sigma_3$ ,  $B_H - \Delta t \Sigma_4$ ,  $B_H$ , and vectors  $\vec{\Omega}_M^{*n+1}$ ,  $\vec{\Omega}_H^{*n+1}$  are defined by equations (81) and (89). Careful observations of the arrays, and the respective elements which make up these arrays, leads to the following conclusions (Lindstrom and Piver, 1985):

- (1) They are all tridiagonal;
- (2) They all have strongly connected, and directed graphs, which implies that they are all irreducible (Varga, 1962);
- (3) They are all weakly diagonally dominant for realistic values of  $\theta$  and  $T$ ;
- (4) The diagonal entries are strictly negative;
- (5) The off-diagonal entries are strictly nonnegative;
- (6) In view of (2) and (3) above, they are all nonsingular for each  $(\theta, T)$  fixed (Varga, 1962);
- (7) In view of (2) to (5), the eigenvalues of each array have negative real parts (Varga, 1962), which implies system stability for all source vectors bounded and measurable over  $(t_0, +\infty)$ .

Therefore, the matrix is a convergence matrix.

Since the oxygen and carbon dioxide field equations (92) and (95) were computed by explicit scheme, an additional stability criterion arises. According to Cheng et al. (1984) and Lindstrom et al. (1989), the sufficient condition for the stability of equation (81) is:

$$\left[ \left\{ (\epsilon - \theta) + \theta H_{O_2} + (1 - \epsilon)\omega_{O_2} \right\}_i^n - \frac{2\Delta t}{\Delta z_{i-1} + \Delta z_i} \left\{ \frac{(\epsilon - \theta)_{i+1}^n + (\epsilon - \theta)_i^n}{2} \left( \frac{D_{O_2 i+1}^n + D_{O_2 i}^n}{2} \right) \right. \right. \\
+ \left. \left. \frac{(\epsilon - \theta)_i^n + (\epsilon - \theta)_{i-1}^n}{2} \left( \frac{D_{O_2 i}^n + D_{O_2 i-1}^n}{2} \right) \right\} \right. \\
\left. - \Delta t (Re)_i^n - \Delta t (S_{O_2}^{rt} + S_{O_2}^{mo})_i^n \right] \geq 0, \quad (110)$$

and the sufficient condition for the stability of equation (89) is

$$\left[ \left\{ (\epsilon - \theta) + \theta H_{CO_2} + (1 - \epsilon)\omega_{CO_2} \right\}_i^n - \frac{2\Delta t}{\Delta z_{i-1} + \Delta z_i} \left\{ \frac{(\epsilon - \theta)_{i+1}^n + (\epsilon - \theta)_i^n}{2} \left( \frac{D_{CO_2 i+1}^n + D_{CO_2 i}^n}{2} \right) \right. \right. \\
+ \left. \left. \frac{(\epsilon - \theta)_i^n + (\epsilon - \theta)_{i-1}^n}{2} \left( \frac{D_{CO_2 i}^n + D_{CO_2 i-1}^n}{2} \right) \right\} \right. \\
\left. - \Delta t (Re)_i^n \right] \geq 0. \quad (111)$$

Iteration Solution Algorithm for the Four Field Equations

Rearrangement of equations (108) and (109), with  $u$  as the iteration index on the variables obtains:

$$(B_M^{[u]} - \Delta t \Sigma_1^{[u]}) \vec{\theta}_{[u+1]}^{n+1} = B_M \vec{\theta}^{n+1} + \Delta t \Sigma_2^{[u]} \vec{T}_{[u]}^{n+1} + \vec{\Omega}_{M[u]}^{*n+1}, \quad (112)$$

$$(B_H^{[u]} - \Delta t \Sigma_4^{[u]}) \vec{T}_{[u+1]}^{n+1} = B_H \vec{T}^{n+1} + \Delta t \Sigma_3^{[u]} \vec{\theta}_{[u]}^{n+1} + \vec{\Omega}_{H[u]}^{*n+1}. \quad (113)$$

The algorithm steps for solving these two equations are as follows:

- Step 1. The iteration index,  $u$ , is set equal to zero, and initial guesses for vectors  $\vec{\theta}_{[0]}^{n+1}$  and  $\vec{T}_{[0]}^{n+1}$  are made. With this information, all four matrices of  $\Sigma_1^{[0]}$ ,  $\Sigma_2^{[0]}$ ,  $\Sigma_3^{[0]}$ , and  $\Sigma_4^{[0]}$  are calculated. The vectors,  $\vec{\Omega}_{H[0]}^{*n+1}$  and  $\vec{\Omega}_{M[0]}^{*n+1}$ , are also calculated.
- Step 2. Equation (112) is used to find  $\vec{\theta}_{[1]}^{n+1}$ . The actual solution is easily found by using the Thomas algorithm.
- Step 3.  $\vec{\theta}_{[1]}^{n+1}$  is now substituted into equation (113), and  $\vec{T}_{[1]}^{n+1}$  found by applying the Thomas algorithm.
- Step 4. A component-by-component check is made on the differences of the absolute values of the vector components between the initial guesses of  $\theta$  and  $T$  and new calculated values of  $\theta$  and  $T$ , in order to get accurate results. That is, for each  $K$ ,  $K = 1, 2, 3, \dots, N_z - 1$ , checks

$$\left| \left| \theta_{[1]}^{n+1} \right| - \left| \theta_{[0]}^{n+1} \right| \right| < e_1$$

and

$$\left| \left| T_{[1]}^{n+1} \right| - \left| T_{[0]}^{n+1} \right| \right| < e_2$$

are made, where  $e_1$  and  $e_2$  are the tolerance error values for the water and heat fields, respectively. If any components violate these tests, go to Step 4a. If all components satisfy the tests, go to Step 5.

Step 4a. Reset all the initial guesses to be  $\vec{\theta}_{[1]}^{n+1}$  and  $\vec{T}_{[1]}^{n+1}$  and go to Step 1 with  $u$  updated by 1.

Step 5. When satisfied with the convergence test, the values of  $\vec{\theta}_{[1]}^{n+1}$  and  $\vec{T}_{[1]}^{n+1}$  are obtained by making  $\theta_{[1]}^{n+1}$  and  $T_{[1]}^{n+1}$  equivalent to the smallest values of  $\vec{\theta}_{[1]}^{n+1}$  and  $\vec{T}_{[1]}^{n+1}$ .

Rearranging equations (112) and (113) yields:

$$\begin{aligned} \vec{\theta}_{[u+1]}^{n+1} = & (B_M^{[u]} - \Delta t \Sigma_1^{[u]})^{-1} (B_M \vec{\theta}^n + \Delta t \Sigma_2^{[u]} \vec{T}_{[u]}^{n+1} \\ & + \vec{\Omega}_{M[u]}^{*n+1}) \end{aligned} \quad (114)$$

and

$$\begin{aligned} \vec{T}_{[u+1]}^{n+1} = & (B_H^{[u]} - \Delta t \Sigma_4^{[u]})^{-1} (B_H \vec{T}^n + \Delta t \Sigma_3^{[u]} \vec{\theta}_{[u]}^{n+1} \\ & + \vec{\Omega}_{H[u]}^{*n+1}) \end{aligned} \quad (115)$$

Substituting  $\vec{\theta}_{[u+1]}^{n+1}$  from equation (114) into equation (115) obtains:

$$\begin{aligned}
\vec{T}_{[n+1]}^{n+1} &= (B_H^{[u]} - \Delta t \Sigma_4^{[u]})^{-1} (B_H \vec{T}^n + \vec{\Omega}_{H[u]}^{*n+1}) \\
&+ (B_H^{[u]} - \Delta t \Sigma_4^{[u]})^{-1} (\Delta t \Sigma_3^{[u]}) (B_M^{[u]} - \Delta t \Sigma_1^{[u]})^{-1} \\
&\quad (B_M \vec{\theta}^n + \vec{\Omega}_{M[u]}^{*n+1}) \\
&+ (B_H^{[u]} - \Delta t \Sigma_4^{[u]})^{-1} (\Delta t \Sigma_3^{[u]}) (B_M^{[u]} - \Delta t \Sigma_1^{[u]})^{-1} \\
&\quad (\Delta t \Sigma_2^{[u]}) \vec{T}_{[u]}^{n+1}, \tag{116}
\end{aligned}$$

which is an iterative system of the form:

$$\vec{T}_{[u+1]}^{n+1} = M \vec{T}_{[u]}^{n+1} + \vec{Y}, \tag{117}$$

where the iterative matrix M (Varga, 1962) is defined to be:

$$M = (B_H^{[u]} - \Delta t \Sigma_4^{[u]})^{-1} (\Delta t \Sigma_3^{[u]}) (B_M^{[u]} - \Delta t \Sigma_1^{[u]})^{-1} (\Delta t \Sigma_2^{[u]}), \tag{118}$$

and the constant source vector  $\vec{Y}$  is defined as:

$$\vec{Y} = (B_H^{[u]} - \Delta t \Sigma_4^{[u]})^{-1} \left[ B_H \vec{T}^n + \vec{\Omega}_{H[u]}^{*n+1} + (\Delta t \Sigma_3^{[u]}) \right. \\
\left. (B_M^{[r]} - \Delta t \Sigma_1^{[r]})^{-1} (B_M \vec{\theta}^n + \vec{\Omega}_{M[r]}^{*n+1}) \right]. \tag{119}$$

Since the special radius  $\rho(M) < 1$  for all  $\Delta t > 0$ , the iterative matrix M, is a convergent matrix (Varga, 1962; Lindstrom and Piver, 1985).

Therefore,  $\vec{T}_{[u+1]}^{n+1}$  can be calculated from equation (115).

Step 6. After calculating  $\vec{T}_{[u+1]}^{n+1}$  and  $\vec{\theta}_{[u+1]}^{n+1}$ ,  $\vec{C}_{o_2}^{n+1}$  and  $\vec{C}_{co_2}^{n+1}$  will be calculated using equations (92) and (95), respectively. No iteration is needed for this explicit scheme.

- Step 7. The distributions of  $\bar{\theta}^{n+1}$ ,  $\bar{T}^{n+1}$ ,  $\bar{C}_{o_2}^{n+1}$  and  $\bar{C}_{co_2}^{n+1}$  are now ready to be stored, or printed out.
- Step 8. Either stop computing by a check on total running time, or reset all initial guesses to  $\bar{\theta}^{n+1}$ ,  $\bar{T}^{n+1}$ ,  $\bar{C}_{o_2}^{n+1}$ ,  $\bar{C}_{co_2}^{n+1}$  and go to Step 1 to start again.

DESCRIPTION OF EXAMPLES TO BE SOLVED AND DISCUSSION  
OF SIMULATION RESULTS

The purpose of this chapter was to apply the mathematical model developed in previous chapters, as well as the corresponding computer program, to examine the simultaneous transport of water, heat, oxygen, and carbon dioxide through soils under different climatic, soil physical, and biological conditions.

Example 1

Statement of the Problem

An example was chosen for the evaluation of the simultaneous transport of water, heat, oxygen, and carbon dioxide through Indio loam soil during infiltration, redistribution, and evaporation of soil water, starting with an initially low water content. Effects of oxygen consumption and carbon dioxide production by plant roots and soil microorganisms on the transport of oxygen and carbon dioxide was also evaluated. Evaluations were made with computer simulations. Using these simulations, conditions which lead to deficiency of oxygen and build up of carbon dioxide in the root zone could be evaluated.

## Input Parameters

Input parameters for running the simulation were obtained from several sources. Attempts were made to obtain realistic values for the input parameters. These included soil depth, simulation time, weather conditions, soil physical properties, biological activities, the coefficients of activity, diffusion, and adsorption of oxygen and carbon dioxide, and the initial distributions of water, temperature, oxygen, and carbon dioxide in the soil profile. All these input parameters are discussed in detail in the following sections.

Simulation Soil Depth and Simulation Time. The model for the simultaneous transport of water, heat, oxygen, and carbon dioxide through the soil will be solved simultaneously in this example for a soil depth of 150 cm with each depth interval  $\Delta z = 1$  cm, except for the first layer where  $\Delta z$  is small ( $\Delta z = 0.1$ ), in order to obtain better results. Numerical experimentation by Lindstrom and Piver (1985) showed that convergence is easily achieved with  $\Delta z = 1$  cm and that a good mass balance and heat balance are obtained with the numerical error less than  $0.001 \text{ cm}^3 \text{ cm}^{-3}$  for water content and less than  $0.01^\circ\text{C}$  for temperature. Although a smaller depth interval would obtain more accurate results, a price paid is a longer computing times and a need for more computer memory. A simulation time of five days (120 hours) was chosen with two 12-hour periods (totally 24 hours) of infiltration of rain water and the rest of the time for redistribution and evaporation. The first 12-hour period of rainfall started at 0 hours and ended at 12 hours on the first day. The second 12-hour period of rainfall started from 76 hours and ended at

88 hours on the fourth day. Time step chosen for in this example is  $\Delta t = 0.0005$  hour. Such a small time step is required to meet the convergence criteria for solving the oxygen and carbon dioxide field equations by the explicit scheme. Although a smaller time step would be better for getting more accurate results, this would require longer computing times and a need for more computer memory.

Weather Conditions. In order to solve the water and heat field equations, the weather conditions needed to be prescribed as input parameters. The climatic parameters used for this simulation were extracted from the weather conditions that occurred during October in Western Oregon (Redmond, 1988).

(1) Air temperature. When the incoming solar radiation reaches the earth, it heats the air in the atmosphere. The intensity of solar radiation changes over time (Figure 9). The air temperature which depends on the intensity of solar radiation, therefore, is also a function of time (Figure 10). When simulating the heat transport through the soil, the air temperature at the atmosphere-soil interface, which is an upper boundary condition, must be known. The effect of air temperature on soil temperature is not negligible. In many cases, the daily course of the air temperature can be characterized by a Fourier Series (Lindstrom and Piver, 1985):

$$T_{\text{air}}(t) = \bar{T} + \sum_{n=1}^N [A_{\text{temp}}(n) \cos(\omega_{1n} t) + B_{\text{temp}}(n) \sin(\omega_{1n} t)], \quad (120)$$

where  $T_{\text{air}}(t)$  is the air temperature ( $^{\circ}\text{C}$ ) at time  $t$ ,  $\bar{T}$  is the mean air temperature ( $^{\circ}\text{C}$ ),  $N$  is the number of the Fourier frequency,  $A_{\text{temp}}(n)$  and  $B_{\text{temp}}(n)$  are the temperature coefficients,  $\omega_{1n}$  is the  $n^{\text{th}}$  temperature Fourier frequency, and  $t$  is the time (hr). The input

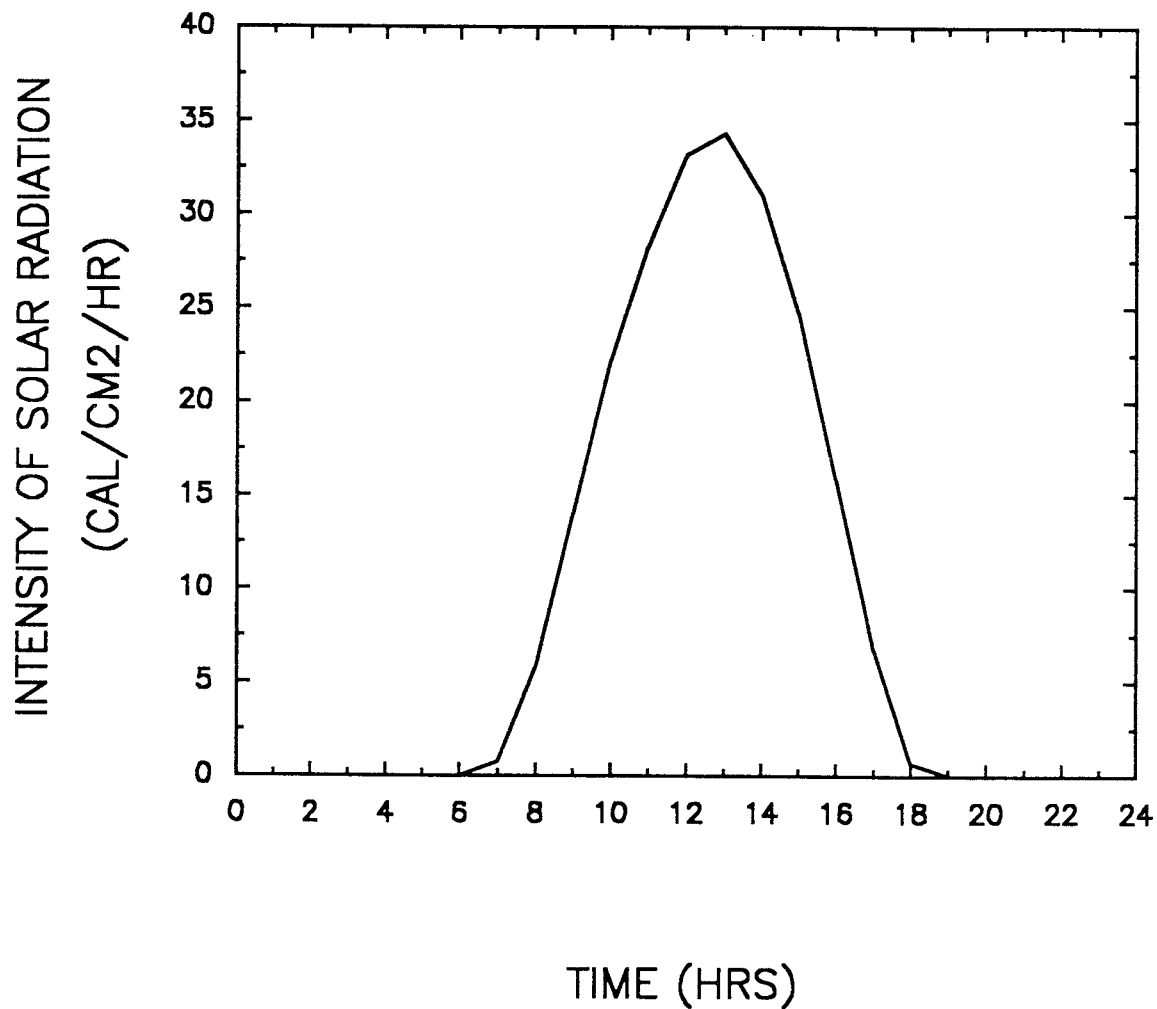


Figure 9. Intensity of solar radiation as a function of time. Data shown are the hourly average intensities of solar radiation during October for the period from 1975 to 1986 in Western Oregon (Solar Monitoring Lab., 1987).

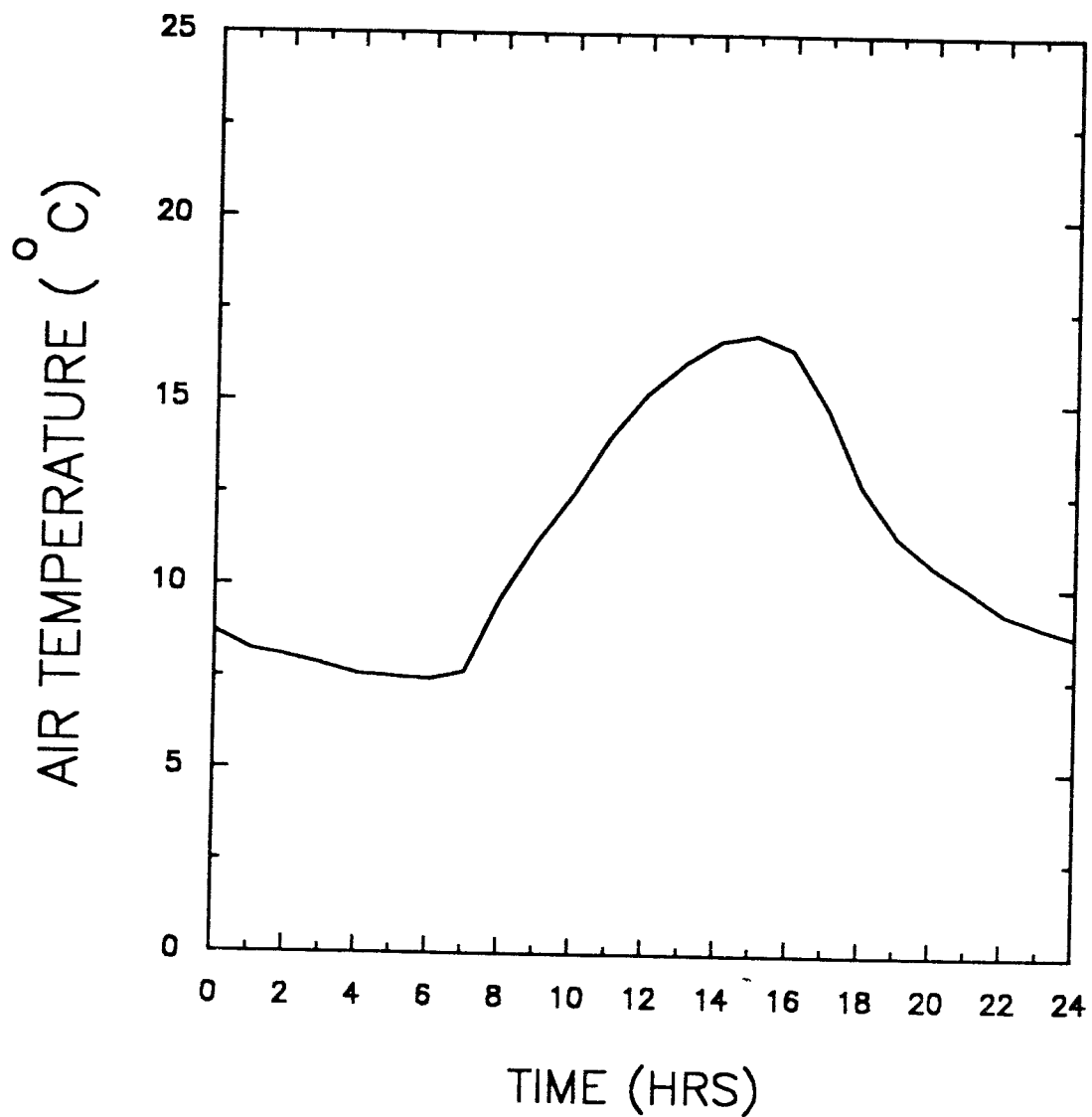


Figure 10. Air temperature as a function of time. Data shown are the hourly average air temperatures during October for the period from 1975 to 1986 in Western Oregon (Redmond, 1988).

data used for the air temperature are listed in Table 4 and shown on Figure 10. The Least Square Method was used to fit the input data to obtain the coefficients in equation (120). After the determination of coefficients in equation (120), air temperature at a given time was calculated by the computer program using equation (120).

(2) Relative Humidity in the Atmosphere. The relative humidity is the ratio of the mass of water vapor present in air to the mass of water at saturation at the existing temperature. The ratio depends on mass of water vapor as well as air temperature in the atmosphere. As the water vapor content increases, the relative humidity increases. The relative humidity decreases with increasing temperature (Wallace and Hobbs, 1977). The relative humidity of the atmosphere during a daily radiation cycle is a function of time of day (Figure 11). Since the soil water content and soil temperature at the soil surface are affected by the relative humidity in the atmosphere, the daily course of relative humidity in the atmosphere must be known, when simulating of the transport of water and heat through the soil. Usually, the relative humidity in the atmosphere can be characterized by a Fourier Series (Lindstrom and Piver, 1985) as follows:

$$RH_{air}(t) = \overline{RH} + \sum_{n=1}^N [A_{rh}(n) \cos(\omega_{2n}t) + B_{rh}(n) \sin(\omega_{2n}t)], \quad (121)$$

where  $RH_{air}(t)$  is the relative humidity in the atmosphere (dimensionless) at time  $t$ ,  $\overline{RH}$  is the mean relative humidity in the atmosphere (dimensionless),  $N$  is the number of the Fourier frequency,  $A_{rh}(n)$  and  $B_{rh}(n)$  are the relative humidity coefficients,  $\omega_{2n}$  is the  $n^{th}$  relative humidity Fourier frequency, and  $t$  is the time (hr).

Table 4. The hourly averages of air temperatures, relative humidities, and solar radiation during October for the period of 1975 to 1986 (Solar Monitoring Lab., 1987; Redmond, 1988).

Time	Air temperature	Relative humidity	Solar radiation
hr	°C	dimensionless	cal cm <sup>-2</sup> hr <sup>-1</sup>
0	8.72	0.892	0.000
1	8.22	0.897	0.000
2	8.06	0.906	0.000
3	7.83	0.914	0.000
4	7.56	0.912	0.000
5	7.50	0.920	0.000
6	7.44	0.923	0.000
7	7.67	0.915	0.774
8	9.67	0.880	5.762
9	11.22	0.826	14.018
10	12.50	0.773	22.188
11	14.06	0.715	28.294
12	15.22	0.670	33.196
13	16.06	0.635	34.314
14	16.67	0.610	31.046
15	16.83	0.608	24.682
16	16.44	0.619	15.824
17	14.89	0.682	6.708
18	12.72	0.766	0.688
19	11.39	0.804	0.000
20	10.61	0.837	0.000
21	10.00	0.859	0.000
22	9.33	0.867	0.000
23	9.00	0.886	0.000

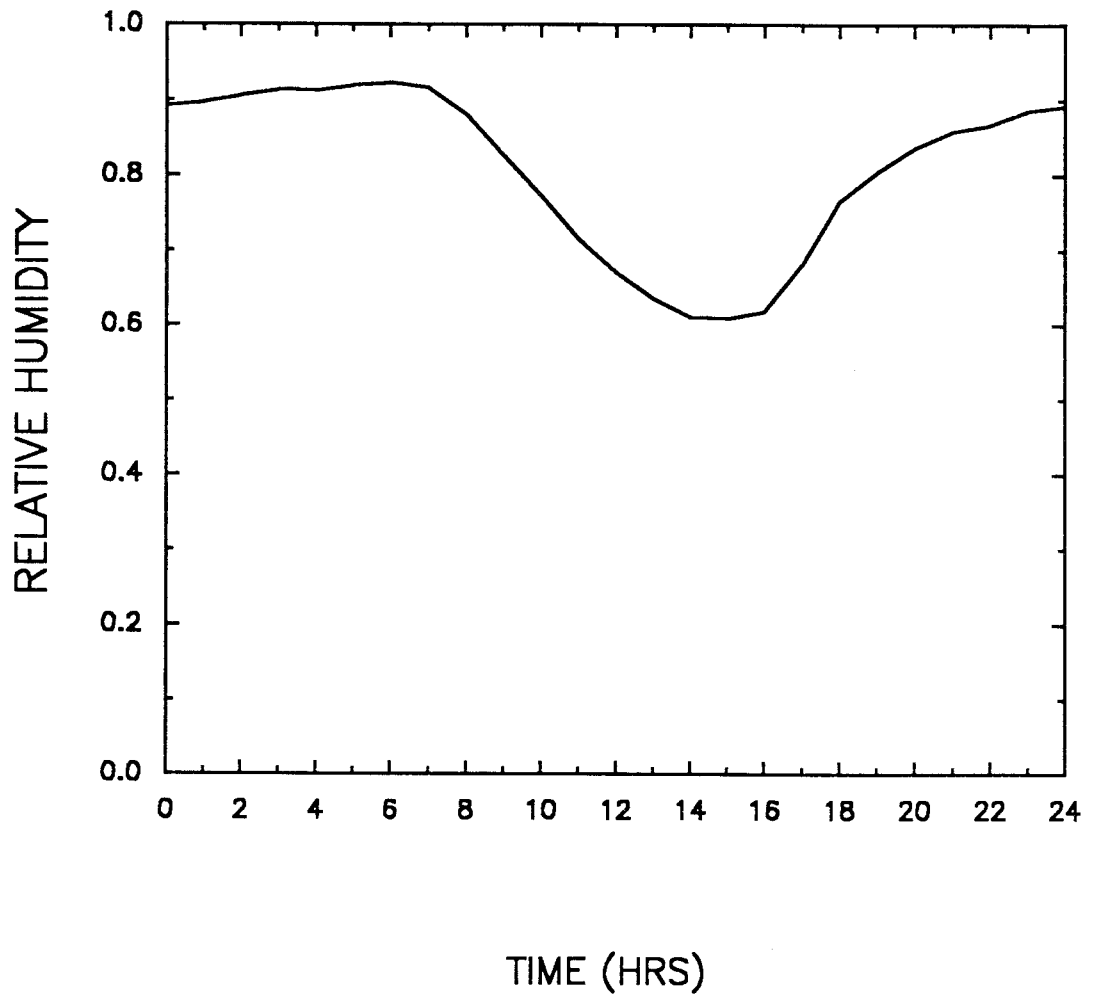


Figure 11. Relative humidity as a function of time. Data shown are the hourly average relative humidities during October for the period from 1975 to 1986 in Western Oregon (Redmond, 1988).

The input data used for the relative humidity in the atmosphere are listed in Table 4 and shown on Figure 11. The Least Square Method was used to fit the input data to obtain the coefficients in equation (121). After determination of the coefficients in equation (121), relative humidity in the atmosphere at a given time was calculated by the computer program using equation (121). During rain events, the relative humidity was set equal to one, the air temperature and solar radiation were assumed to be reduced 50% and 85%, respectively, of the values for conditions without rain.

(3) Solar Radiation. The source of heat for the soil and adjacent atmosphere is the solar radiation. The rate at which the radiant energy reaches the upper boundary of the earth's atmosphere is called the solar constant, and has a value of about  $120 \text{ cal cm}^{-2} \text{ hr}^{-1}$  (Ghildyal and Tripathi, 1987). Only a part of this energy is available for heating the soil because, before reaching the soil surface, much of the radiation is scattered and distributed by the earth's atmosphere. The intensity of solar radiation (short wave radiation), which reaches the soil surface, changes with latitude and season. It also changes during the day. The daily course of intensity of solar radiation during October in Western Oregon is shown in Figure 9. Since the solar radiation is the source of heat for the soil, the intensity of solar radiation as a function of the time must be known for simulating the transport of heat through the soil. Figure 9 suggests that the intensity of solar radiation as a function time may be assumed to be a Gaussian Normal Distribution. Therefore, the Gaussian Normal Distribution function of the form (Dixon and Massey, 1983):

$$QSR(t) = E_1 \exp\left[(-1/2)\left(\frac{t - E_2}{E_3}\right)^2\right], \quad (122)$$

was used to characterize the relationship between the intensity of solar radiation and the time, where  $QSR(t)$  is the intensity of solar radiation ( $\text{cal cm}^{-2} \text{ hr}^{-1}$ ) at time  $t$ ,  $E_1$ ,  $E_2$ , and  $E_3$  are coefficients of the equation, and  $t$  is the time (hr). The input data for the intensity of solar radiation over time are listed in Table 4. The Least Square Method was used to fit the input data to obtain the coefficients in equation (122). After determination of the coefficients in equation (122), the intensity of solar radiation at a given time was calculated by the computer program using equation (122).

(4) Sunrise and Sunset Schedule. Times for sunrise and sunset were chosen to correspond to the conditions for Western Oregon during October. The sun rises at 7:00 a.m. and sets at 6:00 p.m. (Solar Monitoring Lab, 1987). During this period, the intensity of solar radiation changes with time (Figure 9). The period when the intensity of solar radiation is not zero is called "time light on" in the model. The period when the intensity of solar radiation is zero is defined as "time light off" in the model. The time schedule for light on and light off for the five day simulation period is in Table 5.

(5) Wind Speed. The evaporation transfer of water vapor and temperature from the soil surface is affected by the wind velocity. Therefore, the wind velocity must be considered when simulating the transport of water and heat through the soil. The wind velocity was assumed to be constant during the simulation period and was set equal to  $9991.89 \text{ m hr}^{-1}$  (Redmond, 1988).

Table 5. Time schedule for rain on and rain off, and for light on and light off during the five day simulation period. Hours are counted consecutively, starting with 0 at the beginning of the first day and ending at the midnight of the fifth day, for a total simulation time of 120 hours.

Time rain on	Time rain off	Time light on	Time light off
hr	hr	hr	hr
0	12	6.1	19
76	88	30.1	43
--	-	54.1	67
--	-	78.1	91
--	-	102.1	115

(6) Rainfall Rate and Duration. Rainfall rate has direct as well as indirect effects on infiltration. If the infiltration rate exceeds the rainfall intensity, the rain water will not be retained on the soil surface. When the rainfall intensity exceeds the infiltration rate, surface ponding occurs. In this example the intensity of rainfall was chosen to be equal to  $5.0 \text{ mm hr}^{-1}$  (Redmond, 1988) which is lower than the infiltration rate into loam soil ( $5\text{-}10 \text{ mm hr}^{-1}$ , Hillel, 1982). Since the initial soil water content was chosen to be low ( $0.15 \text{ cm}^3 \text{ cm}^{-3}$ ), the duration of rainfall was chosen to be 12 hours in order to allow more water to enter the soil and to allow meaningful changes of water content in the soil profile during infiltration, redistribution, and evaporation. The large changes in soil water content result in large changes in soil temperature, soil oxygen and carbon dioxide concentrations, because soil temperature, soil oxygen and carbon dioxide concentrations are affected by soil water content. These relatively large changes of water, temperature,

oxygen and carbon dioxide concentrations in the soil profile help to demonstrate the applications of the model.

Two 12-hour periods of rainfall were chosen for the simulation. The first 12-hour period of rainfall was chosen to start at 0 hours and end at 12 hours on the first day. The second 12-hour period of rainfall was set to begin at 76 hours and to stop at 88 hours on the fourth day. The period when the rainfall begins is called "time rain on". The period when the rainfall stops is defined as "time rain off". The time schedule for the rain on and rain off in the five-day simulation period is listed in Table 5.

Soil Properties. The soil properties required as input parameters are: hydraulic conductivity; water potential; water diffusivity; thermal conductivity; particle density; total porosity; tortuosity factor; specific heat of solids, water, and air; albedo of solids, water, and air; emissivity of solids, water, and air; and percent of sand, silt, and clay.

(1) Hydraulic Conductivity  $K(\theta)$ . The hydraulic conductivity,  $K(\theta)$ , is a measure of the ability of the soil to conduct water. It depends on properties of both the soil matrix and the fluid. The soil characteristics which affect the hydraulic conductivity are related to pore geometry, i.e., the total porosity, the pore size distribution and the tortuosity of the path through the soil pores. The hydraulic conductivity is a function of the volumetric soil water content (Figure 12). No universal function exists relating hydraulic conductivity and soil water content. Nevertheless, several empirical relationships have been proposed (Hillel, 1982). The Kozeny function proposed by Mualem (1976) of the form:

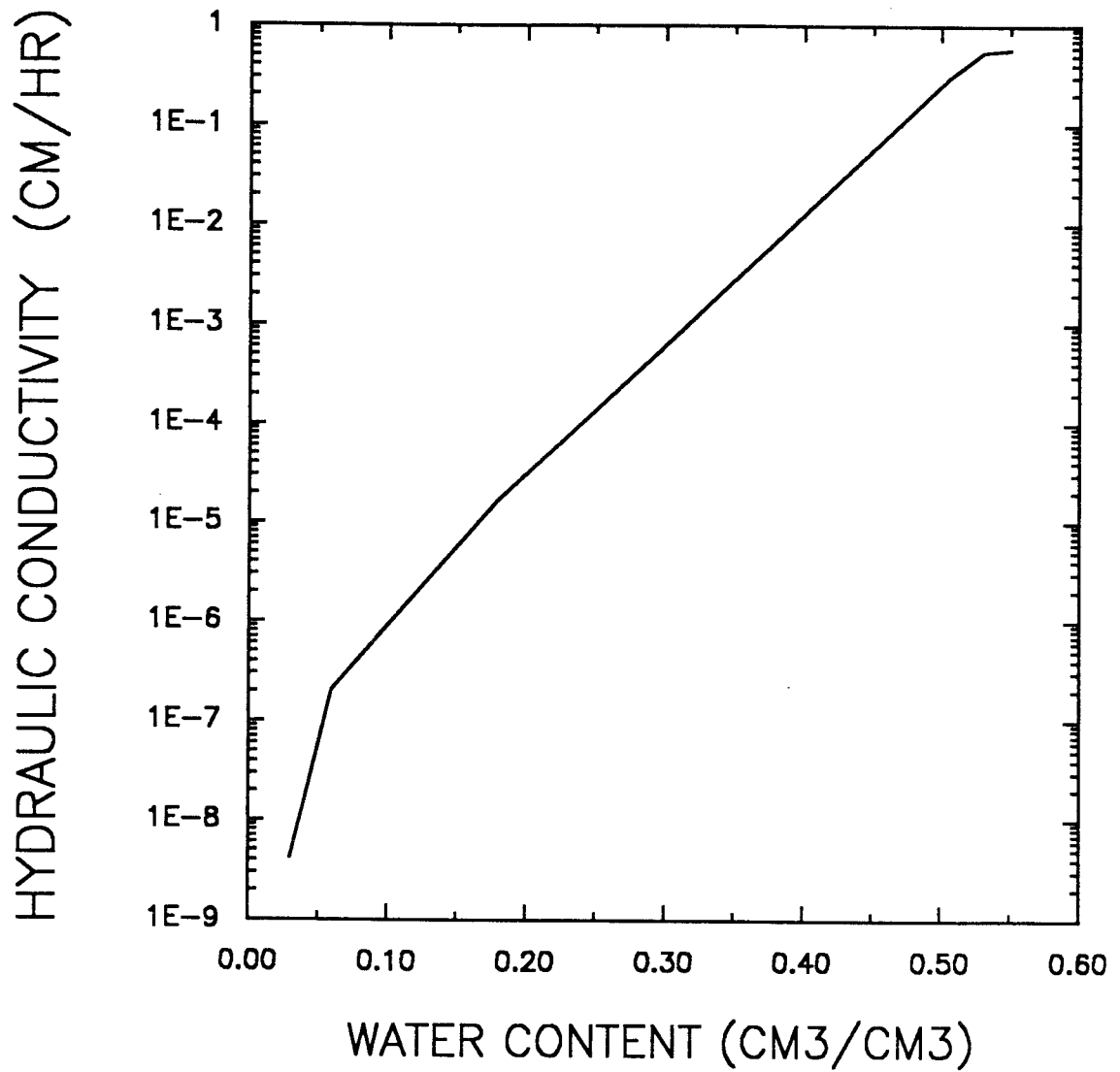


Figure 12. Hydraulic conductivity as a function of soil water content for Indio loam soil. Data taken from McCoy et al. (1984).

$$K = K_S \left[ \frac{\theta - \theta_r}{\theta_s - \theta_r} \right] \gamma_c \quad (123)$$

was used to fit the experimental data for the hydraulic conductivity at different water contents (Table 6), where  $K$  is the hydraulic conductivity ( $\text{cm hr}^{-1}$ ),  $K_S$  is the hydraulic conductivity at saturation ( $\text{cm hr}^{-1}$ ),  $\theta$  is the volumetric soil water content ( $\text{cm}^3 \text{ cm}^{-3}$ ),  $\theta_r$  is the residual volumetric soil water content at air dry conditions ( $\text{cm}^3 \text{ cm}^{-3}$ ),  $\theta_s$  is the saturated volumetric soil water content ( $\text{cm}^3 \text{ cm}^{-3}$ ), and  $\gamma_c$  is a coefficient characterizing the soil. After the determination of the coefficient constants in equation (123), hydraulic conductivity at a given water content was calculated by the computer program using equation (123).

(2) Water Potential  $\psi(\theta)$ . The soil water potential, or matrix potential, is a negative pressure resulting from capillary and adsorptive forces due to the soil matrix and is a function of the volumetric soil water content (Figure 13). No universal function

Table 6. Soil hydraulic conductivity and water potential at different water contents. Data taken from McCoy et al. (1984).

Water content range $\theta$	Hydraulic conductivity $K$	Water potential $\psi$
$\text{cm}^3 \text{ cm}^{-3}$	$\text{cm hr}^{-1}$	cm
0.03	$0.417 \times 10^{-8}$	-102300.00
0.06	$0.208 \times 10^{-6}$	-10226.93
0.18	$0.167 \times 10^{-4}$	-1021.98
0.505	0.296	-102.10
0.53	0.545	-10.23
0.55	0.579	-1.02

describes the relationship between water potential and water content. The power law function proposed by Van Genuchten (1980) of the form:

$$\psi = -\alpha_{\theta} \left[ \left\{ \frac{\theta_s - \theta_r}{\theta - \theta_r} \right\}^{\beta_{\theta}} - 1.0 \right] \quad (124)$$

was used to fit the experimental data for the water potential at different water contents (Table 6), where  $\psi$  is the water potential (cm),  $\alpha_{\theta}$  is the coefficient characterizing the soil (cm),  $\theta_s$  is the saturated volumetric soil water content ( $\text{cm}^3 \text{ cm}^{-3}$ ),  $\theta_r$  is the residual volumetric soil water content ( $\text{cm}^3 \text{ cm}^{-3}$ ),  $\theta$  is the volumetric soil water content ( $\text{cm}^3 \text{ cm}^{-3}$ ), and  $\beta_{\theta}$  is the coefficient characterizing the soil (dimensionless). After the determination of the coefficient constants in equation (124), water potential at a given water content was calculated by the computer program using equation (124).

(3) Water Diffusivity  $D(\theta)$ . The soil water diffusivity,  $D(\theta)$ , is the product of the hydraulic conductivity and the reciprocal of the slope of the soil water characteristic curve at a given water content.  $D(\theta)$  is a function of the volumetric soil water content. No universal function is available relating water diffusivity to the water content. The theoretical formulation of the form (Hillel, 1982):

$$D(\theta) = K(\theta) \frac{d\psi}{d\theta} \quad (125)$$

was used to calculate the water diffusivity at a given water content since  $K(\theta)$  could be calculated from equation (123) and  $d\psi/d\theta$  could be calculated by derivative equation (124) with respect to  $\theta$ .

(4) Other Soil Properties. The soil particle density is defined as the mass per unit volume of soil solids ( $\text{g cm}^{-3}$ ). In most mineral

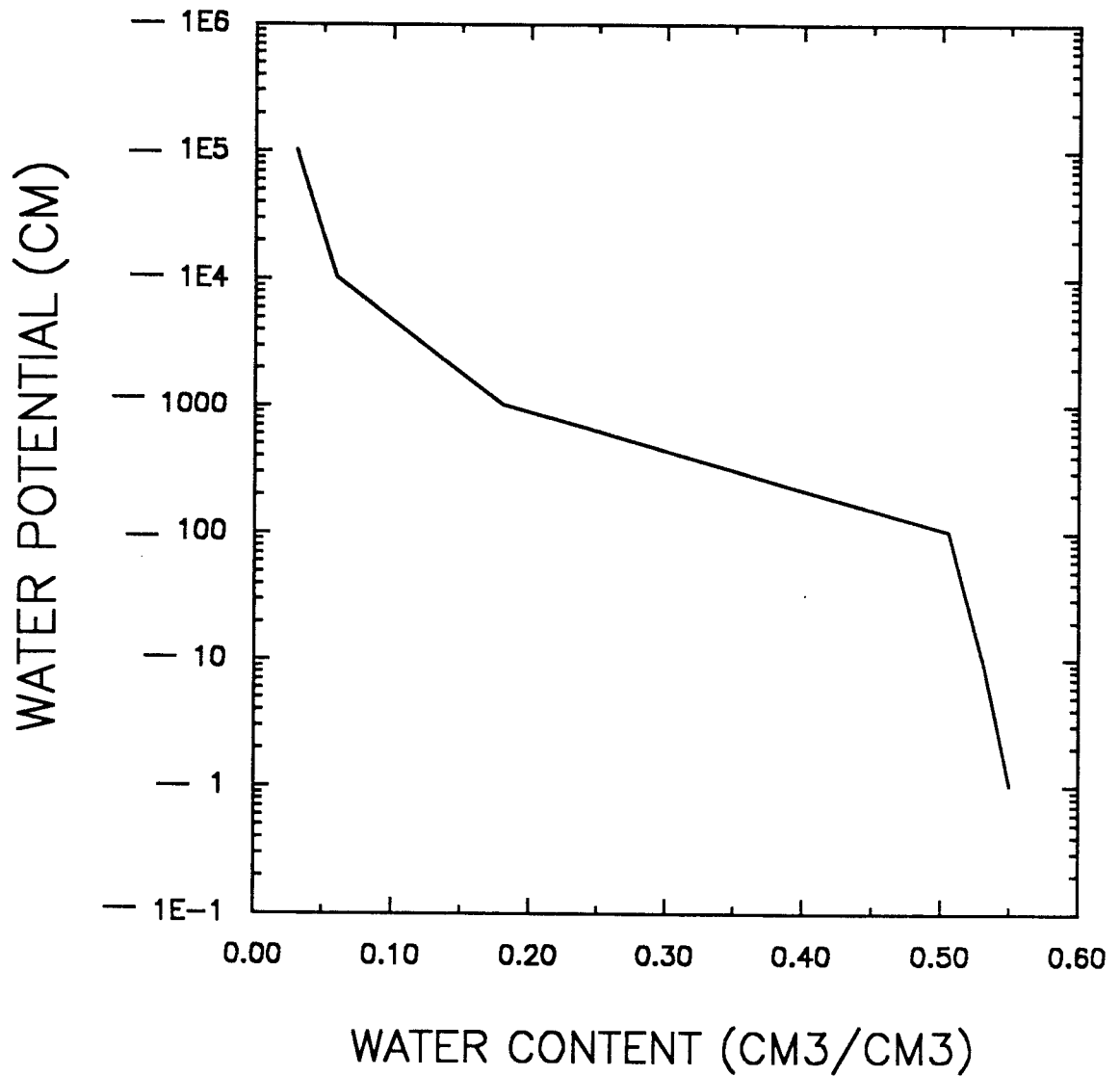


Figure 13. The water potential as a function of soil water content for Indio loam soil. Data taken from McCoy et al. (1984).

soils, the mean density of the solid particles is in the range of 2.6 to 2.7 g cm<sup>-3</sup> (Hillel, 1982). The particle densities of the constituents of the Indio loam soil, used in the simulation, are in Table 7.

The total soil porosity is an index of the total pore volume in the soil. Its value generally is in the range of 0.3 to 0.6 cm<sup>3</sup> cm<sup>-3</sup> (Hillel, 1982). The soil porosity for the Indio loam soil is 0.55 cm<sup>3</sup> cm<sup>-3</sup> (McCoy et al., 1984).

The soil tortuosity is defined as the average ratio of the actual path length to the apparent, or straight, flow path length. The tortuosity factor is defined as the inverse of the tortuosity. It always has a value less than 1. The tortuosity factor chosen for the soil of this example is 0.66 (Hillel, 1982).

The specific heat is defined as the quantity of heat, in cal, required to raise the temperature of 1 g of the substance by 1°C. Values of the specific heat for the soil constituents, such as sand, silt, clay, water, and air, are in Table 7.

The albedo is the reflection coefficient for short-wave radiation and is related to the soil color. The albedo of light colored soils is generally twice as large as that of dark colored soils (Ghildyal and Tripathi, 1987). Water content darkens the surface and decreases the reflection of short-wave radiation. Values of albedo for the soil surface, water, and air are in Table 7.

The emissivity is the emitance of a specimen of the material that is thick enough to be completely opaque and has an optically smooth surface (Weast, 1986). The emissivity of the soil surface, water, and air are in Table 7.

Table 7. Values of the soil parameters used for the Indio loam soil that remain constant throughout the simulation.

Symbol	Meaning	Value/Units	Reference
$\rho_{\text{sand}}$	Density of sand	2.66 g cm <sup>-3</sup>	Ghildyal and Tripathi, 1987
$\rho_{\text{silt}}$	Density of silt	2.65 g cm <sup>-3</sup>	Ghildyal and Tripathi, 1987
$\rho_{\text{clay}}$	Density of clay	2.64 g cm <sup>-3</sup>	Ghildyal and Tripathi, 1987
$\rho_{\text{air}}$	Density of air	0.0011 g cm <sup>-3</sup>	Weast, 1986
$\rho_{\text{water}}$	Density of water	1.00 g cm <sup>-3</sup>	Weast, 1986
$\epsilon$	Total porosity	0.55	McCoy, et al., 1984
$\alpha_{\text{tort}}$	Tortuosity factor	0.66	Hillel, 1982
$c_{\text{sand}}$	Specific heat of sand	0.175 cal g <sup>-1</sup> °C <sup>-1</sup>	Ghildyal and Tripathi, 1987
$c_{\text{silt}}$	Specific heat of silt	0.175 cal g <sup>-1</sup> °C <sup>-1</sup>	Ghildyal and Tripathi, 1987
$c_{\text{clay}}$	Specific heat of clay	0.175 cal g <sup>-1</sup> °C <sup>-1</sup>	Ghildyal and Tripathi, 1987
$c_{\text{water}}$	Specific heat of water	1.0 cal g <sup>-1</sup> °C <sup>-1</sup>	Weast, 1986
$c_{\text{air}}$	Specific heat of air	0.24 cal g <sup>-1</sup> °C <sup>-1</sup>	Weast, 1986
$\alpha_{\text{air}}$	Albedo of air	0.05	Weast, 1986
$\alpha_{\text{water}}$	Albedo of water	0.07	Weast, 1986
$\alpha_{\text{soil}}$	Albedo of soil	0.09	Ghildyal and Tripathi, 1987
$\epsilon_{\text{air}}$	Emissivity of air above the soil	0.9	Weast, 1986
$\epsilon_{\text{water}}$	Emissivity of water	0.95	Weast, 1986

Table 7. Continued.

Symbol	Meaning	Value/Units	Reference
$\epsilon_{\text{soil}}$	Emissivity of soil surface	0.5	Ghildyal and Tripathi, 1987
$\lambda_{\text{solid}}$	Thermal conductivity of solids	18.9 cal $\text{cm}^{-1} \text{hr}^{-1}$	Ghildyal and Tripathi, 1987
$\lambda_{\text{water}}$	Thermal conductivity of water	5.14 cal $\text{cm}^{-1} \text{hr}^{-1}$	Ghildyal and Tripathi, 1987
$\lambda_{\text{air}}$	Thermal conductivity of air	0.2214 cal $\text{cm}^{-1} \text{hr}^{-1}$	Ghildyal and Tripathi, 1987

The thermal conductivity,  $\lambda$ , is defined as the quantity of heat passing per unit time through a unit area of material when the gradient of temperature is also unity. Thermal conductivities of solid, water, and air are in Table 7.

The percentages of sand, silt, and clay of Indio loam soil were chosen to be 30, 60, and 10, respectively. These percentages were used to calculate the specific heat of the soil solids.

Biological Activities. When solving the oxygen and carbon dioxide field equations, the rate of oxygen consumption and carbon dioxide production by plant roots and soil microorganisms during the simulation conditions needs to be known. The oxygen is consumed by plant roots and soil microorganisms for respiration, an activity referred to as an oxygen sink. On the other hand, the respiration by plant roots and soil microorganisms produces carbon dioxide. This activity is referred to as a carbon dioxide source. Input data, for

the rate of oxygen use and carbon dioxide production, are discussed as follows.

(1) Sink of Oxygen by Plant Roots. The rate of oxygen consumption by plant roots varies among species and varies with ages, root length, and growing conditions such as soil oxygen concentration, soil temperature, and soil water content. Lambers and Steingrover (1978) found that the rate of oxygen use by the roots of several plant species is in the range of 390-1430 mg kg<sup>-1</sup> dry roots hr<sup>-1</sup>. The rate of oxygen consumption and carbon dioxide production by roots declines with both age and root length (Lemon and Wiegand, 1962). The influences of soil oxygen concentration, soil temperature, and soil water content on the rates of oxygen consumption by roots were discussed in the Introduction.

For this simulation, the plant species Maize (Zea mays) was chosen. A form of the Michaelis-Menten Kinetics for enzyme reactions was chosen to represent the respiratory sink strength for oxygen by roots as a function of soil oxygen concentration (Luxmoore, et al., 1970) as follows:

$$Srt(i) = \frac{Srt_{max} C(i)}{HRC + C(i)}, \quad (126)$$

where  $Srt(i)$  is the average rate of the respiratory use of oxygen by the  $i^{th}$  section of roots of average length ( $\mu\text{g cm}^{-3}$  fresh tissue hr<sup>-1</sup>),  $Srt_{max}$  is the maximum rate of the respiratory use of oxygen by roots ( $240 \mu\text{g cm}^{-3}$  fresh tissue hr<sup>-1</sup>),  $C(i)$  is the concentration of oxygen in the air-filled pore space of the soil in the  $i^{th}$  section of soil depth corresponding to the  $i^{th}$  section of roots ( $\mu\text{g cm}^{-3}$  soil

air), HRC is the concentration of oxygen at which the respiration rate is one half of  $Sr_{t_{max}}$  ( $114 \mu\text{g cm}^{-3}$  soil air).

(2) Root Length. In order to solve equation (126), the root length needs to be known. Rather than choosing a fixed root length for the entire the five day period of simulation, the root length was chosen to be a function of time and increased as time progressed. In this example, the simulation starts from 0 hours. Therefore, the growth of roots into the soil was assumed to begin at 0 hours. The root length as a function of time was calculated using the following linear function (Oates and Barber, 1987):

$$L = L_0 + a_1 t, \quad (127)$$

where  $L$  is the root length (cm),  $L_0$  is the initial root length (2 cm),  $a_1$  is a constant characterizing the root growth characteristics ( $0.4 \text{ cm hr}^{-1}$ ), and  $t$  is time (hr).

(3) Sink of Oxygen by Soil Microorganisms. The respiratory use of oxygen by the soil microorganisms changes with species and soil conditions such as soil oxygen concentration, soil temperature, soil water content, and time. Glinski and Stepniewski (1985) found that the rate of oxygen consumption by soil microorganisms normally falls within the range of  $0.2$  to  $20 \text{ cm}^3 \text{ kg}^{-1} \text{ dry soil hr}^{-1}$ . The effects of soil oxygen concentration, soil temperature, soil water content, and time on the rate of the respiratory sink of oxygen were discussed in the Introduction.

In this simulation, the soil microorganisms were assumed to have a uniform density from the soil surface to a depth of 20 cm (Alexander, 1961). Aerobic, heterotrophic microorganisms whose

growth is limited by lack of substrate or oxygen sources, or both simultaneously were selected for the simulation. The rate of the respiratory use of oxygen by these soil microorganisms was assumed to depend on the oxygen concentration in the soil. In the processes of the respiratory activities of soil microorganisms, oxygen is required for energy of synthesis as well as energy of maintenance. With the assumption that the oxygen required for the energy of gross biomass production is proportional to substrate utilization and that the oxygen required for the energy of maintenance follows Monod Kinetics, the rate of the respiratory use of oxygen by soil microorganisms can be expressed as (Molz et al., 1986):

$$S_{mO} = \gamma_o Y_o r_s + \alpha_o k_o m_c \left[ \frac{C_{col}}{K_o + C_{col}} \right] \quad (128)$$

and

$$r_s = \frac{\mu_o m_c}{Y_o} \left[ \frac{s}{K_{sb} + s} \right] \left[ \frac{C_{col}}{K_o + C_{col}} \right], \quad (129)$$

where  $S_{mO}$  is the rate of the respiratory use of oxygen by soil microorganisms ( $\text{g colony}^{-1} \text{hr}^{-1}$ ),  $\gamma_o$  is the oxygen use coefficient for the synthesis of heterotrophic biomass (dimensionless),  $Y_o$  is the yield coefficient for heterotrophic microorganisms (dimensionless),  $r_s$  is the rate of substrate utilization per colony ( $\text{g colony}^{-1} \text{hr}^{-1}$ ),  $\alpha_o$  is the oxygen use coefficient for the energy of maintenance for heterotrophic microorganisms (dimensionless),  $k_o$  is the microbial decay coefficient for aerobic respiration ( $\text{hr}^{-1}$ ),  $m_c$  is the cell mass per colony ( $\text{g colony}^{-1}$ ),  $K_o$  is the oxygen saturation constant for decay ( $\text{g cm}^{-3}$  soil air),  $C_{col}$  is the concentration of oxygen within the

colony ( $\text{g cm}^{-3}$  soil air),  $\mu_o$  is the maximum specific growth rate ( $\text{hr}^{-1}$ ),  $s$  is the concentration of substrate within the colony ( $\text{g cm}^{-3}$  soil), and  $K_{sb}$  is the substrate saturation constant ( $\text{g cm}^{-3}$ ). In the unsaturated soil, the diffusion of oxygen from the soil air-filled pore space into the colony is assumed to be rapid since the microorganisms are thin and quite small (10 to 100 organisms) in numbers (Harvey et al., 1984). Therefore, the concentration of oxygen within the colony ( $C_{co1}$ ) was assumed to be equal to the concentration of oxygen in the soil air-filled pore space ( $C_{o2}$ ).

Putting equation (129) into equation (128) and replacing  $C_{co1}$  by  $C_{o2}$  obtains:

$$S_{mo} = \left[ \gamma \mu_o m_c \left\{ \frac{s}{K_{sb} + s} \right\} + \alpha_o k_o m_c \right] \left[ \frac{C_{o2}}{K_o + C_{o2}} \right], \quad (130)$$

where  $C_{co2}$  has the unit  $\text{g cm}^{-3}$  soil air.

Equation (130) shows that the rate of the respiratory use of oxygen by soil microorganisms depends on the concentrations of the substrate and oxygen in the soil. The equation was used in the simulation. The input data used for solving equation (130) are listed in Table 8.

The unit for  $S_{mo}$  in equation (130) is  $\text{g colony}^{-1} \text{hr}^{-1}$ , which is different from the unit for  $S_{mo}$  ( $\mu\text{g cm}^{-3}$  soil air  $\text{hr}^{-1}$ ) in the oxygen field equation. Therefore, the conversion of  $\text{g colony}^{-1} \text{hr}^{-1}$  to  $\mu\text{g cm}^{-3}$  soil air  $\text{hr}^{-1}$  is needed (Appendix III).

(4) Production of Carbon Dioxide by Roots and Soil Microorganisms. The respiratory production of carbon dioxide by plant roots and soil microorganisms were calculated, using the definition of respiratory quotient. That is:

Table 8. Parameters of microbial kinetics for solving equation (130) in the simulation. Data are adopted from Molz et al. (1986) and Widdowson et al. (1988).

<u>Parameter</u>	<u>Value/Unit</u>
$\gamma_o$	1.4
$\mu_o$	0.18 hr <sup>-1</sup>
$m_c$	2.8 x 10 <sup>-11</sup> g colony <sup>-1</sup>
$s$	2 x 10 <sup>-6</sup> g cm <sup>-3</sup>
$K_s$	120 x 10 <sup>-6</sup> g cm <sup>-3</sup>
$K_o$	0.77 x 10 <sup>-6</sup> g cm <sup>-3</sup>
$\alpha_o$	0.0402
$k_o$	0.77 x 10 <sup>-6</sup> g cm <sup>-3</sup>

$$\text{Respiratory Quotient (RQ)} = \frac{\text{moles of CO}_2 \text{ produced}}{\text{moles of O}_2 \text{ consumed}} \quad (131)$$

In this simulation, it was assumed that the RQ value for both roots (Levitt, 1969) and soil microorganisms (Bridge and Rixon, 1976) was equal to one. Since the rate of consumption of oxygen by roots and soil microorganisms had been calculated previously, the rates of production of carbon dioxide could be calculated using the RQ value of one and the equation (131).

Initial Distribution of Water Content, Temperature, Oxygen and Carbon Dioxide Concentrations in the Soil Profile. The initial soil water content was assumed to be constant with soil depth. Although the minimum value of soil water content for Indio loam soil given by McCoy et al. (1984) is 0.03 cm<sup>3</sup> cm<sup>-3</sup>, which is close to air-dry soil, this minimum water content is unlikely to exist under the weather conditions occurring in October in Western Oregon. The value of the initial soil water content chosen for this example was 0.15 cm<sup>3</sup> cm<sup>-3</sup> which is a relatively low soil water content. In order to prevent ponding of water on the soil surface during infiltration, an

initially low soil water content, as well as a low rate of rainfall, is needed. The initial soil temperature was also assumed to be constant with soil depth. Since the simulation began from the 0 hours of the first day, the value of the initial soil temperature chosen for this example was 8.72°C, which corresponded to the air temperature at this time. The initial soil oxygen and carbon dioxide concentrations were assumed to be constant with soil depth. The values of initial oxygen and carbon dioxide concentrations in the soil were chosen to be the same as those of the atmosphere, which are 300  $\mu\text{g oxygen cm}^{-3}$  soil air and 0.6134  $\mu\text{g carbon dioxide cm}^{-3}$  soil air, respectively.

Activity Coefficients of Oxygen and Carbon Dioxide. In order to solve the oxygen and carbon dioxide field equations, the activity coefficients of oxygen and carbon dioxide must be known. The activity of a gas is defined by:

$$a = \gamma C, \quad (132)$$

where  $a$  is the activity of the gas or the effective concentration of the gas ( $\text{mol liter}^{-1}$ ),  $\gamma$  is the activity coefficient of the gas (dimensionless), and  $C$  is the concentration of the gas ( $\text{mol liter}^{-1}$ ). According to the behavior of a gas under a given condition, the gas can be classified as an ideal gas or as a non-ideal gas. The standard state of an ideal gas is established at the pressure of one atmosphere. When a gas behaves as an ideal gas, the individual gas molecules have no interaction upon one another and the activity coefficient ( $\gamma$ ) is unity, so that the activity of an ideal gas equals its concentration. However, at high pressures or concentrations much higher than in the atmosphere, the individual gas molecules may

interact with each other. Under those conditions the gas does not behave as an ideal gas and the activity coefficient is not unity (Moore, 1983).

During mixed transport of oxygen and carbon dioxide through the soil pores, two kinds of behavior of oxygen and carbon dioxide molecules may occur.

Case I. Oxygen and carbon dioxide behave as ideal gases. The individual molecules of the gases have no interaction with each other. Molecules of the same gas do not affect each other, nor is there interaction between the molecules of the unlike gases. The molecules behave completely independently. For such an ideal mixture, the activity coefficients of oxygen and carbon dioxide are both unity (Moore, 1983), so that

$$\gamma_{O_2} = \gamma_{CO_2} = 1. \quad (133)$$

In the soil environment, the concentration of oxygen is either equal to that of the atmosphere ( $300 \text{ mg cm}^{-3}$ ) or lower. The actual concentration depends on the rate of use of the oxygen by roots and soil microorganisms, and the rate of supply of the oxygen from the atmosphere to the soil. When the rate of use of oxygen is larger than the rate of supply of oxygen, the concentration of oxygen in the soil air-filled pore space is less than that of the atmosphere. Conversely, when the rate of use of oxygen is smaller than the rate of supply of oxygen, the concentration of the oxygen could become equal to that of the atmosphere. Since the concentration of oxygen in the soil usually does not exceed that of the atmosphere, the oxygen in the soil air-filled pore space will behave ideally.

Carbon dioxide is produced by roots and soil microorganisms in the soil. Its concentration can be much higher (300 times) than that of the atmosphere (Brady, 1984). The actual concentration depends on the rate of production of carbon dioxide by roots and microorganisms, and the rate of diffusion of carbon dioxide from the soil to the atmosphere. When the rate of production of carbon dioxide in the soil is low and the rate of diffusion of carbon dioxide to the atmosphere is high, the carbon dioxide can be treated as an ideal gas in the gaseous phase. This condition may exist in a well-aerated soil.

Case II. Oxygen in the soil pores behaves as an ideal gas, but carbon dioxide may not. As was discussed above, the concentration of oxygen in the soil pores is usually either equal to or less than that of the atmosphere. Therefore, the oxygen in the soil air-filled pore space can be treated as an ideal gas. Carbon dioxide, however, is produced in the soil by roots and soil microorganisms during respiration. The concentration of carbon dioxide in the atmosphere is 0.034 percent by volume, while that in the soil pores may be as high as 10 percent by volume, which is about 300 times higher (Brady, 1984). The molecules of carbon dioxide may interact with each other and behave in a non-ideal manner. This case may exist in a poorly aerated soil. Thus, the activity coefficient of carbon dioxide may not be unity.

As was discussed above, the activity of gas can be calculated by equation (132). However, there is little data available about the activity coefficients of gases. For a gas, the fugacity, instead of the activity, is commonly used and is given as:

$$f = \gamma_f P , \quad (134)$$

where  $f$  is the fugacity of the gas (atm),  $\gamma_f$  is the fugacity coefficient of the gas (dimensionless), and  $P$  is the pressure of the gas (atm). Since it is more convenient to express the mass of carbon dioxide in units of concentration than in units of pressure in this thesis, we chose to use the activity coefficients rather than the fugacity coefficients. This presents the problem of relating the activity coefficient with the fugacity coefficient. Data and methods for calculating the fugacity coefficients of gases are available in the literature. According to Moore (1983), the activity of a gas is equal to its fugacity. Equating equations (132) and (134) and taking care of the dimensions obtains:

$$\gamma = \gamma_f \frac{P}{CRT} . \quad (135)$$

For a non-ideal gas, the pressure of the gas can be calculated using the Virial Equation (Moore, 1983) as follows:

$$\frac{PV}{nRT} = 1 + \frac{B(T)n}{V} , \quad (136)$$

with

$$C = \frac{n}{V} , \quad (137)$$

so that

$$P = [1 + B(T) C] CRT, \quad (138)$$

where  $P$  is the pressure of the gas (atm),  $V$  is the volume of the gas (liter),  $n$  is the number of moles (mol),  $R$  is the gas constant (liter atm mol<sup>-1</sup> K<sup>-1</sup>),  $T$  is the absolute temperature (K),  $B(T)$  is the second

Virial Coefficient, which is a function of temperature (liter mol<sup>-1</sup>), and C is the concentration of the gas (mol liter<sup>-1</sup>). Substituting equation (138) into equation (135) yields:

$$\gamma = \gamma_f [1 + B(T) C] . \quad (139)$$

The parameters of  $\gamma_f$  and B(T) in equation (139) can be calculated using equations proposed by Berthelot (Lewis and Randall, 1961), which are:

$$\gamma_f = 1 + \frac{9R T_c P}{128 P_c T} \left[ 1 - 6 \frac{T_c^2}{T^2} \right] , \quad (140)$$

and

$$B(T) = \frac{9R T_c}{128 P_c} \left[ 1 - 6 \frac{T_c^2}{T^2} \right] , \quad (141)$$

where  $T_c$  and  $P_c$  are the critical temperature (K) and pressure (atm) of the gas, respectively. For carbon dioxide,  $T_c$  is 304.2 K and  $P_c$  is 72.8 atm. Using equations (139), (140), and (141), the activity coefficients of carbon dioxide can be calculated.

Note that the unit of carbon dioxide in equation (136) is mol liter<sup>-1</sup>, while the unit of carbon dioxide in the mathematical model in this thesis is  $\mu\text{g cm}^{-3}$  air. Thus, a unit conversion is necessary before using equation (141). This was done by the computer program.

In this simulation, the activity coefficients of oxygen and carbon dioxide were chosen to be unity.

Other Coefficients for Oxygen and Carbon Dioxide. The other coefficients needed as input parameters were the diffusion coefficients of oxygen and carbon dioxide in soil air-filled pores, the physical adsorption coefficients of oxygen and carbon dioxide, and

the solubility constants of oxygen and carbon dioxide [inverse Henry's Law constants, see equations (42) and (43)].

The equation for the diffusion coefficient of oxygen and carbon dioxide was chosen to be a function of soil water content and tortuosity from Collin and Rasmuson (1988). They studied several diffusion equations and verified them with the experimental data for different soil waters. They proposed the equation:

$$D(\theta) = D_o(\theta) \left(1 - \frac{\theta}{\epsilon}\right)^2 (\epsilon - \theta)^{2x}, \quad (142)$$

where  $D(\theta)$  is the effective diffusion coefficient of oxygen or carbon dioxide in soil air-filled pore space ( $\text{cm}^2 \text{hr}^{-1}$ ),  $D_o(\theta)$  is the diffusion coefficient of oxygen or carbon dioxide ( $\text{cm}^2 \text{hr}^{-1}$ ) at reference state,  $\theta$  is the soil water content ( $\text{cm}^3 \text{cm}^{-3}$ ),  $\epsilon$  is the total soil porosity ( $\text{cm}^3 \text{cm}^{-3}$ ), and  $x$  is the constant depending on total soil porosity. Equation (142) was used in the simulation.

In addition to the effects of soil water on the diffusion coefficients of oxygen and carbon dioxide, soil temperature also plays a role. The equation for temperature effects on diffusion coefficients of oxygen and carbon dioxide is (Partington, 1949):

$$D(T) = D_o(T) \left(\frac{T}{T_o}\right)^m, \quad (143)$$

where  $D(T)$  is the diffusion coefficient of oxygen or carbon dioxide in soil air-filled pore space ( $\text{cm}^2 \text{hr}^{-1}$ ),  $T$  is the temperature (K),  $m$  is constant ( $m = 1.75$  for oxygen and  $m = 2$  for carbon dioxide), and  $D_o(T)$  and  $T_o$  are diffusion coefficients of oxygen or carbon dioxide ( $\text{cm}^2 \text{hr}^{-1}$ ) and temperature ( $^{\circ}\text{C}$ ) at reference state, respectively.

Multiplying equations (142) and (143) together obtains:

$$D(\theta, T) = D_o(\theta, T) \left(1 - \frac{\theta}{\epsilon}\right)^2 (\epsilon - \theta)^{2x} \left(\frac{T}{T_o}\right)^m, \quad (144)$$

where  $D(\theta, T)$  is the diffusion coefficient of oxygen or carbon dioxide which is a function of soil water and temperature ( $\text{cm}^2 \text{hr}^{-1}$ ),  $D_o(\theta, T)$  is the diffusion coefficient of oxygen or carbon dioxide at reference water content and temperature ( $640 \text{ cm}^2 \text{hr}^{-1}$  for oxygen and  $482 \text{ cm}^2 \text{hr}^{-1}$  for carbon dioxide). Equation (144) accounts for both water content and temperature effects on the diffusion coefficient of oxygen or carbon dioxide and was used in the simulation.

Adsorption and Solubility. The physical adsorption coefficients of both oxygen and carbon dioxide were chosen to be  $3.6 \times 10^{-8} \text{ cm}^{-1}$  (Molz et al., 1986). The solubility constants for oxygen and carbon dioxide were 0.03086 and 0.8333, respectively (Stumm and Morgan, 1981).

### Discussion of Simulation Results

Soil Water Content. Changes in soil water content during the 120 hours simulation period are in Figures 14, 15, and 16. These diagrams show the volumetric water content as a function of soil depth at several points in time since the start of the simulation. The simulation started with a rainfall period, which lasted for 12 hours. The rainfall rate was quite low when compared with the infiltration capacity of the soil. As a result, the infiltration profiles at 6 and 12 hours did not show the constant water content of a transmission zone followed by a rapid decrease in water content in the wetting zone or wetting front.

Following the 12 hours with rainfall was a period of change in the water content of the soil profile, due to evaporation at the soil surface and further penetration of the water into the soil due to water potential gradients at the wetting front. The evaporative demand was quite low, so that the soil was always able to satisfy the evaporative demand without substantial drying at the soil surface.

The pattern of rainfall followed by evaporation and redistribution was repeated, starting with rain during the period from at 76 to 88 hours. The water content increased substantially to a depth of about 65 cm. Following the rain, redistribution occurred, increasing the water content down to a depth of 80 cm at 120 hours.

Surface Evaporation. Daily cycles of evaporation are in Figures 17 through 21. Each figure shows the rate of evaporation cycle at the soil surface as a function of time. Figure 17 shows that the condensation of water onto the soil surface occurred from 6 to 12 hours during the period of rainfall. The rate of surface condensation is controlled by the gradients of water vapor pressure and temperature between the atmosphere and the soil surface. In this simulation, it was assumed that the water vapor in the atmosphere was saturated during the rain. The air temperature and solar radiation were assumed to be reduced by 50 percent and 80 percent, respectively, as compared to condition without rain. The temperature of rainwater was set to be 4°C. As a result, the air temperature was low. When the pressure of water vapor of the air is higher and the temperature of the air is lower in the atmosphere than it is at the soil surface, condensation of water onto the soil surface occurs. As soon

as the rain stopped at 12 hours, radiation started to heat the soil. The change in the rate of evaporation during the period from 12 to 24 hours shows the characteristic evaporation cycle (Ghildyal and Tripathi, 1987).

The rate of evaporation changed during the second and third day (Figures 18 and 19) showing the more characteristic surface evaporation behavior, with the rate decrease during the night followed by a gradual increase during the day.

The fourth day involved a period of rainfall, which started at 76 hours and ended at 88 hours. The evaporation rate was close to zero from 82 to 88 hours due to the low temperature of soil surface during the rainfall and the lack of evaporative energy. Then after 88 hours, there was a rise in the rate of evaporation as a result of an increase in evaporative demand. The rain stopped during a time when the rate of radiation was low, so that the rate of evaporation increase was small. During the fifth day, the typical soil surface evaporation cycle repeated.

Soil Temperature. Daily cycles of soil temperature at several depths are shown in Figures 22 through 26. Figure 22 shows that the temperature at the soil surface was close to the temperature of the rain, which was falling during the first 12 hours. This rain, which completely wetted the soil surface, decreased the temperature of the soil surface layers to the temperature of the rainwater after about 6 hours. At the lower depths, the temperature of the rainwater was never reached, because the amount of heat remaining in the soil was sufficient to warm the incoming rain. The rainwater never reached the 50 cm depth, so that the temperature at this depth was constant

during the rain period. However, the rainwater did reach the 20 cm depth, so that at this depth, the temperature of the soil slowly decreased. As soon as the rain stopped at 12 hours, radiation started to warm the soil surface and then deeper layers. The change in soil temperature during the period from 12 to 24 hours showed the characteristic temperature cycle (Hillel, 1982). During the warming part of the cycle, e.g. at 14 and 16 hours, the temperature decreased with soil depth. At each depth, the temperature slowly increased, showing the characteristic decrease in amplitude and time lag with increasing soil depth.

The temperature changes during the second and third day (Figures 23 and 24) show the more characteristic soil temperature behavior, with a decreasing temperature during the night followed by warming during the day. These diagrams more clearly show the decrease in amplitude and increase in lag time of the temperature as a function of soil depth. The fourth day included a rainfall period, which started at 76 hours and ended at 88 hours. From 76 hours to 80 hours, the soil showed a cooling profile with the lowest temperature at the soil surface and the highest temperature at the 20 cm depth. Starting at 76 hours, the temperature of the soil surface decreased more than indicated by the rate of cooling due to radiation. This cooling resulted from the arrival of the cold rainwater. Then at 88 hours when rainfall stopped, the temperature started to increase. The rain stopped during a time of low rate of radiation, so that the temperature rise was small. During the fifth day the typical soil temperature cycle occurred.

Concentrations of Oxygen and Carbon Dioxide. Changes in oxygen and carbon dioxide concentrations are shown in Figures 27, 28, and 29. Each figure shows the concentrations of the two gases side by side. Generally the behavior of oxygen and carbon dioxide show mirror images. The oxygen is depleted through respiration by roots and microorganisms, and the carbon dioxide concentration is released at the same time. When comparing the behavior of oxygen and carbon dioxide, it must be kept in mind that the oxygen enters the soil by diffusion, whereas carbon dioxide leaves the soil by the same mechanism.

Figure 27 shows that at the depth of 5 cm, the oxygen concentrations decreased and carbon dioxide increased rapidly and quite substantially at the depth of about 5 cm during the 12 hour period of simulation. From the depth of 5 cm towards the soil surface, oxygen concentration increased and carbon dioxide concentration decreased rapidly, to reach the concentrations of air at the soil surface. The oxygen concentration from 5 cm to the deeper layers increased slowly to the initial concentration in the soil profile, whereas the opposite occurred with the carbon dioxide concentration.

Figure 28 shows the changes in concentrations during a period with more constant conditions. Oxygen concentrations continued to decrease, and carbon dioxide concentrations continued to increase, throughout the soil profile from 24 to 48 hours and again from 48 to 72 hours. These continued decreases in oxygen concentrations and increases in carbon dioxide concentrations were the results of continued growth of roots. Root length was 2 cm at 0 hours, but increased from 11.6 at 24 hours to 21.2 cm at 48 hours and to 30.8 cm

at 72 hours. In this simulation, the rate of oxygen consumption was the same over the entire root length if the oxygen concentration is constant along the root. Thus, oxygen was depleted more and more from deeper soil depths. Since the total consumption capacity of roots also continued to increase, the minimum concentration continued to decrease.

Figure 29 shows the consequences of rainfall. The minimum concentration of oxygen decreased and the maximum concentration of carbon dioxide increased dramatically as a result of the increase in water content. At 76 hours the concentration profile was very similar to that at 72 hours. Then, from 76 to 88 hours, the minimum concentration of oxygen decreased to  $35 \mu\text{g cm}^{-3}$  at the depth of 10 cm. This rapid decrease occurred because rainwater decreased the soil air-filled pore spaces available for the diffusion of oxygen from the atmosphere to supply the respiring roots. At the same time the concentration of carbon dioxide increased rapidly for the same reason.

Rates of Oxygen Consumption by Roots and Microorganisms. The rates of oxygen consumption by roots and microorganisms used in the simulations are shown in Figures 30, 31, and 32. Each figure shows the rate of oxygen consumption in  $\mu\text{g cm}^{-3} \text{ soil hr}^{-1}$ . The rate of oxygen consumption by roots was converted from  $\mu\text{g cm}^{-3} \text{ fresh roots hr}^{-1}$  to  $\mu\text{g cm}^{-3} \text{ soil hr}^{-1}$  (Appendix III), as was required by the unit used in the oxygen field equation.

The rate of root elongation is a function of time. The initial root length was 2 cm and reached 50 cm at the end of the simulation (120 hours). Figures 30, 31, and 32 show the sequence of the change

in oxygen use as a function of soil depth and time. For this simulation, the rate of oxygen consumption by the roots is constant along the entire root length. However, the rate was a function of soil oxygen concentration as shown on the figures.

The rate of oxygen use by microorganisms was chosen to be a function of soil oxygen concentration. Soil microorganisms were assumed to be uniformly distributed from the soil surface down to the depth of 20 cm. The large decreases in the rates of oxygen use from 76 through 96 hours at the depth of 20 cm shown in Figure 32 were due to a rapid decrease in oxygen concentrations (Figure 29).

### Conclusions

This simulation shows that the transport of oxygen and carbon dioxide through soil was strongly dependent on soil water content and the respiratory activities of roots and soil microorganisms. Soil water governed the soil air content and distribution and arrangement of air spaces in the soil, thereby affecting the transport of oxygen and carbon dioxide through soil. When water infiltrated into the soil, the oxygen and carbon dioxide in the soil pores were squeezed out of the soil and left less spaces for the transport of oxygen and carbon dioxide. This results in the decrease of soil oxygen content. On the other hand, when water evaporated out of the soil, more soil pore spaces are available for the transport of oxygen and carbon dioxide in the soil. This results in the increase of oxygen supply from the atmosphere to the soil as was discussed above. Root growth is assumed to be a function of time in this simulation. The rate of

oxygen consumption was the same over the entire root length if the oxygen concentration was constant along the root. As a results, the oxygen was depleted more and more from the deeper depths. Since the total consumption capacity of roots also continue to increase, the minimum concentration continue to increase. The opposite was true for carbon dioxide.

This simulation should be repeated with the conditions, where the rate of root elongation is a function of soil oxygen concentration in addition to be a function of time, and where the maximum rate of consumption of oxygen remains constant at the root tip but decreases along the roots starting from root tips to its base in addition to be a function of soil oxygen concentration.

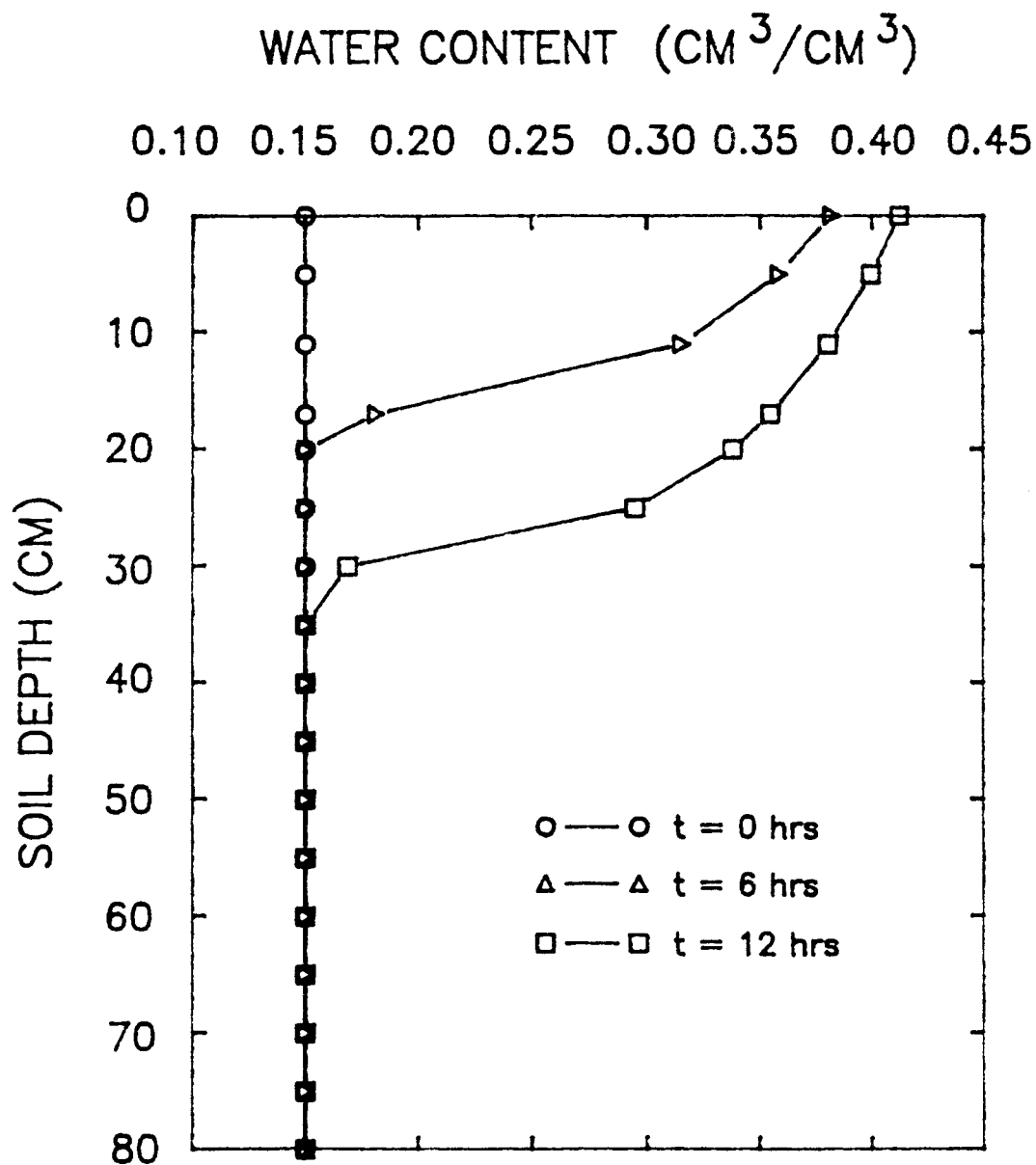


Figure 14. Water content as a function of soil depth at 0, 6, and 12 hours. Rain fell during this period at the rate of  $0.5 \text{ cm hr}^{-1}$ . The rainfall started at 0 hours and stopped at 12 hours. The initial soil water content was  $0.15 \text{ cm}^3 \text{ cm}^{-3}$ .

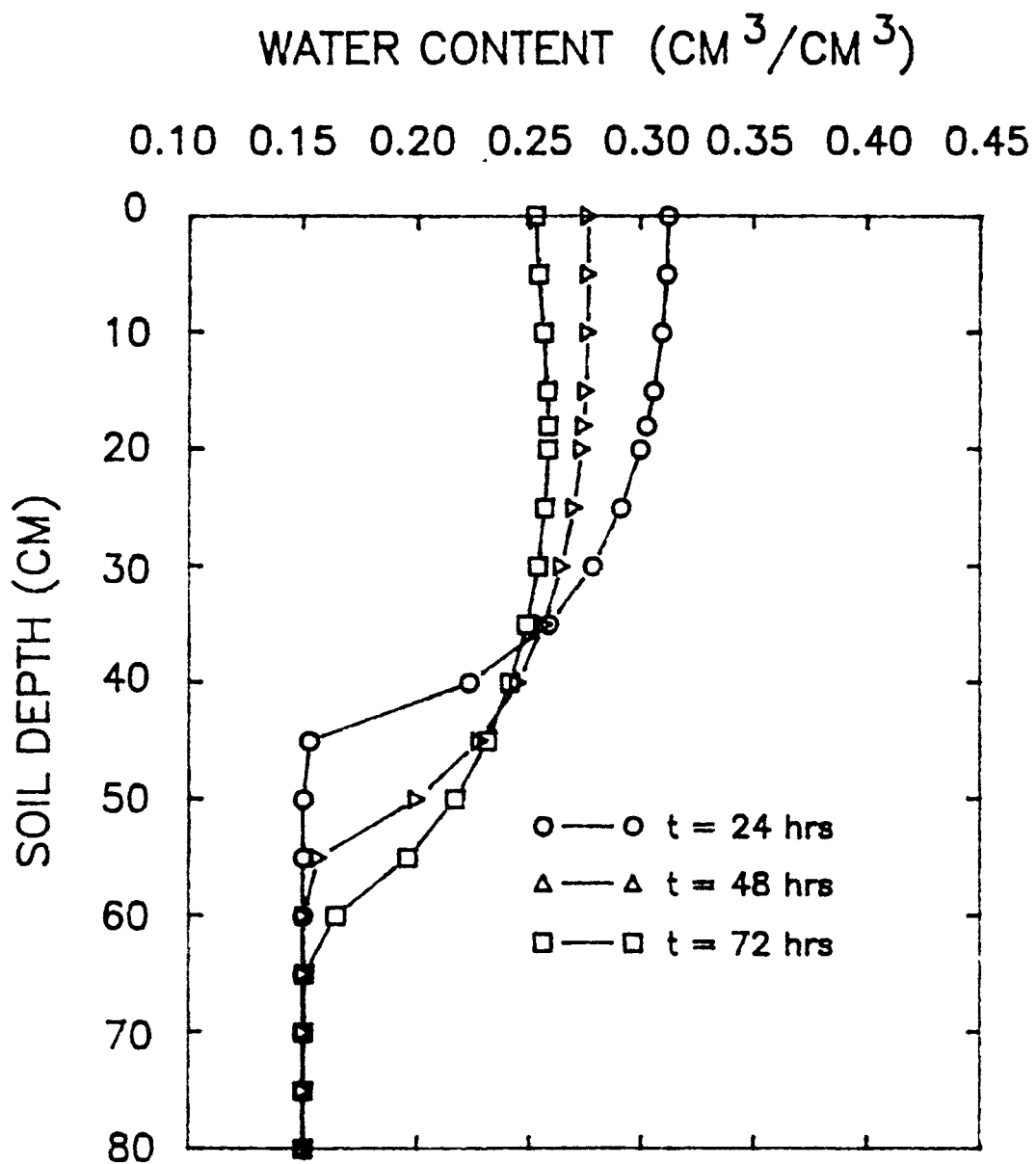


Figure 15. Water content as a function of soil depth at 24, 48, and 72 hours since start. Evaporation and redistribution processes occurred during this period.

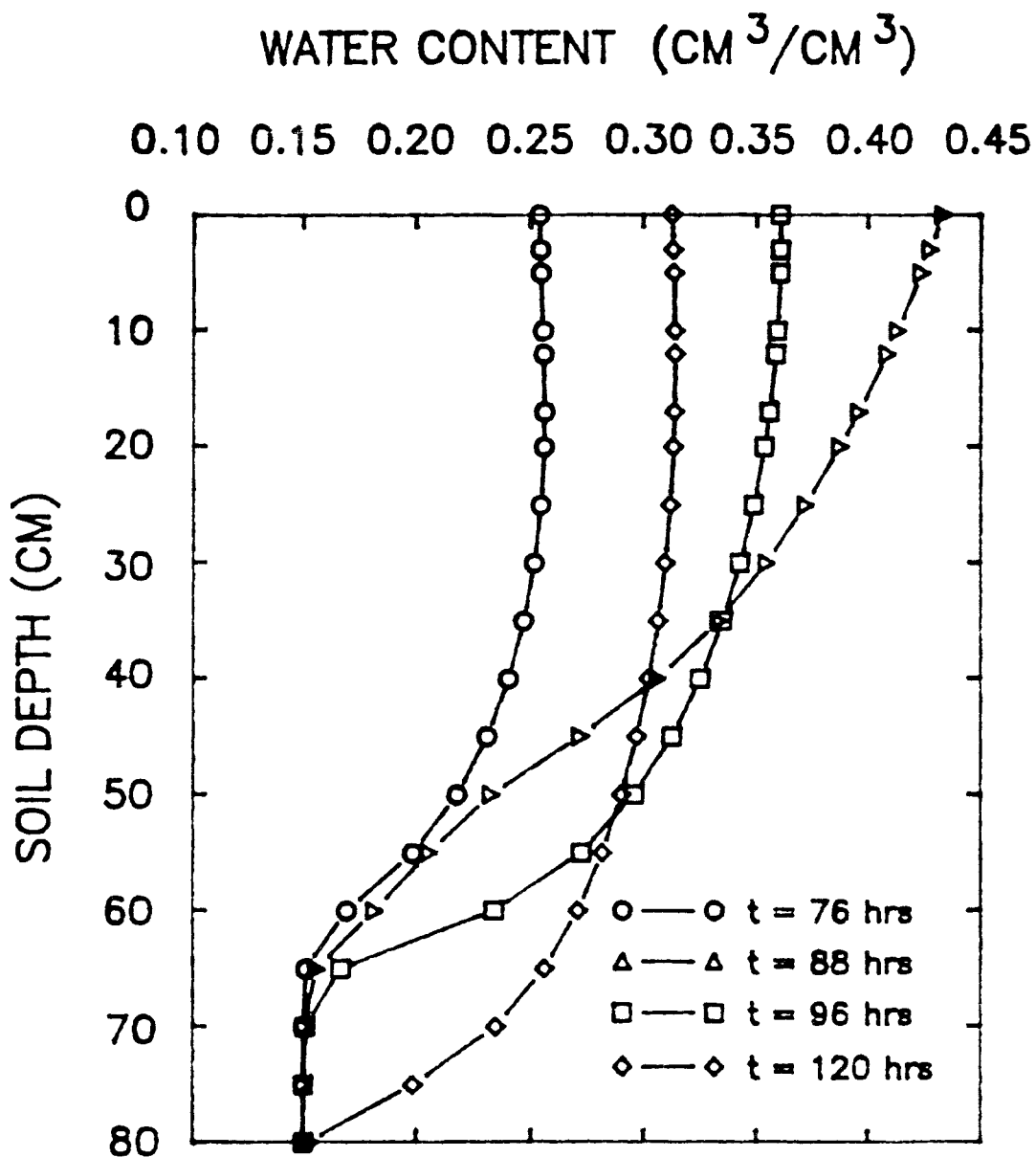


Figure 16. Water content as a function of soil depth at 76, 88, 96, and 120 hours since start. Rainfall started at 76 hours and stopped at 88 hours. The rainfall rate was  $0.5 \text{ cm hr}^{-1}$ . During the period from 88 hours to 120 hours, redistribution and evaporation occurred.

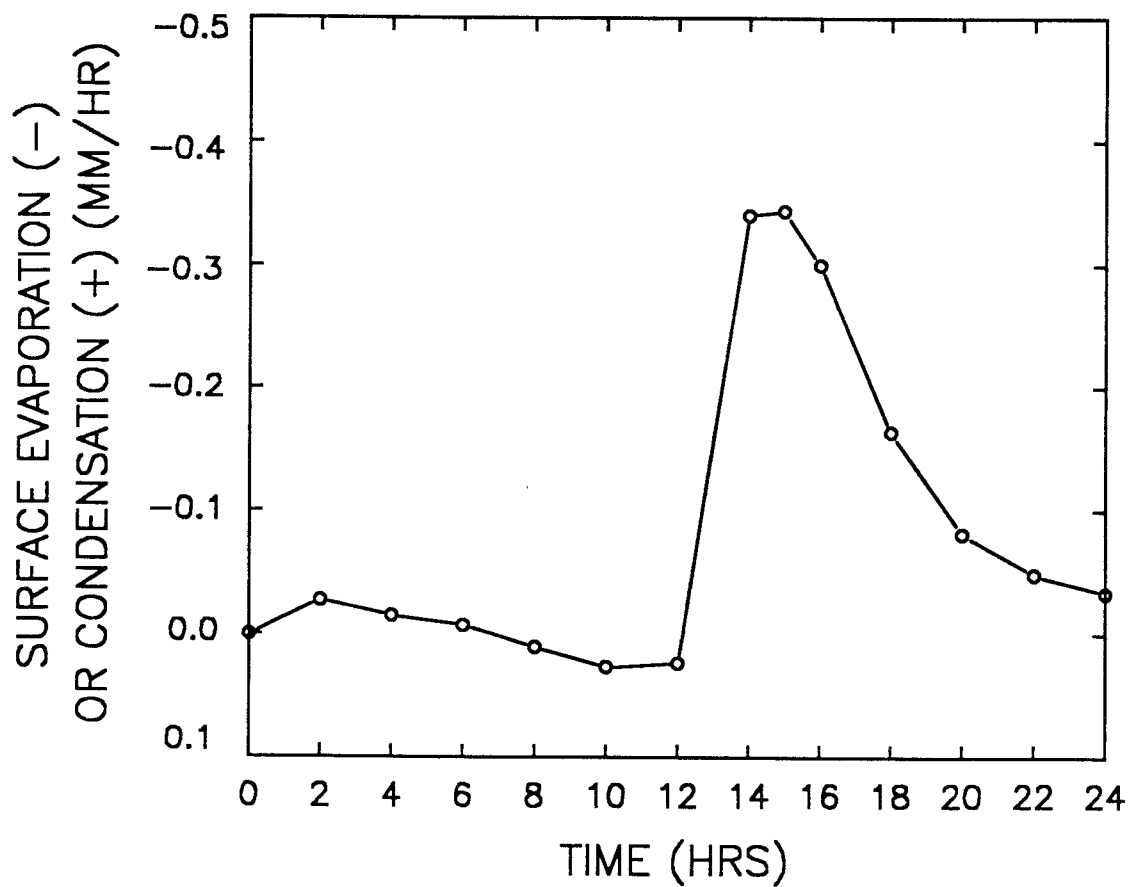


Figure 17. Rate of surface evaporation (-) or condensation (+) of water as a function of time from 0 to 24 hours. Rainfall started at 0 hours and stopped at 12 hours.

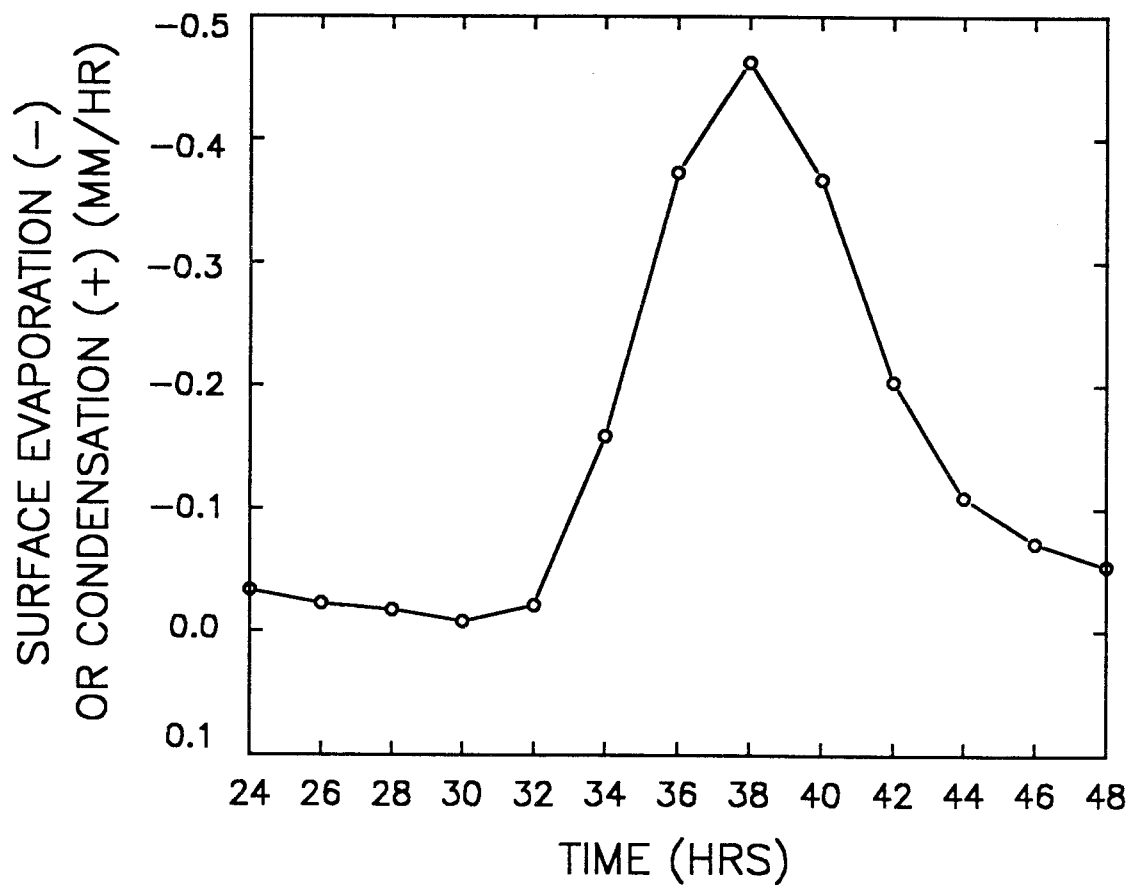


Figure 18. Rate of surface evaporation (-) or condensation (+) of water as a function of time during the period from 24 to 48 hours.

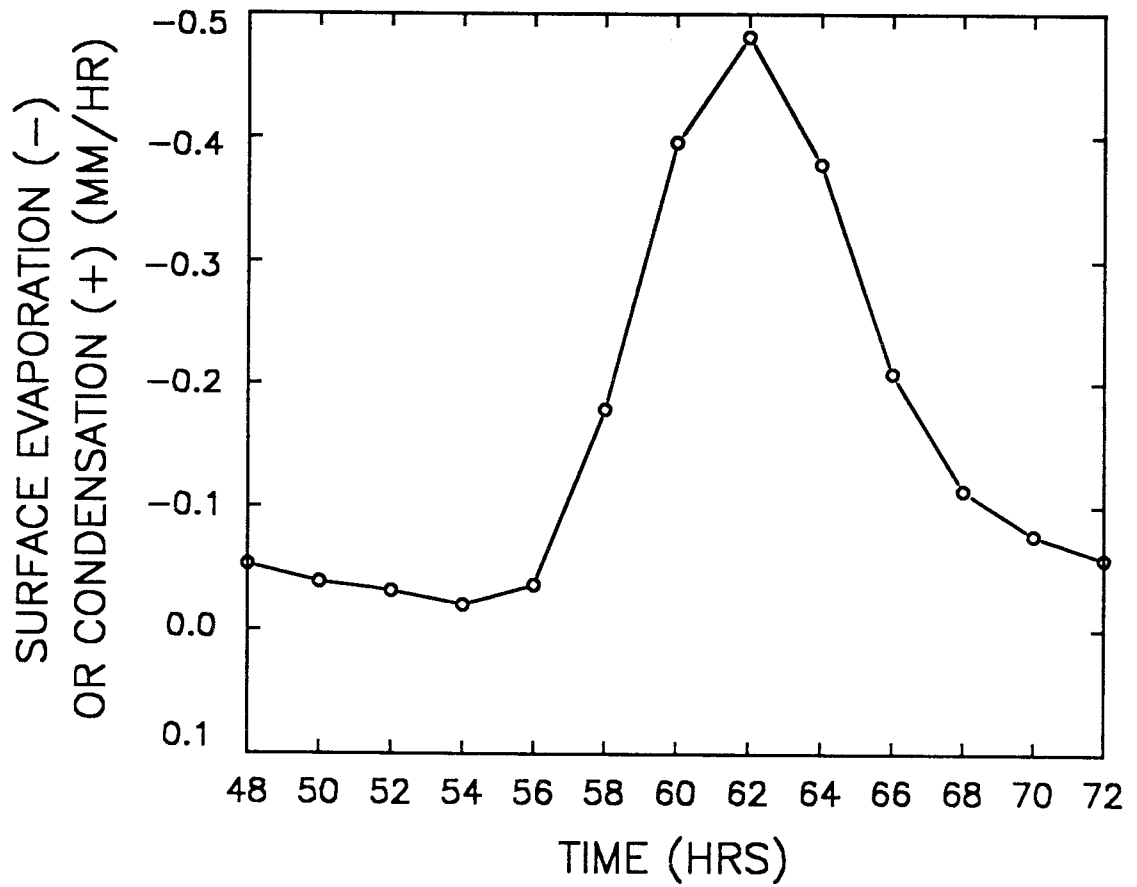


Figure 19. Rate of surface evaporation (-) or condensation (+) of water as a function of time during the period from 48 to 72 hours.

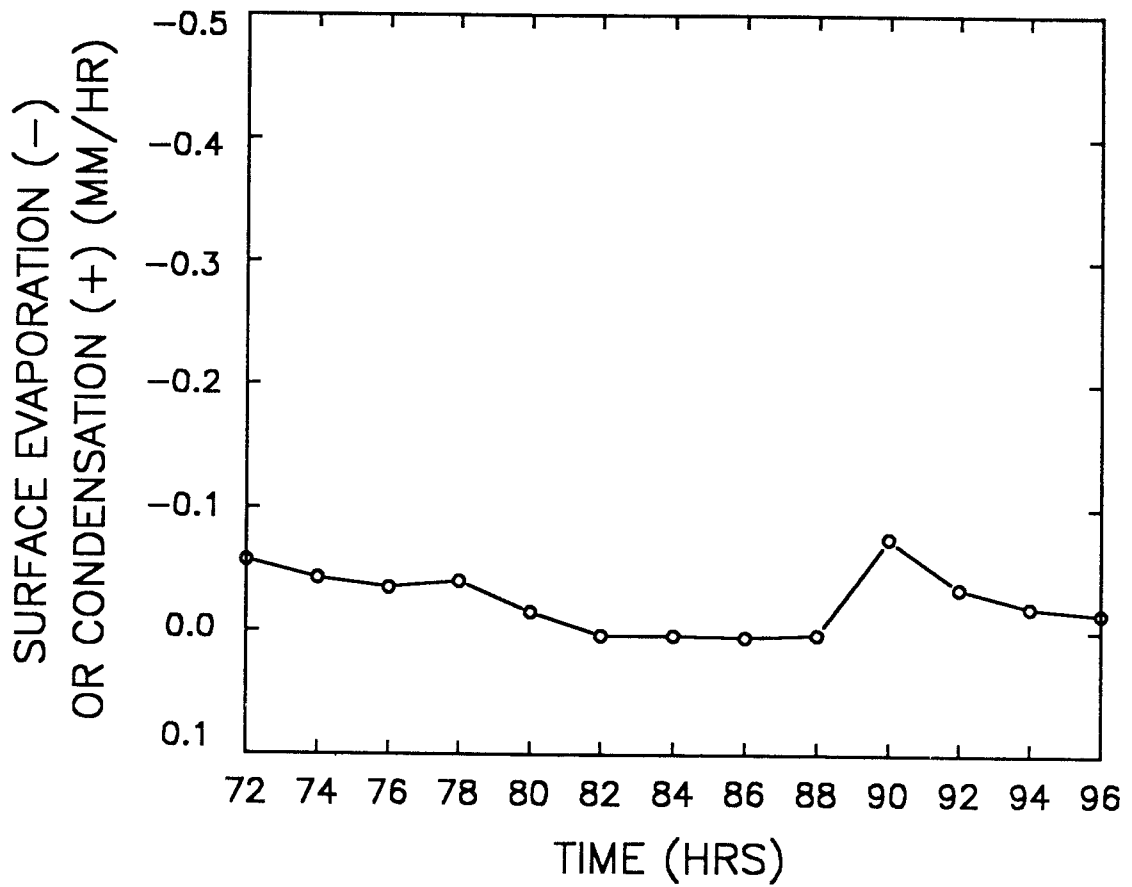


Figure 20. Rate of surface evaporation (-) or condensation (+) of water as a function of time during the period from 72 to 96 hours. Rainfall started at 76 hours and stopped at 88 hours.

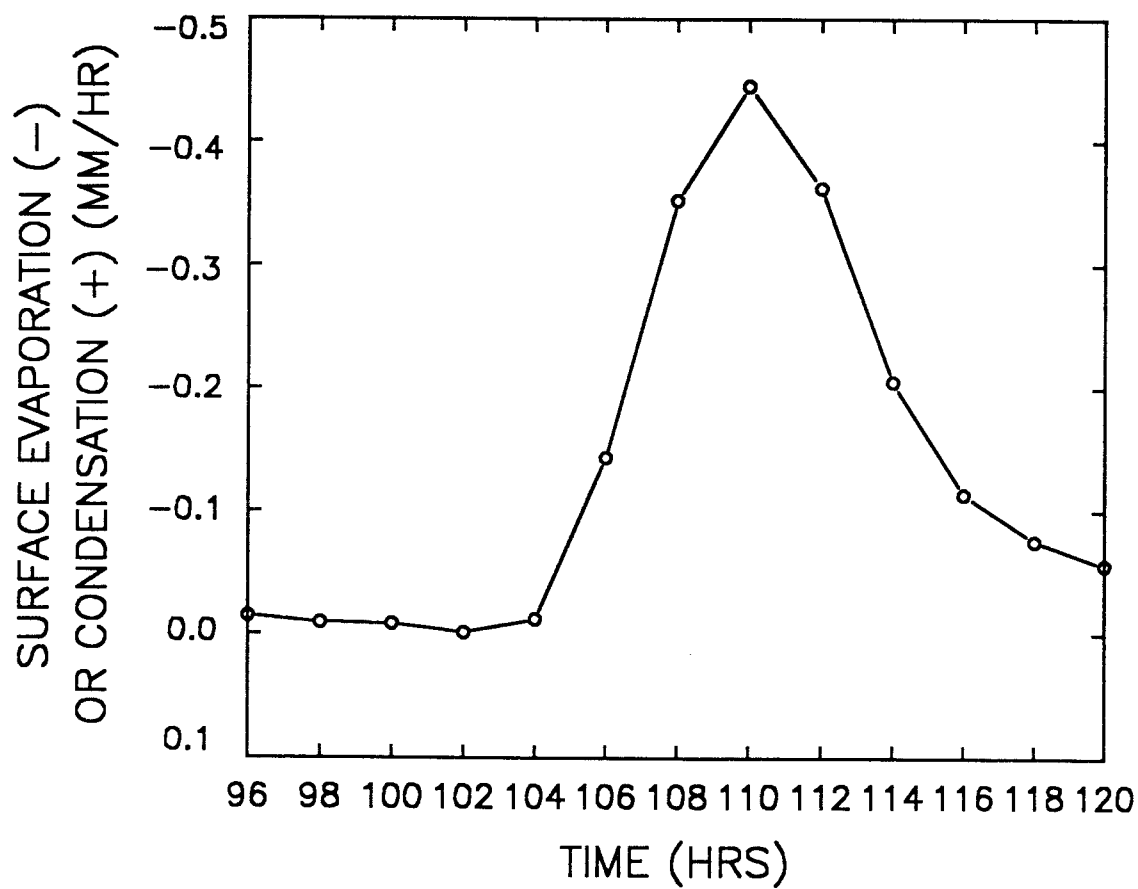


Figure 21. Rate of surface evaporation (-) or condensation (+) of water as a function of time during the period from 96 to 120 hours.

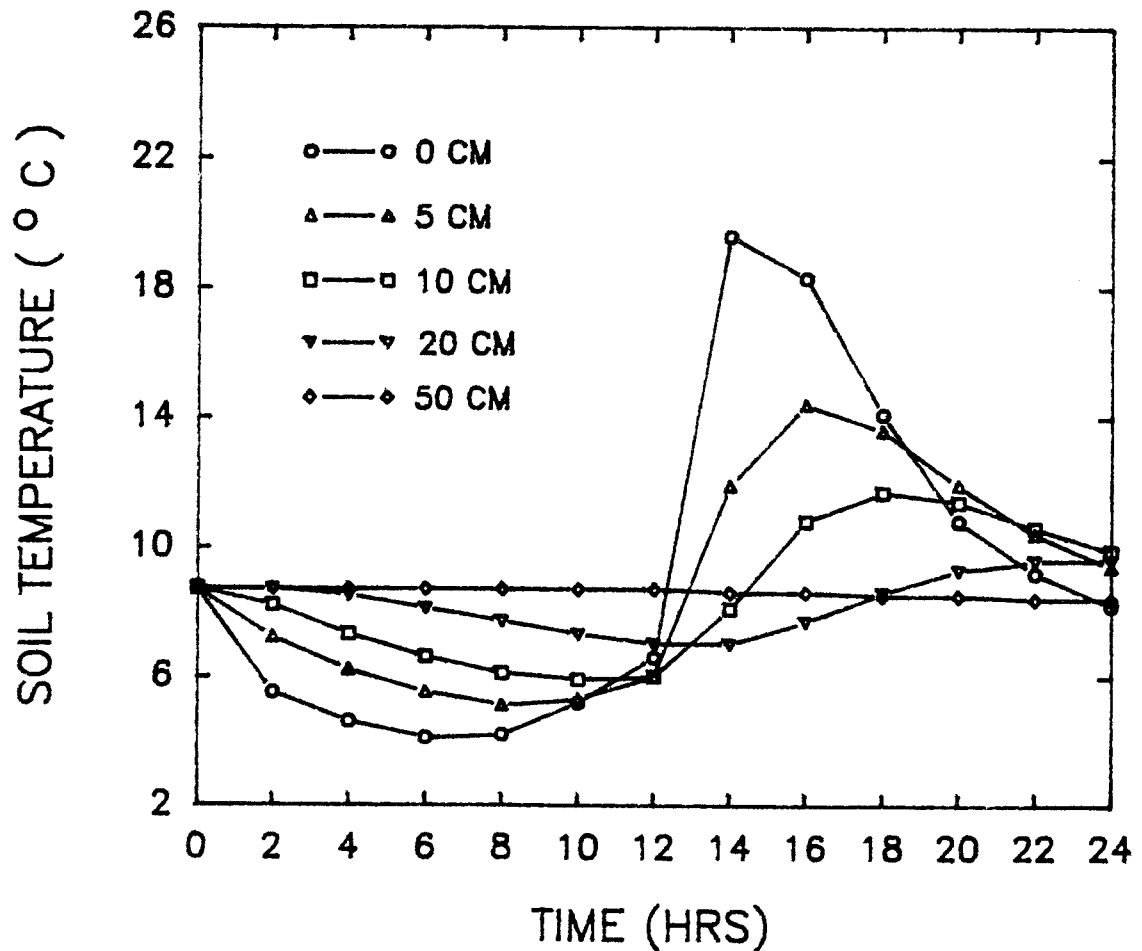


Figure 22. Soil temperature as a function of time at the soil depths of 0, 5, 10, 20, and 50 cm. Initial soil temperature was 8.7 °C. Rainfall started at 0 hours and stopped at 12 hours. Rain water temperature was 4 °C. During the rainy period, the air temperature was assumed to be reduced by 50 percent and solar radiation was assumed to be reduced by 85 percent compared to conditions without rain.

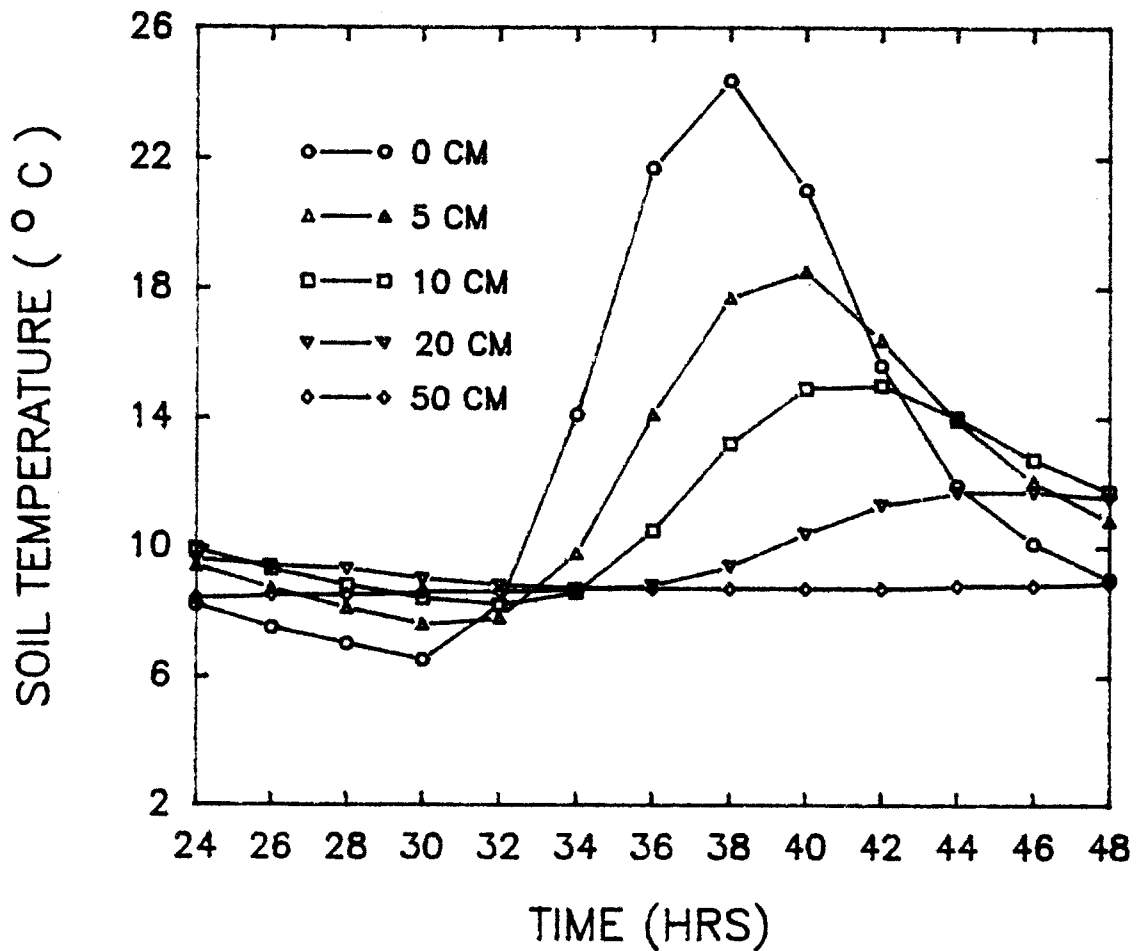


Figure 23. Soil temperature as a function of time at the soil depths of 0, 5, 10, 20, and 50 cm during the period of 24 to 48 hours.

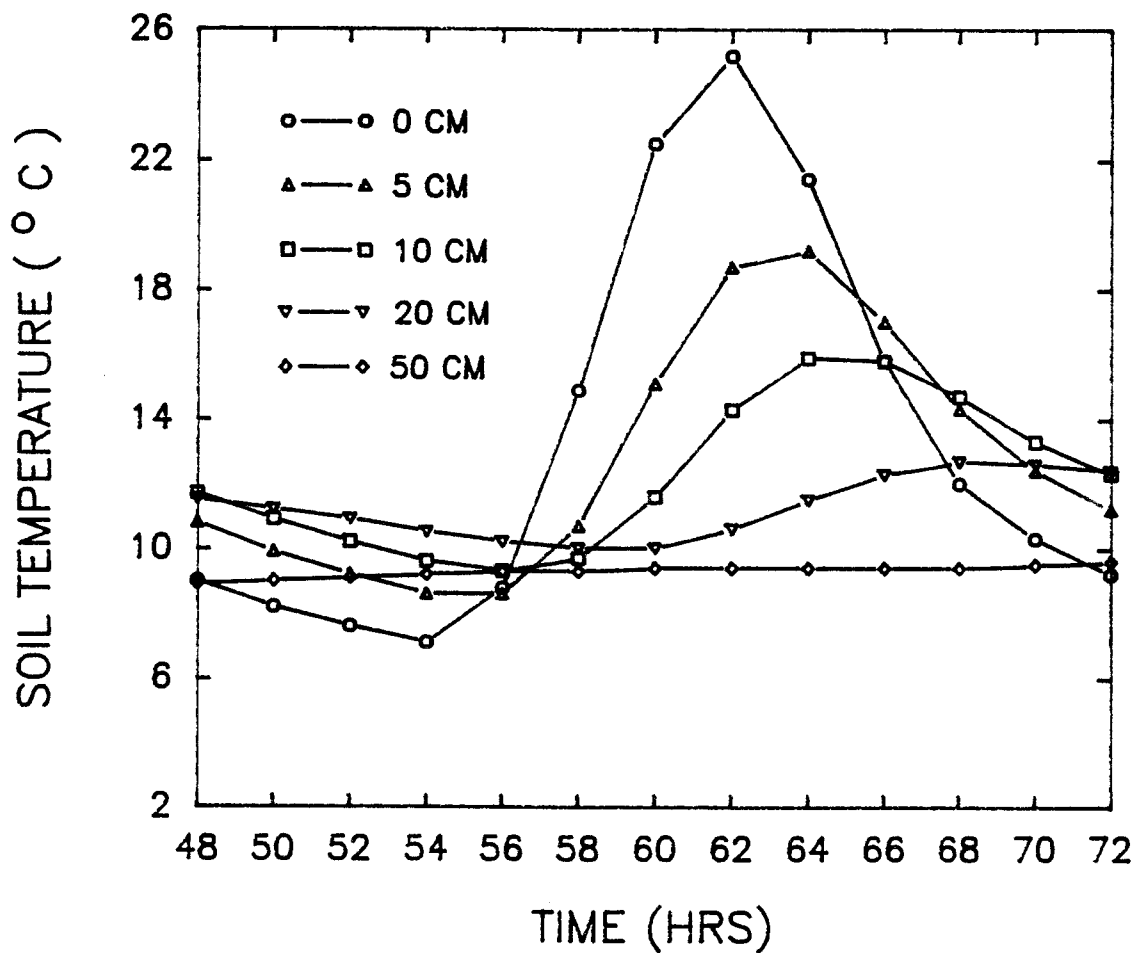


Figure 24. Soil temperature as a function of time at the soil depths of 0, 5, 10, 20, and 50 cm during the period of 48 to 72 hours.

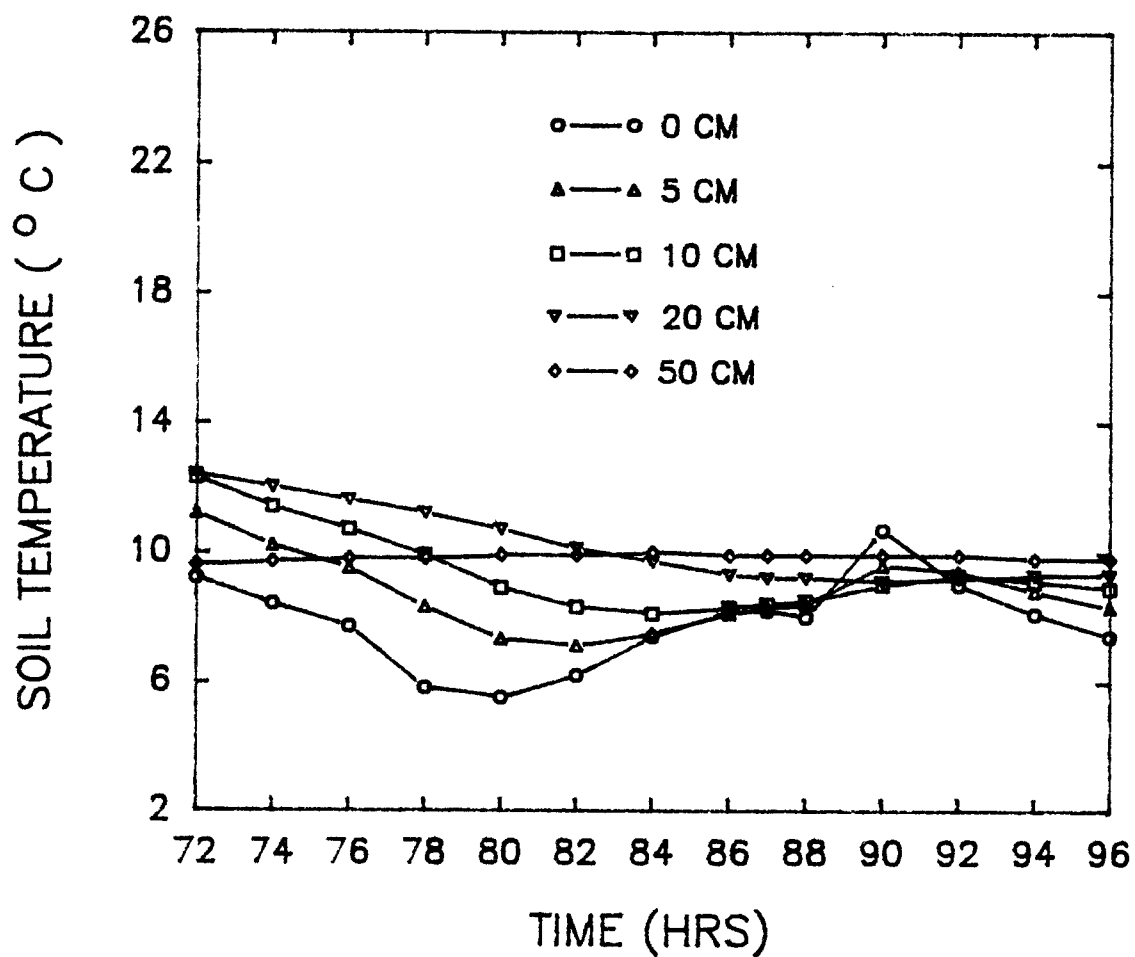


Figure 25. Soil temperature as a function of time at the soil depths of 0, 5, 10, 20, and 50 cm during the period of 72 to 96 hours. Rainfall started at 76 hour and ended at 88 hours. Conditions were the same as during the first rain shown in Figure 22.

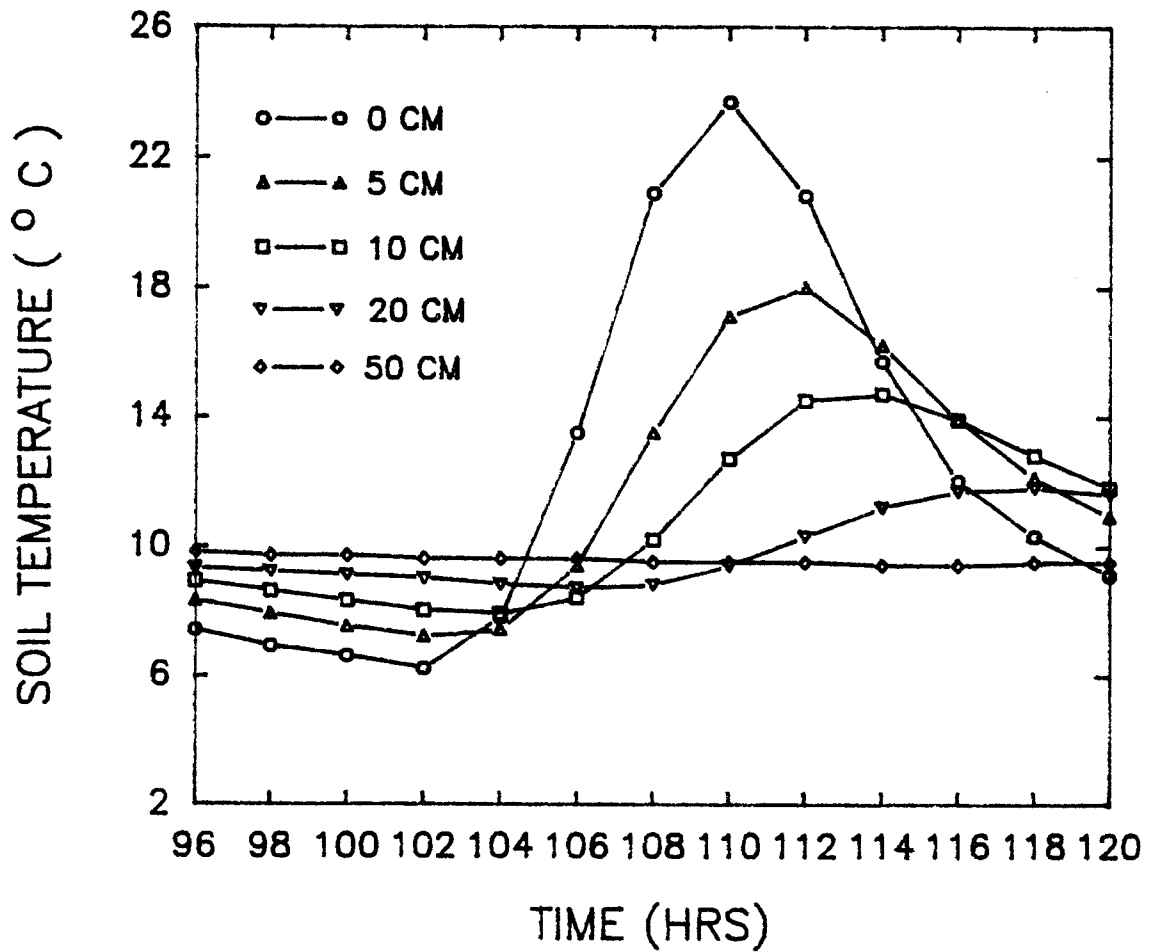


Figure 26. Soil temperature as a function of time at the soil depths of 0, 5, 10, 20, and 50 cm during the period from 96 to 120 hours.

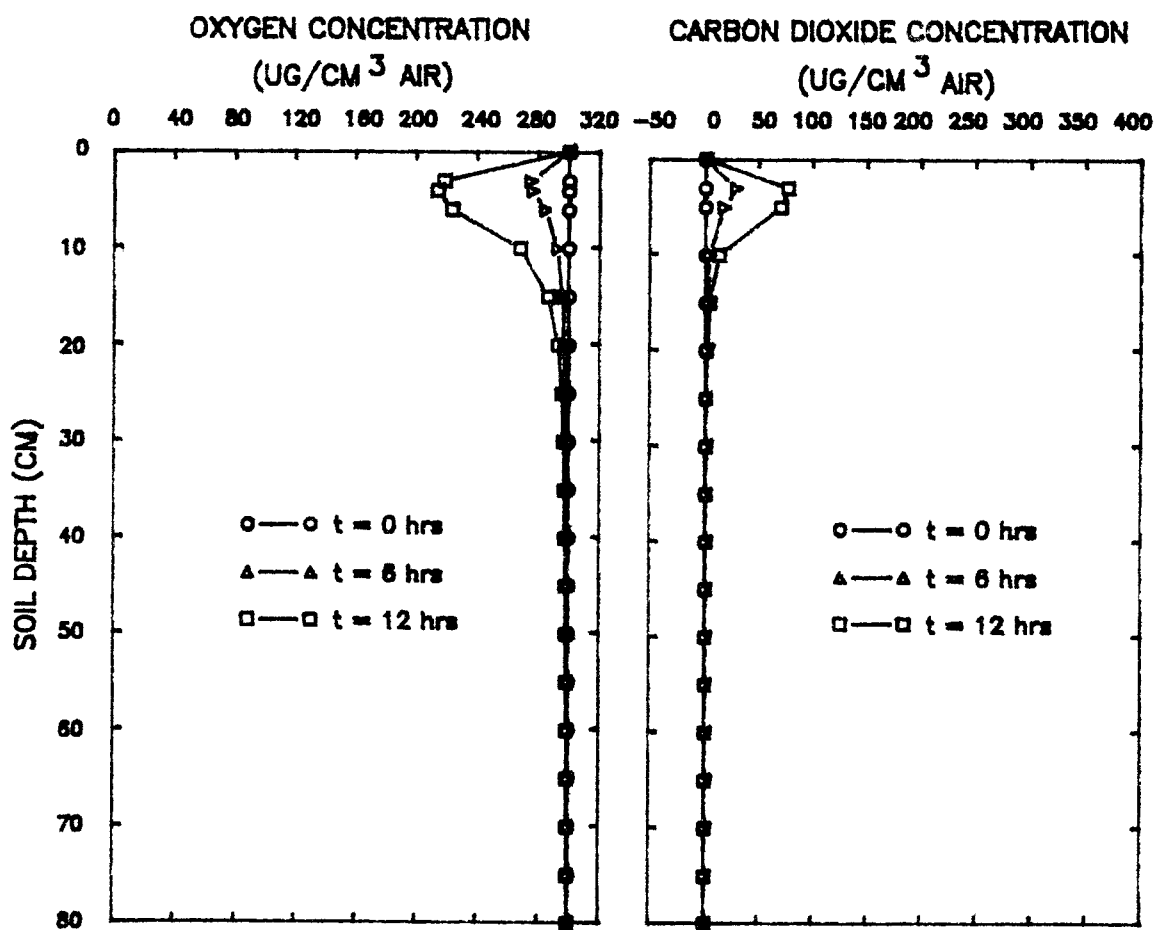


Figure 27. Oxygen and carbon dioxide concentrations as a function of soil depth at 0, 6, and 12 hours since start. The rainfall started at 0 hours and stopped at 12 hours.

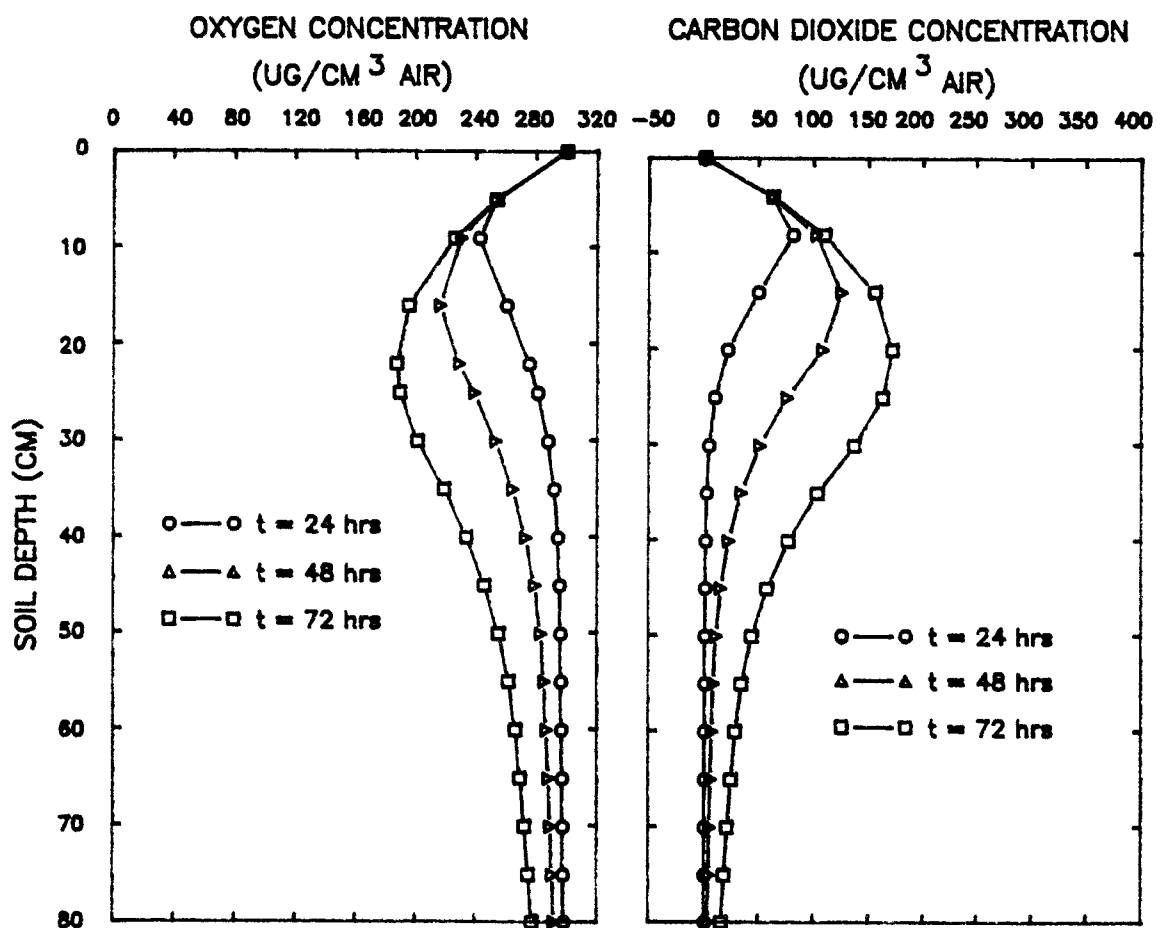


Figure 28. Oxygen and carbon dioxide concentrations as a function of soil depth at 24, 48, and 72 hours since start.

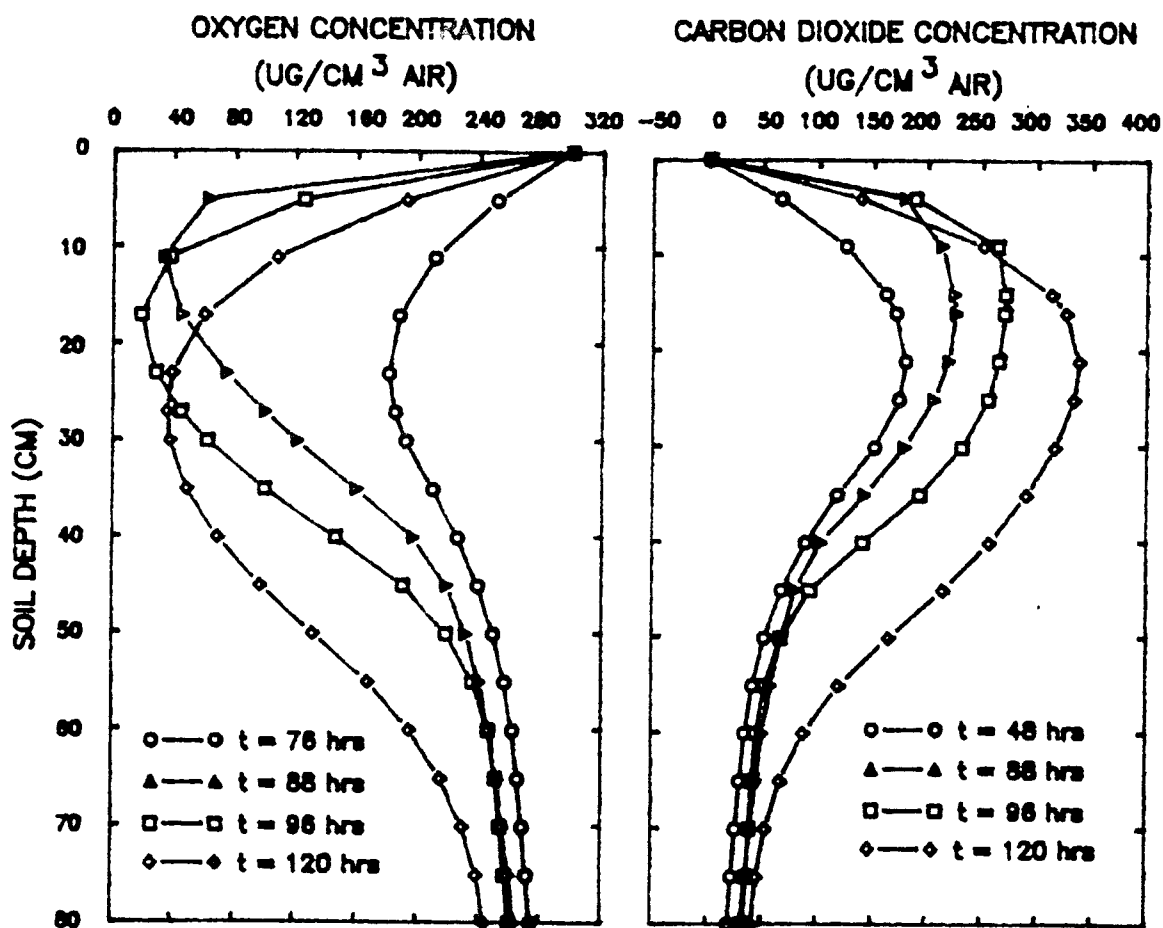


Figure 29. Oxygen and carbon dioxide concentrations as a function of soil depth at 76, 88, 96, and 120 hours since start. Rainfall, evaporation, and redistribution occurred during the period. The rainfall started at 76 hours and stopped at 88 hours.

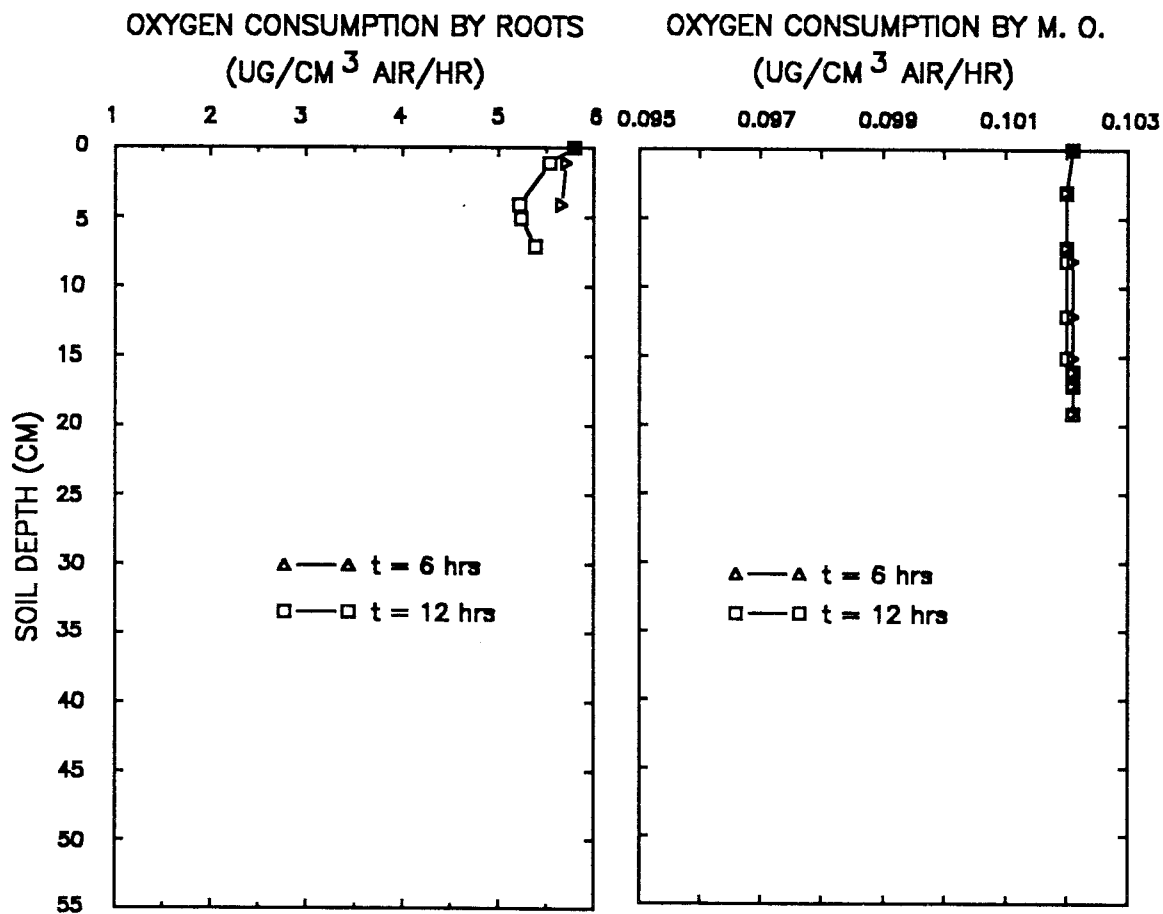


Figure 30. Oxygen consumption rates by plant roots and soil microorganisms as a function of soil depth at times of 6 and 12 hours. The rate of oxygen consumption in  $\mu\text{g cm}^{-3}$  fresh roots  $\text{hr}^{-1}$  was converted to  $\mu\text{g cm}^{-3}$  air  $\text{hr}^{-1}$  as shown on the Figure.

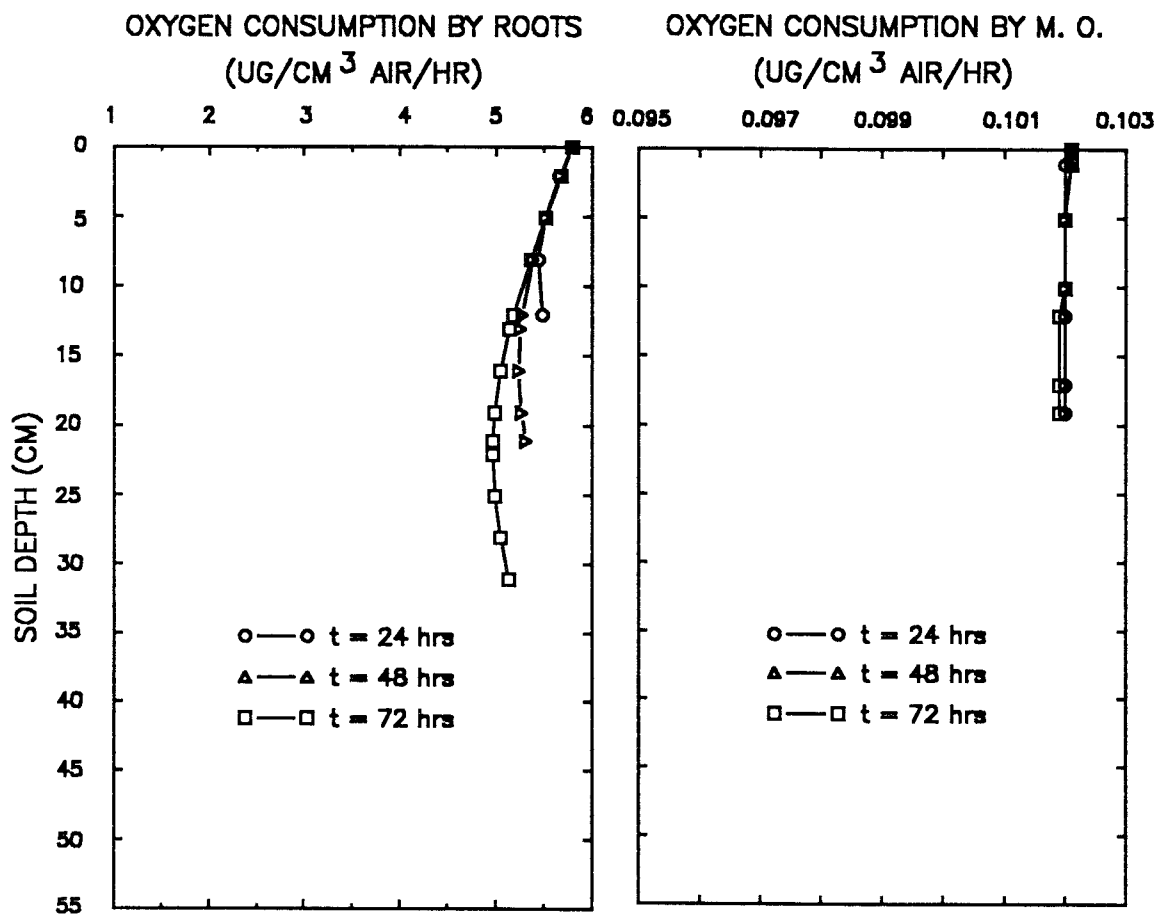


Figure 31. Oxygen consumption rates by plant roots and soil microorganisms as a function of soil depth at times of 24, 48, and 72 hours. The rate of oxygen consumption in  $\mu\text{g cm}^{-3}$  fresh roots  $\text{hr}^{-1}$  was converted to  $\mu\text{g cm}^{-3}$  air  $\text{hr}^{-1}$  as shown on the Figure.

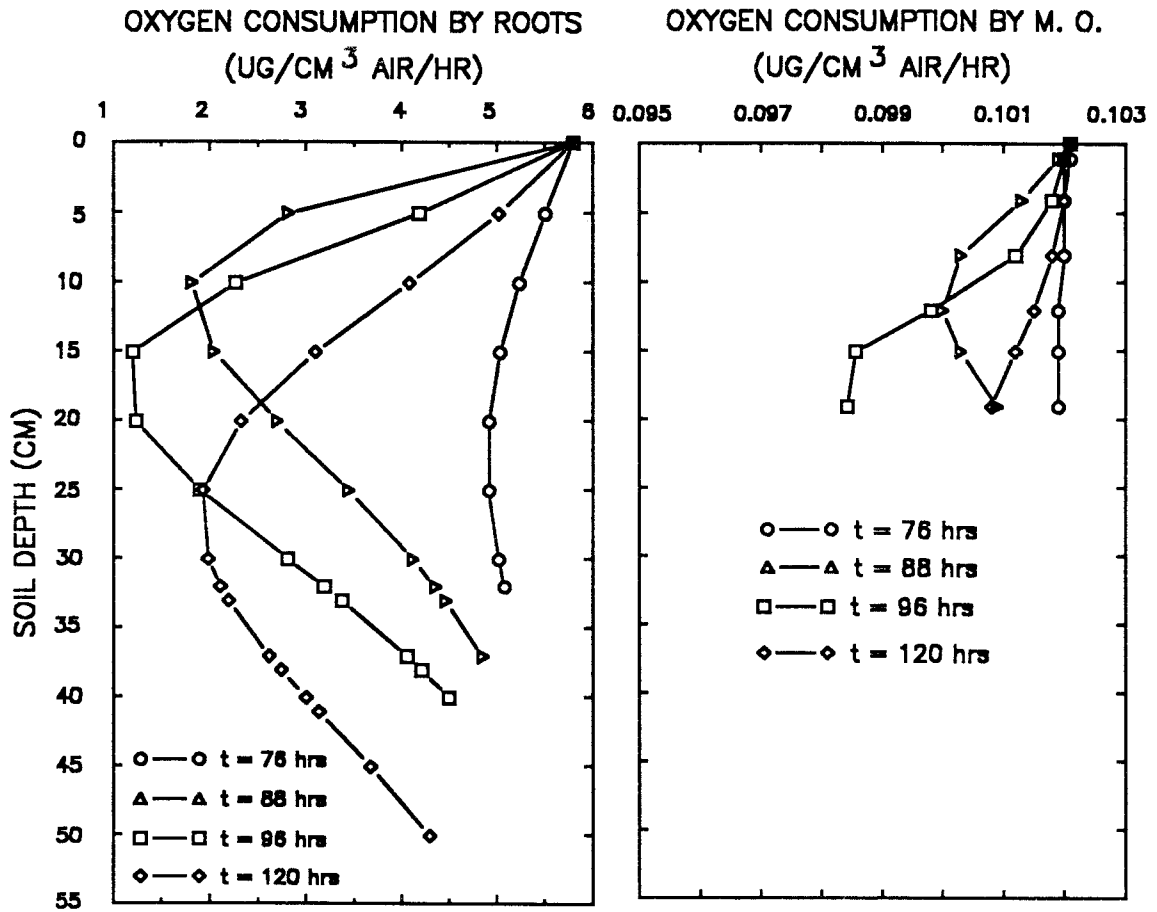


Figure 32. Oxygen consumption rates by plant roots and soil microorganisms as a function of soil depth at times of 76, 88, 96, and 120 hours. The rate of oxygen consumption in  $\mu\text{g cm}^{-3}$  fresh roots  $\text{hr}^{-1}$  was converted to  $\mu\text{g cm}^{-3}$  air  $\text{hr}^{-1}$  as was shown on the Figure.

Example 2aStatement of the Problem

This example differs from the first example in the use of different functions for the root elongation and the rate of root oxygen consumption. The root elongation was chosen to depend on soil oxygen concentration, in addition to being proportional to time. The rate of oxygen consumption by roots was assumed to be a function of root age, in addition to being a function of soil oxygen concentration. Since the rate of carbon dioxide production by roots was calculated from the rate of oxygen consumption, using the definition of the respiratory quotient, i.e.  $RQ = 1$ , the rate of carbon dioxide production was also a function of root age.

Input Parameters

All input parameters were the same as in Example 1 except the parameters for biological activities. These changes are discussed as follows.

Root Elongation. In this simulation, the root elongation was chosen to be a function of time and of soil oxygen concentration. It was assumed that, when the soil is well aerated, the root elongation is only a function of time. The root elongation for this condition is given by equation (145) and is shown in Figure 33:

$$L = L_0 + a_1 t, \quad (145)$$

where  $L$  is the root length (cm),  $L_0$  is the initial root length (2 cm),  $a_1$  is the constant characterizing the root elongation characteristics ( $0.4 \text{ cm hr}^{-1}$ ), and  $t$  is the time (hr).

When the soil is not fully aerated, the root elongation is also a function of soil oxygen concentration. This implies that a factor is needed to correct equation (145) to account for the effects of soil oxygen concentration on the root elongation. It was assumed that, when the soil is well aerated, the correction factor equals to unity, which means that the root elongation is only a function of time. When the soil is not fully aerated, the correction factor decreases as soil oxygen concentration decreases. A logistic function was chosen to define the correction factor for the soil oxygen concentration (Figure 34) as follows:

$$F_1 = \frac{A_1}{1 + B_1 \text{ EXP} \left[ -C_1 (C_{\text{o}_2}^{\text{tip}} - C_{\text{o}_2}^{\text{th}}) \right]}, \quad (146)$$

where  $F_1$  is the correction factor,  $A_1$ ,  $B_1$ , and  $C_1$  are constants characterizing the shape of the equation with  $A_1 = 1$ ,  $B_1 = 200$ , and  $C_1 = 0.04$ ,  $C_{\text{o}_2}^{\text{tip}}$  is the soil oxygen concentration at the root tip ( $\mu\text{g cm}^{-3}$  air), and  $C_{\text{o}_2}^{\text{th}}$  is the threshold soil oxygen concentration below which the root elongation rate approaches zero ( $50 \mu\text{g cm}^{-3}$  air). Multiplying equation (145) and equation (146) yields:

$$L(t, \text{o}_2) = [L_0 + a_1 t] F_1, \quad (147)$$

where  $L(t, \text{o}_2)$  represents the root elongation as a function of time and of soil oxygen concentration.

Rate of Oxygen Consumption By Roots. In this simulation, the rate of oxygen consumption by roots was chosen to be a function of soil oxygen concentration and of root age. The rate of oxygen consumption by roots as a function of soil oxygen concentration was represented by the logistic function (Figure 35):

$$SRT(i) = \frac{A2}{1 + B2 \text{ EXP} \left[ -C2(C_{o_2}^i - C_{o_2}^{th}) \right]}, \quad (148)$$

where  $SRT(i)$  is the root oxygen consumption rate by the  $i^{\text{th}}$  section of root length converted to  $\mu\text{g cm}^{-3}$  soil  $\text{hr}^{-1}$ ,  $A2$ ,  $B2$ , and  $C2$  are constants characterizing the shape of the equation with  $A2 = 8$ ,  $B2 = 200$ , and  $C2 = 0.04$ ,  $C_{o_2}^i$  is the soil oxygen concentration in the  $i^{\text{th}}$  section of soil depth corresponding to the  $i^{\text{th}}$  section of root length ( $\mu\text{g cm}^{-3}$  soil air), and  $C_{o_2}^{th}$  is the threshold soil oxygen concentration below which the root oxygen consumption rate approaches zero ( $50 \mu\text{g cm}^{-3}$  air).

Equation (148) implies that the rate of oxygen consumption is the same along the root length when the soil oxygen concentration is constant. This is not true for root respiratory characteristics. The rate of oxygen consumption decreases exponentially with the root length from the root tip to root base (Lemon, 1962). A correction factor to account for these changes was introduced by assuming that the correction factor at the root tip is unity and that it decreases exponentially with the root length, starting at the root tip. The following equation was proposed (Figure 36):

$$F3 = A3 \text{ EXP}(-B3*L) + C3, \quad (149)$$

where F3 is the correction factor, A3, B3, and C3 are constants characterizing the shape of the equation with A3 = 0.9, B3 = 0.5, and C3 = 0.1, and L is the root length (cm).

Multiplying equation (148) and equation (149) obtains:

$$\text{SRT}(\text{co}_2, i) = \frac{A2}{1 + B2 \text{EXP}[-C2(C_{\text{o}_2}^i - C_{\text{o}_2}^{\text{th}})]} F3, \quad (150)$$

where SRT(co<sub>2</sub>, i) represents the rate of oxygen consumption by roots as functions of soil oxygen concentration and of the root length.

The choice of the logistic function to describe the rate of oxygen consumption by the roots as a function of soil oxygen concentration was based on the consideration that this function represents changes in the rate of oxygen consumption at low oxygen concentration. When the soil oxygen concentration falls below a certain level (50 μg cm<sup>-3</sup> air in this example), the rate of oxygen consumption approaches zero. This approach describes respiratory characteristics of roots in soil (Lemon and Wiegand, 1962).

Rate of Oxygen Consumption by Soil Microorganisms. The rate of oxygen consumption by soil microorganisms was set to be five times larger than it was in Example 1. The oxygen saturation constant for microbial decay, K<sub>O</sub>, (equation (130)) was chosen to be 150 μg cm<sup>-3</sup> air.

## Discussion of Simulation Results

Concentrations of Oxygen and Carbon Dioxide. Changes in oxygen and carbon dioxide concentrations are shown in Figures 37, 38, and 39. Each Figure shows the concentrations of the two gases side by side at several times since the start of simulation. The oxygen is depleted by respiration by roots and microorganisms, and the carbon dioxide is released as a result. Figure 37 shows that oxygen concentrations decreased and carbon dioxide concentrations increased rapidly. The lowest oxygen concentration was at 4.5 cm and the highest carbon dioxide concentration was at 4.0 cm at 12 hours.

Figure 38 shows that oxygen concentrations continued to decrease throughout the soil profile from 24 hours to 48 hours and again from 48 hours to 72 hours, whereas carbon dioxide concentrations continued to increase during these periods. This continued decrease in oxygen concentration and increase in carbon dioxide was the result of continued growth of roots. Root length was 2 cm at 0 hours, but increased from 9.1 cm at 24 hours to 18.1 cm at 48 hours and to 27.1 cm at 72 hours. In this simulation, the maximum rate of oxygen consumption remained close to the root tip, and decreased along the roots starting from root tip. As a result, the minimum oxygen concentration and the maximum carbon dioxide concentration existed close to the root tip.

Figure 39 shows conditions where the minimum concentration of oxygen decreased dramatically as a result of the occurrence of rainfall. At 76 hours the concentration profile was very similar to that at 72 hours. Then, from 76 to 88 hours, the minimum concentration of

oxygen decreased from 232 to 179  $\mu\text{g cm}^{-3}$  air. This occurred because rainwater decreased the soil air-filled pore spaces available for the diffusion of oxygen from the atmosphere to supply the respiring roots.

Figure 40 shows soil depth, where the minimum oxygen concentration occurred, as a function of time since the start of the simulation. The depth where the minimum oxygen concentration occurred moved down dramatically starting at the soil depth of about 4 cm at 12 hours to the depth of about 23 cm at 72 hours due to the continue penetration of root tip into the deeper soil. Then, 76 hours to 88 hours, the depth moved up from about 23 cm to 17 cm as a result of rainfall at that period. Rainwater infiltrated into the soil and replaced the soil air simultaneously, and left less soil pore spaces for the oxygen. As a result, the oxygen concentration at the soil depth is lower. After the rain stop at 88 hours, the depth move down again to about 31 cm at 120 hours. This is so because of the penetration of root tip.

Figures 41 and 42 show oxygen and carbon dioxide concentrations as a function of time at the soil depths of 5, 20, and 40 cm, respectively. The oxygen concentration at 5 cm in Figure 41 decreased dramatically starting from 300  $\mu\text{g cm}^{-3}$  air at 0 hours to about 240  $\mu\text{g cm}^{-3}$  air at 12 hours and increased to about 280  $\mu\text{g cm}^{-3}$  air at 76 hours, and again decreased to about 230  $\mu\text{g cm}^{-3}$  air at 88 hours and increased to about 260  $\mu\text{g cm}^{-3}$  air at 120 hours. Such decreases in oxygen concentration from 0 to 12 hours and from 76 to 88 hours are the results of rainwater infiltration into the soil. Rainwater did reach the soil depth of 5 cm (Figures 14 and 16) and reduced the soil

air-filled pore spaces for the oxygen diffusion. As a result, the oxygen concentration decreased. After the rain stop, soil water evaporated out of the soil at 5 cm. This left more air-filled pore spaces for the oxygen diffusion. As a result, the oxygen concentration increased. As was shown in Figure 41, the oxygen concentration at 20 cm did not show the pattern as it was at 5 cm. The oxygen concentration decreased gradually from 0 hours to 88 hours. This is so because the soil water content was lower at 20 cm than it was at 5 cm. Therefore more soil pore spaces are available for the oxygen diffusion at 20 cm. However, the oxygen concentration did decrease from 76 to 88 hours and increased from 88 to 120 hours due to the same reason as at 5 cm. The oxygen concentration at 40 cm decreased more gradually from 0 hours to 88 hours indicates the less effect of water content on the oxygen diffusion as compare with that of at 5 and 20 cm.

Similar but opposite results were obtained for carbon dioxide concentration in Figure 42.

Rates of Oxygen Consumption by Roots and Microorganisms. The rates of oxygen consumption by roots and microorganisms are shown in Figures 43, 44, and 45. Each figure shows the rate of oxygen consumption in  $\mu\text{g cm}^{-3}$  air  $\text{hr}^{-1}$ . The rate of oxygen consumption by roots was calculated in the program in  $\mu\text{g cm}^{-3}$  fresh roots  $\text{hr}^{-1}$  and then converted to  $\mu\text{g cm}^{-3}$  air  $\text{hr}^{-1}$  (Appendix III), as was required by the unit used for the oxygen field equation. The sequence of the three diagrams shows the change in oxygen use as a function of soil depth at several times. The growth of the plant roots can be deduced from the diagrams. The roots grew from the 2 cm soil depth at the

start of the simulation to the 40 cm depth at the end of the 120 hour simulation. The population of microorganisms was distributed uniformly from the soil surface down to the depth of 20 cm throughout the simulations. The diagrams clearly show the increased rate of oxygen consumption as a function of distance along the root length. The highest rate is always at the root tip. Since the rate of oxygen consumption also is a function of oxygen concentration, the maximum rate varies according to the oxygen concentration in the soil air. The rate at the root tip was highest with the simulation at 6 hours, namely  $7.7 \mu\text{g cm}^{-3} \text{ soil hr}^{-1}$ , and lowest with the simulation at 96 hours, namely  $4.6 \mu\text{g cm}^{-3} \text{ soil hr}^{-1}$ .

Comparison of Root Length Changes in root length in Example 1 and 2a are shown in Figure 46. This diagram shows root length in the soil profile as a function of time since the start of the simulation. Example 1 assumed that the root elongation was only a function of time. Example 2a assumed that the root elongation was a function of oxygen concentration in addition to being a function of time. Starting with the initial root length of 2 cm in both Example 1 and Example 2a, root elongation is slower in Example 2a than that of Example 1. As the time elapsed, the differences in root length between the examples increased. Root length was 6.8 cm at 12 hours and 50 cm at 120 hours in Example 1 but was 5.1 cm at 12 hours and 40.1 cm at 120 hours in Example 2a. This is so because that the rate of root elongation in Example 2a was assumed to be governed by soil oxygen concentration in addition to being governed by time. As more oxygen was depleted by roots and microorganisms, the rate of root

elongation, which is a function of oxygen concentration, would decrease.

### Conclusions

This simulation points to the problem which needed to be done as concluded in Example 1. Results show that the root elongation and the rate of oxygen consumption by roots are functions of soil oxygen availability, in addition to being functions of time. The maximum rate of oxygen consumption remains close to the root tip, and decreases along the root starting from the root tip. This approach describes respiratory characteristic of roots in soil better than that of Example 1, which assumed that the root elongation was only a function of time. The oxygen and carbon dioxide concentrations were strongly controlled by soil water content. As the rainfall began, the oxygen concentration decreased and carbon dioxide concentration increased dramatically at the soil surface due to the increase of soil water content. After the rain stopped, water evaporated from the soil surface and more soil pore spaces are available for gases diffusion. As a result, the oxygen concentration increased and carbon dioxide concentration decreased.

A further simulation should be conducted by assuming that the root elongation and the rate of oxygen consumption by roots are functions of carbon dioxide concentration instead of oxygen concentration, in addition to being functions of time.

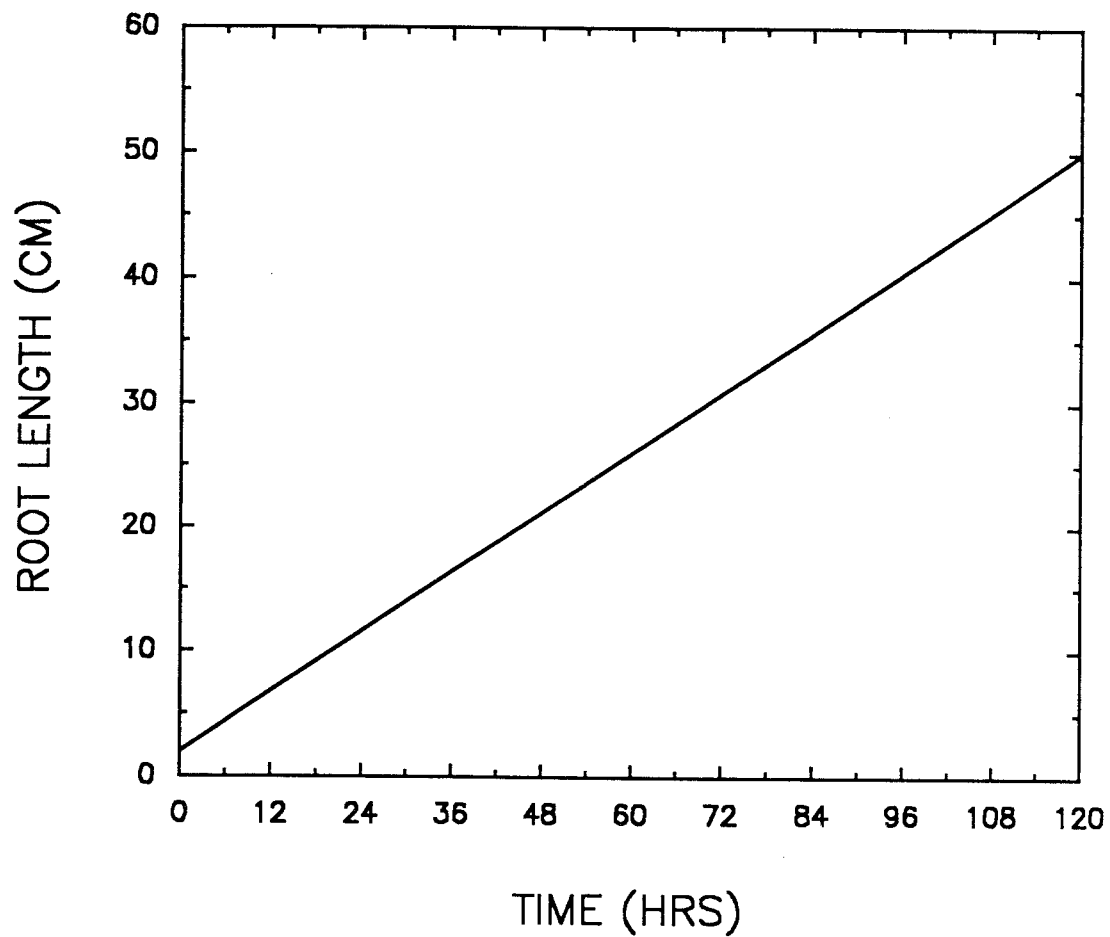


Figure 33. Root length as a function of time calculated from equation (145).

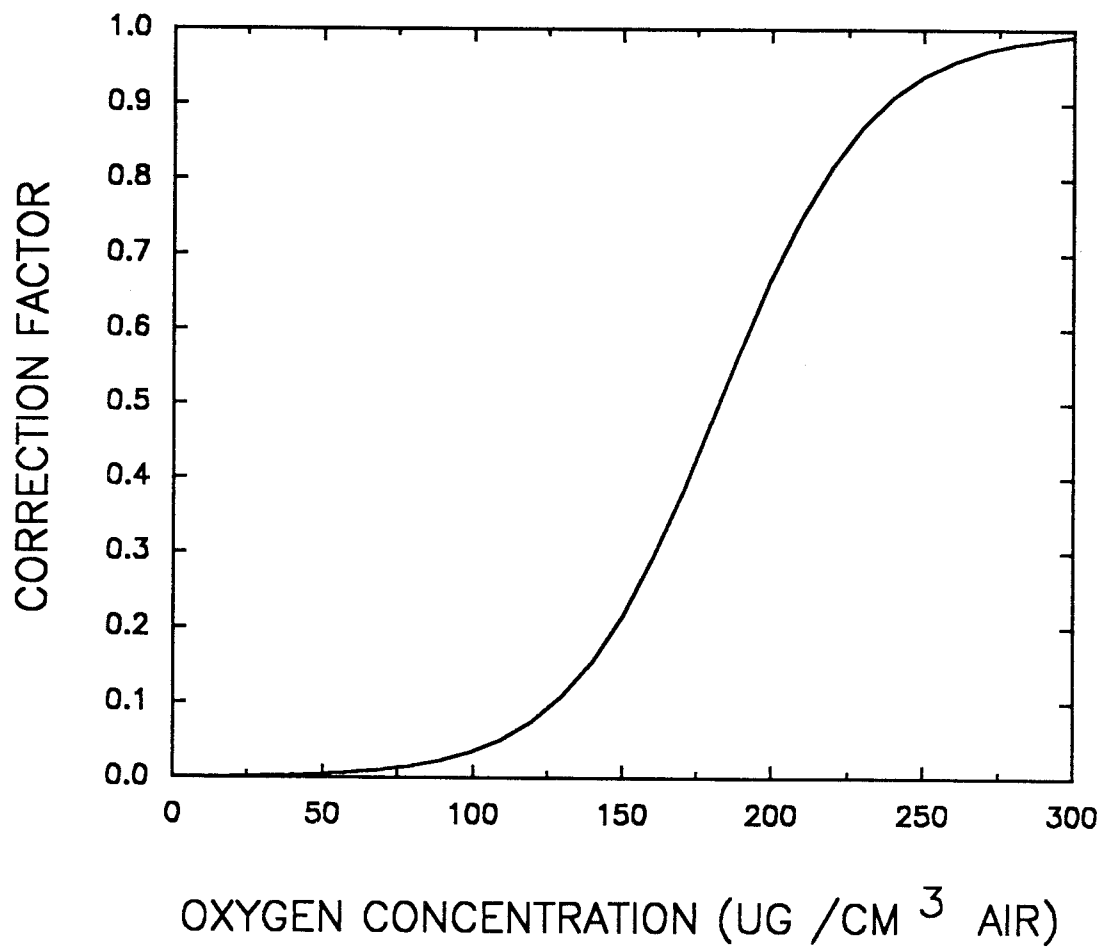


Figure 34. Correction factor for the root elongation rate as a function of soil oxygen concentration, calculated from equation (146).

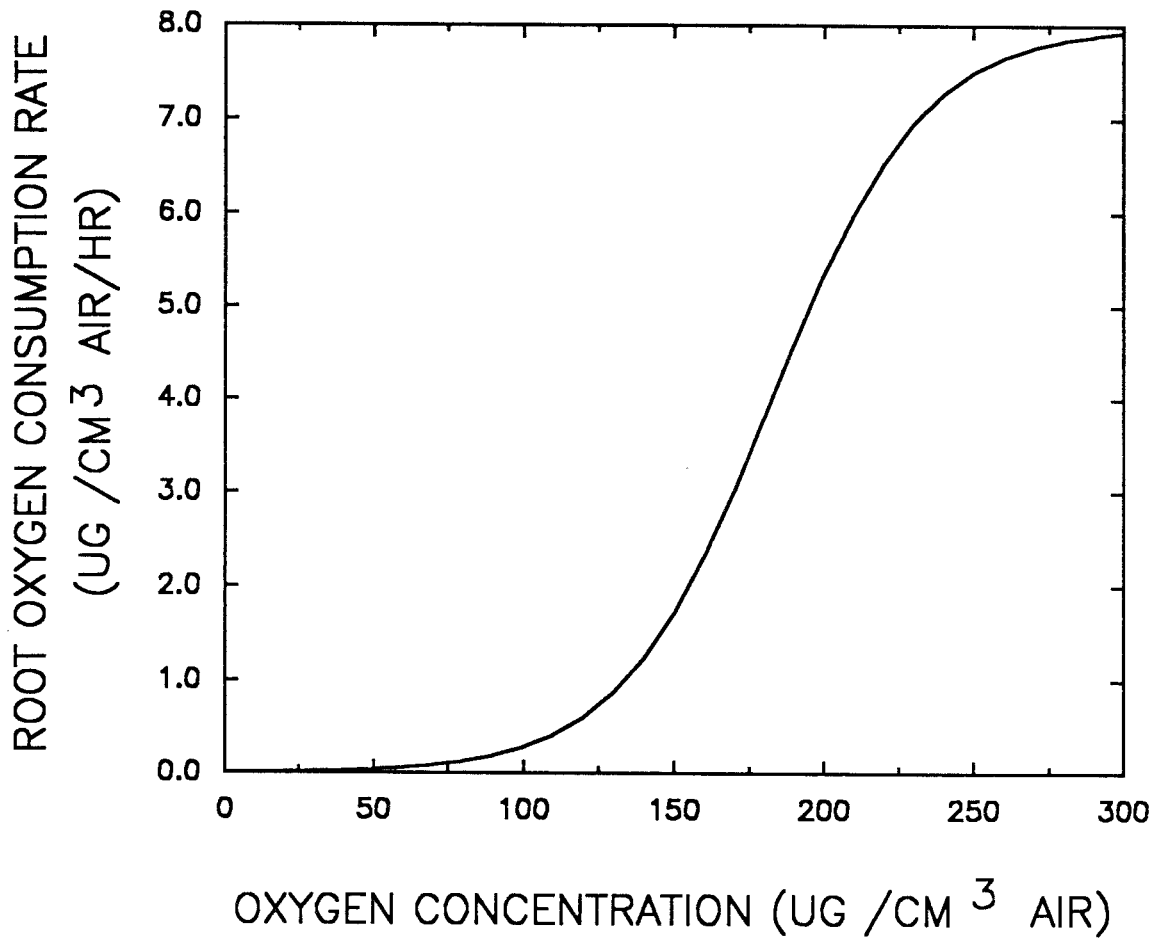


Figure 35. Oxygen consumption rate of roots as a function of soil oxygen concentration calculated from equation (148).

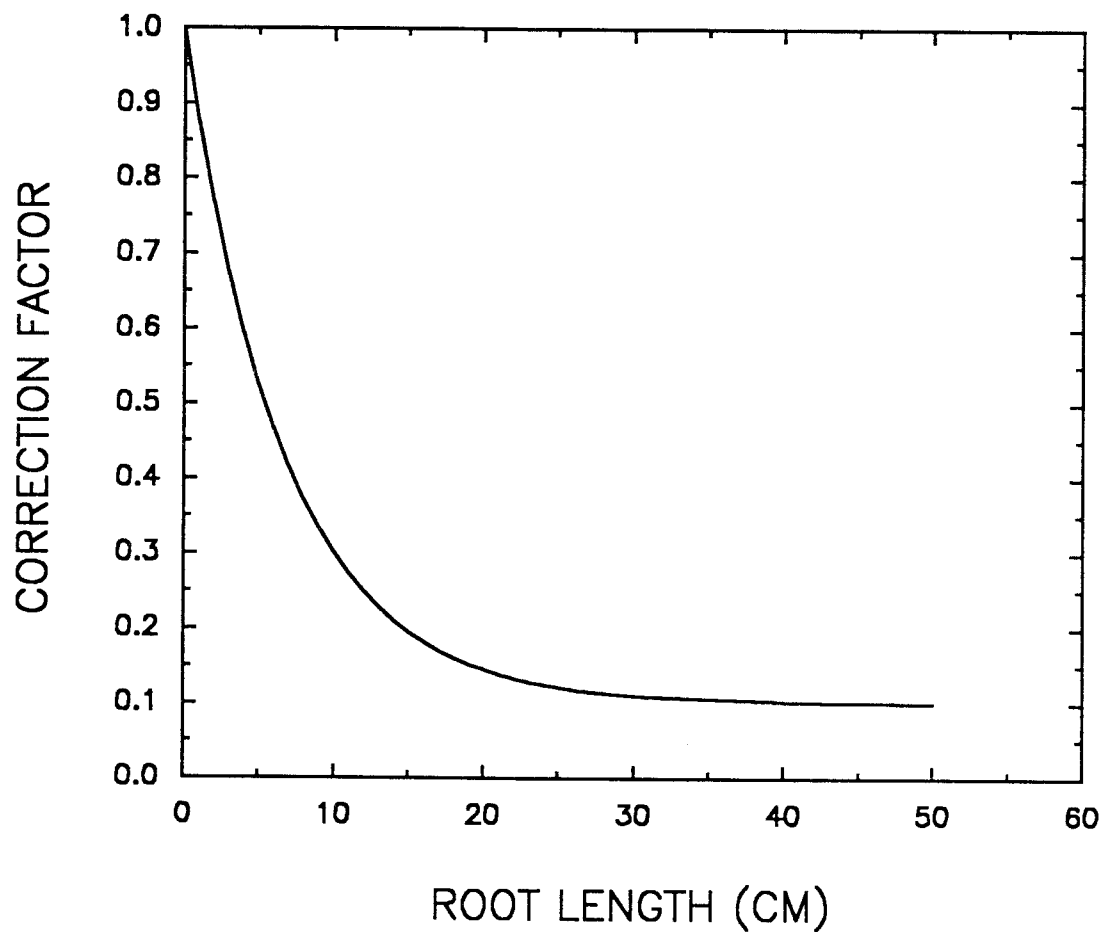


Figure 36. Correction factor for the oxygen consumption rate of roots as a function of root length starting from the root tip, calculated from equation (149).

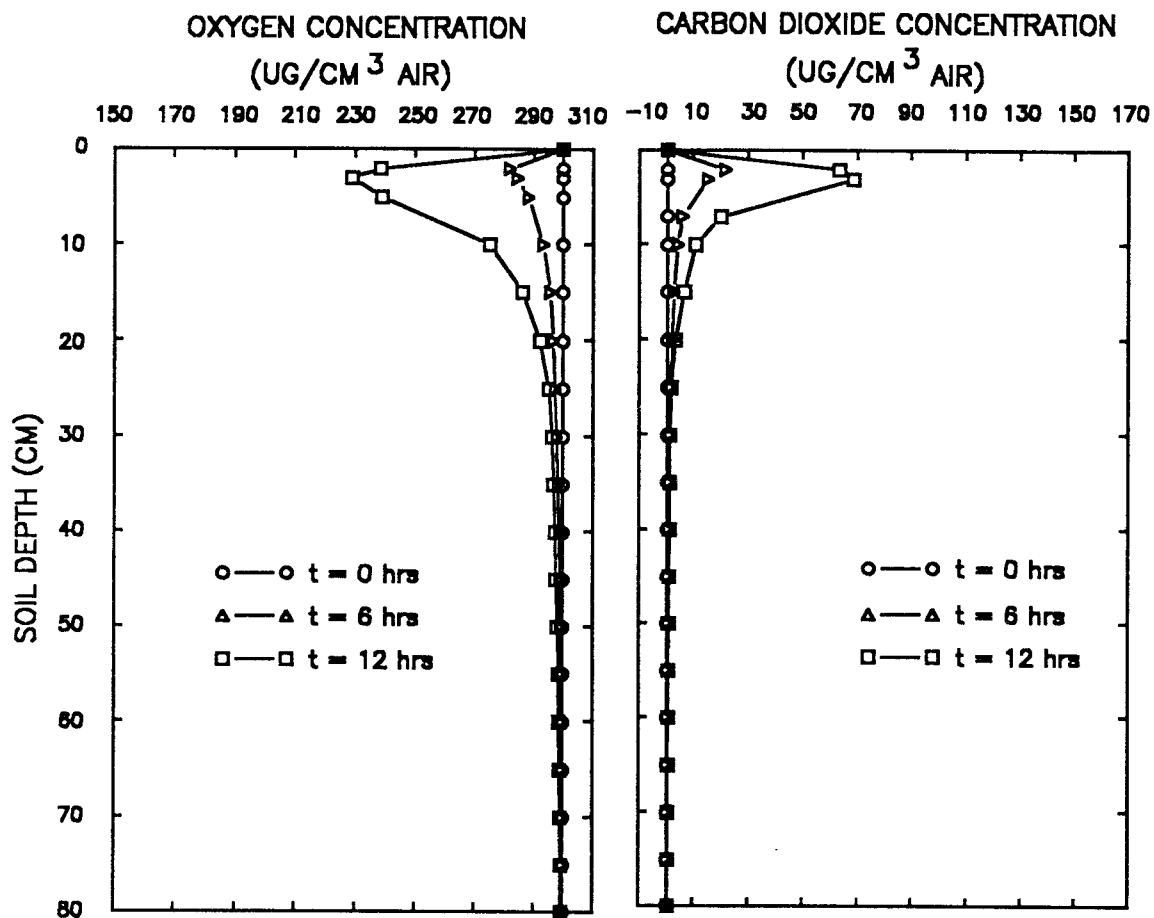


Figure 37. Oxygen and carbon dioxide concentrations as a function of soil depth at 0, 6, and 12 hours since start. The rainfall started at 0 hours and stopped at 12 hours.

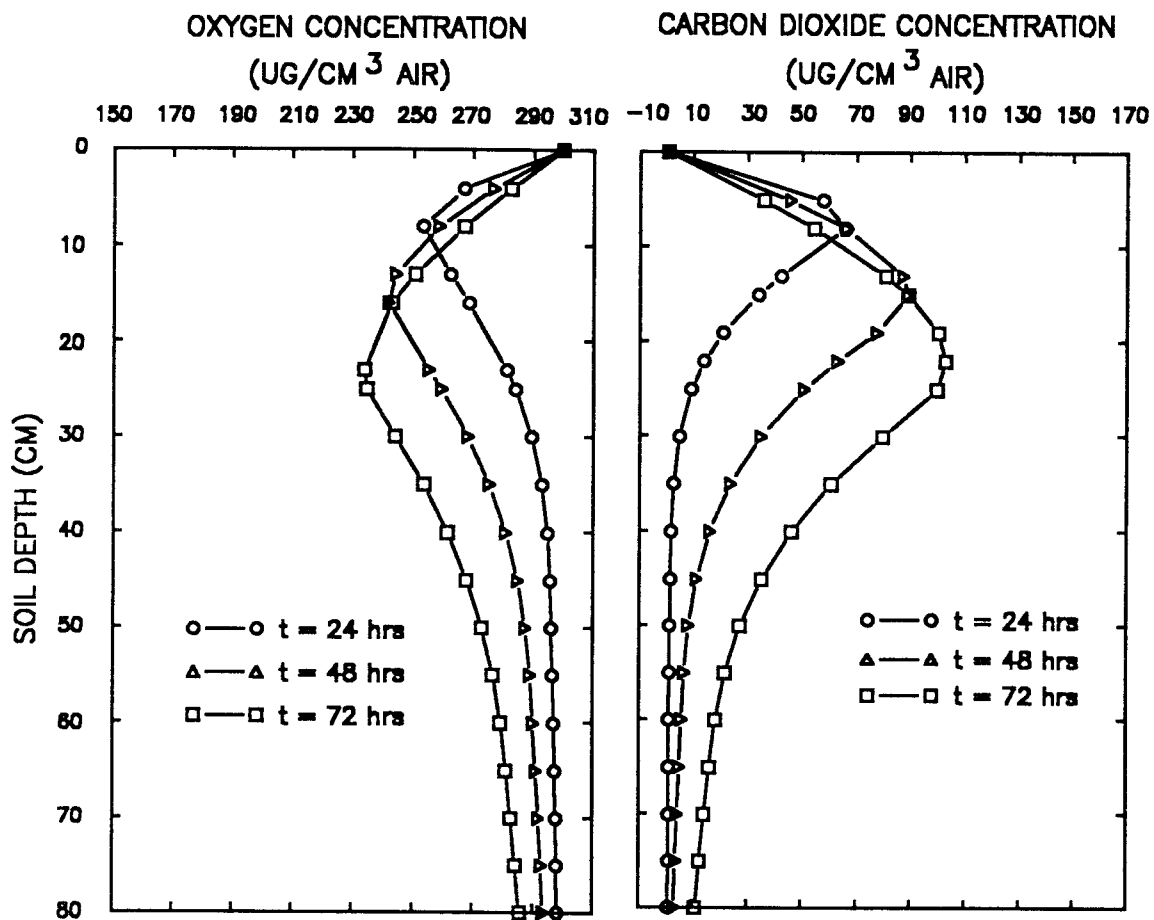


Figure 38. Oxygen and carbon dioxide concentrations as a function of soil depth at 24, 48, and 72 hours.

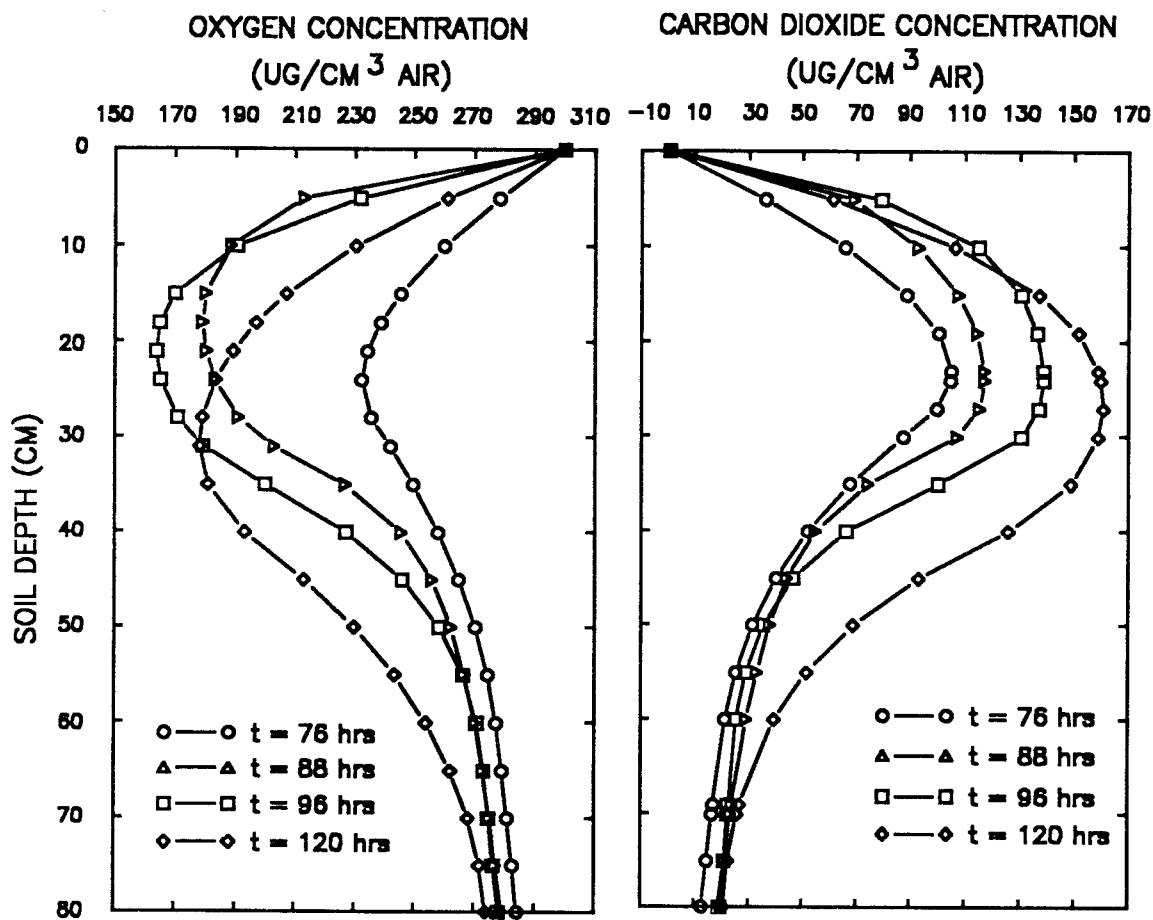


Figure 39. Oxygen and carbon dioxide concentrations as a function of soil depth at 76, 88, 96, and 120 hours since start. Rain, evaporation, and redistribution occurred during the period. The rainfall started at 76 hours and stopped at 88 hours.

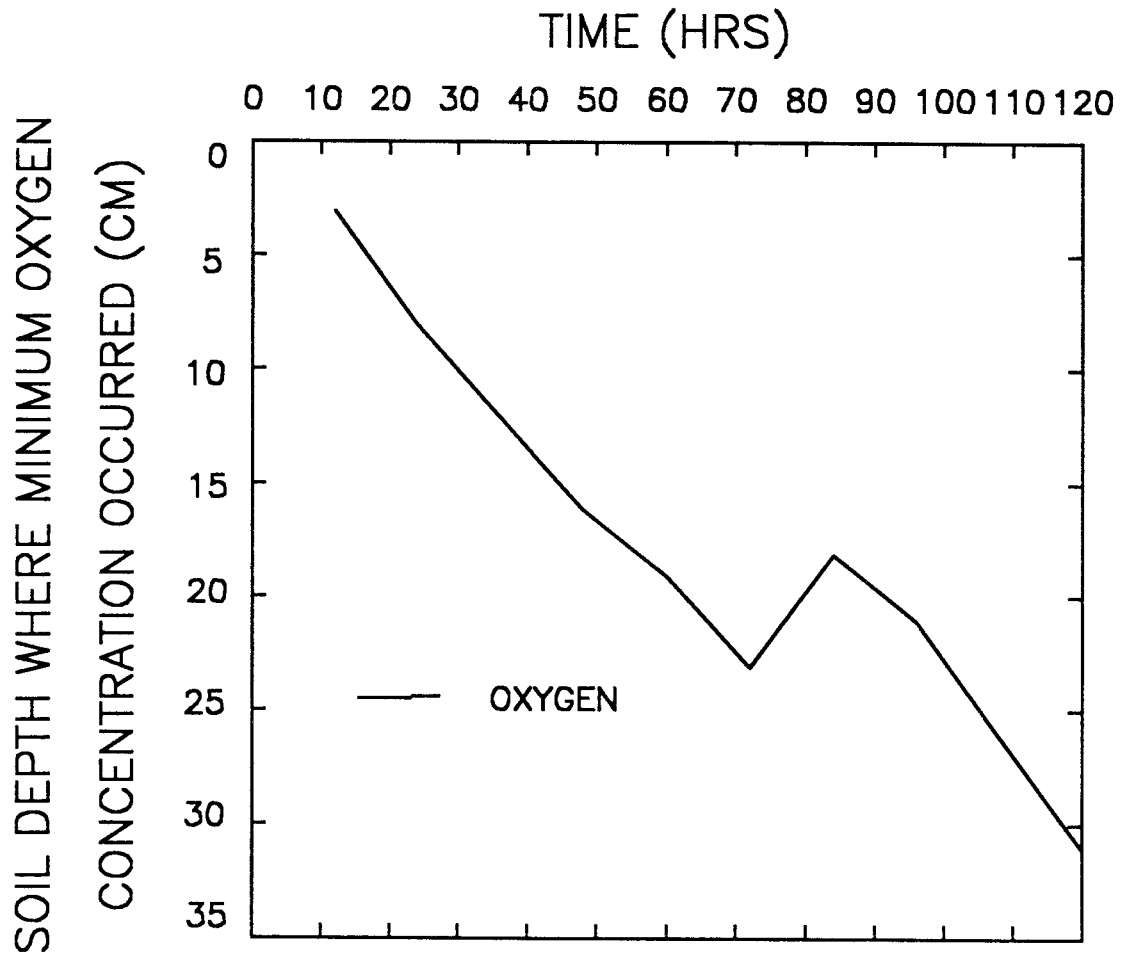


Figure 40. Soil depth where the minimum oxygen concentration occurred as a function of time from 0 to 120 hours.

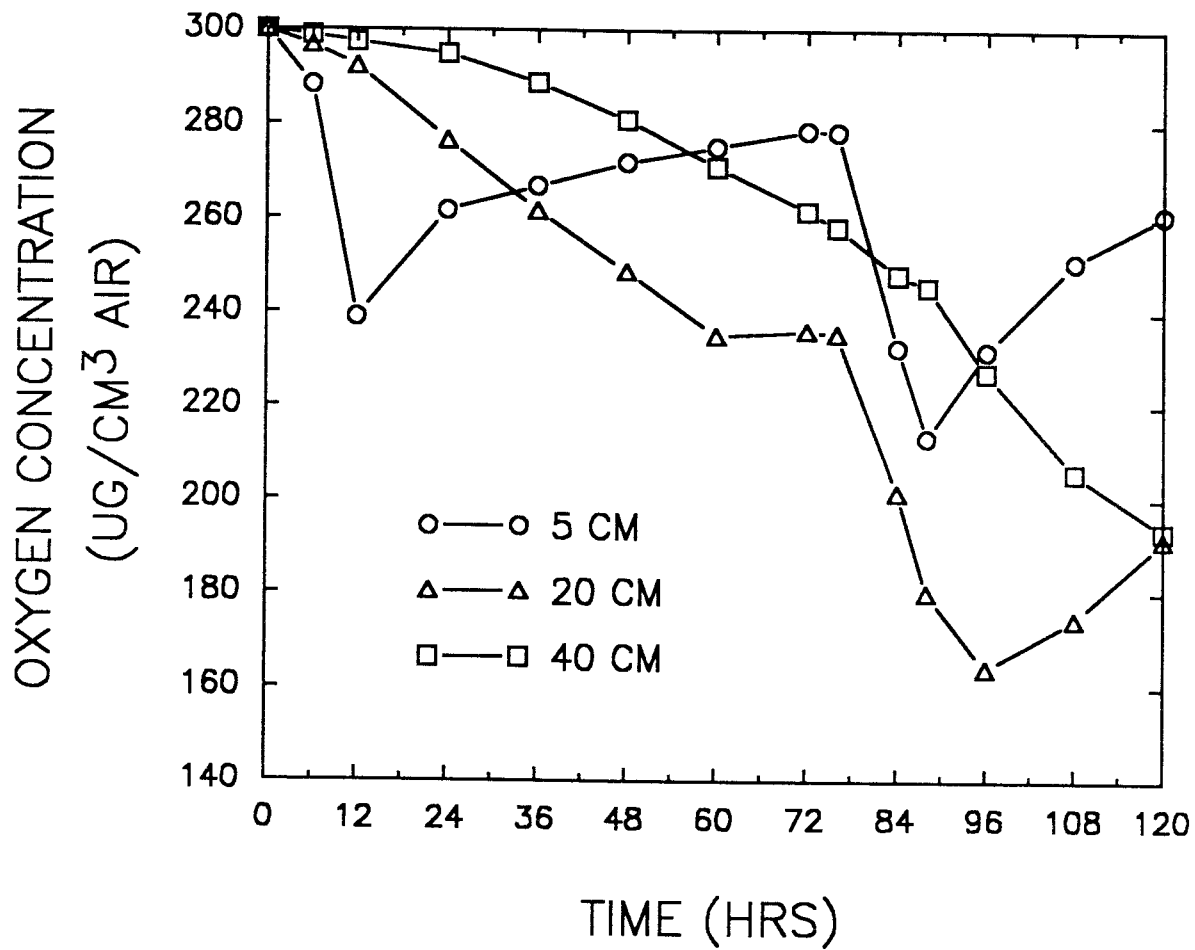


Figure 41. Oxygen concentration as a function of time at the soil depths of 5, 20, and 40 cm.

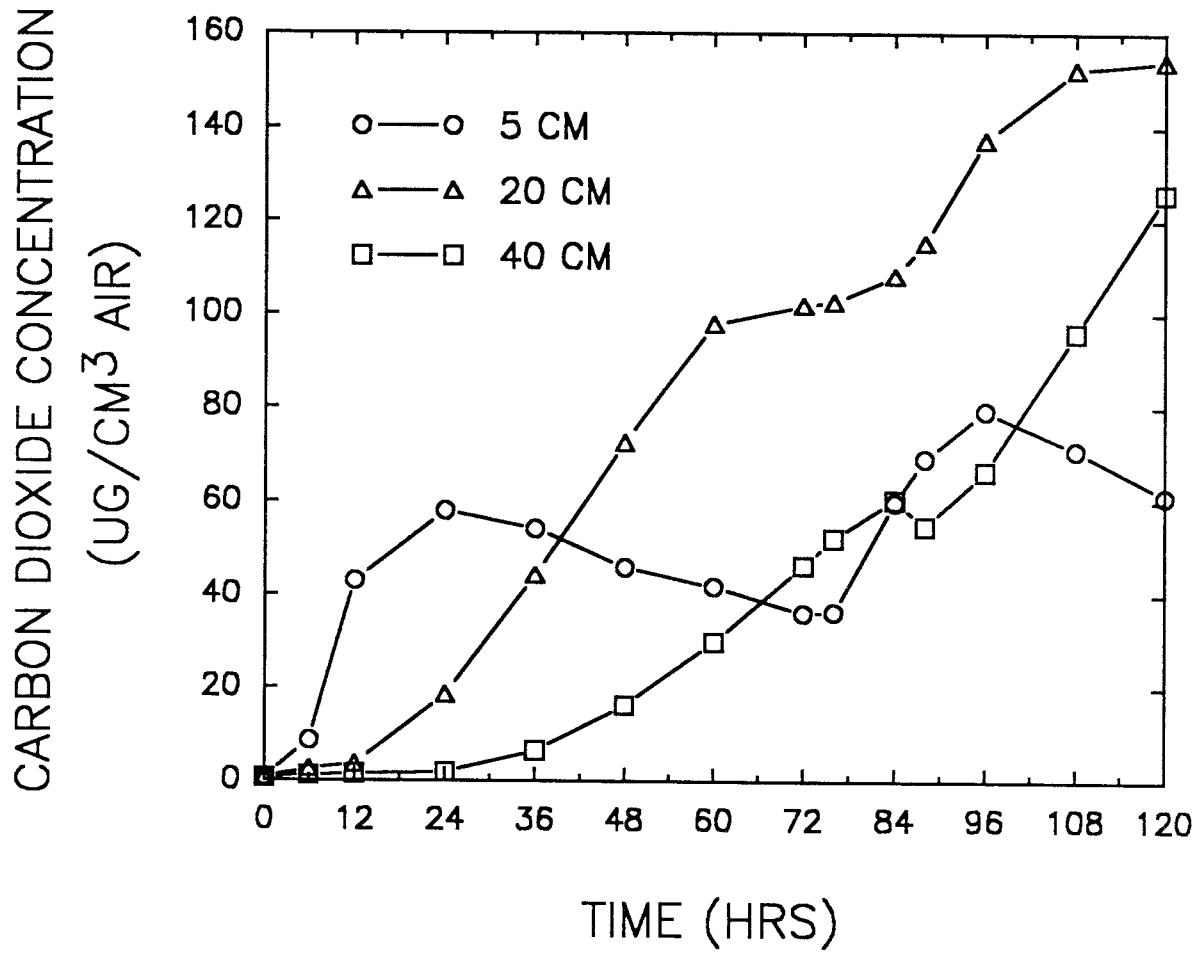


Figure 42. Carbon dioxide concentration as a function of time at the soil depths of 5, 20, and 40 cm.

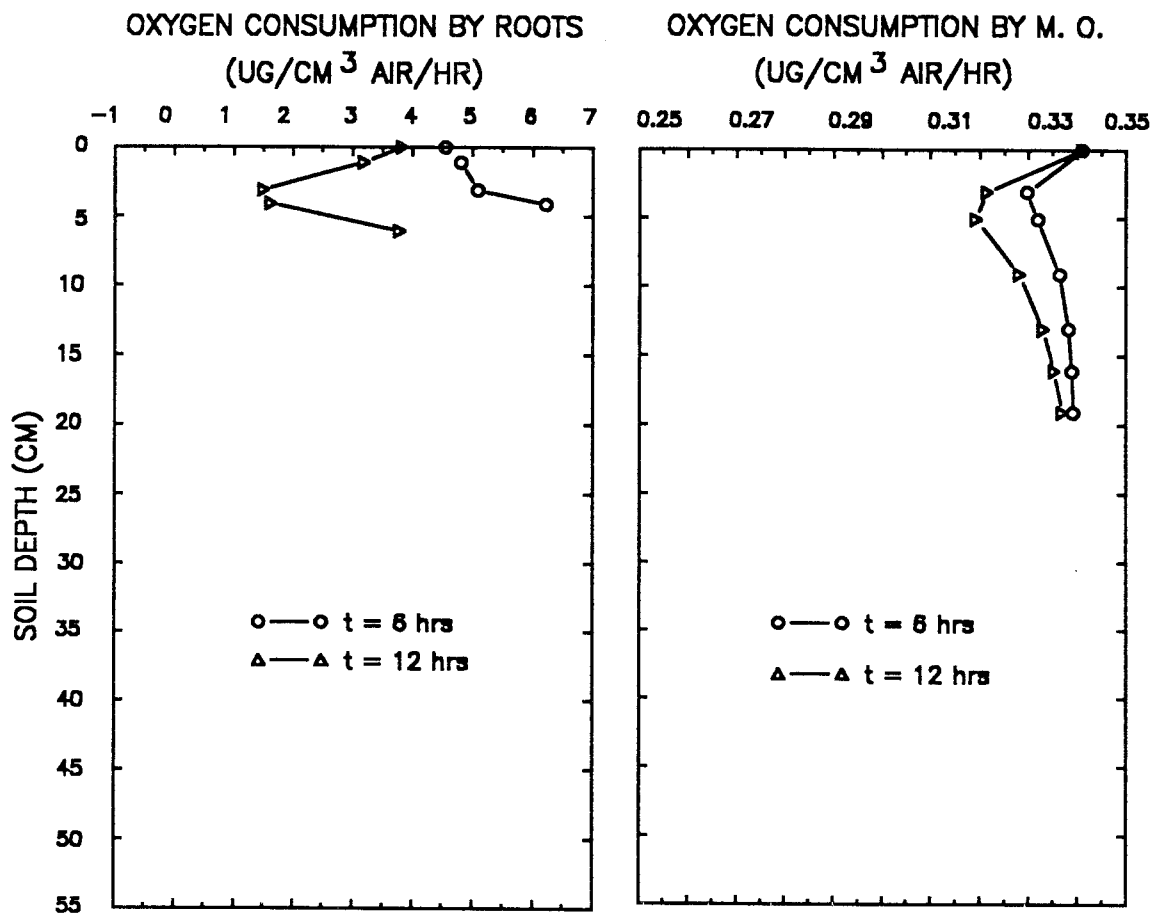


Figure 43. Oxygen consumption rates by plant roots and soil microorganisms as a function of soil depth at times of 6 and 12 hours. The rate of oxygen consumption in  $\mu\text{g cm}^{-3}$  fresh roots  $\text{hr}^{-1}$  was converted to  $\mu\text{g cm}^{-3}$  air  $\text{hr}^{-1}$  as shown on the Figure.

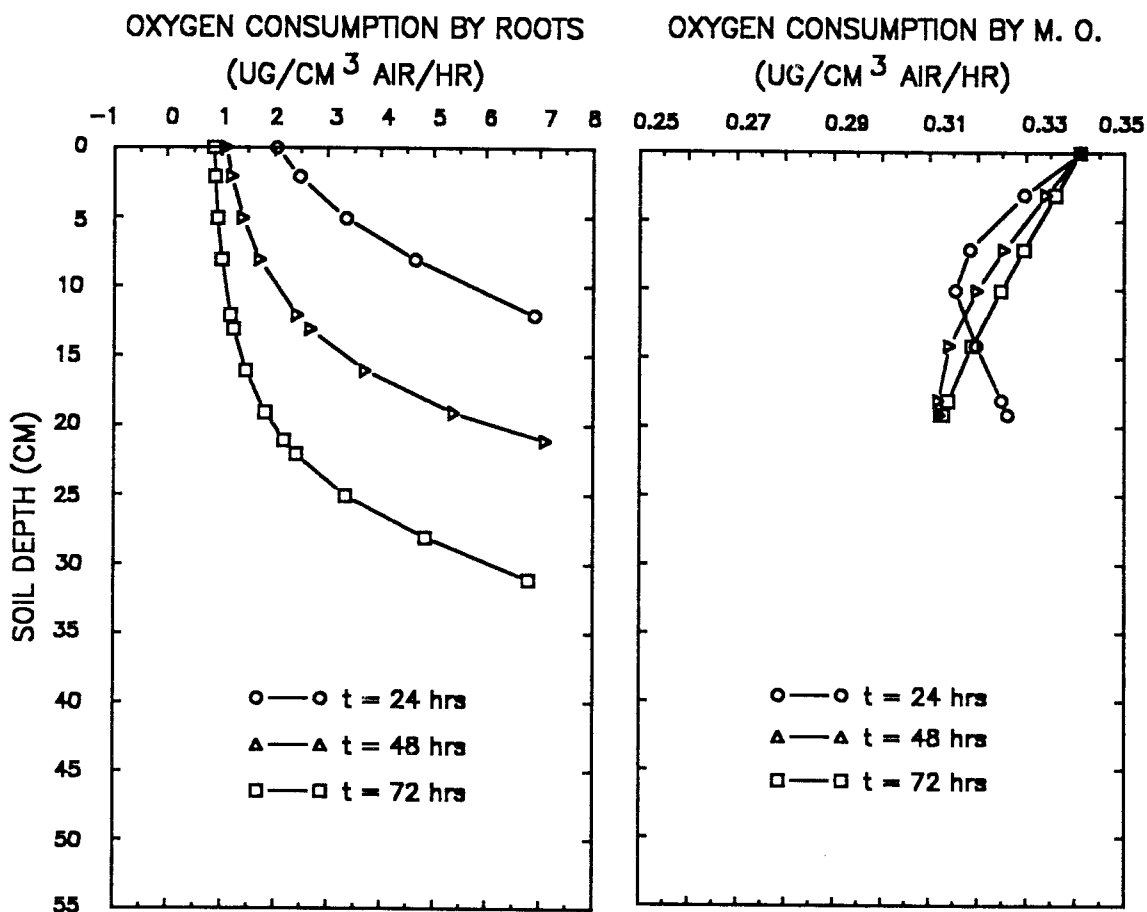


Figure 44. Oxygen consumption rates by plant roots and soil microorganisms as a function of soil depth at times of 24, 48, and 72 hours. The rate of oxygen consumption in  $\mu\text{g cm}^{-3}$  fresh roots  $\text{hr}^{-1}$  was converted to  $\mu\text{g cm}^{-3}$  air  $\text{hr}^{-1}$  as shown on the Figure.

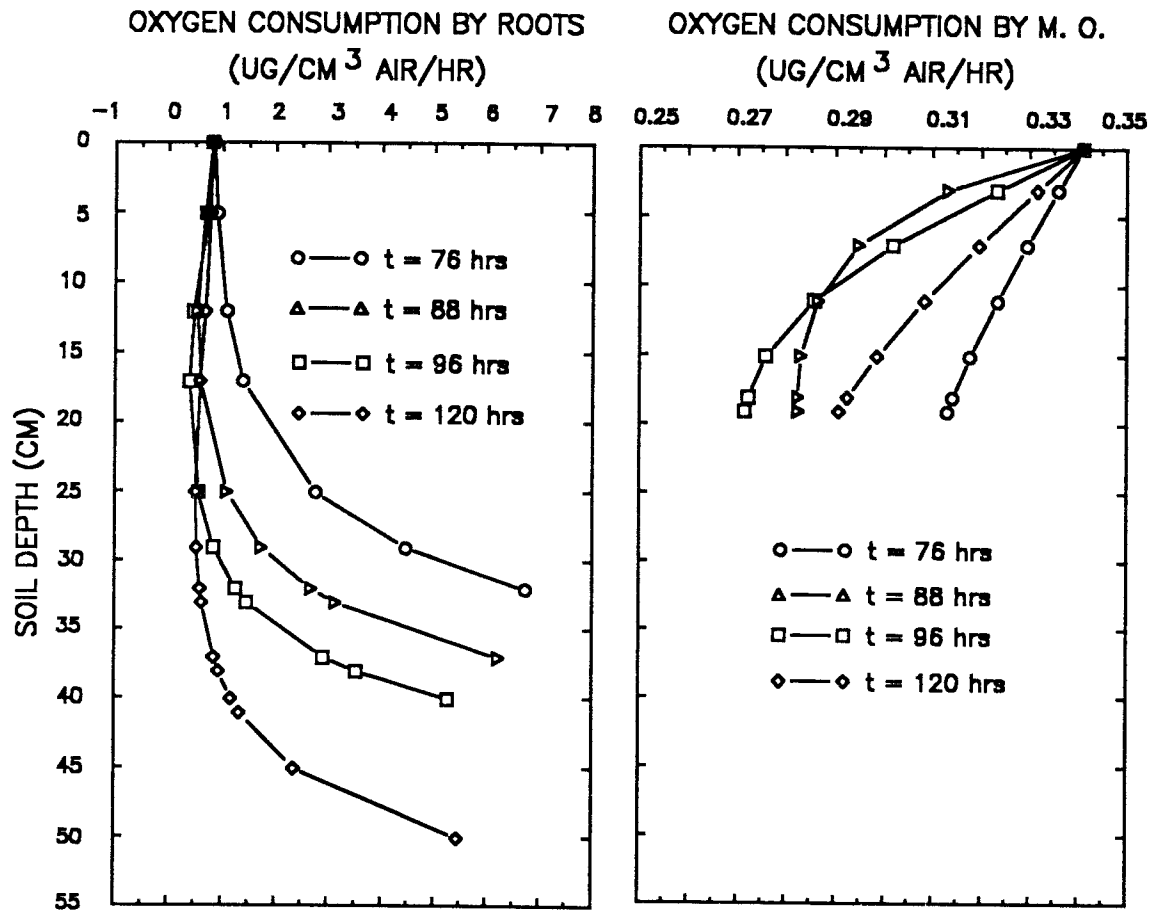


Figure 45. Oxygen consumption rates by plant roots and soil microorganisms as a function of soil depth at times of 76, 88, 96, and 120 hours. The rate of oxygen consumption in  $\mu\text{g cm}^{-3}$  fresh roots  $\text{hr}^{-1}$  was converted to  $\mu\text{g cm}^{-3}$  air  $\text{hr}^{-1}$  as shown on the Figure.

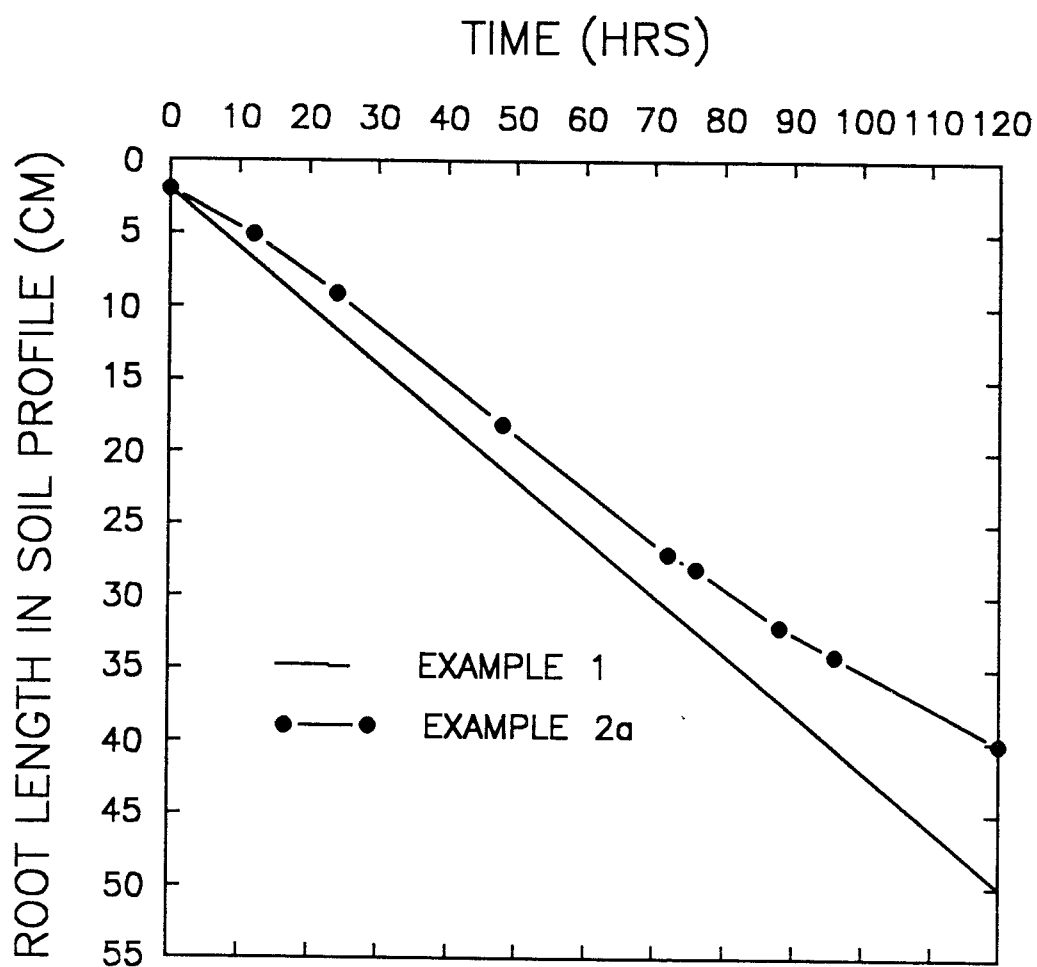


Figure 46. Root length in soil profile as a function of time in Example 1 and Example 2a since the start of the simulation.

## Example 2b

### Statement of the Problem

This example differs from Example 2a by assuming that the root elongation and the rate of root oxygen consumption are functions of carbon dioxide concentration instead of oxygen concentration. Comparison of the two examples allows evaluation of the effects of oxygen and carbon dioxide on the root growth and on the soil aeration conditions.

### Input Parameters

All input parameters were the same as in Example 2a except for the follows.

Root Elongation. The root elongation was chosen to be a function of the carbon dioxide concentration instead of the oxygen concentration. It was assumed that, when the soil is well aerated and carbon dioxide concentration is at the level of the atmosphere, the root elongation is only a function of time, as described by equation (145).

When the soil is not fully aerated, the root elongation is also a function of the carbon dioxide concentration. This implies that a factor is needed to correct equation (145) to account for the effects of soil carbon dioxide concentration on the root elongation. It was assumed that, when the soil is well aerated, the correction factor is equal to unity which means that the root elongation is only a

function of time. When the soil is not fully aerated, the correction factor decreases as the carbon dioxide concentration increases. A logistic function was chosen to define the correction factor for the soil carbon dioxide concentration (Figure 47) as follows:

$$F4 = \frac{A4}{1 + B4 \text{ EXP } \left[ C4(C_{\text{co}_2}^{\text{tip}} - C_{\text{co}_2}^{\text{th}}) \right]}, \quad (151)$$

where F4 is the correction factor, A4, B4, and C4 are constants characterizing the shape of the equation with A4 = 1, B4 = 200, and C4 = 0.11,  $C_{\text{co}_2}^{\text{tip}}$  is the soil carbon dioxide concentration at the root tip ( $\mu\text{g cm}^{-3}$  air), and  $C_{\text{co}_2}^{\text{th}}$  is the threshold soil carbon dioxide concentration below which the root elongation rate approaches zero ( $90 \mu\text{g cm}^{-3}$  air). Multiplying equation (145) and equation (151) yields:

$$L(t, \text{co}_2) = [L_0 + a_1 t] F4. \quad (152)$$

Equation (152) represents the root elongation as a function of time and of soil carbon dioxide concentration.

Rate of Oxygen Consumption By Roots. The rate of oxygen consumption by the roots was chosen to be a function of carbon dioxide concentration instead of oxygen concentration. The rate of oxygen consumption by the roots as a function of carbon dioxide concentration was represented by the logistic function (Figure 48):

$$\text{SRT}(i) = \frac{A5}{1 + B5 \text{ EXP } \left[ C5(C_{\text{co}_2}^i - C_{\text{co}_2}^{\text{th}}) \right]}, \quad (153)$$

where SRT(i) is the root oxygen consumption rate by the  $i^{\text{th}}$  section of root length converted to  $\mu\text{g cm}^{-3}$  air  $\text{hr}^{-1}$  (Appendix III), A5, B5,

and C5 are constants characterizing the shape of the equation with  $A5 = 8$ ,  $B5 = 200$ , and  $C5 = 0.11$ ,  $C_{\text{co}_2}^i$  is the carbon dioxide concentration in the  $i^{\text{th}}$  section of soil depth corresponding to the  $i^{\text{th}}$  section of root length ( $\mu\text{g cm}^{-3}$  soil air), and  $C_{\text{co}_2}^{\text{th}}$  is the threshold carbon dioxide concentration below which the root oxygen consumption rate approaches zero ( $90 \text{ mg cm}^{-3}$  air).

Multiplying equation (149) and equation (153) obtains:

$$\text{SRT}(i, \text{co}_2) = \frac{A5}{1 + B5 \text{EXP}[-C5(C_{\text{co}_2}^i - C_{\text{co}_2}^{\text{th}})]} F5. \quad (154)$$

Equation (154) represents the rate of oxygen consumption by root as a function of carbon dioxide concentration and of root length.

### Discussion of Simulation Results

Concentrations of Oxygen and Carbon Dioxide. Changes in oxygen and carbon dioxide concentrations are shown in Figures 49, 50, and 51. Each figure shows the concentrations of the two gases side by side at several times since the start of simulation. The oxygen is depleted by respiration by roots and microorganisms, and the carbon dioxide is released as a result. Comparisons of Example 2a and Example 2b show that the depletion of oxygen and the production of carbon dioxide in the soil were much smaller in Example 2b than that in Example 2a. For instance, the oxygen concentration was about  $240 \mu\text{g cm}^{-3}$  air in Figure 51 in Example 2b at the depth of 10.0 cm at 96 hours, but was about  $190 \mu\text{g cm}^{-3}$  air in Figure 39 in Example 2a at the same depth and time. Similar results were obtained for the

carbon dioxide concentrations. This is so because that the rate of oxygen use and the rate of carbon dioxide production by roots were lower in Example 2b. These lower rates were due to the restriction of carbon dioxide concentration on the root respiratory activities. By comparing Figure 48 with Figure 35, one sees that in order to decrease the rate of oxygen use by roots to  $4.0 \mu\text{g cm}^{-3} \text{ hr}^{-1}$ , the oxygen concentration needs to decrease  $117 \mu\text{g cm}^{-3}$  air (from  $300 \mu\text{g cm}^{-3}$  air to  $183 \mu\text{g cm}^{-3}$  air), but the carbon dioxide concentration only needs to increase about  $40 \mu\text{g cm}^{-3}$  air (from  $0.6134 \mu\text{g cm}^{-3}$  air to  $40 \mu\text{g cm}^{-3}$  air). This implies that soil carbon dioxide concentration is more sensitive to the rate of oxygen use by roots. As a result, the rate of oxygen use, as well as the rate of carbon dioxide production, by roots was smaller in Example 2b than that of Example 2a.

Rates of Oxygen Consumption by Roots and Microorganisms. The rates of oxygen consumption by roots and microorganisms are shown in Figures 52, 53, and 54. Each Figure shows the rate of oxygen consumption in  $\mu\text{g cm}^{-3} \text{ air hr}^{-1}$ . The rate of oxygen consumption by roots was calculated in the program in  $\mu\text{g cm}^{-3}$  fresh roots  $\text{hr}^{-1}$  and then converted to  $\mu\text{g cm}^{-3}$  soil  $\text{hr}^{-1}$  (Appendix III), as was required by the unit used for the oxygen field equation. The sequence of the three diagrams shows the change in oxygen use as a function of soil depth at several times.

Comparisons of Example 2a and Example 2b show that the rate of oxygen consumption by roots was much lower in Example 2b than that in Example 2a. For instance, the maximum rate of oxygen consumption by roots was about  $1 \mu\text{g cm}^{-3}$  soil  $\text{hr}^{-1}$  in Figure 54 in Example 2b at 96

hours, but was about  $4.7 \text{ mg cm}^{-3} \text{ soil hr}^{-1}$  in Figure 45 in Example 2a at the same time, which is about five fold larger than that in Example 2b. This is so because that the rate of root elongation and the rate of oxygen consumption by roots was chosen to be a function of carbon dioxide concentration. As the carbon dioxide concentration increases, the rate of oxygen consumption by roots decreases.

Comparison of Root Length. Changes in root length between Example 2a and 2b were shown in Figure 55. This diagram shows root length in the soil profile as a function of time since the start of the simulation. Example 2a assumed that the rate of root elongation was a function of oxygen concentration in addition to being a function of time. Example 2b assumed that the rate of root elongation was a function of carbon dioxide concentration in addition to being a function of time. Start with the initial root length of 2 cm in both Example 2a and 2b, root elongation rate was lower in Example 2b than that in Example 2a. As the time elapsed, the differences in root length of two examples increased. Root length was about 21.0 cm at 120 hours in Example 2b, but was about 40.0 cm at the same time in Example 2a, which was twice as long as that in Example 2b. This is so because that the rate of root elongation was more sensitive to soil carbon dioxide concentrations. As more carbon dioxide was produced by roots and microorganisms, the rate of root elongation decreased.

## Conclusions

This example together with Example 2a shows that the root elongation and the rate of oxygen use by roots were stronger restricted by the soil carbon dioxide concentration than that by the soil oxygen concentration. This is so because the rate of oxygen use by roots is more sensitive to the carbon dioxide concentration.

A interesting simulation which need to be conducted is to choose the root elongation and the rate of oxygen use by roots as functions of both oxygen and carbon dioxide concentrations, in addition to being a function of time. This simulation should allow complete evaluation of how soil oxygen and carbon dioxide affect root growth.

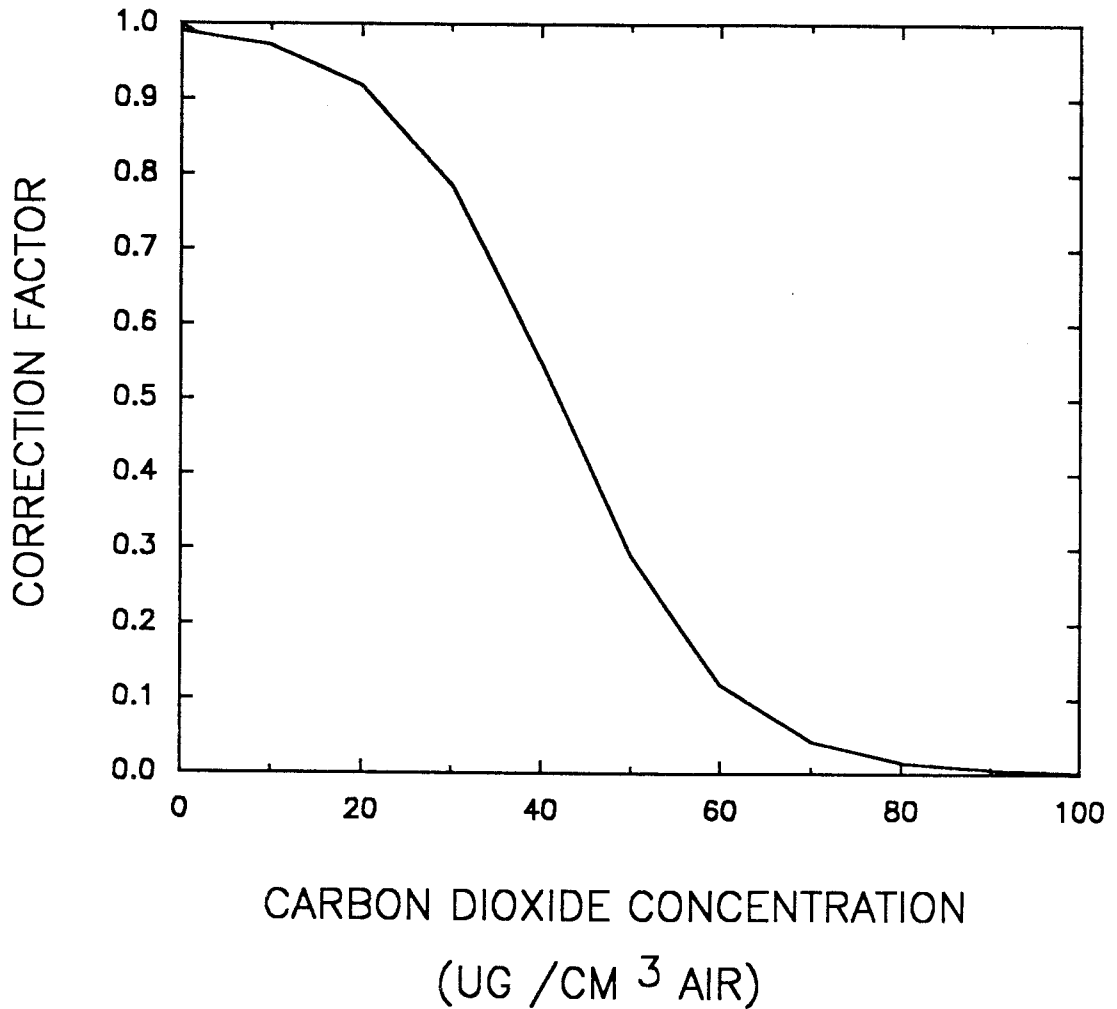


Figure 47. Correction factor for the root elongation rate as a function of soil carbon dioxide concentration, calculated from equation (151).

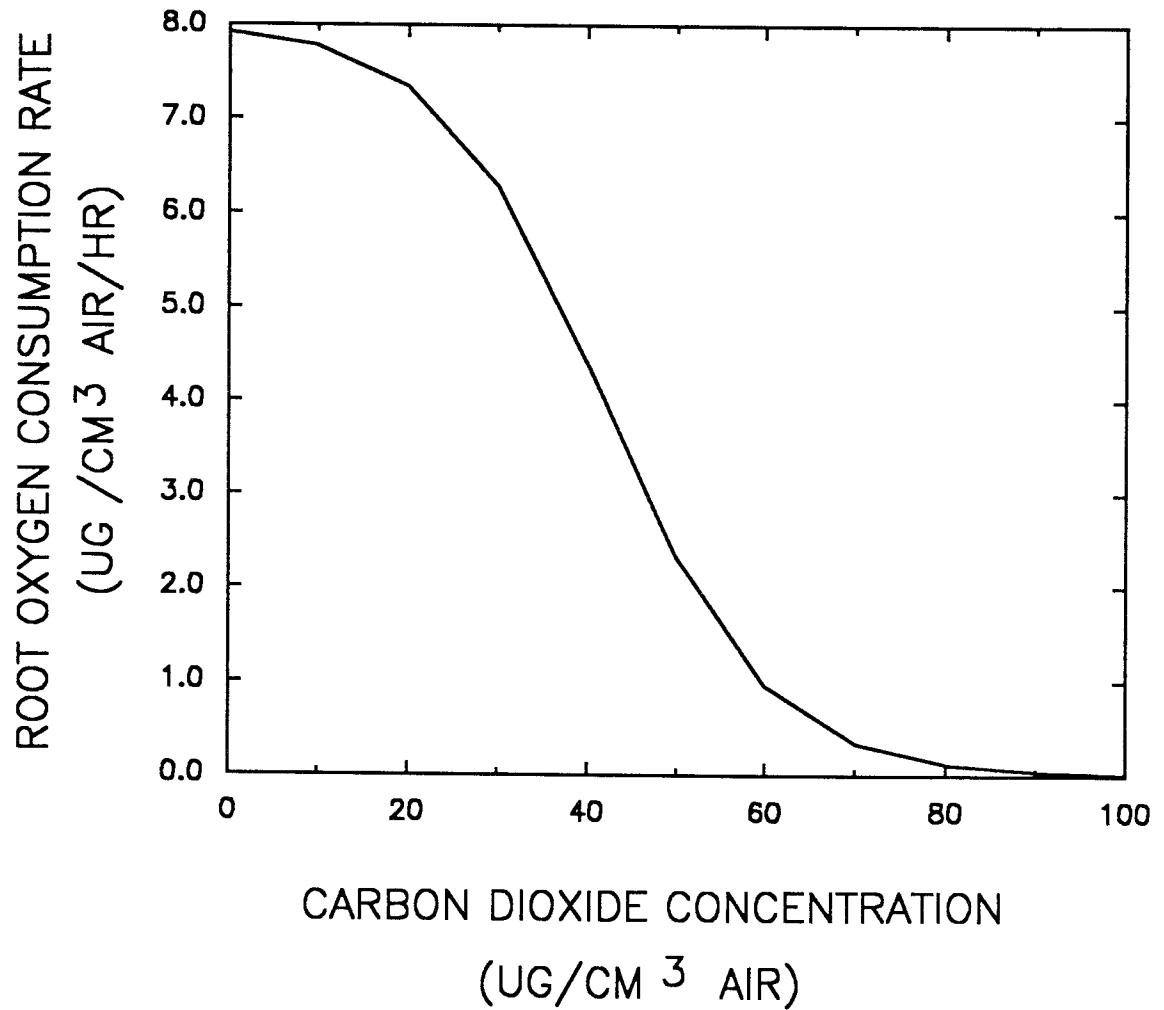


Figure 48. Oxygen consumption rate of roots as a function of soil carbon dioxide concentration, calculated from equation (153).

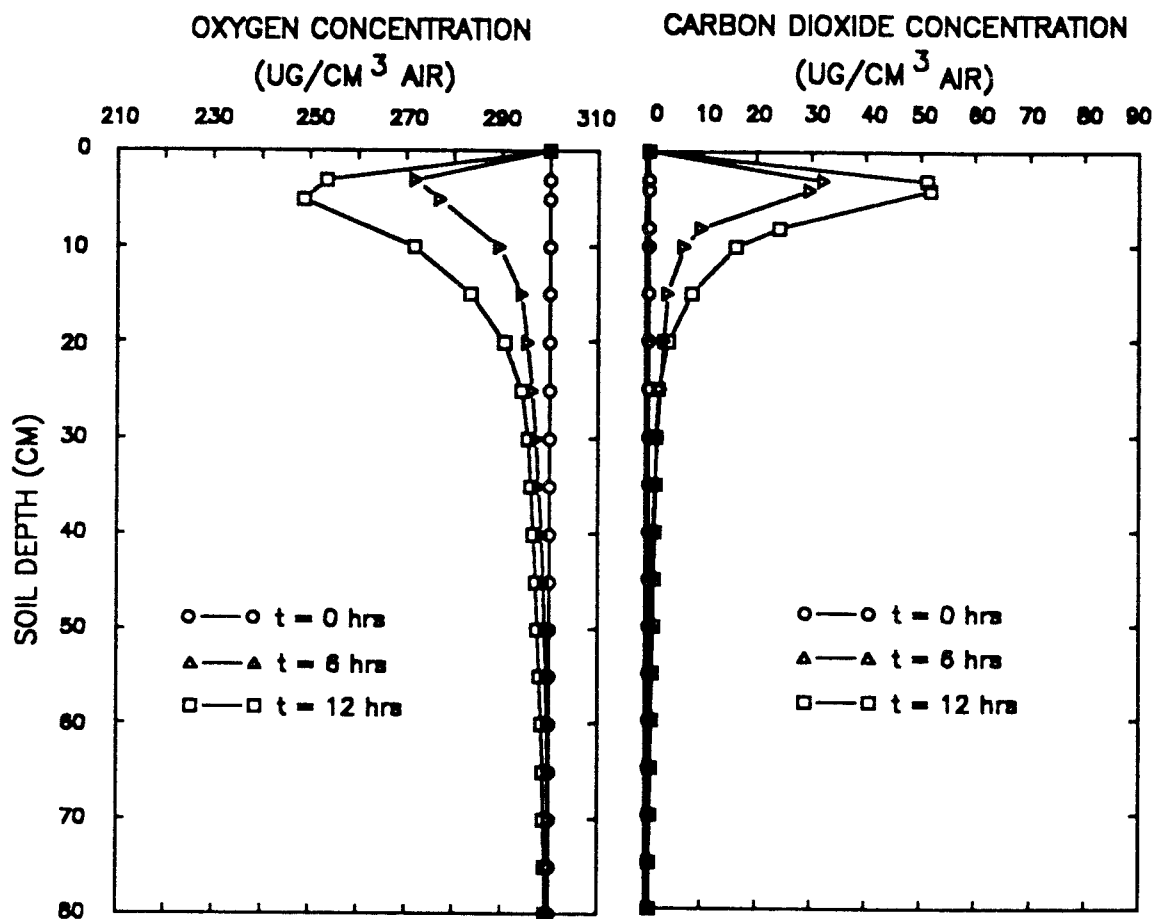


Figure 49. Oxygen and carbon dioxide concentrations as a function of soil depth at 0, 6, and 12 hours since start. The rainfall started at 0 hour and stopped at 12 hours.

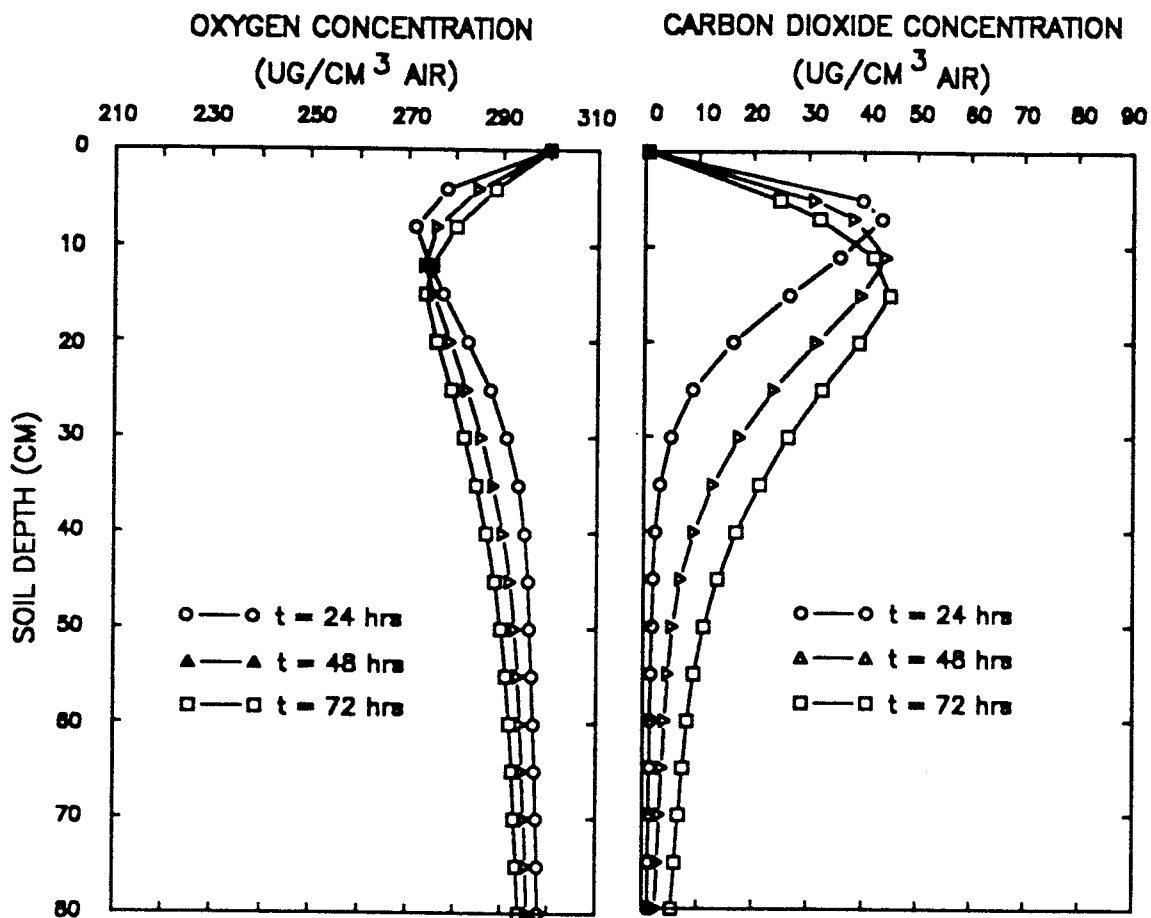


Figure 50. Oxygen and carbon dioxide concentrations as a function of soil depth at 24, 48, and 72 hours.

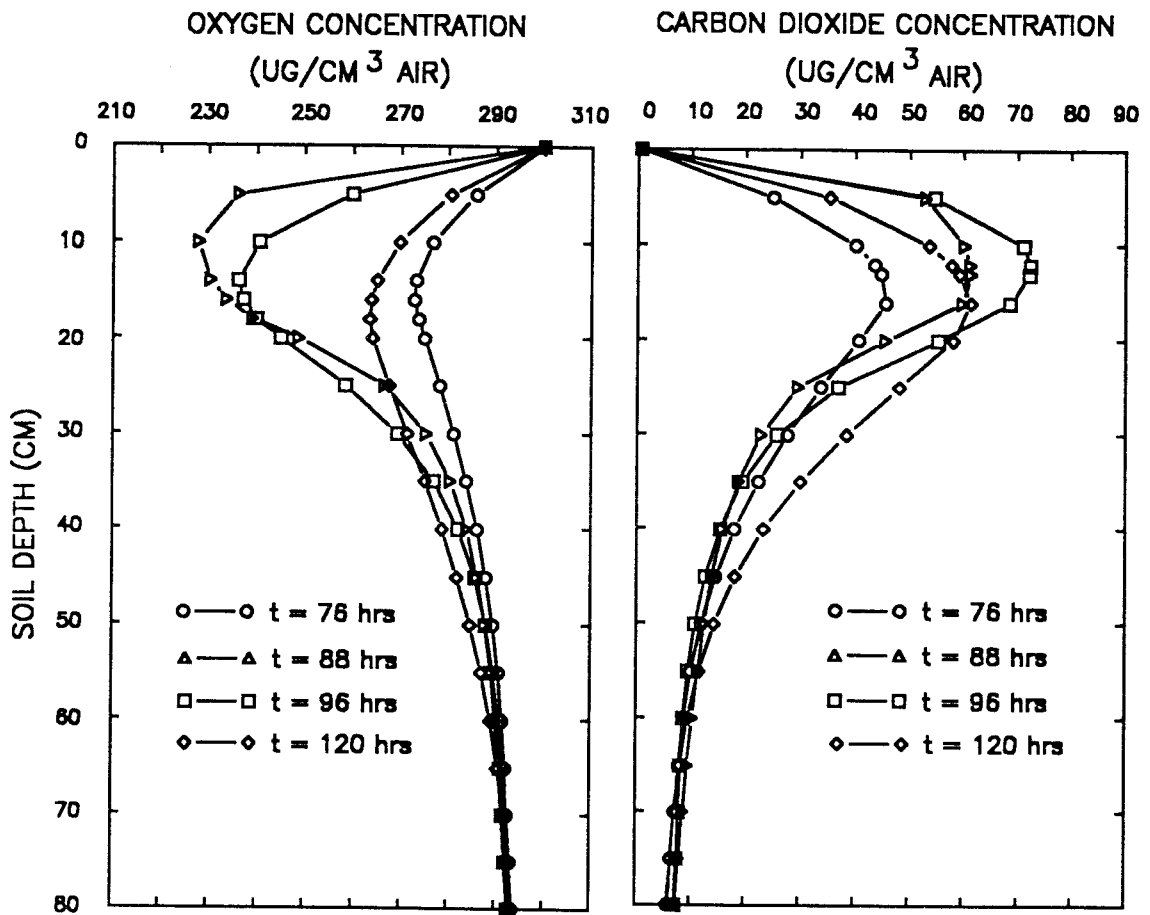


Figure 51. Oxygen and carbon dioxide concentrations as a function of soil depth at 76, 88, 96, and 120 hours since start. Rain, evaporation, and redistribution occurred during the period. The rainfall started at 76 hours and stopped at 88 hours.

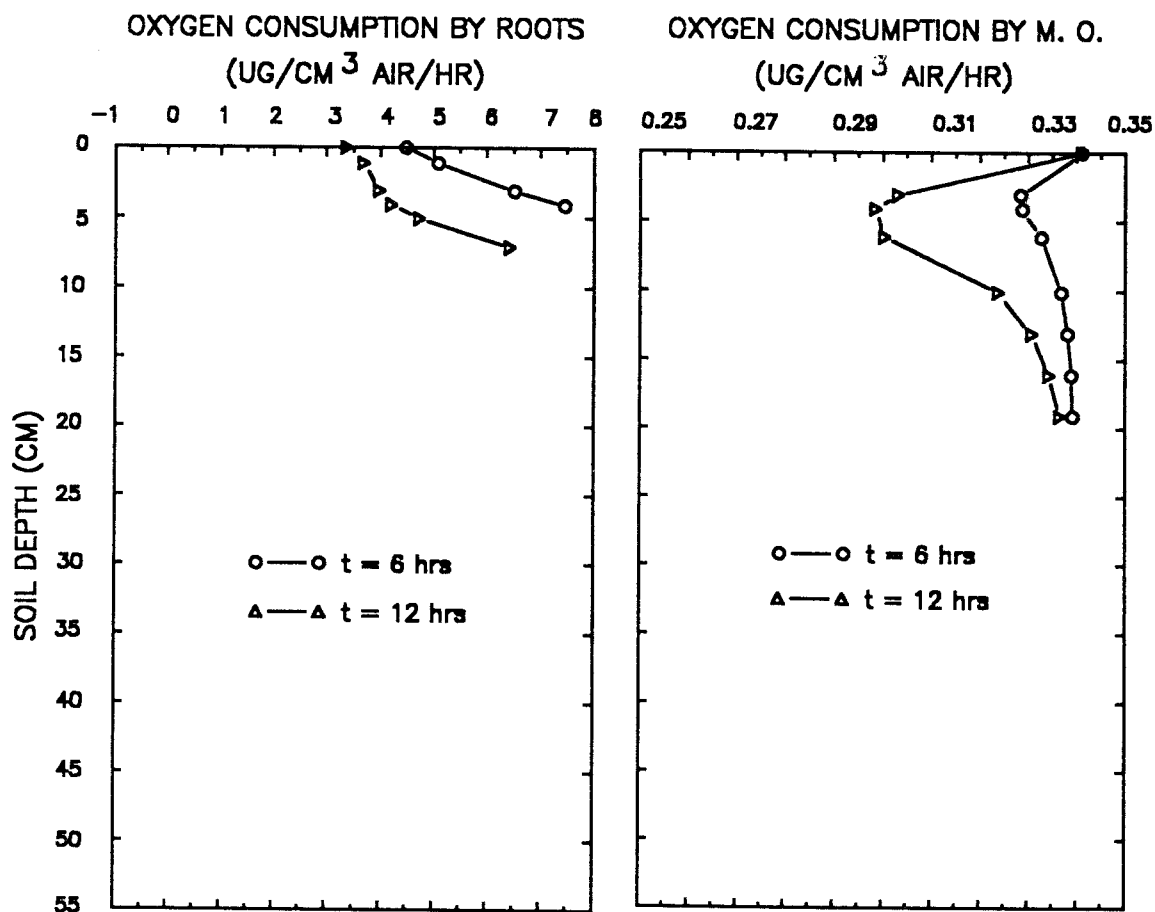


Figure 52. Oxygen consumption rates by plant roots and soil microorganisms as a function of soil depth at times of 6 and 12 hours. The rate of oxygen consumption in  $\mu\text{g cm}^{-3}$  fresh roots  $\text{hr}^{-1}$  was converted to  $\mu\text{g cm}^{-3}$  air  $\text{hr}^{-1}$  as shown on the figure.

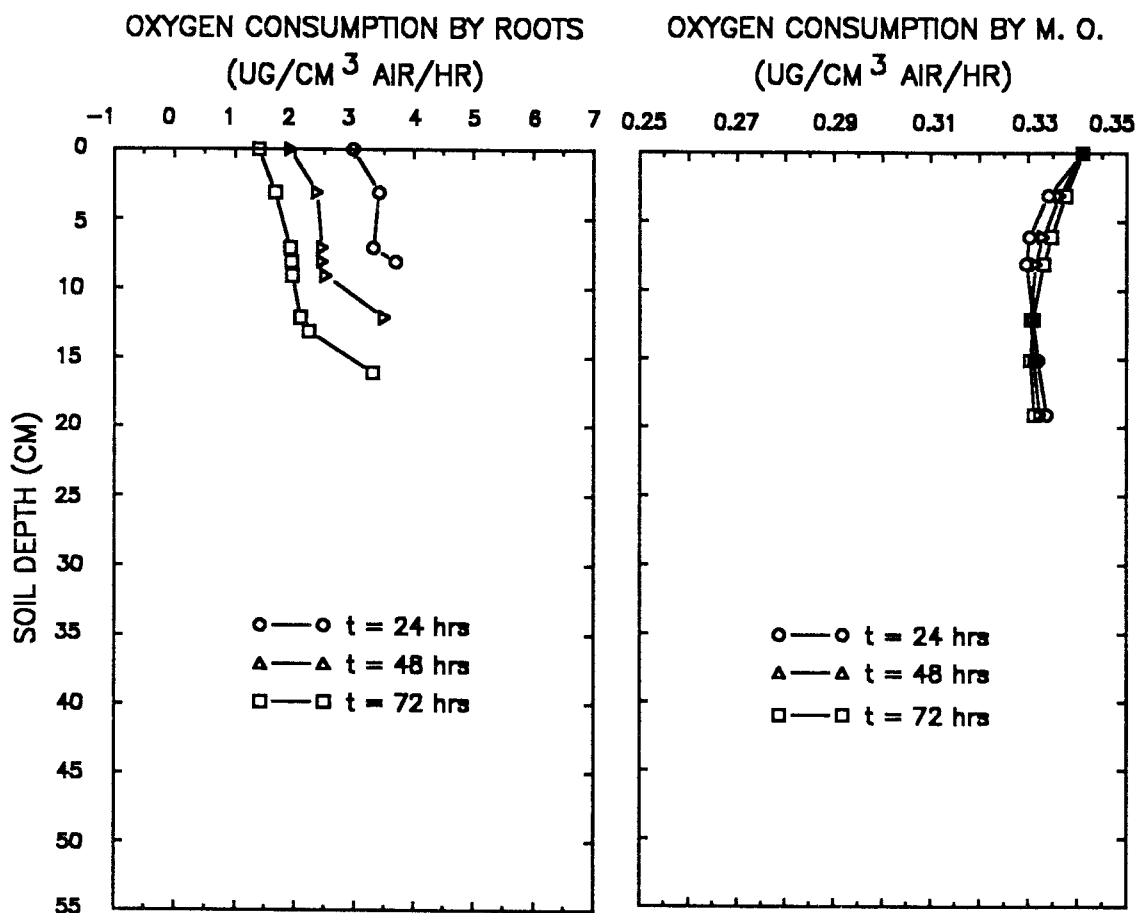


Figure 53. Oxygen consumption rates by plant roots and soil microorganisms as a function of soil depth at times of 24, 48, and 72 hours. The rate of oxygen consumption in  $\mu\text{g cm}^{-3}$  fresh roots  $\text{hr}^{-1}$  was converted to  $\mu\text{g cm}^{-3}$  air  $\text{hr}^{-1}$  as shown on the figure.

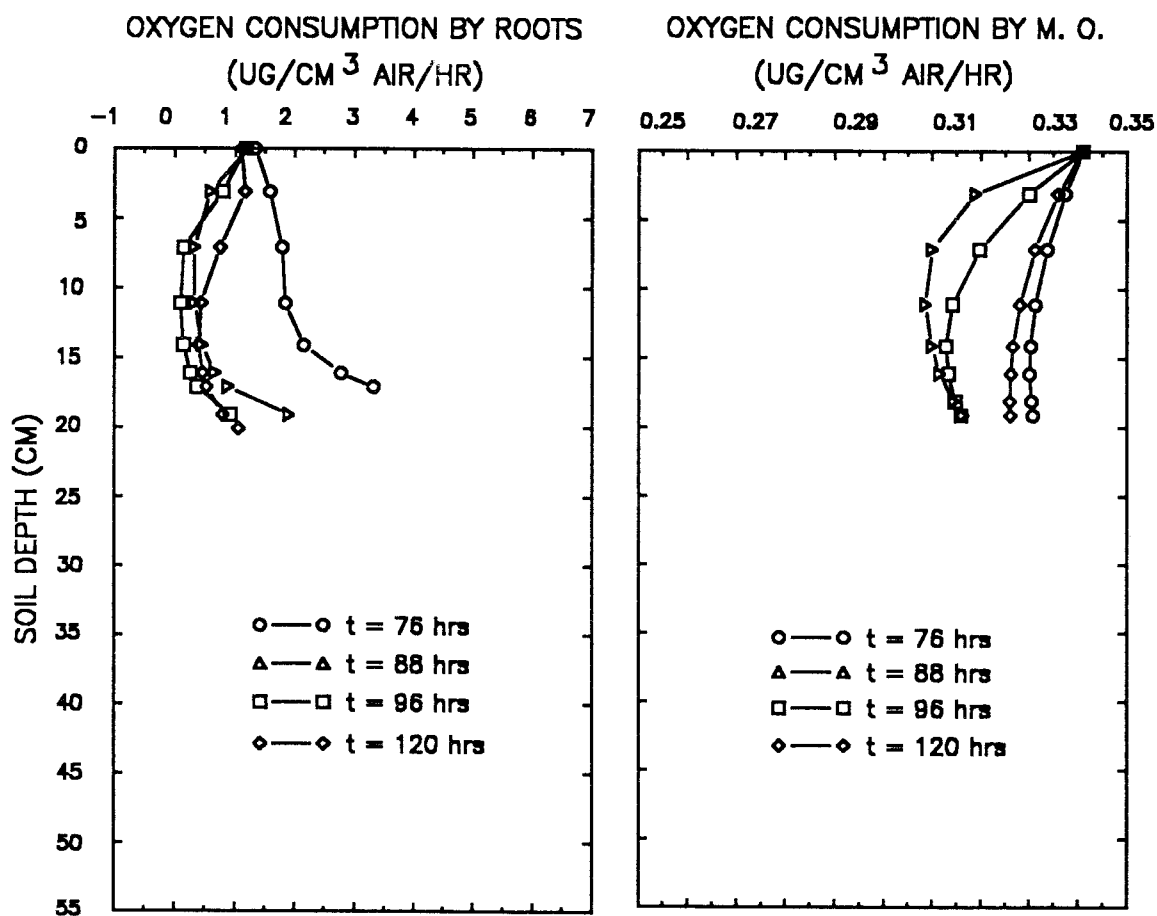


Figure 54. Oxygen consumption rates by plant roots and soil microorganisms as a function of soil depth at times of 76, 88, 96, and 120 hours. The rate of oxygen consumption in  $\mu\text{g cm}^{-3}$  fresh roots  $\text{hr}^{-1}$  was converted to  $\mu\text{g cm}^{-3}$  air  $\text{hr}^{-1}$  as shown on the figure.

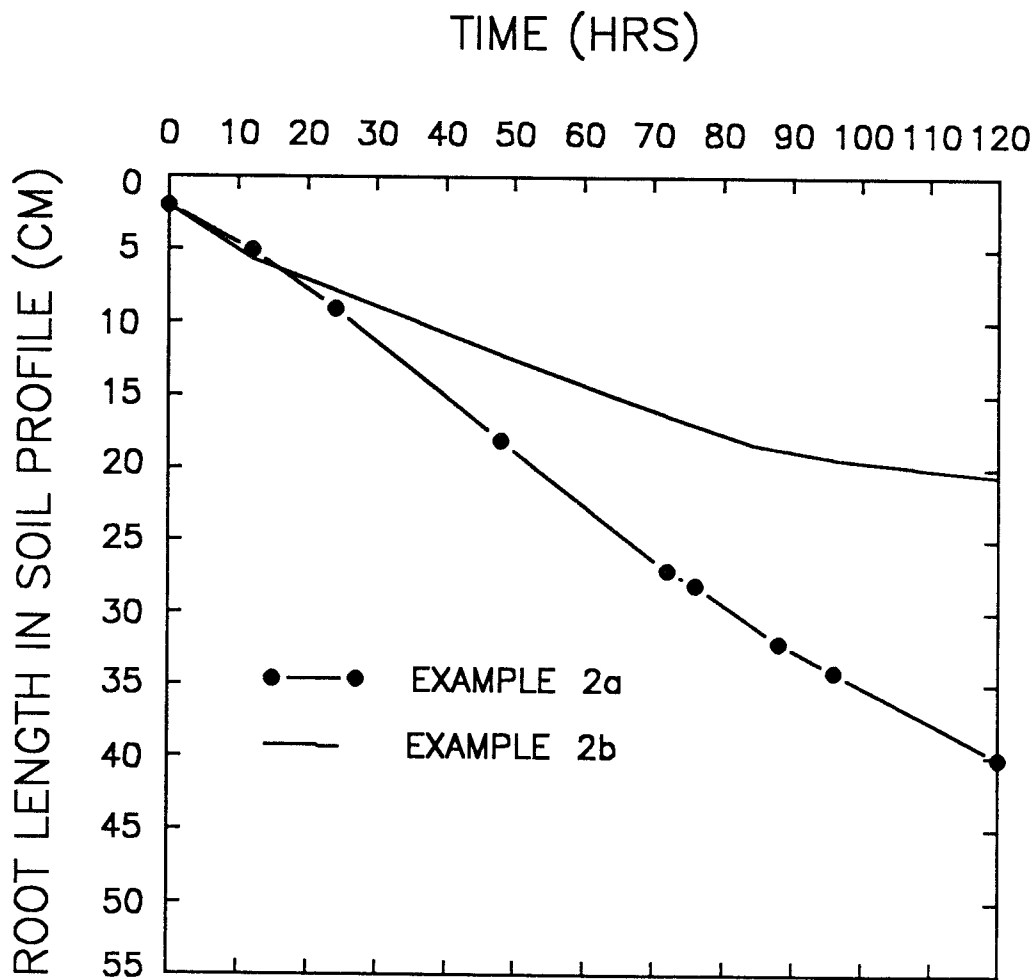


Figure 55. Root length in soil profile as a function of time in Example 2a and Example 2b since the start of the simulation.

### Example 3

#### Statement of the Problem

This example was chosen to compare the differences in carbon dioxide concentrations resulting from ideal versus non-ideal behavior of carbon dioxide diffusion through soil under poorly aerated conditions. Two simulations were made. The first simulation assumed that both oxygen and carbon dioxide molecules behave as ideal gases. This assumption implies that the activity coefficients of oxygen and carbon dioxide are unity. The second simulation assumed that the oxygen molecules behave as an ideal gas, while carbon dioxide molecules behave as a non-ideal gas. The activity coefficient of carbon dioxide was chosen to be a function of carbon dioxide concentration. Comparison of the two simulations allows the evaluation of the rate of carbon dioxide diffusion under ideal and non-ideal assumptions in poorly aerated conditions.

#### Input Parameters

All the input parameters were the same as in Example 2 except for the follows:

- (1) Initial oxygen and carbon dioxide concentrations were chosen to be a function of soil depth (Figures 56 and 57);
- (2) The activity coefficient of carbon dioxide in the second simulation was chosen to be a function of carbon dioxide concentration, calculated using equation (139); and

(3) The respiration quotient (RQ) was assumed to be 1.2 for soil microorganisms.

### Discussion of Simulation Results

Differences in carbon dioxide concentrations resulting from ideal versus non-ideal behavior of carbon dioxide diffusion through soil is in Figure 58. This diagram shows the difference in carbon dioxide concentrations as a function of soil depth at 76 hours since the start of the simulation. The activity coefficients of carbon dioxide in the non-ideal diffusion were calculated by using equation (139). This equation states that the activity coefficients are functions of carbon dioxide concentration and temperature. The activity coefficients of carbon dioxide in the ideal diffusion were set to be unity. As was indicated in Figure 58, the maximum difference in carbon dioxide concentration in the non-ideal versus ideal diffusion is about  $0.0175 \mu\text{g cm}^{-3}$  air at the depth of about 25 cm. This is quite small in comparison with the carbon dioxide concentration in the atmosphere, namely  $0.6134 \mu\text{g cm}^{-3}$  air (Nobel and Palta, 1989).

### Conclusions

Although the difference of carbon dioxide concentrations in ideal and non-ideal behaviors was detected, such a small difference does not have a significant effect on the activities of roots and microorganisms.

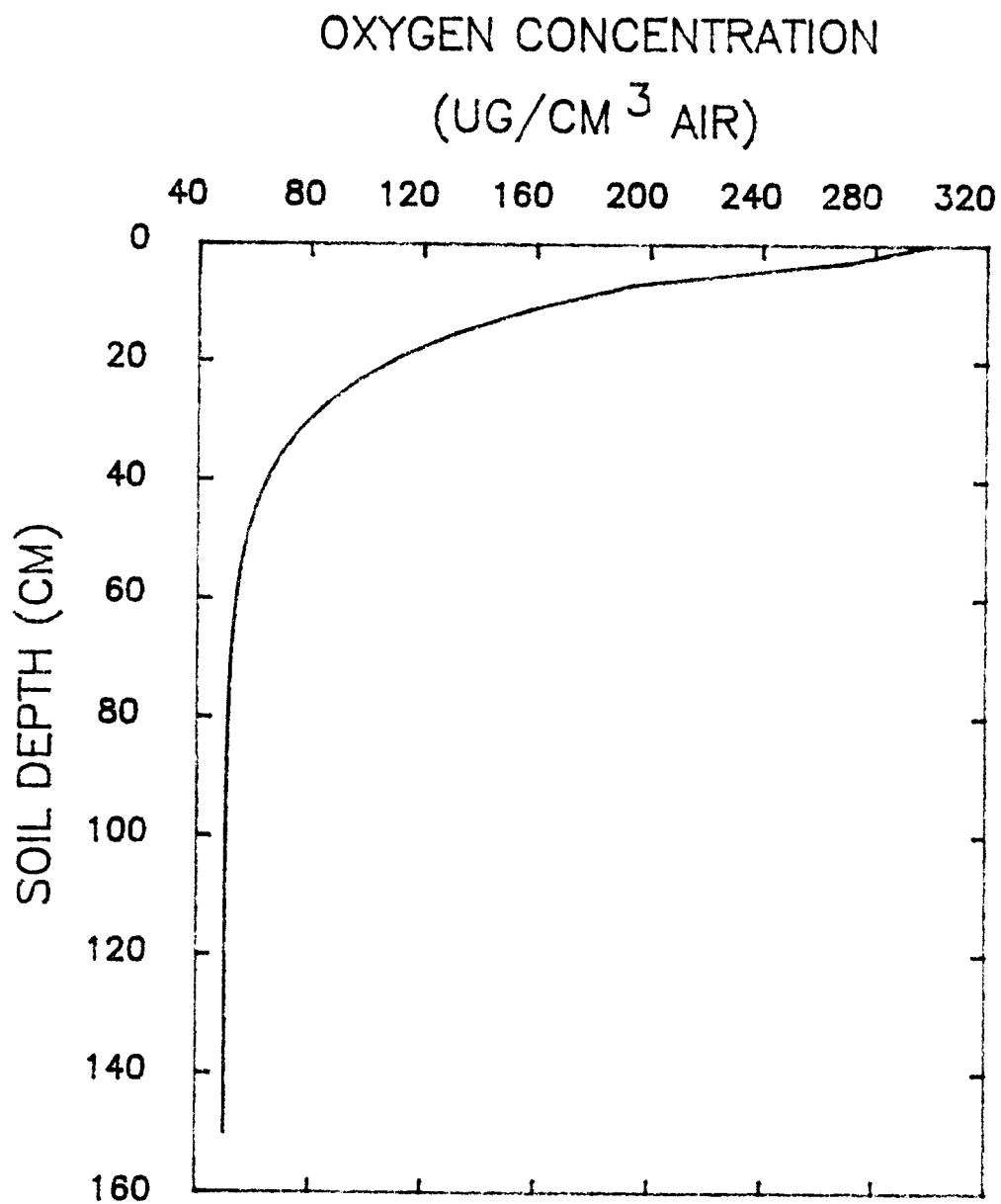


Figure 56. Initial oxygen concentration as a function of soil depth.

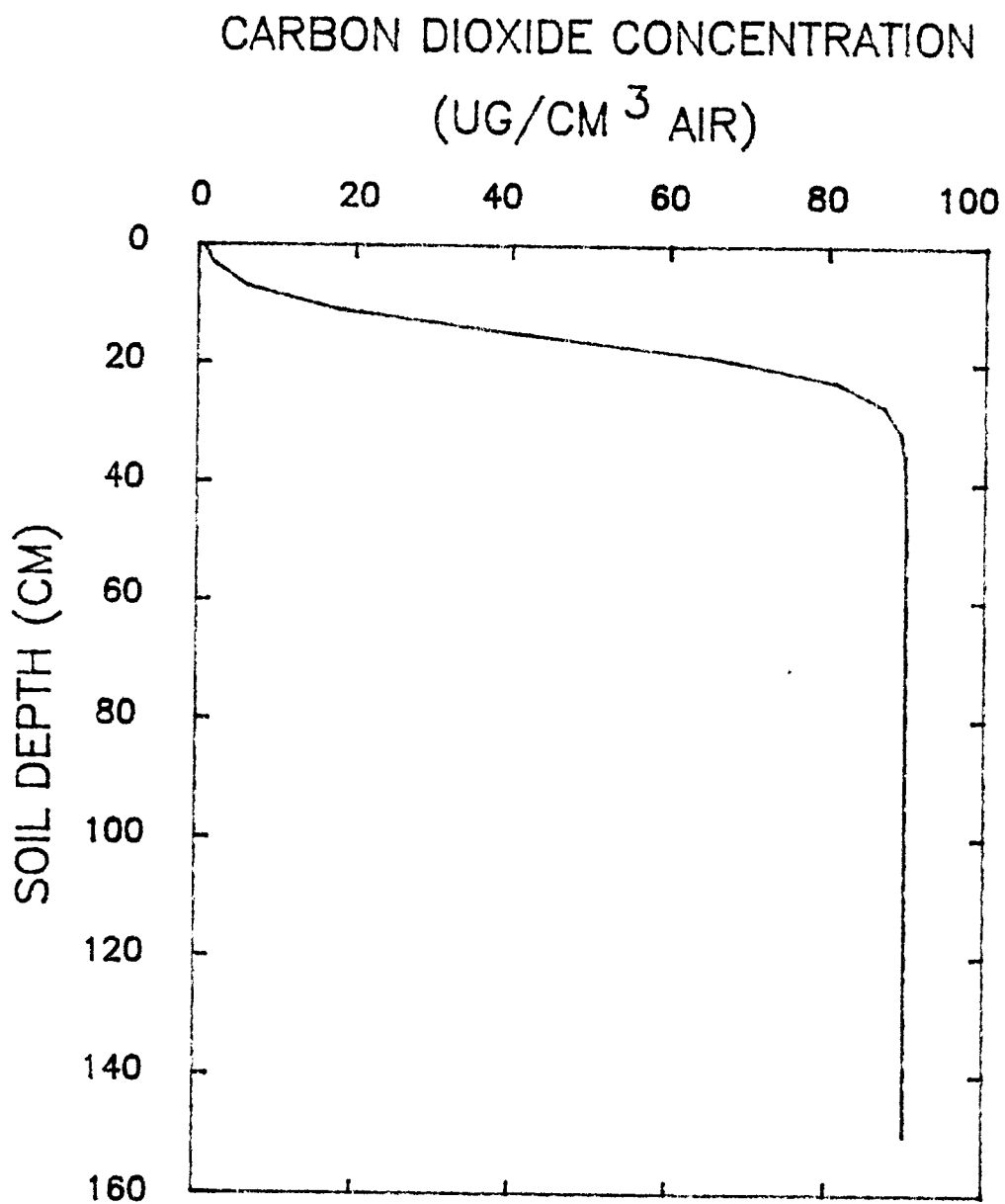


Figure 57. Initial carbon dioxide concentration as a function of soil depth.

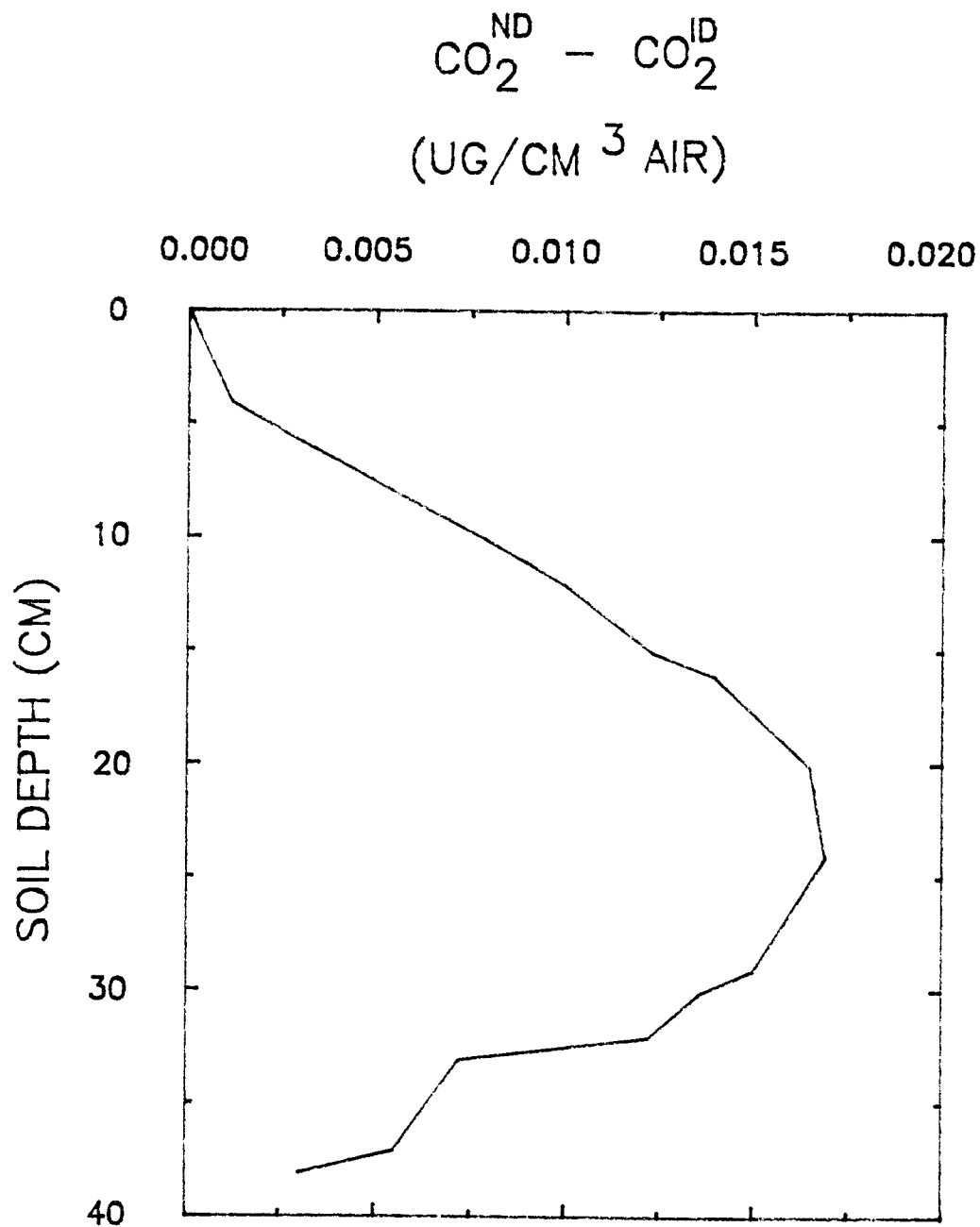


Figure 58. Difference of carbon dioxide concentrations between non-ideal and ideal diffusion as a function of soil depth at 76 hours.  $\text{CO}_2^{\text{ND}}$  and  $\text{CO}_2^{\text{ID}}$  are the concentrations of carbon dioxide in non-ideal and ideal diffusion, respectively.

#### Example 4

##### Statement of the Problem

This example was chosen to compare the results of the simultaneous transport of water, heat, oxygen, and carbon dioxide through a compacted versus non-compacted soil. A compacted soil layer was assumed to exist between the soil depths of 15 cm and 20 cm. Comparisons of the simulation results may allow to evaluate the conditions which lead to deficiency of oxygen and build up of carbon dioxide within and below the compacted soil layer.

##### Input Parameters

All the input parameters were the same as used in Example 2a except for those discussed below.

Hydraulic Conductivity and Water Potential. In this simulation, the hydraulic conductivity and soil water potential of the compacted soil layer were assumed to be the functions of soil depth in addition to soil water content. The hydraulic conductivity and soil water potential in the compacted soil layer were calculated using equations (123) and (124), respectively, with the parameters such as  $K_S$ ,  $\theta_r$ ,  $\theta_s$ ,  $\gamma_c$ ,  $\alpha_\theta$ , and  $\beta_\theta$  chosen to be functions of soil depth (Table 9).

Table 9. Some parameters used to calculate the hydraulic conductivity and water potential in a compacted soil layer by using equations (123) and (124).

Soil depth	$K_s$	$\theta_r$	Parameters			
			$\theta_s$	$\gamma_c$	$\alpha_\theta$	$\beta_\theta$
cm	cm hr <sup>-1</sup>	cm <sup>3</sup> cm <sup>-3</sup>	cm <sup>3</sup> cm <sup>-3</sup>	-	cm	-
15.0	0.6100	0.029	0.55	6.50	1241.39	0.7079
16.3	0.1500	0.025	0.44	8.89	1242.00	2.5000
17.5	0.0001	0.020	0.40	9.00	1243.00	3.5000
18.9	0.1500	0.024	0.44	8.70	1242.00	2.5000
20.0	0.6100	0.029	0.55	6.50	1241.39	0.7079

Figures 59 and 60 show the hydraulic conductivity and soil water potential in non-compacted and compacted soil as a function of soil water content. The values of hydraulic conductivity and water potential for the compacted soil were calculated at a depth of 17.5 cm.

Initial Root Length. The initial root length was assumed to be 30 cm for both the compacted and the non-compacted soil.

Initial Soil Water Content. The initial soil water content was set up to change with soil depth (Figure 61).

Simulation Time. The simulation time was chosen to be 72 hours.

#### Discussion of Simulation Results

Soil Water Content. Changes in soil water content in compacted and non-compacted soil during the 72 hours simulation period is shown Figure 61. This diagram shows the volumetric water content as a

function of soil depth at several points in time since the start of the simulation. The simulation started with the same initial soil water content in both the compacted and the non-compacted soil and with a rainfall period, which lasted for 12 hours. The infiltration profile of the non-compacted soil at 12 hours shows a smooth curve with substantially decreasing soil water content starting at about  $0.415 \text{ cm}^3 \text{ cm}^{-3}$  at the soil surface to  $0.15 \text{ cm}^3 \text{ cm}^{-3}$  at the depth of 35 cm. In contrast, the infiltration profile of the compacted soil at 12 hours shows a discontinuous curve at the depth of 15 to 20 cm, as a result of the existing compacted soil layer. The water content decreased from  $0.42 \text{ cm}^3 \text{ cm}^{-3}$  at the soil surface to about  $0.38 \text{ cm}^3 \text{ cm}^{-3}$  at the depth of 15 cm, and then increased to about  $0.43 \text{ cm}^3 \text{ cm}^{-3}$  at 16 cm, and again decreased to  $0.42 \text{ cm}^3 \text{ cm}^{-3}$  at 20 cm, finally decreased to  $0.15 \text{ cm}^3 \text{ cm}^{-3}$  at depth of 35 cm. The hanging of soil water within the compacted layer is thoroughly controlled by the sizes of soil pores. Small soil pores have a lower soil water potential which has a larger suction force to retain the soil water.

Following the 12 hours with rainfall was a period of change in the water content of the soil profile caused by evaporation at the soil surface and deeper infiltration of water into the soil due to the water potential at the wetting front. Compared with the non-compacted soil, the retention of soil water in the compacted soil from 15 cm to 20 cm at 48 and 72 hours was clearly a result of the existence of the compacted soil layer.

Concentration of Oxygen. Changes in oxygen concentrations in compacted and non-compacted soil during the 72 hour simulation period is shown in Figure 62. This diagram shows oxygen concentration as a

function of soil depth at several points in time since the start of the simulation. The simulation started with a rainfall period, which lasted for 12 hours. This rainwater infiltrated into the soil and increased the water content rapidly at the compacted soil layer (Figure 61), which reduced the soil pore spaces for the diffusion of oxygen. As a result, the rapid depletion of oxygen occurred in the compacted soil layer with the minimum oxygen concentration  $80 \mu\text{g cm}^{-3}$  air at the depth of 17.5 cm at 12 hours. Compared with that of the non-compacted soil, the depletion of oxygen was small, namely  $210 \mu\text{g cm}^{-3}$  air.

At 48 and 72 hours, the oxygen concentrations increased in both the compacted and the non-compacted soil above the depth of 15 cm. This is so because more soil pore spaces were available for the supply of oxygen from the atmosphere because of the evaporative loss of soil water (Figure 61) and because of the rate of oxygen supply from the atmosphere was higher than the rate of oxygen use by roots and microorganisms. The existence of the compacted soil layer restricted the further diffusion of oxygen across below 15 cm and retained more oxygen in above 15 cm. As a result, the increase in oxygen concentration was faster in the compacted soil than it was in the non-compacted soil at above 15 cm.

Below the depth of 20 cm, there was an increasing depletion of oxygen from 12 to 48 and to 72 hours for both the compacted and non-compacted soil due to the growth of roots. Compared with that of the non-compacted soil, the increased in depletion of oxygen was large. For example, the oxygen concentration at the depth of 30 cm at 48 hours was about  $180 \mu\text{g cm}^{-3}$  air in the compacted soil, whereas

was about  $210 \mu\text{g cm}^{-3}$  air in the non-compacted soil. This larger depletion of oxygen in the compacted soil below 20 cm was due to a restriction of the oxygen supply from above the compacted layer.

Changes in oxygen concentrations in the compacted and the non-compacted is shown in Figure 63. This diagram shows oxygen concentration at the soil depth of 35 cm as a function of time since the start of the simulation. Start with the initial oxygen concentration  $300 \mu\text{g cm}^{-3}$  air in both the compacted and the non-compacted soil, oxygen concentration decreases were the same in both soils from 0 to 24 hours. Then, from 48 to 72 hours, the differences in the oxygen concentration of two simulations increased. Oxygen concentration was  $205 \mu\text{g cm}^{-3}$  air at 72 hours in the non-compacted soil, but was about  $187 \mu\text{g cm}^{-3}$  air at the same time in the compacted soil. This is so because the diffusion of oxygen in the compacted soil was restricted by the compacted layer.

Concentration of Carbon Dioxide. Changes in carbon dioxide concentrations in the compacted and the non-compacted soil during the 72 hour simulation period is shown in Figure 64. This diagram shows carbon dioxide concentration as a function of soil depth at several points in time since the start of the simulation.

As was shown in Figure 64, the carbon dioxide concentrations continued to increase in both the compacted and the non-compacted soil from 0 hours through 72 hours due to the release of carbon dioxide by the respiratory activities of roots and microorganisms. However, the carbon dioxide concentration from the soil depths of 20 cm to 25 cm at 72 hours in the compacted soil was higher than that in the non-compacted soil. For example, the carbon dioxide

concentration at 25 cm at 72 hours was about  $170 \mu\text{g cm}^{-3}$  air in compacted soil, but was  $150 \mu\text{g cm}^{-3}$  in the non-compacted soil. This indicates that more carbon dioxide was accumulated within the depth of 20 to 25 cm. This is so because of the restriction of carbon dioxide diffusion out of the soil by the compacted layer above.

Rates of Oxygen Consumption by Roots and Microorganisms. The rates of oxygen consumption by roots and microorganisms used in compacted and non-compacted soil are shown in Figures 65 and 66. Each figure shows the rate of oxygen consumption in  $\mu\text{g cm}^{-3}$  soil  $\text{hr}^{-1}$ . The rate of oxygen consumption by roots was converted from  $\mu\text{g cm}^{-3}$  fresh roots  $\text{hr}^{-1}$  to  $\mu\text{g cm}^{-3}$  air  $\text{hr}^{-1}$  (Appendix III), as was required by the unit used in the oxygen field equation. The sequence of the two diagrams shows the changes in oxygen use as a function of soil depth. The growth of the plant roots can be deduced from the diagrams. The roots grew from the 30 cm soil depth at the start of the simulation to the 44 cm depth at the end of the 72 hour simulation. The population of microorganisms was distributed uniformly from the soil surface down to the depth of 20 cm throughout the simulations. The diagram clearly shows the increased rate of oxygen consumption as a function of distance along the root length. The highest rate is always at the root tip. Since the rate of oxygen consumption also is a function of oxygen concentration, the maximum rate varies according to the oxygen concentration in the soil air. The rate at the root tip was highest with the simulation at 12 hours namely  $7.2 \mu\text{g cm}^{-3}$  soil  $\text{hr}^{-1}$  and lowest with the simulation at 24 hours, namely  $5.1 \mu\text{g cm}^{-3}$  soil  $\text{hr}^{-1}$  in compacted soil. Similar results were obtained in the non-compacted soil.

The interesting result shown in Figure 66 is that the maximum rate of oxygen consumption at 72 hours in the compacted soil was  $5.1 \mu\text{g cm}^{-3} \text{ soil hr}^{-1}$ , while that in the non-compacted soil is  $5.9 \mu\text{g cm}^{-3} \text{ soil hr}^{-1}$ . Such lower in the maximum rate of oxygen consumption in the compacted soil implies the lower supply of oxygen from the above soil due to restriction of the compacted layer, since the rate was a function of oxygen concentration. If the simulation time would last longer than 72 hours, a larger difference in the maximum rate of oxygen consumption between the compacted and the non-compacted soil would be observed.

Comparison of Root Length. Changes in root length in the compacted and the non-compacted soil are shown in Figure 67. This diagram shows root length in the soil profile as a function of time since the start of the simulation. Start with the initial root length of 30 cm, which is far deeper than the compacted layer, in both the compacted and the non-compacted soil, root elongation rate was the same for both soils from 0 to 48 hours. Then, from 48 to 72 hours, the differences in root length of two simulations increased. Root length was 42.0 cm at 72 hours in the non-compacted soil. But was 39 cm at the same time in the compacted soil. This is so because that the oxygen concentration in the compacted soil was less than that of the non-compacted soil (Figure 64).

### Conclusions

This example simulates the transport of water, oxygen, and carbon dioxide through the compacted soil. Results show that more

oxygen was depleted and more carbon dioxide was produced in the soil below the compacted layer as compared with that in the non-compacted soil. As a result, the root elongation was slower in the compacted soil than in the non-compacted soil.

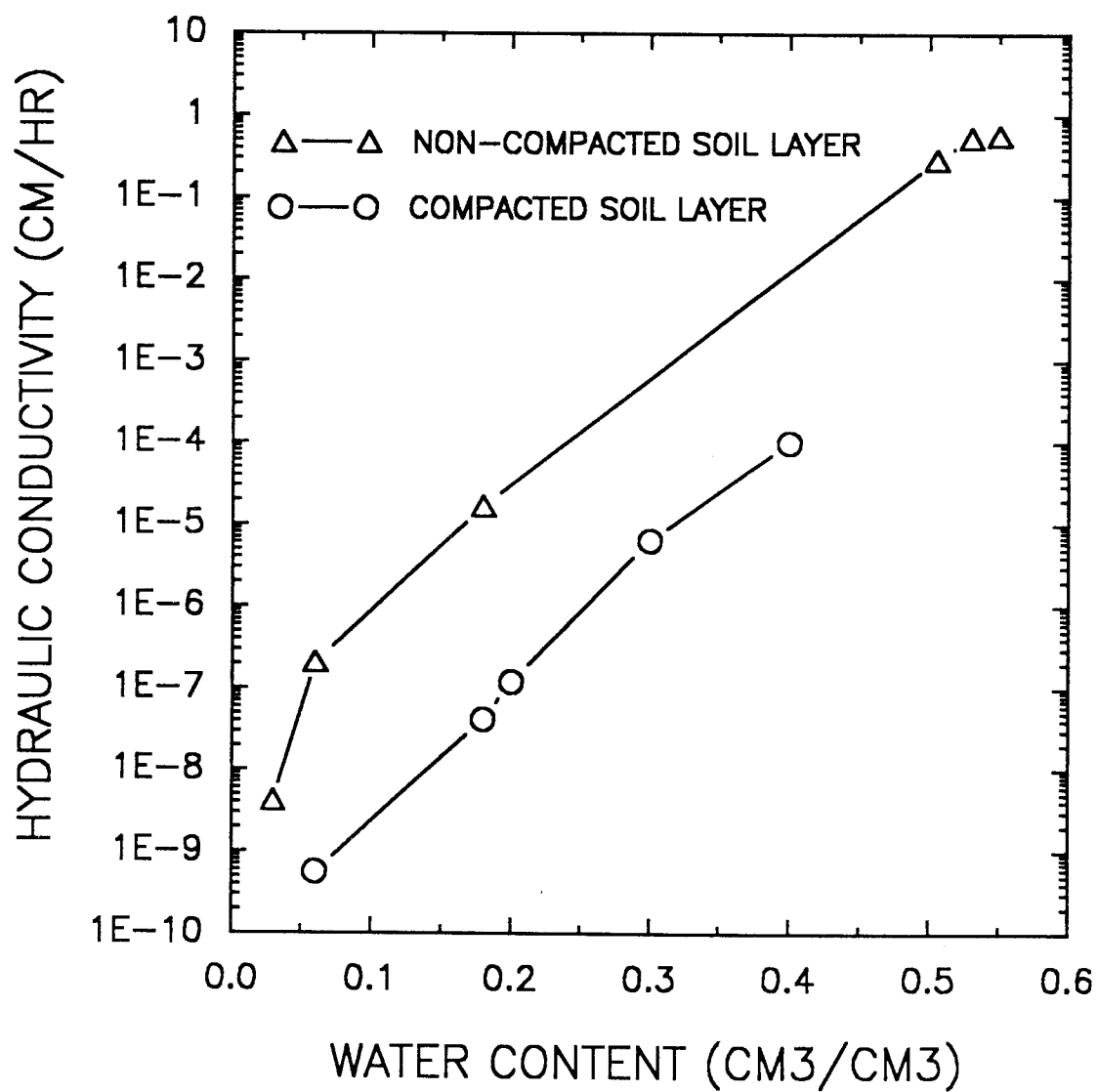


Figure 59. Hydraulic conductivity as a function of soil water content at the soil depth of 17.5 cm.

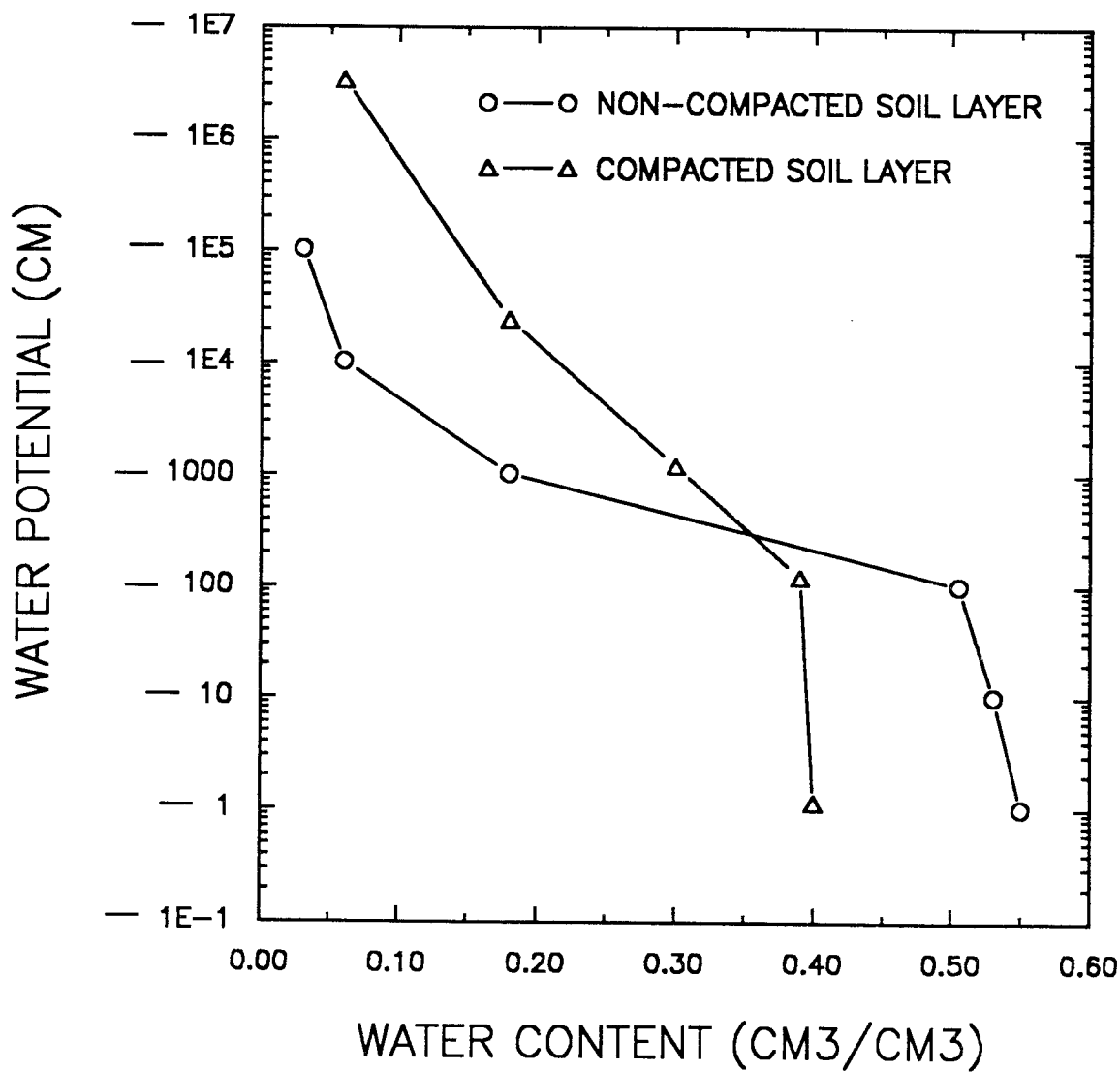


Figure 60. Water potential as a function of soil water content at the soil depth of 17.5 cm.



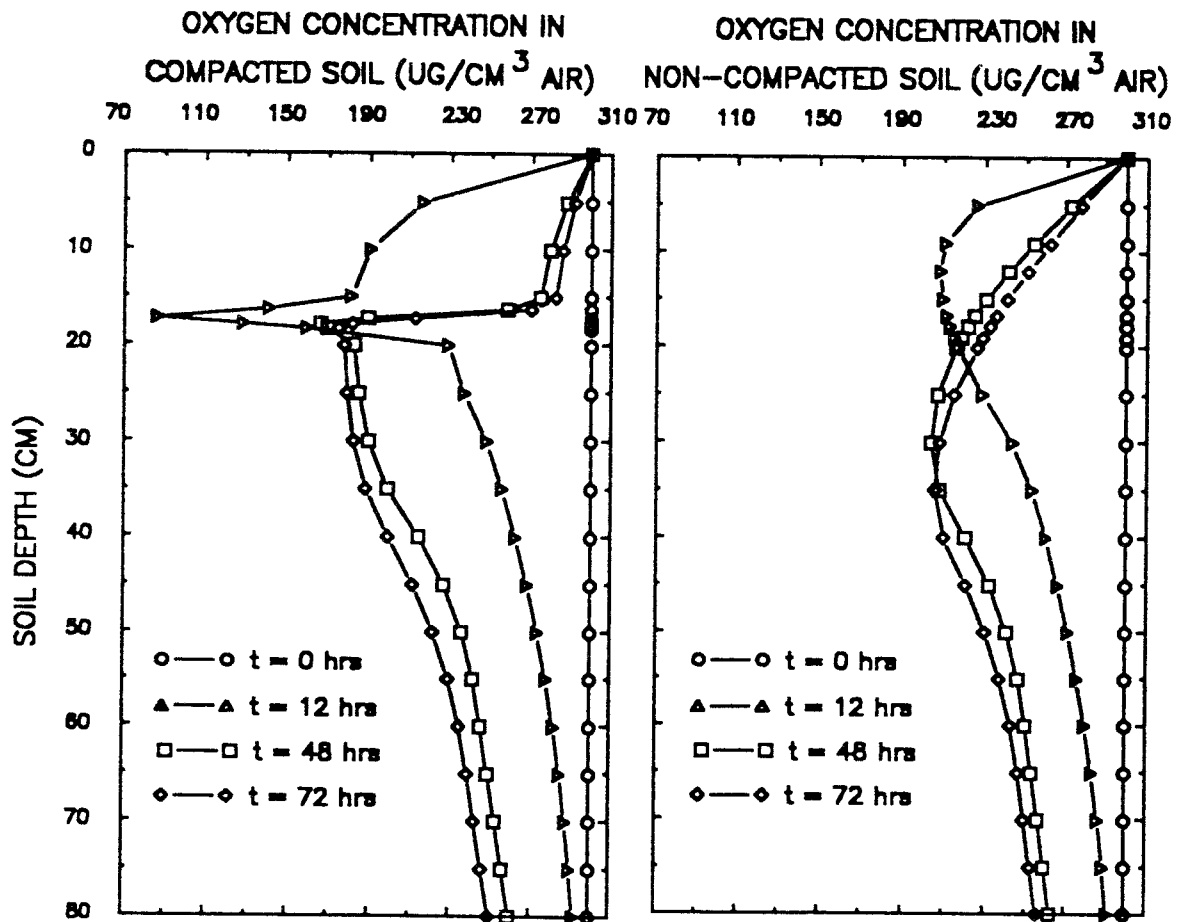


Figure 62. Oxygen concentration as a function of soil depth in the compacted and non-compacted soil at 0, 12, 48, and 72 hours since start. The rainfall started from 0 hour and stopped at 12 hours.

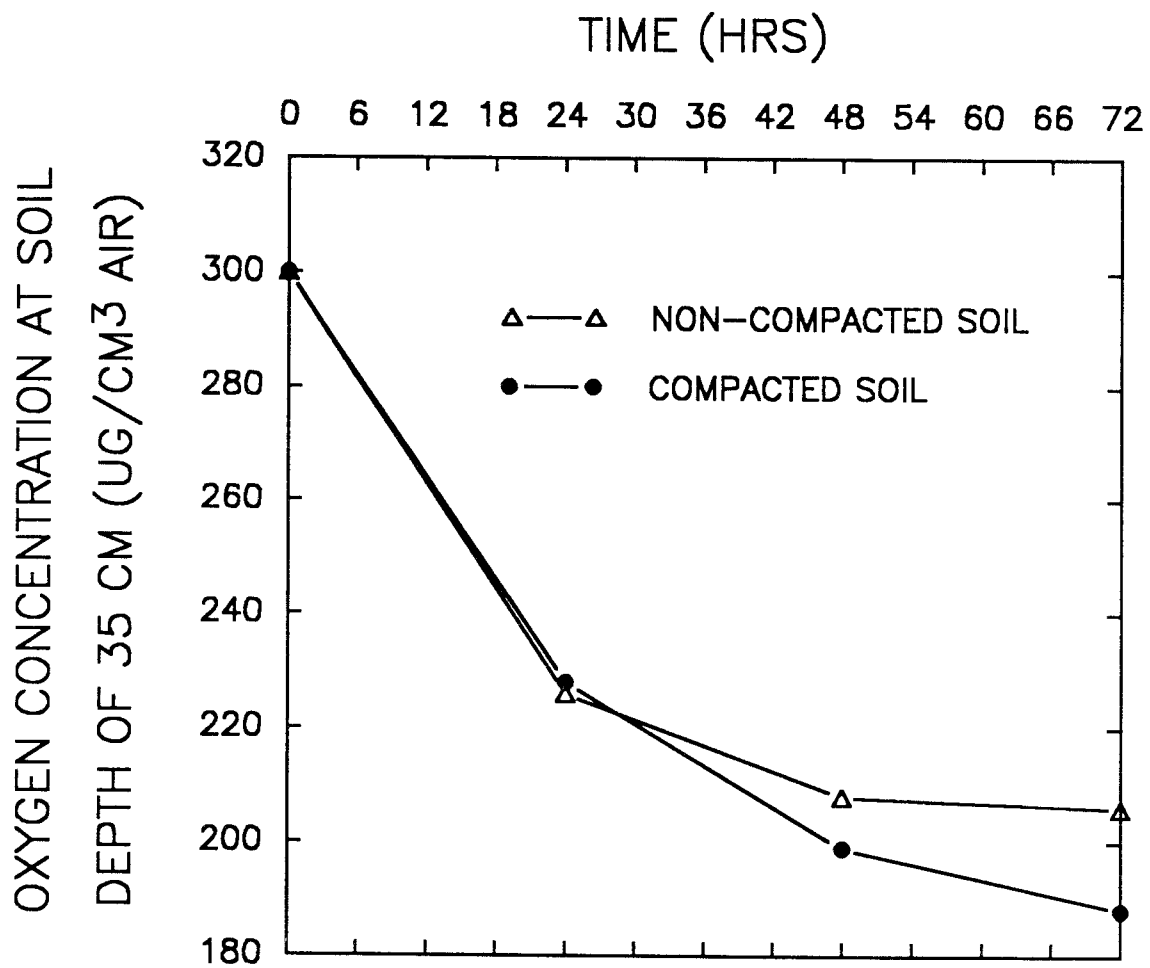


Figure 63. Oxygen concentration as a function of time at the soil depth of 35 cm in compacted and non-compacted soil.

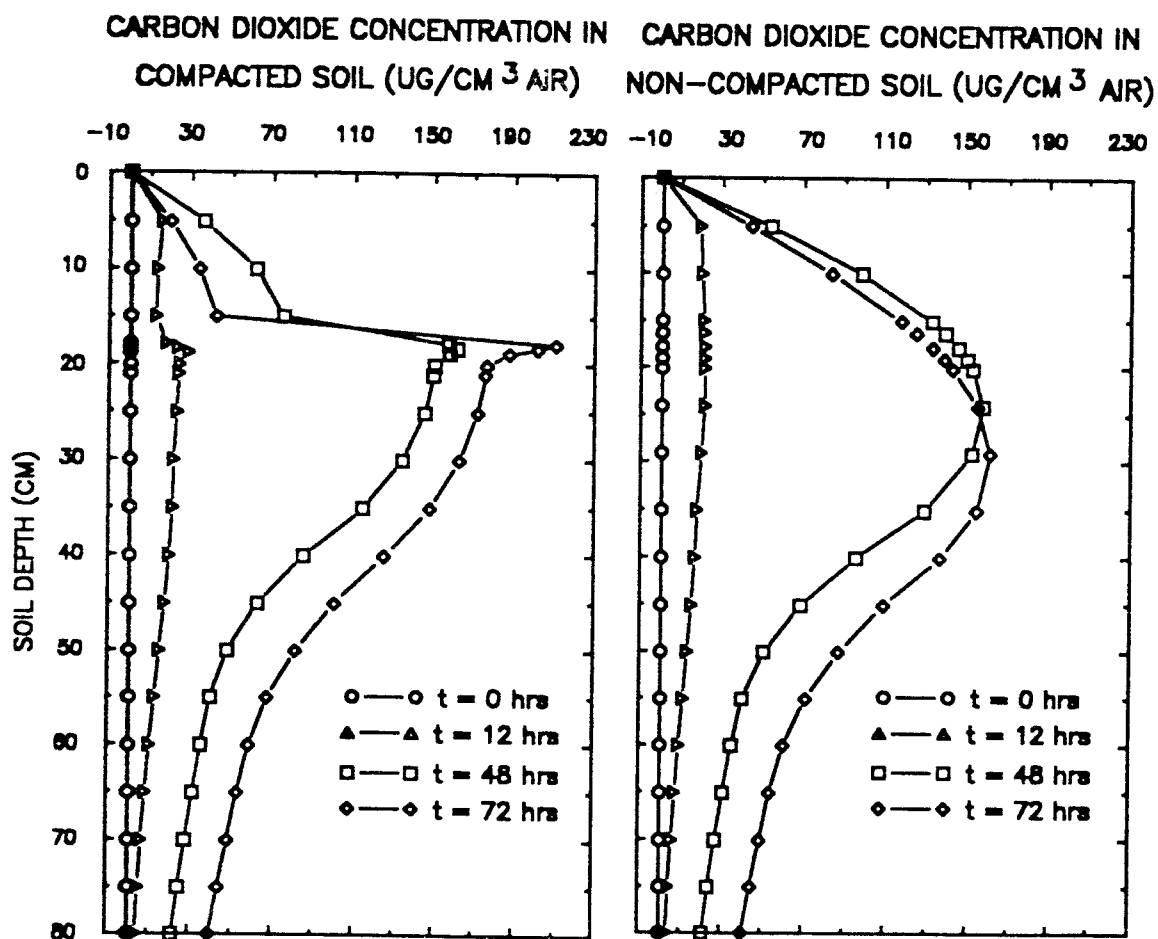


Figure 64. Carbon dioxide concentration as a function of soil depth in the compacted and non-compacted soil at 0, 12, 48, and 72 hours since start.

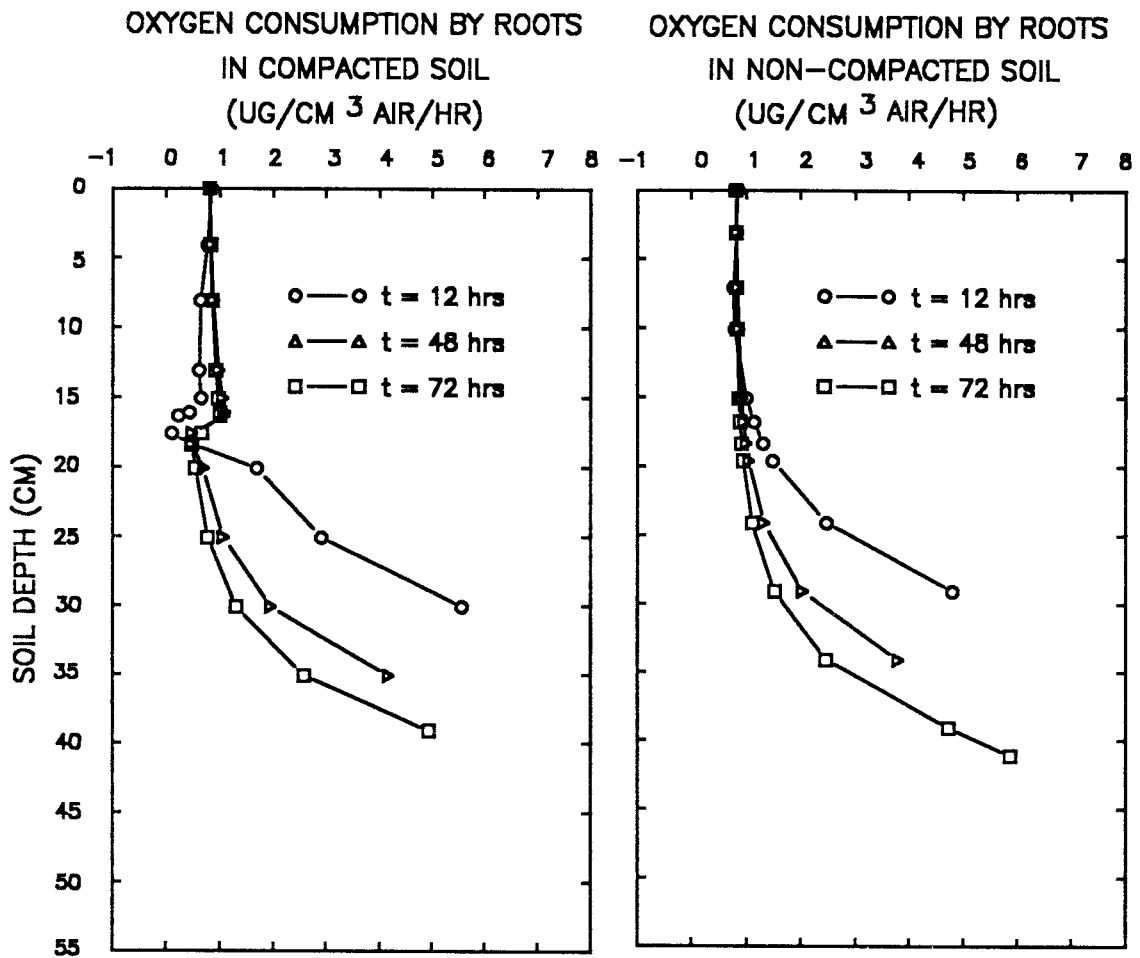


Figure 65. Oxygen consumption rates by plant roots as a function of soil depth in the compacted and non-compacted soil at times of 0, 12, 48 and 72 hours. The rate of oxygen consumption in  $\mu\text{g cm}^{-3}$  fresh roots  $\text{hr}^{-1}$  was converted to  $\mu\text{g cm}^{-1}$  air  $\text{hr}^{-1}$  as shown on the Figure.

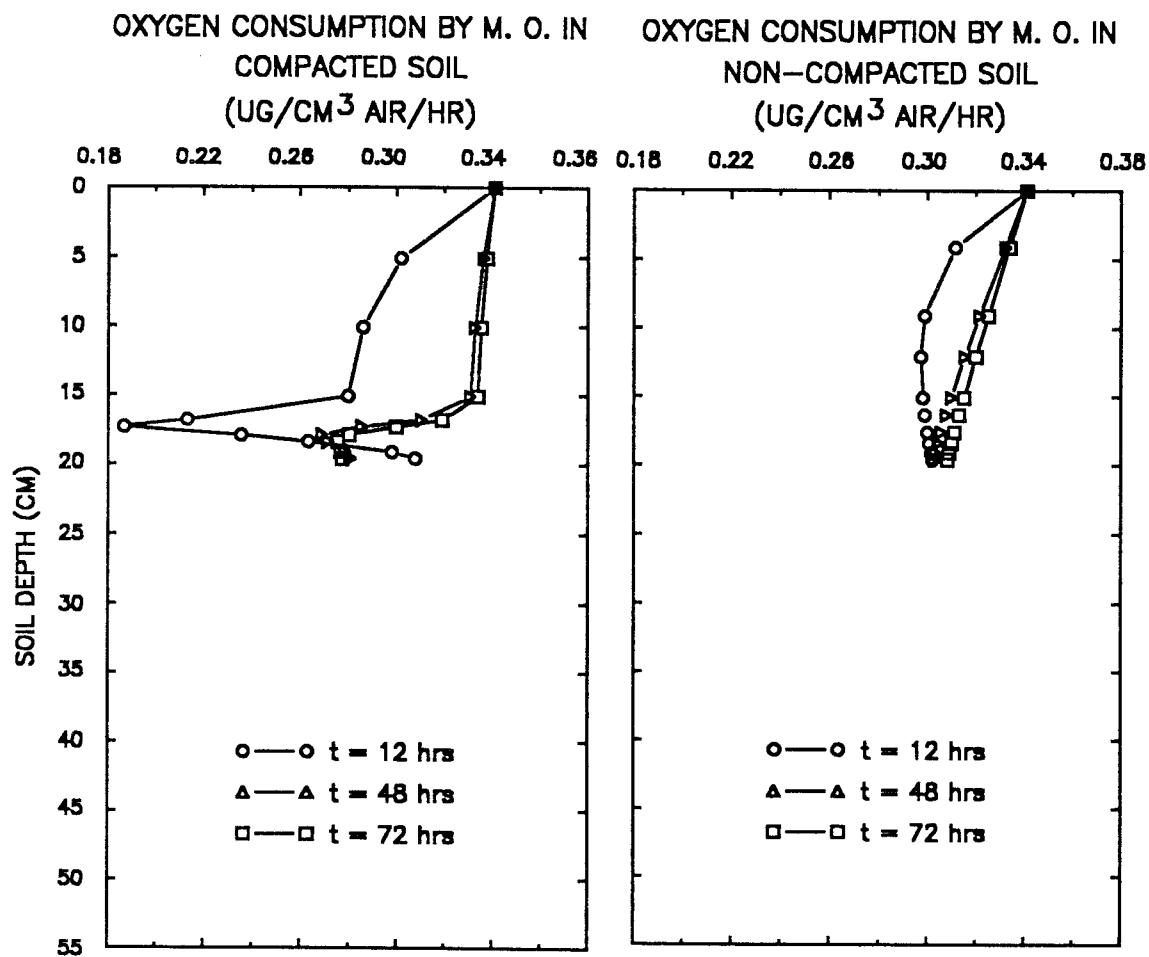


Figure 66. Oxygen consumption rates by microorganisms as a function of soil depth in the compacted and non-compacted soil at times of 12, 48 and 72 hours.

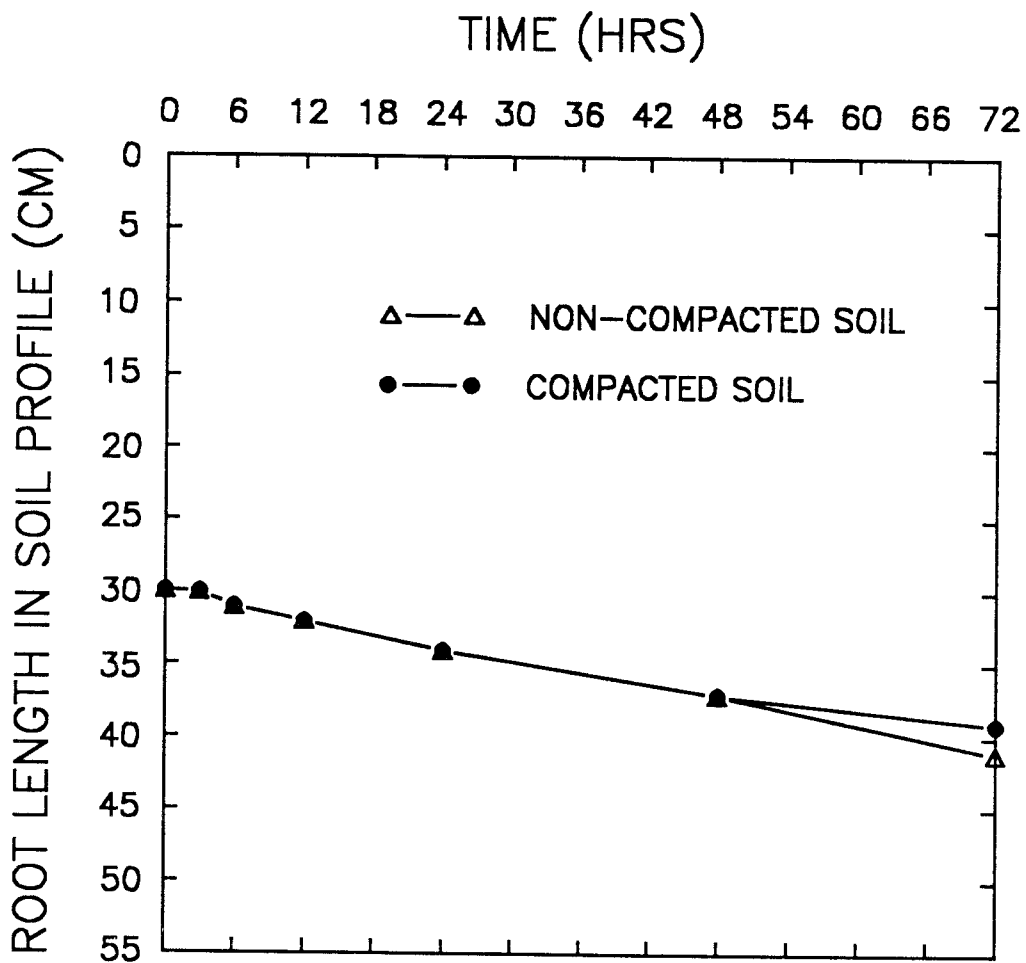


Figure 67. Root length in soil profile as a function of time in the compacted and the non-compacted soil since the start of the simulation.

### Example 5a

#### Statement of the Problem

This example was chosen to simulate the diffusion of oxygen and carbon dioxide within the plant canopy and soil system (Figure 68). Roots penetrate into the soil, as the plant canopy above the ground grows. Plant leaves fix carbon dioxide and evolve oxygen in the processes of photosynthesis and consume oxygen and produce carbon dioxide in the processes of photorespiration and respiration. These processes affect the oxygen and carbon dioxide concentrations at the atmosphere-soil interface (Nobel, 1983). Therefore, when modeling the dynamic exchange of oxygen and carbon dioxide between the atmosphere and the soil, it is necessary to include the transport of oxygen and carbon dioxide within the plant canopy, in addition to the diffusion through the soil. The assumptions and field equations used to simulate the transport of oxygen and carbon dioxide within the plant canopy are now discussed.

Assumptions. It was assumed that the transport of oxygen and carbon dioxide within the plant canopy is governed only by diffusion. Mass flow of oxygen and carbon dioxide was not considered here. This is justified by assuming that the wind speed is close to zero, so that no mass flow of oxygen and carbon dioxide occurs within the plant canopy. In addition, the diffusion of oxygen and carbon dioxide within the plant canopy was also assumed to be controlled by photosynthesis, photorespiration, and respiration of plant leaves.

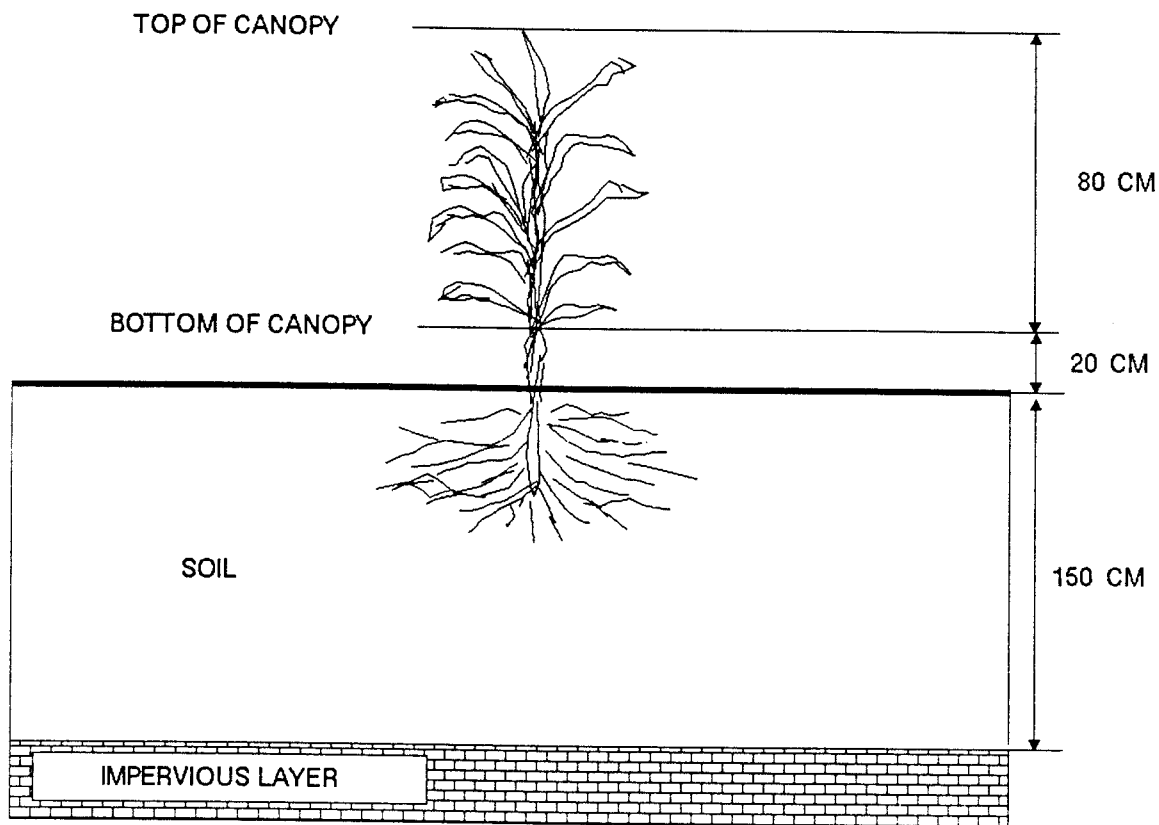


Figure 68. Schematic diagram of a plant and soil profile for which the diffusion of oxygen and carbon dioxide within the plant canopy and through the soil was simulated.

Field Equations. Field equations for the diffusion of oxygen and carbon dioxide within the plant canopy were obtained by modifying equations (52) and (53). By eliminating the terms for soil water content, soil porosity, adsorption of oxygen and carbon dioxide by the surfaces of soil particles, dissolution of oxygen and carbon dioxide in soil water, and sink and source of roots and microorganisms from equations (52) and (53), setting the activity coefficient equal to unity, and adding the terms for photosynthesis, photorespiration, and respiration to equation (52) and (53), equations (155) and (156) are obtained:

$$\frac{\partial}{\partial t} (C_{o_2}^a) = -\nabla \cdot [D_{o_2}^a \frac{\partial C_{o_2}^a}{\partial z}] + Pn_{o_2} - Res_{o_2} \quad (155)$$

for oxygen and

$$\frac{\partial}{\partial t} (C_{co_2}^a) = -\nabla \cdot [D_{o_2}^a \frac{\partial C_{co_2}^a}{\partial z}] - Pn_{co_2} + Res_{co_2} \quad (156)$$

for carbon dioxide, where  $C_{o_2}^a$  and  $C_{co_2}^a$  are the concentrations of oxygen and carbon dioxide within the plant canopy ( $\mu\text{g cm}^{-3}$  air),  $D_{o_2}^a$  and  $D_{co_2}^a$  are the diffusion coefficients of oxygen and carbon dioxide within the plant canopy ( $\text{cm}^2 \text{hr}^{-1}$ ),  $z$  is the height of plant canopy (cm),  $Pn_{o_2}$  and  $Pn_{co_2}$  are the rates of carbon dioxide fixation and oxygen evolution by photosynthesis ( $\mu\text{g cm}^{-3} \text{hr}^{-1}$ ),  $Res_{o_2}$  and  $Res_{co_2}$  represent the rates of oxygen consumption and carbon dioxide production by photorespiration and respiration ( $\mu\text{g cm}^{-3} \text{hr}^{-1}$ ).

Equations (155) and (156) together with equations (52) and (53) describe the diffusion of oxygen and carbon dioxide within the plant canopy and through the soil.

In this simulation, the upper boundary conditions for the diffusion of oxygen and carbon dioxide were set up at the top of plant canopy. These are:

$C_{o_2}^a(0,t)$  = oxygen concentration of the atmosphere ( $300 \mu\text{g cm}^{-3}$  air),

and

$C_{co_2}^a(0,t)$  = carbon dioxide concentration of the atmosphere ( $300 \text{ mg cm}^{-3}$  air).

The lower boundary conditions were the same as used in Example 2a. Finite difference methods, used to solve field equations (155) and (156), are the same as discussed in the section "Solution of Oxygen Field Equation" starting on page 71. The program listing was shown in Appendix V.

Simulations with and without a plant canopy were conducted. Comparison of these two simulations allows evaluation of the effects of plant canopy on the transport of oxygen and carbon dioxide through the soil.

#### Input Parameters

All the input parameters were the same as used in Example 2a except as indicated below.

(1) Solar Radiation. It was assumed that with the plant canopy present, solar radiation could not reach the soil surface directly.

(2) Rainfall. Rainfall was not included with the simulations.

(3) Air Temperature. Air temperature was assumed to be a function of time as shown in Figure 69.

(4) Relative Humidity of the Air. Relative humidity of the air at the soil surface was assumed to be a function of time as shown in Figure 70.

(5) Wind Speed. Wind speed was assumed to be zero, so that no mass flow of oxygen and carbon dioxide within the plant canopy occurred.

(6) Height of Plant and Length of Canopy. The height of plant was chosen to be 100 cm with the length of canopy 80 cm counting from the top of canopy (Figure 68).

(7) Initial Oxygen Concentration. The initial oxygen concentrations within the plant canopy and throughout the soil are  $300 \mu\text{g cm}^{-3} \text{ hr}^{-1}$ , which is equivalent to 21% by volume.

(8) Initial Carbon Dioxide Concentration. The initial carbon dioxide concentrations within the plant canopy and throughout the soil are  $0.6134 \mu\text{g cm}^{-3} \text{ hr}^{-1}$ , which is equivalent to 340 ppm.

(9) Initial Soil Water Content. The initial soil water content is  $0.25 \text{ cm}^3 \text{ cm}^{-3}$ .

(10) Initial Root Length. The initial root length is set to be 5 cm.

(11) Rate of Carbon Dioxide Fixation and Oxygen Evolution by the Photosynthesis Processes. It was assumed that photosynthesis occurs during the day from 6 to 18 hours. The rates of carbon dioxide fixation and oxygen evolution were assumed to be a function of time and carbon dioxide concentration. The rate of carbon dioxide fixation during photosynthesis as a function of time was represented by (Figure 71):

$$Pn_{CO_2}(t) = a_1 + a_2t + a_3t^2 + a_4t^3 + a_5t^4 \quad (157)$$

where  $Pn_{CO_2}(t)$  is the rate of carbon dioxide fixation during photosynthesis ( $\mu\text{g cm}^{-3} \text{ hr}^{-1}$ ),  $a_1$ ,  $a_2$ ,  $a_3$ ,  $a_4$ , and  $a_5$  are coefficients characterizing the shape of the function with  $a_1 = 585.71$ ,  $a_2 = -265.00$ ,  $a_3 = 41.04$ ,  $a_4 = -2.50$ , and  $a_5 = 0.05$ ,  $t$  is the time (hr).

Equation (157) implies that the rate of carbon dioxide fixation during photosynthesis is only a function of time. This is not so within the canopy when the carbon dioxide concentration is lower than its saturated concentration for photosynthesis. In order to include the effects of carbon dioxide concentration on the rate of carbon dioxide fixation during photosynthesis within canopy, a correction factor was introduced by assuming that the correction factor is unity when the carbon dioxide reaches its saturated concentration, and decreases as the carbon dioxide concentration decreases (Figure 72). The following equation was proposed to relate the correction factor to the carbon dioxide concentration:

$$F_6 = \frac{a_6}{1 + b_6 \text{ EXP} \left[ -c_6(C_{CO_2}^a - C_{CO_2}^{th}) \right]}, \quad (158)$$

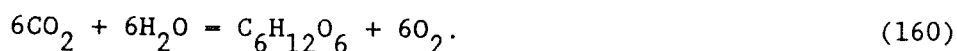
where  $F_6$  is the correction factor,  $a_6$ ,  $b_6$ , and  $c_6$  are constants characterizing the shape of the equation with  $a_6 = 1$ ,  $b_6 = 200$ , and  $c_6 = 0.04$ ,  $C_{CO_2}^a$  is the carbon dioxide concentration within the canopy ( $\mu\text{g cm}^{-3}$  air), and  $C_{CO_2}^{th}$  is the threshold carbon dioxide concentration below which photosynthesis approaches zero ( $\mu\text{g cm}^{-3}$  air).

Multiplying equations (158) and (157) yields:

$$Pn_{\text{CO}_2}(t, \text{CO}_2) = [a_1 + a_2t + a_3t^2 + a_4t^3 + a_5t^4] F_6 \quad (159)$$

Equation (159) shows that the rate of carbon dioxide fixation during photosynthesis is a function of time and carbon dioxide concentration.

The rate of oxygen evolution during photosynthesis was calculated using:



Since the rate of carbon dioxide fixation can be calculated from equation (159), the rate of oxygen evolution can be calculated from equation (160).

(12) Rate of Oxygen Consumption and Carbon Dioxide Production by Respiration. The rates of oxygen consumption and carbon dioxide production during photorespiration and respiration were assumed to be a function of time and oxygen concentration. The rate of carbon dioxide production as a function of time was represented by (Figure 71):

$$\text{Res}_{\text{CO}_2}(t) = e_1 + e_2t + e_3t^2 + e_4t^3 + e_5t^4 \quad (161)$$

where  $\text{Res}_{\text{CO}_2}(t)$  is the rate of carbon dioxide production during photorespiration and respiration ( $\mu\text{g cm}^{-3} \text{ hr}^{-1}$ ),  $e_1$ ,  $e_2$ ,  $e_3$ ,  $e_4$ , and  $e_5$  are coefficients characterizing the shape of the function with  $e_1 = 1.851$ ,  $e_2 = -0.816$ ,  $e_3 = 0.0267$ ,  $e_4 = -0.018$ , and  $e_5 = 0.0003$ ,  $t$  is the time (hr).

Equation (161) implies that the rate of carbon dioxide production is only a function of time. This is not so within the canopy when the oxygen concentration is lower than its atmospheric level

(300  $\mu\text{g cm}^{-3}$  air). In order to include the effects of oxygen concentration on the rate of carbon dioxide production during photorespiration and respiration processes, a correction factor was introduced by assuming that the correction factor is unity when the oxygen concentration is at the level in the atmosphere and decreases as the oxygen concentration decreases (Figure 73). The following equation was proposed to relate the correction factor with oxygen concentration:

$$F7 = \frac{a7}{1 + b7 \text{ EXP } \left[ -c7(C_{\text{O}_2}^a - C_{\text{O}_2}^{\text{th}}) \right]}, \quad (162)$$

where F7 is the correction factor, a7, b7, and c7 are constants characterizing the shape of the equation with a6 = 1, b1 = 200, and c6 = 0.04,  $C_{\text{O}_2}^a$  is the oxygen concentration within canopy ( $\mu\text{g cm}^{-3}$  air), and  $C_{\text{O}_2}^{\text{th}}$  is the threshold oxygen concentration below which the photorespiration and respiration rate approaches zero ( $\mu\text{g cm}^{-3}$  air).

Multiplying equations (161) and (162) yields:

$$\text{Res}_{\text{CO}_2}(t, \text{O}_2) = [e1 + e2t + e3t^2 + e4t^3 + e5t^4] F7. \quad (163)$$

Equation (163) shows that the rate of carbon dioxide production during photorespiration and respiration is a function of time and oxygen concentration.

The rate of oxygen consumption during photorespiration and respiration was calculated using:



Since the rate of carbon dioxide production can be calculated from equation (163), the rate of oxygen consumption can be calculated from equation (164).

(13) Diffusion Coefficient of Oxygen and Carbon Dioxide. The diffusion coefficient of oxygen and carbon dioxide was chosen to be a function of air temperature and was calculated from equation (143).

### Discussion of Simulation Results

Concentrations of Oxygen and Carbon Dioxide Within the Plant Canopy. Changes in oxygen and carbon dioxide concentrations within the plant canopy are shown in Figures 74 and 75. Each Figure shows the concentrations of the two gases side by side at several times since the start of simulation. The oxygen was depleted by respiration and photorespiration by plant leaves, and the carbon dioxide was released as a result.

Figure 74 shows that oxygen concentration decreased and carbon dioxide concentration increased from the top of canopy to the soil surface at the three midnights. The decrease in oxygen concentration and increase in carbon dioxide concentrations were rapid from 0 to 24 hours and became quite substantial from 24 to 48 hours, and finally the equilibrium condition was reached from 48 to 72 hours. The lowest oxygen concentration and the highest carbon dioxide concentration were at the soil surface. This is so because the path for oxygen diffusion into and carbon dioxide diffusion out of the canopy was longer near the soil surface. In addition, the respiration

activities by roots and soil microorganisms also used oxygen and produce carbon dioxide at the soil surface.

Figure 75 shows that the oxygen concentration decreased and carbon dioxide concentration increased from the top of canopy to the soil surface at the three noons. However, the decrease in oxygen concentration and increase in carbon dioxide concentration in Figure 75 were much less than that in Figure 74. This is so because the plant leaves fix carbon dioxide and evolve oxygen by photosynthesis processes during the day. As a result, the oxygen concentration increased and carbon dioxide concentration decreased during the day as compared to that during the night.

Concentration of Oxygen in Soil Profile. Changes in oxygen concentrations in soil profile for the conditions with and without canopy during the 72 hours simulation period are shown in Figures 76. This diagram shows the oxygen concentration as a function of soil depth at several points in time since the start of the simulation. Starting from 0 hours, the oxygen concentrations continued to decrease throughout the soil profile from 0 to 24, 48 and 72 hours for conditions in both with canopy and without canopy. This continued decrease in oxygen concentration was the result of continued growth of roots (Figure 80).

As shown in Figure 76, the depletion of oxygen was smaller for the condition without the canopy than that for the condition with the canopy. For example, the oxygen concentration in the soil profile for the condition without the canopy at the soil depth of 20 cm was about  $270 \mu\text{g cm}^{-3}$  air at 24 hours, but was about  $250 \mu\text{g cm}^{-3}$  air for the condition without the canopy at the same depth and time. Similar

results were obtained at 48 and 72 hours. This is so because less oxygen diffuses into the soil profile for the condition with canopy, due to the respiration used of oxygen by plant leaves.

Figure 76 does not show a reach in equilibrium condition for oxygen concentration in the soil profile as time elapse from 0 to 24, 48, and 72 hours for conditions in both with and without canopy. This is because the rate of oxygen consumption by roots was much faster than the rate of oxygen supply from soil surface. The rate of oxygen consumption by roots was assumed to be a function of oxygen concentration and was the same as used in Example 2a (Figure 35). As was shown in Figure 35, when the soil oxygen concentration decreases  $100 \mu\text{g cm}^{-3}$  air (from  $300$  to  $200 \mu\text{g cm}^{-3}$  air), the rate of oxygen consumption by roots decreases only  $2.5 \mu\text{g cm}^{-3}$  air  $\text{hr}^{-1}$  (from  $8.0$  to  $5.5 \mu\text{g cm}^{-3}$  air  $\text{hr}^{-1}$ ). This implies that the rate of oxygen consumption by roots was still high enough to deplete the soil oxygen. The equilibrium conditions could be expected as the soil oxygen concentration further depletion and the rate of oxygen consumption by roots equal to the rate of oxygen supply from the soil surface.

Concentration of Carbon Dioxide in Soil Profile. Changes in carbon dioxide concentrations in soil profile for the conditions with and without canopy during the 72 hours simulation period are in Figures 77. This diagram shows the carbon dioxide concentration as a function of soil depth at several points in time since the start of the simulation. Starting from 0 hours, the carbon dioxide concentrations continued to increase throughout the soil profile from 0 to 24, 48 and 72 hours for the conditions in both with canopy and without

canopy. This continued increase in carbon dioxide concentration was the result of continued growth of roots (Figure 80).

As shown in Figure 77, the production of carbon dioxide was smaller for the condition without the canopy than that for the condition with the canopy. For example, the carbon dioxide concentration in the soil profile for the condition without the canopy at the soil depth of 20 cm was about  $40 \mu\text{g cm}^{-3}$  air at 24 hours, but was about  $55 \mu\text{g cm}^{-3}$  air for the condition with the canopy at the same depth and time. Similar results were obtained at 48 and 72 hours. This is so because less carbon dioxide diffuses out of the soil profile for condition with the canopy, due to more carbon dioxide was produced within the plant canopy by respiration by plant leaves.

Analogous to Figure 76, Figures 77 does not show a reach in equilibrium condition for carbon dioxide concentration in the soil profile as time elapse from 0 to 24, 48, and 72 hours for conditions in both with and without canopy. The rate of carbon dioxide production by roots was assume to be proportion to the rate of oxygen consumption by roots. Since oxygen concentration does not reach the equilibrium condition, so does the carbon dioxide concentration.

#### Oxygen and Carbon Dioxide Concentration at the Soil Surface.

Daily cycles of oxygen and carbon dioxide concentration at the soil surface for the condition with the canopy are shown in Figures 78 through 79. As shown in Figure 78, the oxygen concentration decreased from 0 to 6 hours, then increased from 6 to 12 hours, and then decreased again from 12 to 24 hours for the first day. The opposite results were obtained for carbon dioxide concentration in Figure 79. Such changes in oxygen and carbon dioxide concentrations

during the day and night were due to the effects of photosynthesis and respiration processes.

The changes in oxygen and carbon dioxide concentrations during the second and third day show the more characteristic surface oxygen and carbon dioxide behaviors, with the oxygen concentration decrease and carbon dioxide concentration increase during the night followed by gradual increase in oxygen concentration and decrease in carbon dioxide concentration during the day.

Figures 78 and 79 also show a gradual approach of equilibrium conditions in oxygen and carbon dioxide concentrations at the soil surface from 24 to 72 hours. For example, the oxygen concentration was about  $262 \mu\text{g cm}^{-3}$  air at 24 hours and was about  $258 \text{ mg cm}^{-3}$  air at 48 and 72 hours. Similar results were obtained for carbon dioxide concentration. The changes of oxygen and carbon dioxide concentrations at the soil surface were mostly controlled by plant leaves in the this example. As the rate of oxygen consumption by plant leaves is equal to the rate of oxygen evolution by photosynthesis and oxygen supply from the atmosphere, the equilibrium conditions would reach as was shown in the figures.

Comparison of Root Length. Changes in root length for conditions with and without the canopy are shown in Figure 80. This diagram shows root length in the soil profile as a function of time since the start of the simulation. Root length is about 14 cm for the conditions in both with and without the canopy at 24 hours. As the time elapsed, the differences in root length for the two conditions started at 24 hours and increase from 24 to 72 hours. Root length was 22 cm at 48 hours and 29 cm at 72 hours for the condition

with the canopy, but was 23 cm at 24 hours and 32 cm at 72 hours for the condition without the canopy. This is so because the root elongation rate was assumed to be governed by soil oxygen concentration in addition to being governed by time. Since less oxygen was supplied from the atmosphere to the soil for the condition with the canopy than for the condition without the canopy, the rate of root growth should be lower for the condition with the canopy.

### Conclusions

This example simulates the diffusion of oxygen and carbon dioxide not only through the soil but also within the canopy. It predicts the daily changes of oxygen and carbon dioxide within the canopy with decrease in oxygen concentration and increase in carbon dioxide concentration during the night followed by gradual increase in oxygen concentration and decrease in carbon dioxide concentration during the day. The oxygen concentration was higher and the carbon dioxide concentration was lower in the soil profile for the condition without the canopy than that for the condition with the canopy. This is because with the present of canopy, more oxygen was depleted and more carbon dioxide was released by plant leaves. So that the diffusion of oxygen into the soil and the diffusion of carbon dioxide out of the soil was slower. This result implies that the canopy has effects on the diffusion of oxygen and carbon dioxide through the soil.

A further simulation should be conducted by assuming that the rate of root elongation and oxygen consumption is a function of

carbon dioxide concentration instead of oxygen concentration, in addition to being function of time. This simulation should allow evaluation of effects of oxygen and carbon dioxide on the root growth and soil aeration conditions.

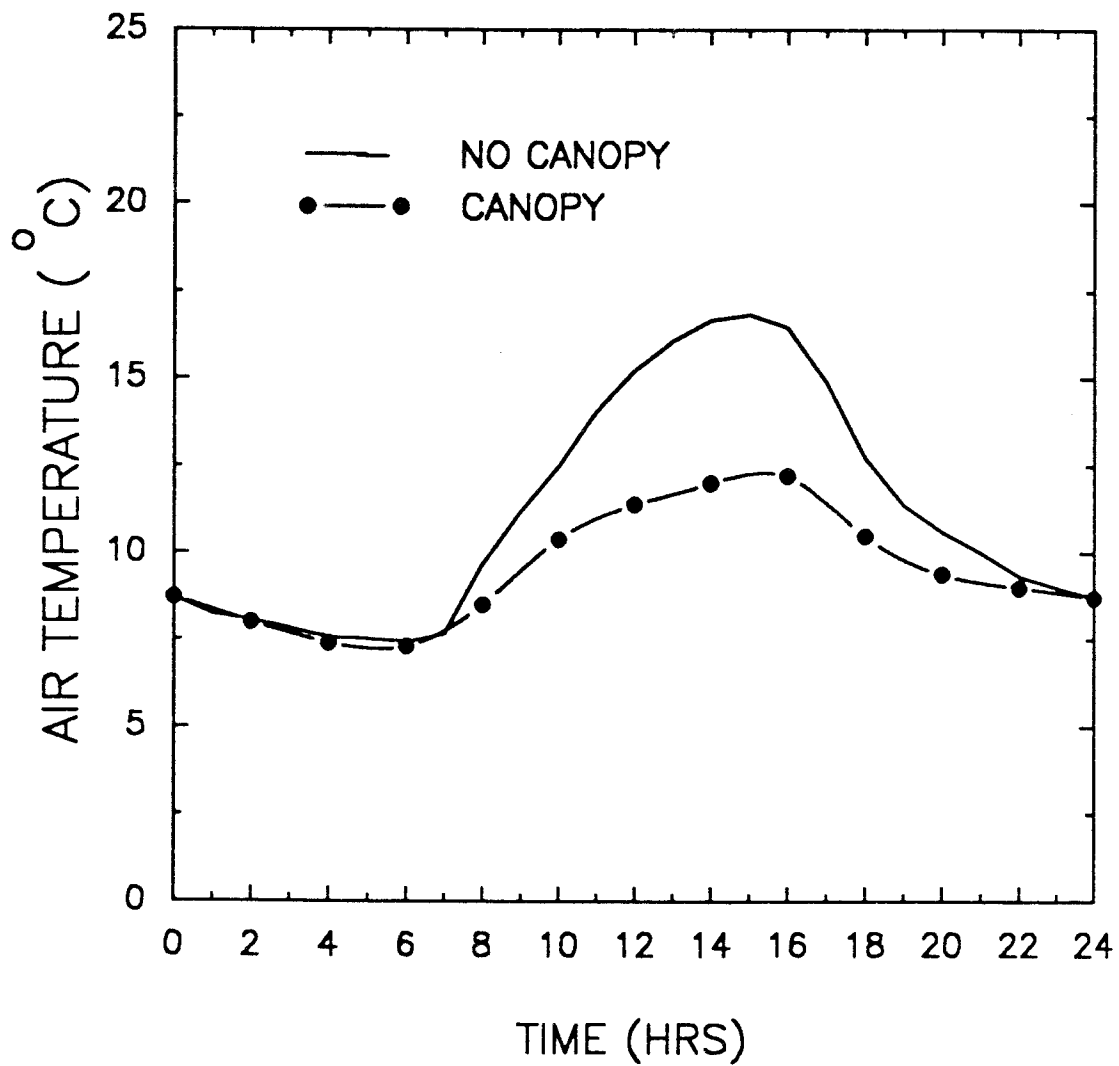


Figure 69. Air temperature as a function of time for conditions with and without the plant canopy.

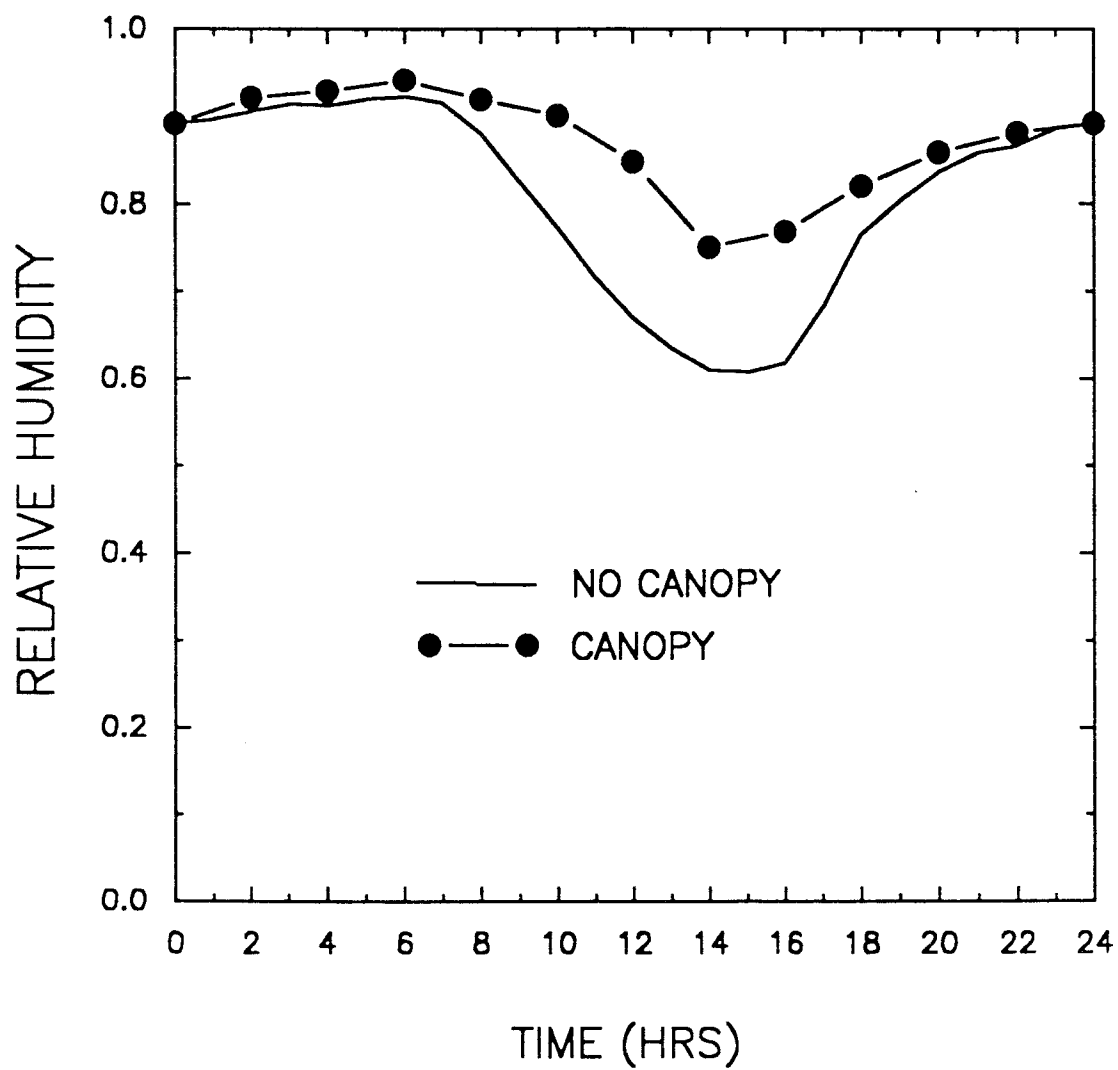


Figure 70. Relative humidity as a function of time for conditions with and without the plant canopy.

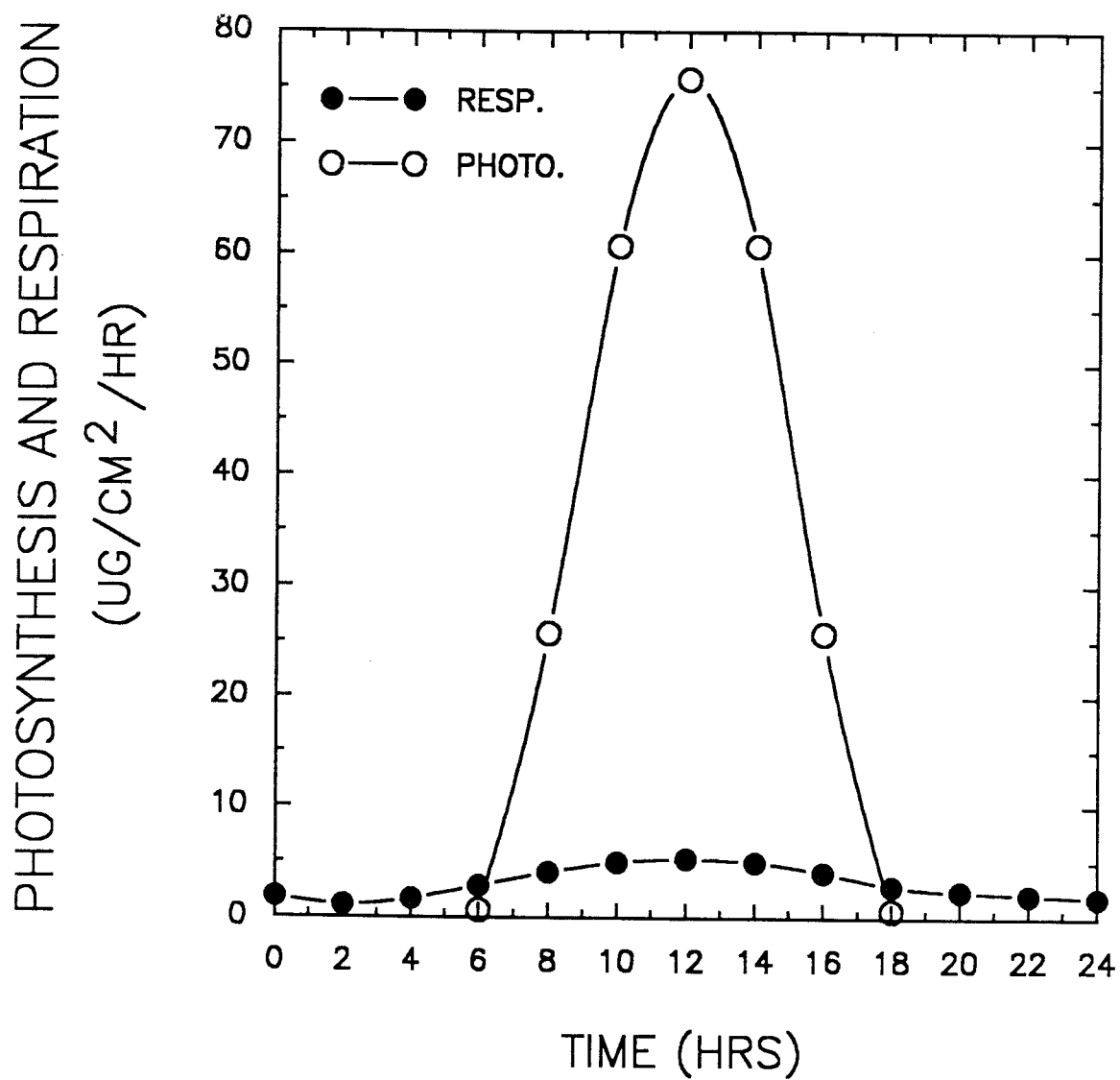


Figure 71. Rates of photosynthesis and respiration as a function of time. Data adapted from Nobel (1983).

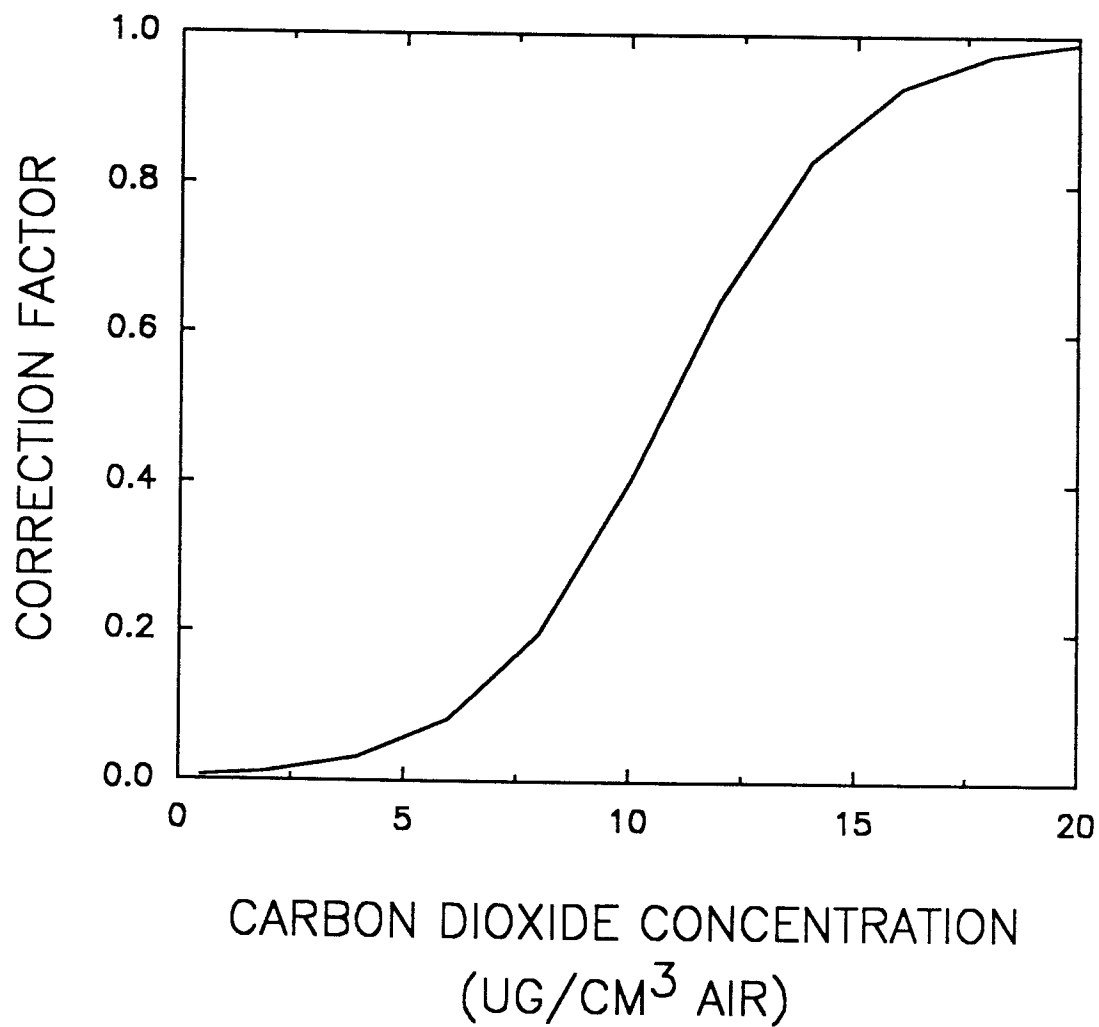


Figure 72. Correction factor for photosynthesis as a function of carbon dioxide concentration within the plant canopy (Devlin and Barker, 1971).

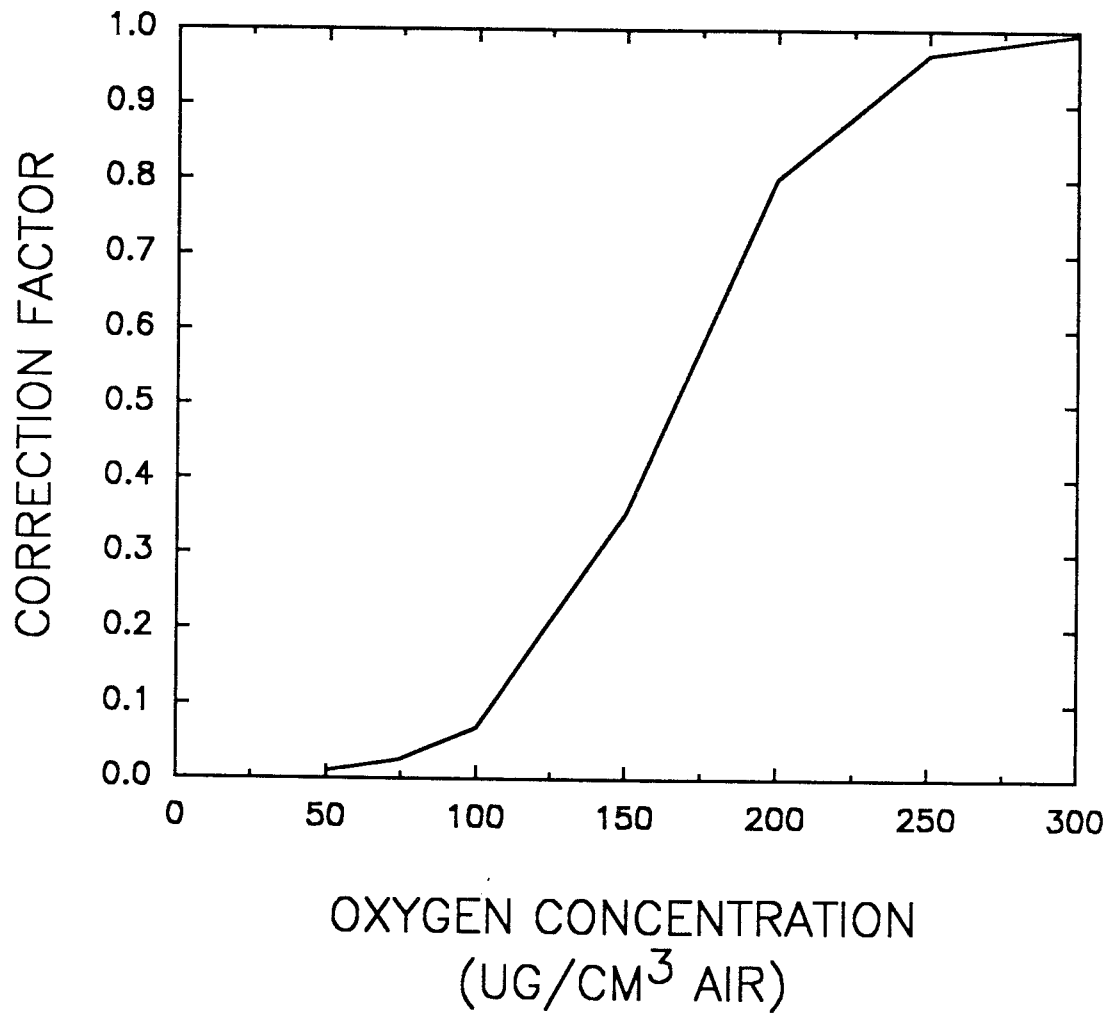


Figure 73. Correction factor for photorespiration and respiration as a function of oxygen concentration within the plant canopy (Devlin and Barker, 1971).

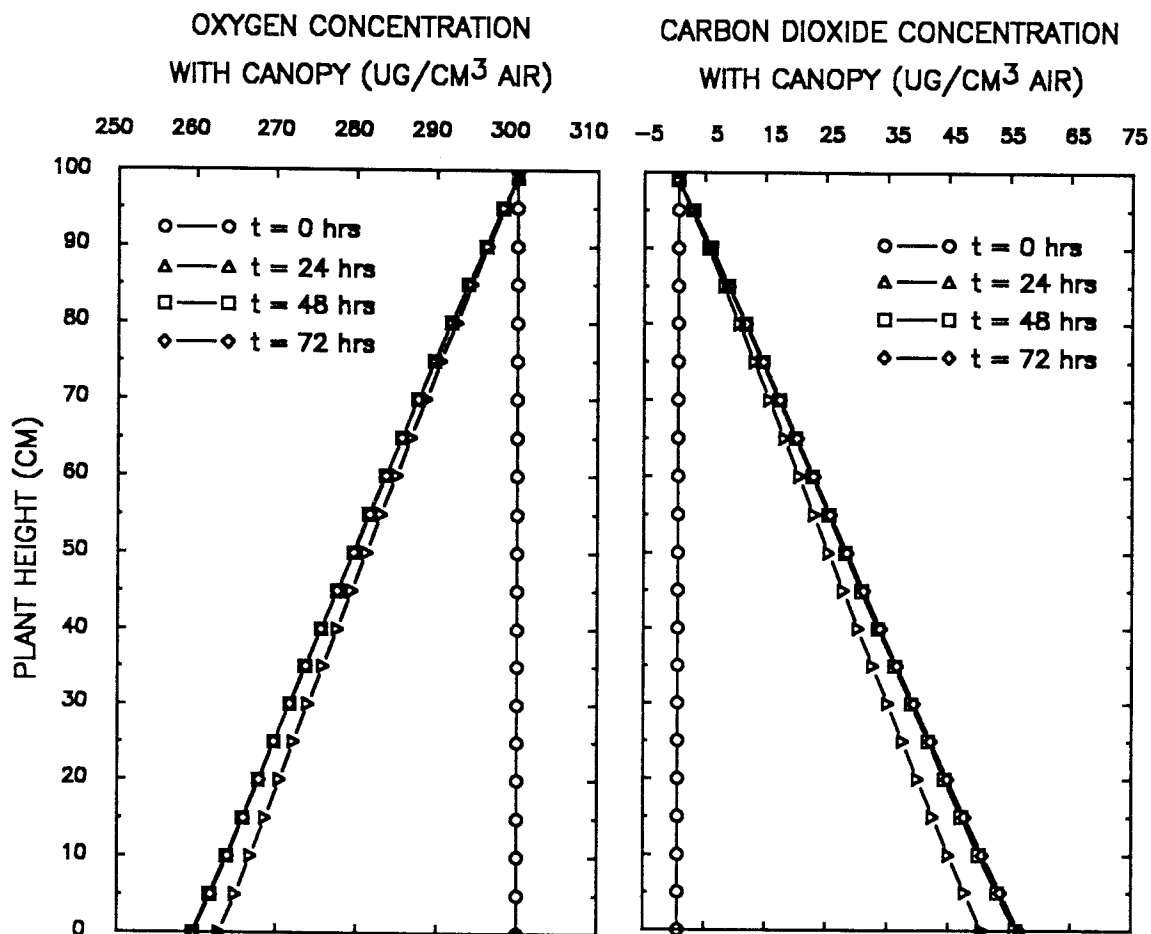


Figure 74. Oxygen and carbon dioxide concentrations as a function of plant height at the three midnights. Initial oxygen and carbon dioxide concentrations are 300 and  $0.6134 \mu\text{g cm}^{-3}$  air, respectively.

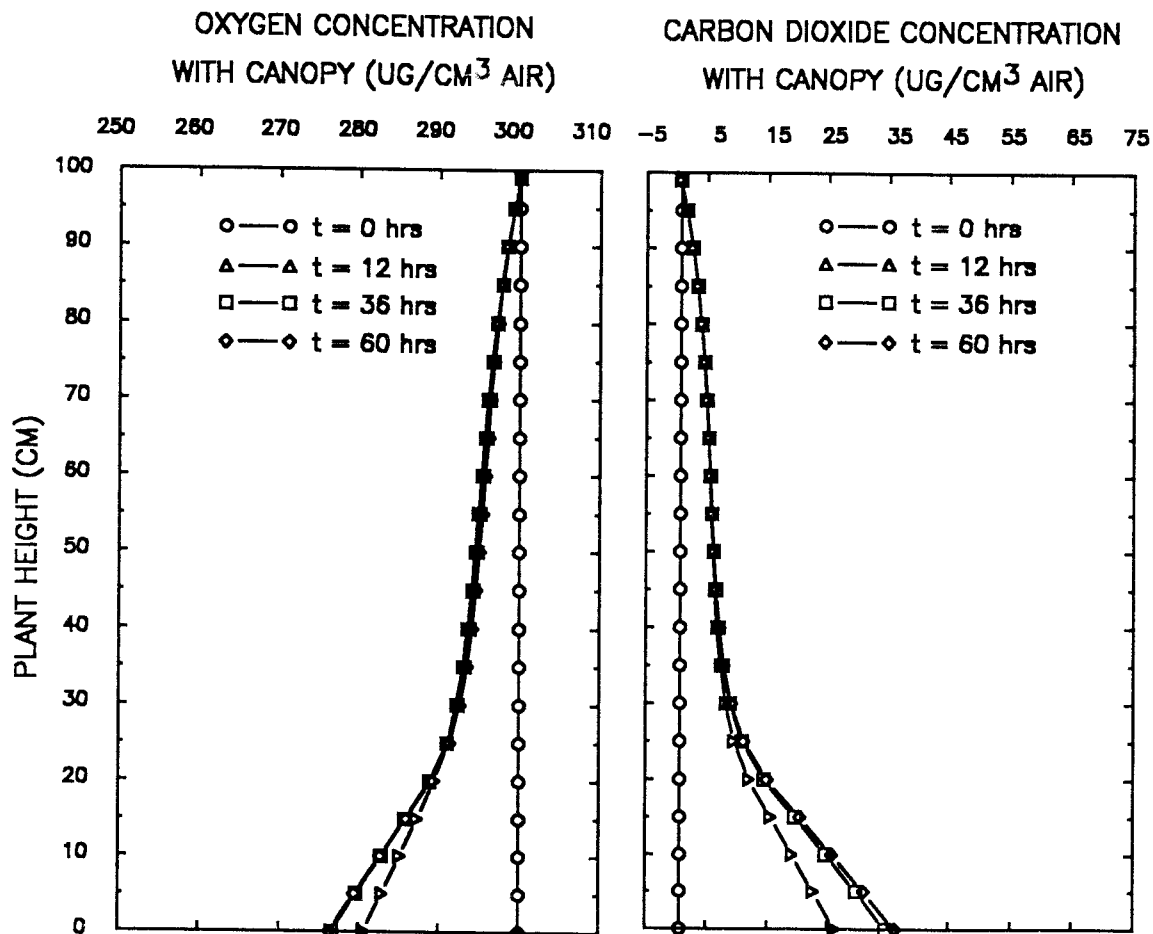


Figure 75. Oxygen and carbon dioxide concentrations as a function of plant height at the three noons. Initial oxygen and carbon dioxide concentrations are 300 and  $0.6134 \mu\text{g cm}^{-3}$  air, respectively.

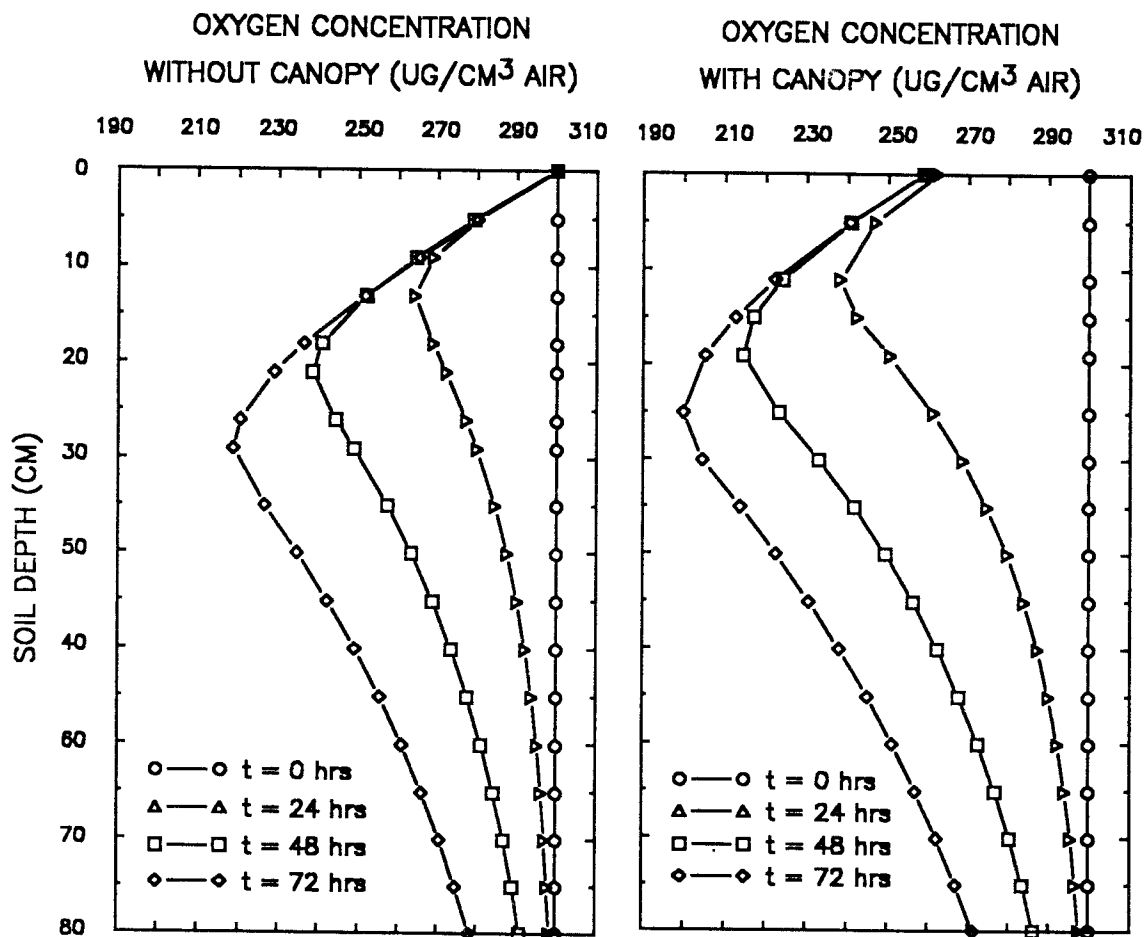


Figure 76. Oxygen concentration as a function of soil depth at times of 0, 24, 48 and 72 hours for conditions with and without the plant canopy.

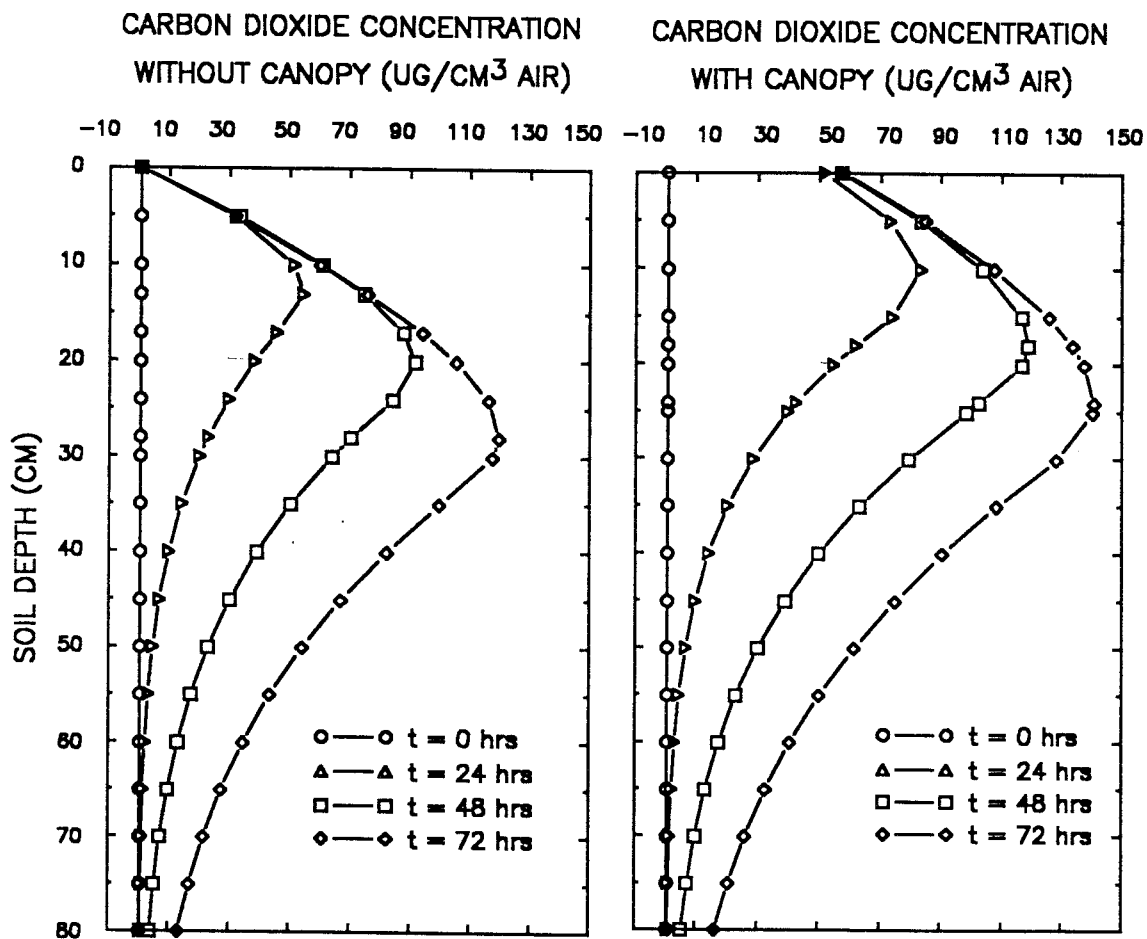


Figure 77. Carbon dioxide concentration as a function of soil depth at times of 0, 24, 48, and 72 hours for conditions with and without the plant canopy.

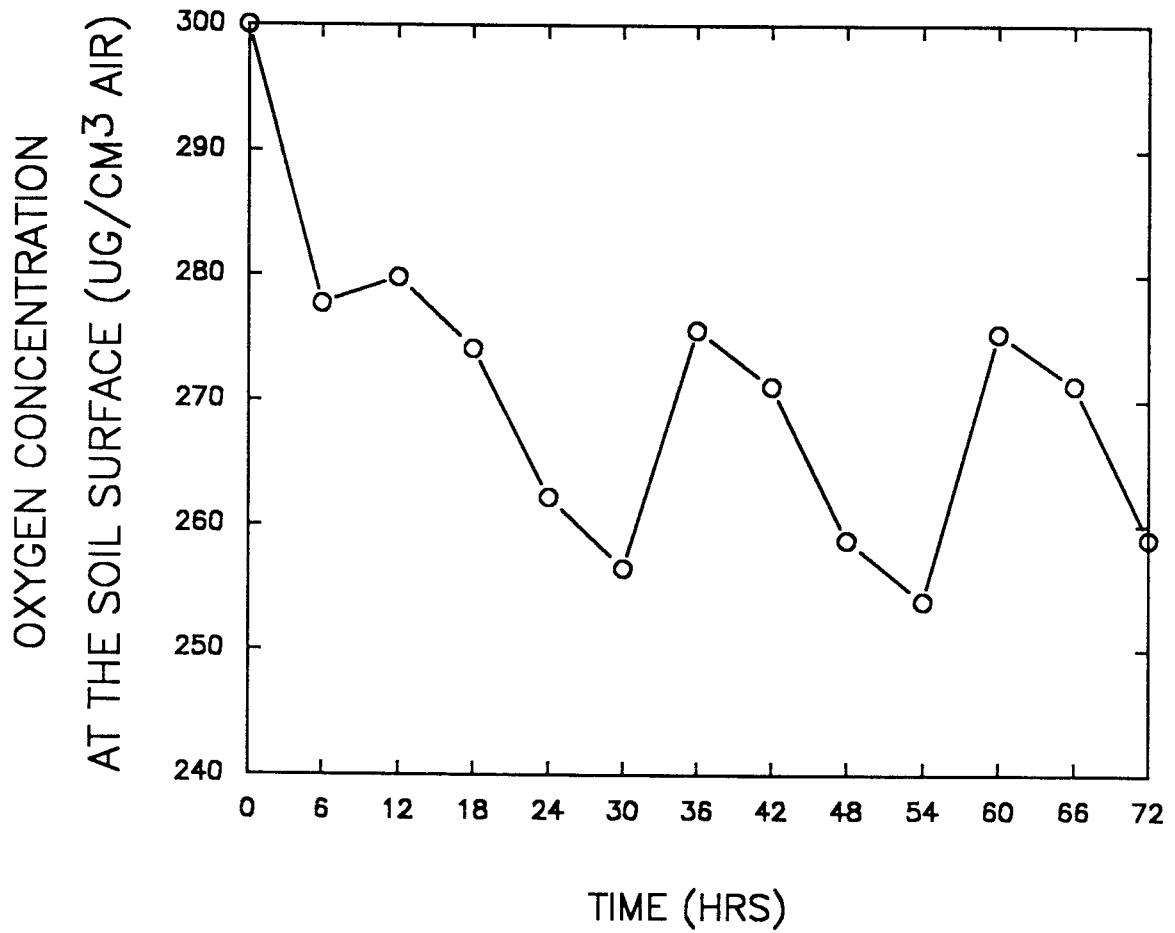


Figure 78. Oxygen concentration as a function of time at the soil surface from 0 to 72 hours for conditions with the plant canopy.

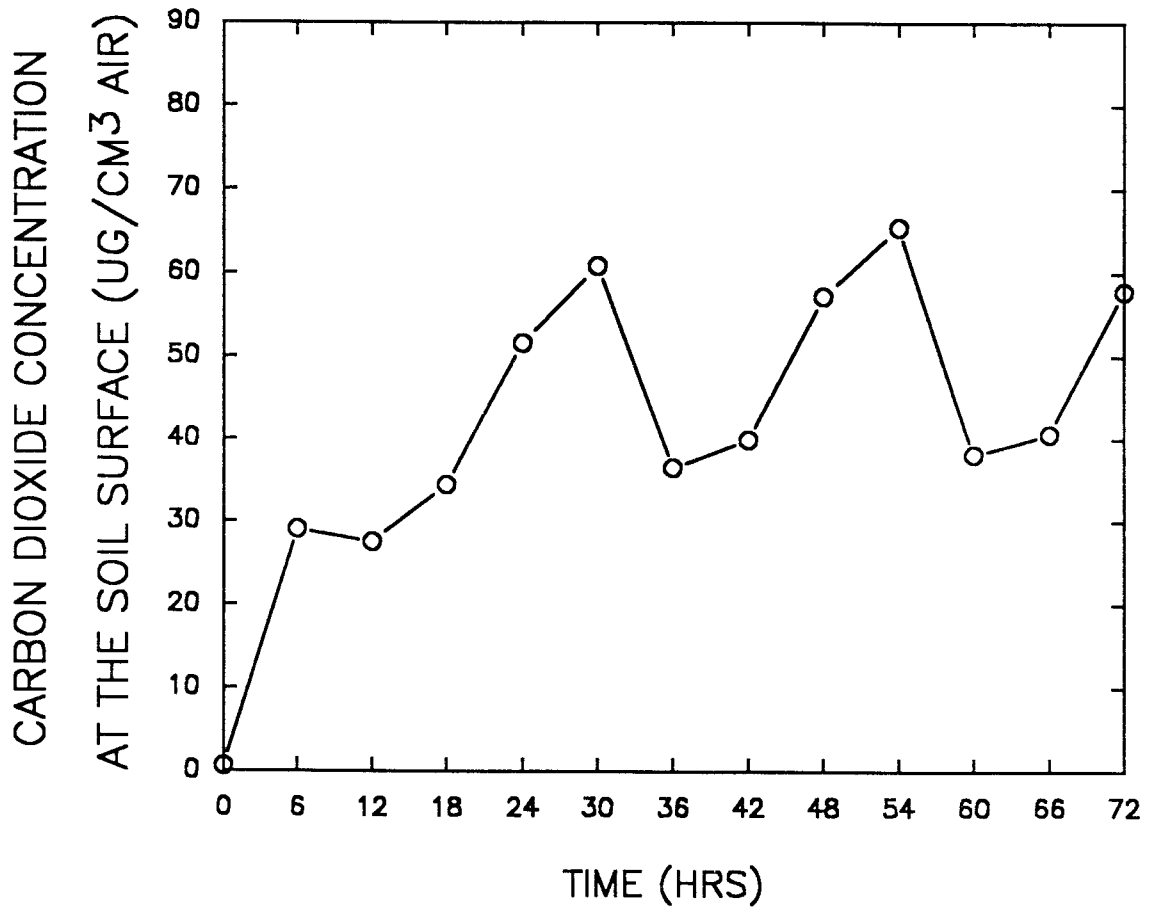


Figure 79. Carbon dioxide concentration as a function of time at the soil surface from 0 to 72 hours for conditions with the plant canopy.

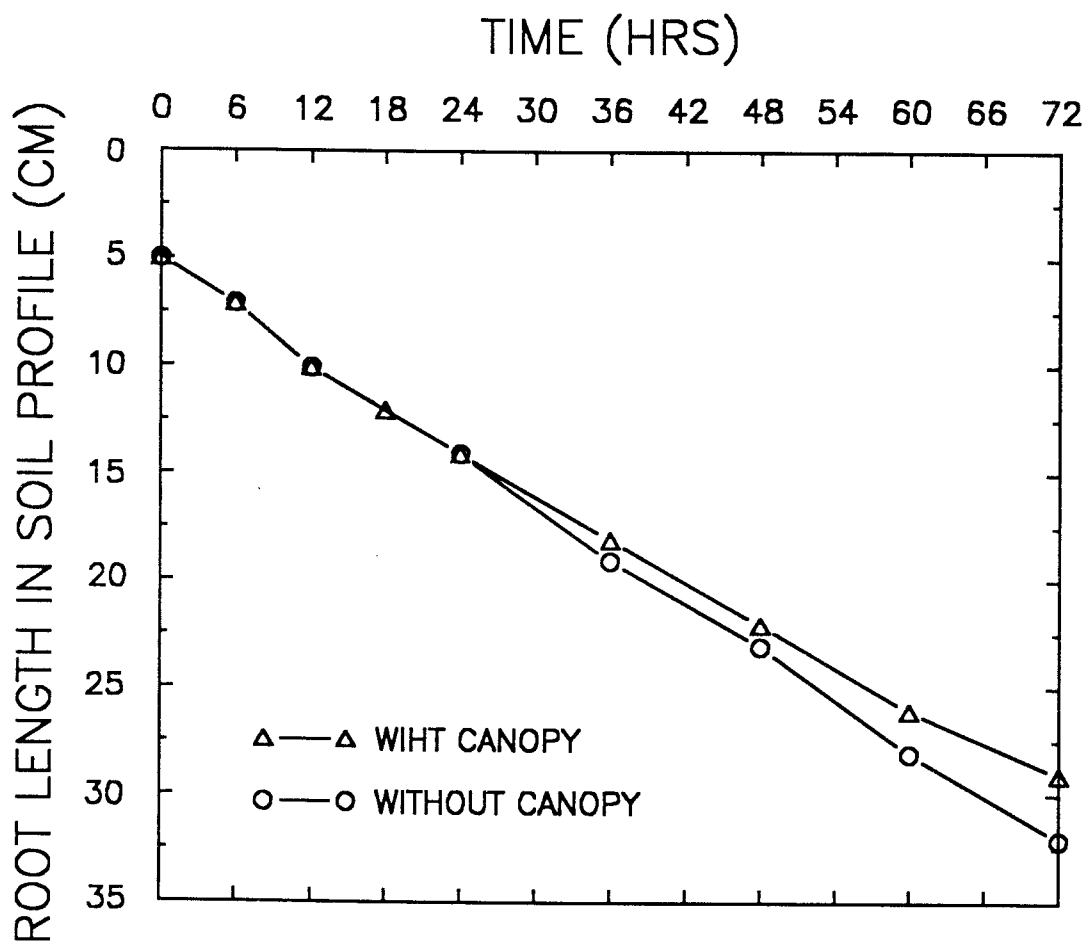


Figure 80. Root length as a function of time in soil profile from 0 to 72 hours for conditions with and without the plant canopy.

### Example 5b

#### Statement of the Problem

This example differs from Example 5a by assuming that the rate of root elongation and the rate of root oxygen consumption are functions of carbon dioxide concentration instead of oxygen concentration. Comparisons of two examples allow evaluation of the effects of oxygen and carbon dioxide on the root growth and on the soil aeration conditions.

#### Input Parameters

All input parameters were the same as in Example 5a except for the following.

Root Elongation Rate. The root elongation rate was chosen to be a function of carbon dioxide concentration instead of oxygen concentration. It was assumed that, when the soil is well aerated and carbon dioxide concentration is at the atmosphere level, the root elongation rate is a function of time only, as described by equation (145).

When the soil is not fully aerated, the root elongation rate is also a function of carbon dioxide concentration (Kursar, 1989). This implies that a factor is needed to correct equation (145) to account for the effects of soil carbon dioxide concentration on the rate of root elongation. It was assumed that, when the soil is well aerated, the correction factor is equal to unity which means that the root

elongation rate is only a function of time. When the soil is not fully aerated, the correction factor decreases as carbon dioxide concentration increases. A logistic function was chosen to define the correction factor for the carbon dioxide concentration (Figure 81) as follows:

$$F8 = \frac{A8}{1 + B8 \text{ EXP} \left[ C8(C_{\text{co}_2}^{\text{tip}} - C_{\text{co}_2}^{\text{th}}) \right]}, \quad (165)$$

where F8 is the correction factor, A8, B8, and C8 are constants characterizing the shape of the equation with  $A8 = 1$ ,  $B8 = 200$ , and  $C8 = 0.2$ ,  $C_{\text{co}_2}^{\text{tip}}$  is the soil carbon dioxide concentration at the root tip ( $\mu\text{g cm}^{-3}$  air), and  $C_{\text{co}_2}^{\text{th}}$  is the threshold soil carbon dioxide concentration below which the root elongation rate approaches zero ( $50 \mu\text{g cm}^{-3}$  air). Multiplying equation (145) and equation (165) yields:

$$L(t, \text{co}_2) = [L_0 + a_1 t] F8. \quad (166)$$

Equation (166) represents the root elongation rate as a function of time and of carbon dioxide concentration.

Rate of Oxygen Consumption By Roots. The rate of oxygen consumption by roots was chosen to be a function of carbon dioxide concentration instead of oxygen concentration. The rate of oxygen consumption by roots as a function of carbon dioxide concentration was represented by the logistic function (Figure 82):

$$\text{SRT}(i) = \frac{A9}{1 + B9 \text{ EXP} \left[ C9(C_{\text{co}_2}^i - C_{\text{co}_2}^{\text{th}}) \right]}, \quad (168)$$

where  $SRT(i)$  is the root oxygen consumption rate by the  $i^{\text{th}}$  section of root length converted to  $\mu\text{g cm}^{-3} \text{ air hr}^{-1}$  (Appendix III),  $A9$ ,  $B9$ , and  $C9$  are constants characterizing the shape of the equation with  $A9 = 10$ ,  $B9 = 2000$ , and  $C9 = 0.3$ ,  $C_{\text{co}_2}^i$  is the carbon dioxide concentration in the  $i^{\text{th}}$  section of soil depth corresponding to the  $i^{\text{th}}$  section of root length ( $\mu\text{g cm}^{-3}$  soil air), and  $C_{\text{co}_2}^{\text{th}}$  is the threshold carbon dioxide concentration below which the root oxygen consumption rate approaches zero ( $50 \text{ mg cm}^{-3}$  air).

Multiplying equation (149) and equation (168) obtains:

$$SRT(i, \text{co}_2) = \frac{A9}{1 + B9 \text{ EXP}[-C9(C_{\text{co}_2}^i - C_{\text{co}_2}^{\text{th}})]} F3. \quad (169)$$

Equation (169) represents the rate of oxygen consumption by the root as a function of carbon dioxide concentration and of root length.

### Discussion of Simulation Results

Concentrations of Oxygen and Carbon Dioxide Within the Plant Canopy. Changes in oxygen and carbon dioxide concentrations within the plant canopy at the three midnights and noons are shown in Figures 83 and 84, respectively. Each Figure shows the concentrations of the two gases side by side at several times since the start of simulation. The oxygen was depleted by respiration and photorespiration by plant leaves, and the carbon dioxide was released as a result.

Comparison of Example 5a and Example 5b shows that the oxygen concentration within the canopy was higher during the day and night

in Example 5b than that in Example 5a. For instance, the oxygen concentration was about  $290 \mu\text{g cm}^{-3}$  air in Figure 83 in Example 5b at the plant height of 50 cm at 72 hours, but was about  $280 \mu\text{g cm}^{-3}$  air in Figure 74 in Example 5a at the same depth and time. Similar results were obtained for the carbon dioxide concentrations. This is so because that the rate of oxygen use and the rate of carbon dioxide production by roots were lower in Example 5b. These lower rates were due to the restriction of carbon dioxide concentration on the photosynthesis and respiration activities of plant leaves. By comparing Figure 73 with Figure 82, one sees that in order to decrease the correction factor to 0.4, the oxygen concentration needs to decrease to about  $155 \mu\text{g cm}^{-3}$  air, but the carbon dioxide concentration only needs to increase to about  $26 \mu\text{g cm}^{-3}$  air. This implies that carbon dioxide concentration is more sensitive to the photosynthesis and respiration of plant leaves. As a result, the rate of oxygen use, as well as the rate of carbon dioxide production, by plant leaves was smaller in Example 5b than that in Example 5a.

#### Concentration of Oxygen and Carbon Dioxide in the Soil Profile.

Changes in oxygen and carbon dioxide concentrations in the soil profile during the 72 hours simulation period were in Figure 85. This diagram shows the oxygen concentration as a function of soil depth at several points in time since the start of the simulation.

Comparisons of Example 5a and Example 5b show that the depletion of oxygen and the production of carbon dioxide in the soil for the condition with the canopy were much smaller in Example 5b than that in Example 5a. For instance, the oxygen concentration was about  $282 \mu\text{g cm}^{-3}$  air in Figure 85 in Example 5b at the soil depth of 20 cm

at 72 hours, but was about  $205 \mu\text{g cm}^{-3}$  air in Figure 76 in Example 5a at the same depth and time. Similar results were obtained for carbon dioxide concentrations. This is so because that the rate of oxygen use and the rate of carbon dioxide production by roots were lower in Example 5b. These lower rates were due to the restriction of carbon dioxide concentration on the roots activities.

#### Oxygen and Carbon Dioxide Concentration at the Soil Surface.

Daily cycles of oxygen and carbon dioxide concentration at the soil surface for the condition with canopy are in Figures 86 and 87. Each Figure shows concentration as a function of time at the soil surface from 0 to 72 hours.

Comparisons of Example 5a and Example 5b show that the oxygen concentration was higher and carbon dioxide concentration was lower at the soil surface in Example 5b than that in Example 5a. For instance, the oxygen concentration was about  $284 \mu\text{g cm}^{-3}$  air in Figure 86 and carbon dioxide concentration was about  $25 \mu\text{g cm}^{-3}$  air in Figure 87 in Example 5b at 72 hours, but the oxygen concentration was about  $259 \mu\text{g cm}^{-3}$  air in Figure 78 and carbon dioxide concentration was about  $58 \mu\text{g cm}^{-3}$  air in Figure 79 in Example 5a at the same time. This is so because the rate of oxygen use and the rate of carbon dioxide production by roots were lower in Example 5b. These lower rates were due to the restriction of carbon dioxide concentration on the activities of the roots.

Comparison of Root Length. Changes in root length between Example 5a and 5b were shown in Figure 88. This diagram shows root length in the soil profile as a function of time since the start of the simulation. Example 5a assumed that the root elongation rate was

a function of oxygen concentration in addition to being a function of time. Example 5b assumed that the root elongation was a function of carbon dioxide concentration in addition to being a function of time. Starting with the initial root length of 5 cm in both Example 5a and 5b, root length was shorter in Example 5b than that in Example 5a. As the time elapsed, the differences in the root length of two examples increased. Root length was about 12.0 cm at 72 hours in Example 5b, but was about 29.0 cm at the same time in Example 5a, which was more than twice as long as that in Example 5b. This result can be explained as follows. In Example 5a, the root elongation rate was assumed to decrease with oxygen concentration (Figure 34). The minimum oxygen concentration in soil profile was  $225 \mu\text{g cm}^{-3}$  air at 72 hours and the correction factor for the root elongation was about 0.7 at this oxygen concentration (Figure 34). In Example 5b, the root elongation rate was assumed to decrease as carbon dioxide concentration increased (Figure 81). The maximum carbon dioxide concentration in the soil profile was about  $33 \mu\text{g cm}^{-3}$  air at 72 hours but the correction factor for the root elongation rate was 0.25 at this carbon dioxide concentration (Figure 81). The lower the correction factor, the slower the roots grow.

### Conclusions

This example together with Example 5a shows that the rate of root elongation and oxygen consumption by roots were stronger restricted by the soil carbon dioxide concentration than that by the soil oxygen concentration. This is because the correction factor

used for the root elongation rate and root oxygen consumption rate as a function of carbon dioxide is lower than that of as a function of oxygen.

A interesting simulation which need to be conducted is to choose the fast diffusion coefficient, instead of diffusion coefficient in still air, for oxygen and carbon dioxide within the plant canopy. This simulation should better describe the diffusion of oxygen and carbon dioxide within the plant canopy.

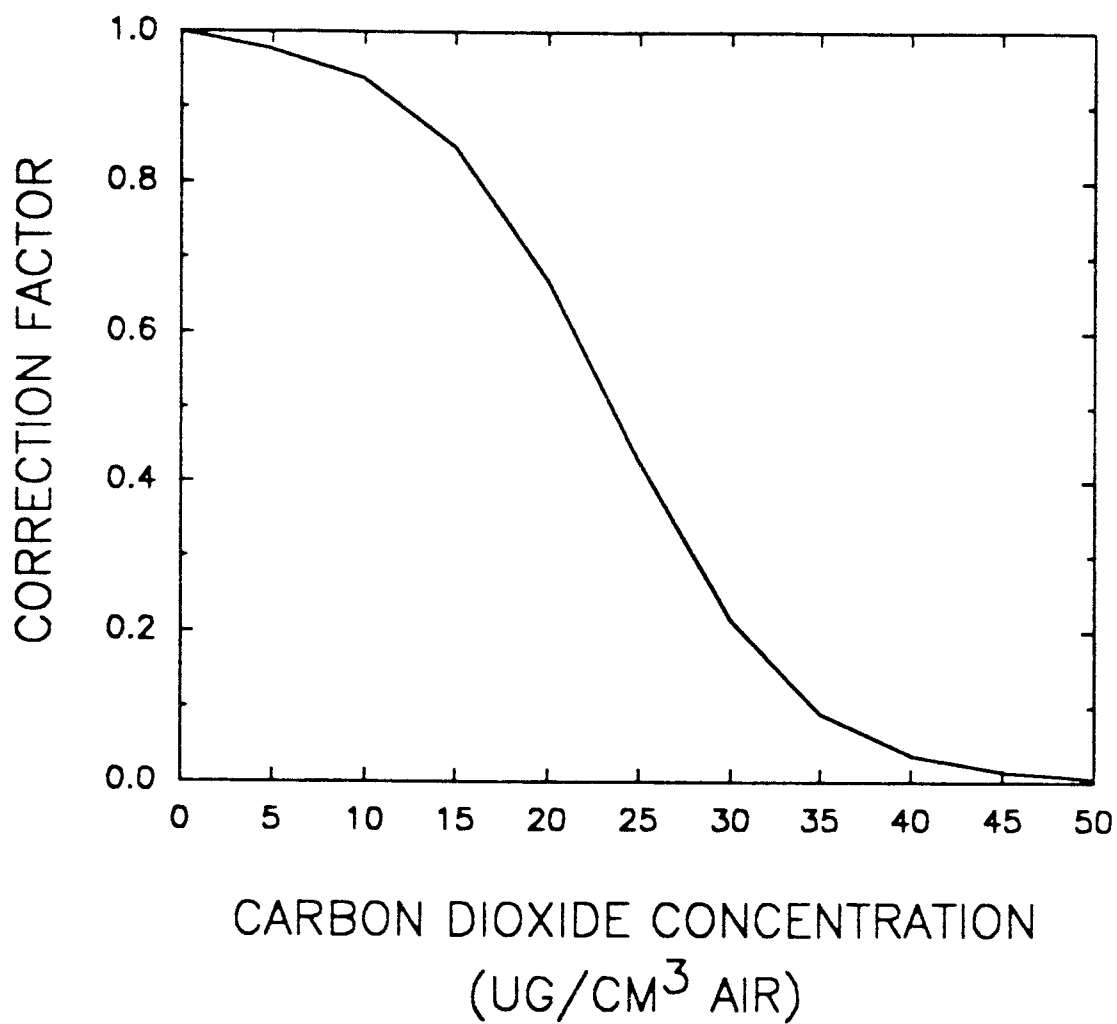


Figure 81. Correction factor for root elongation as a function of carbon dioxide concentration, calculated from equation (165).

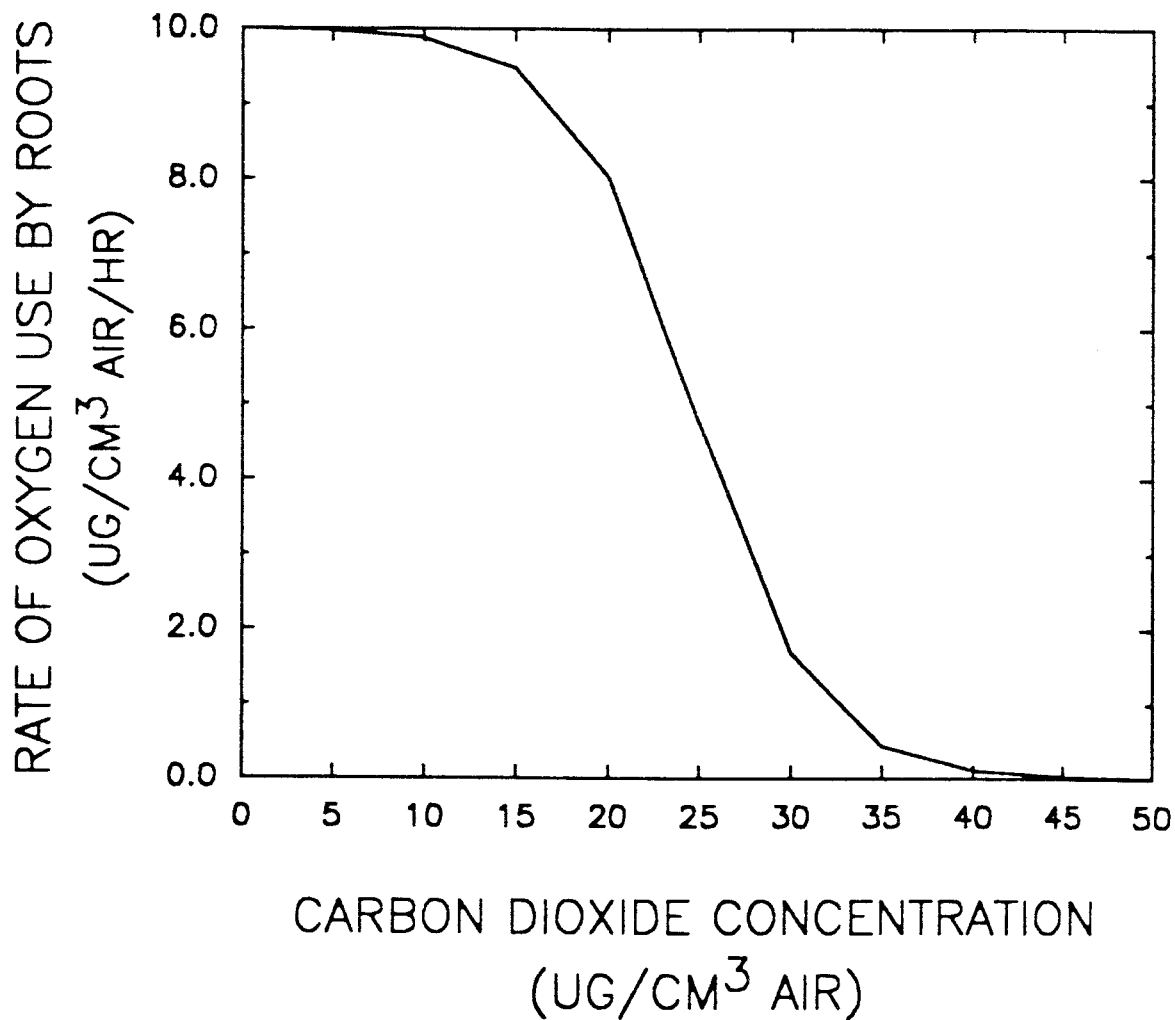


Figure 82. Oxygen consumption rate of roots as a function of soil carbon dioxide concentration, calculated from equation (168).

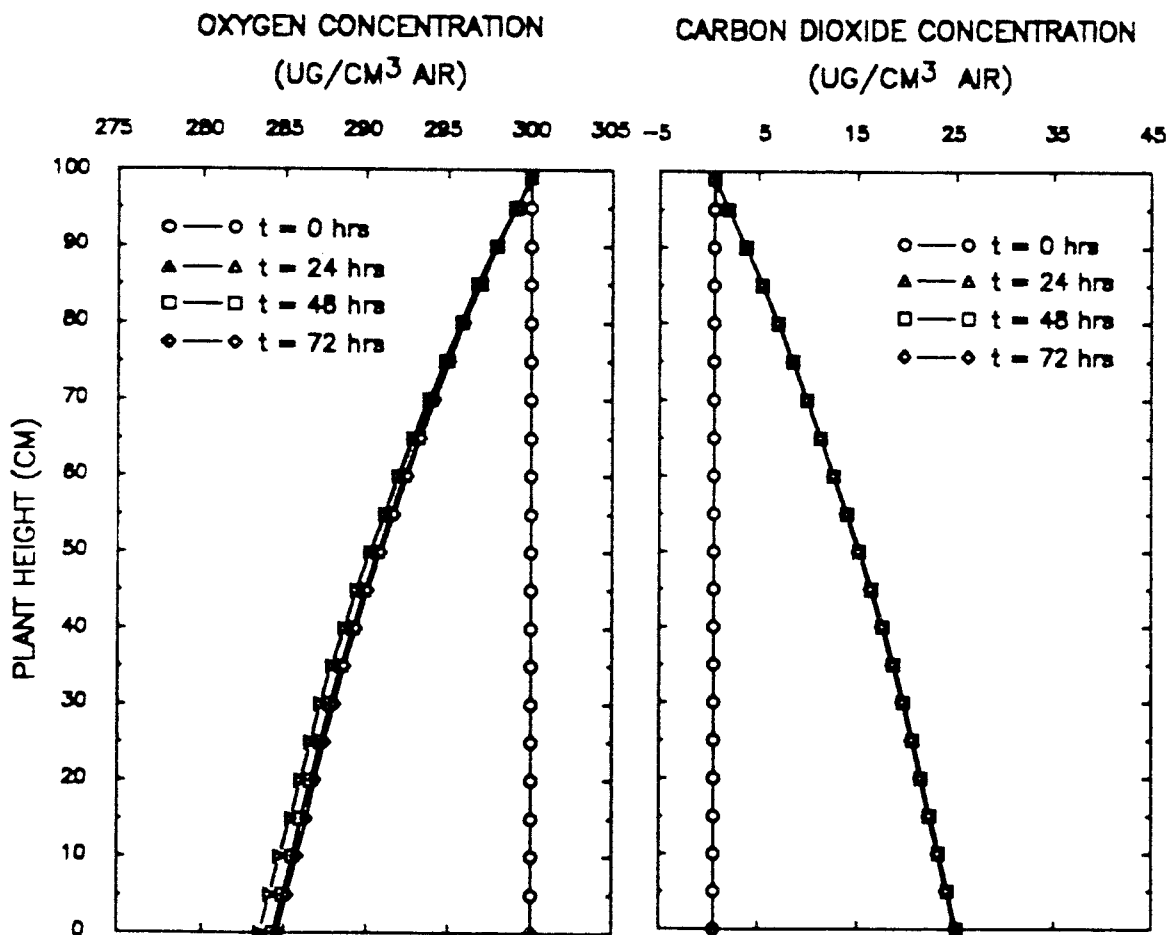


Figure 83. Oxygen and carbon dioxide concentrations as a function of plant height at the three midnights. Initial oxygen and carbon dioxide concentrations are 300 and  $0.6134 \mu\text{g cm}^{-3}$  air, respectively.

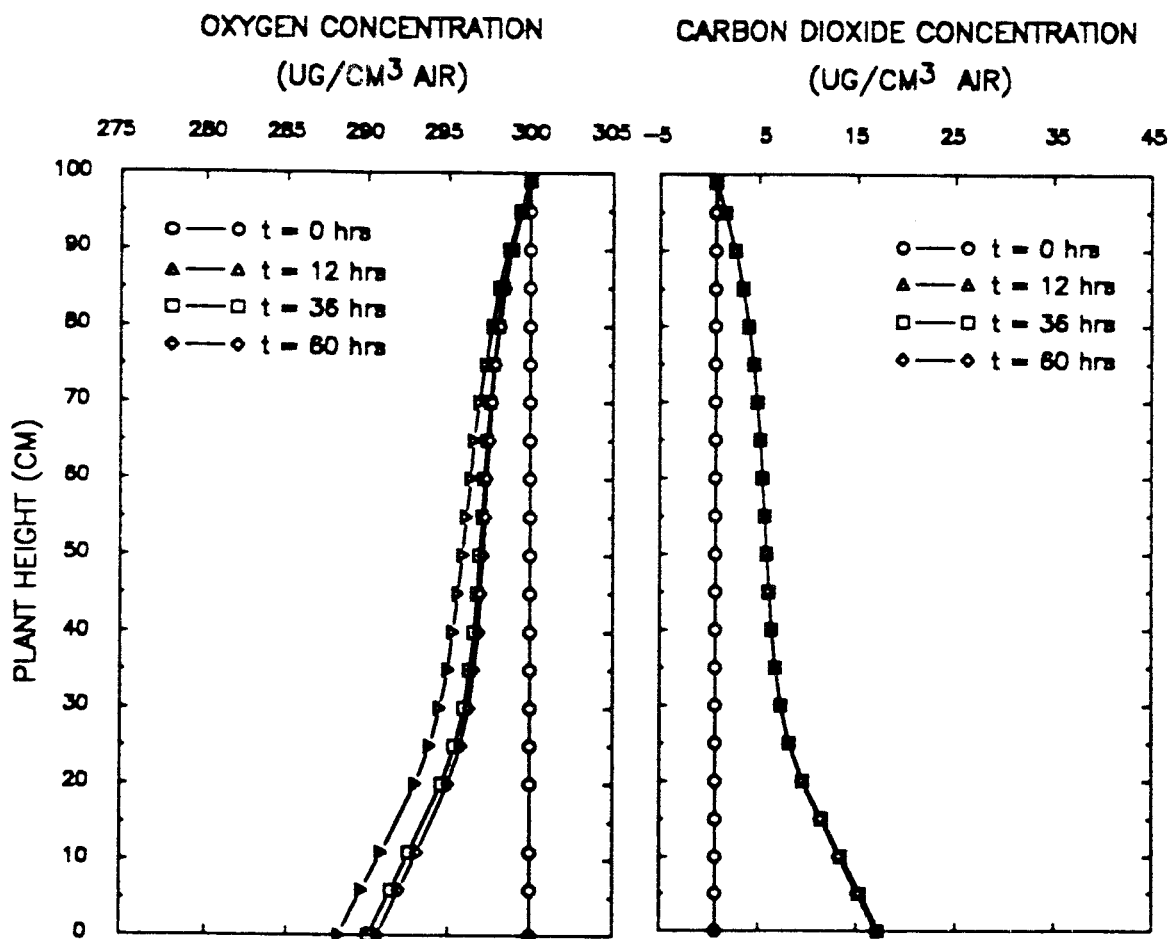


Figure 84. Oxygen and carbon dioxide concentrations as a function of plant height at the three noons. Initial oxygen and carbon dioxide concentrations are 300 and  $0.6134 \mu\text{g cm}^{-3}$  air, respectively.

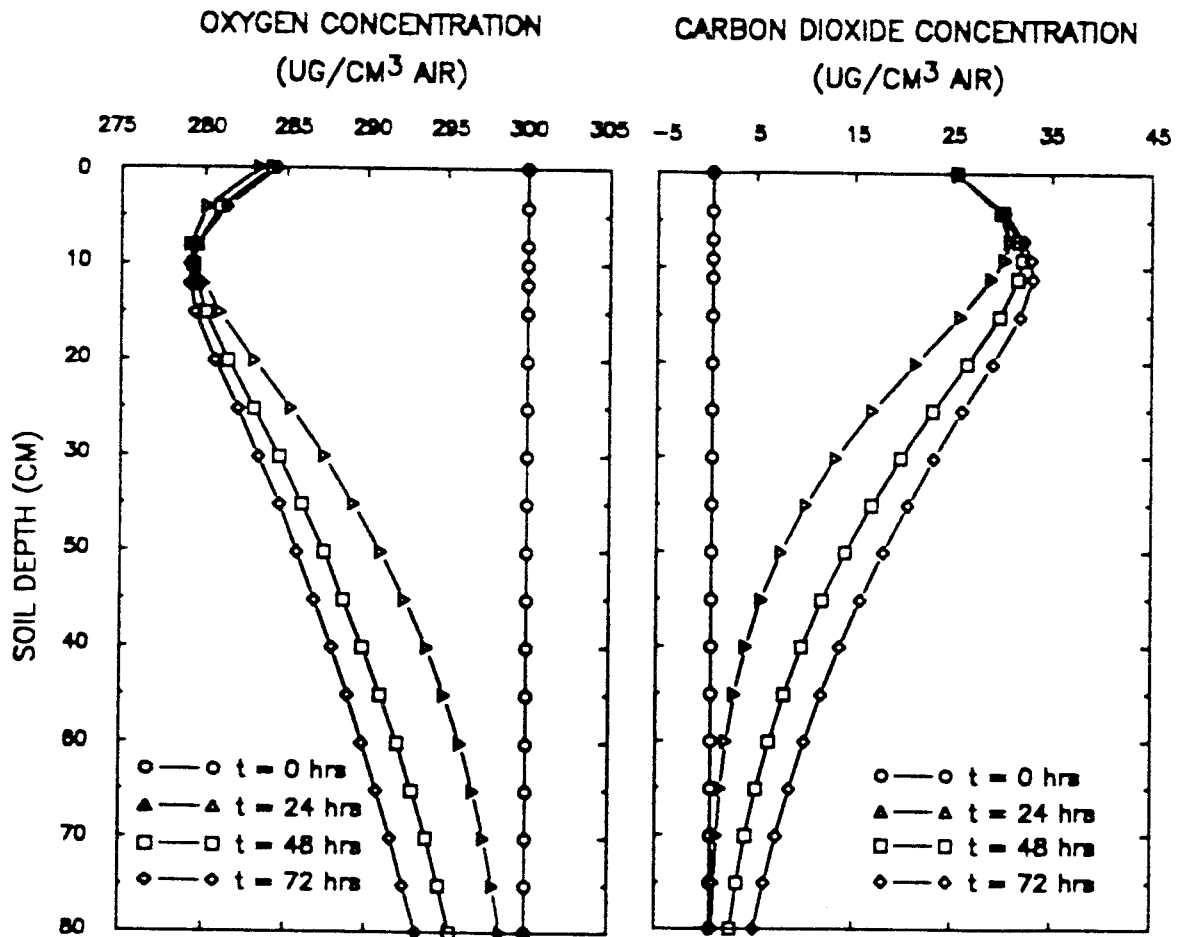


Figure 85. Oxygen and carbon dioxide concentrations as a function of soil depth at times of 0, 24, 48 and 72 hours. Initial oxygen and carbon dioxide concentrations are 300 and 0.6134  $\mu\text{g cm}^{-3}$  air, respectively.

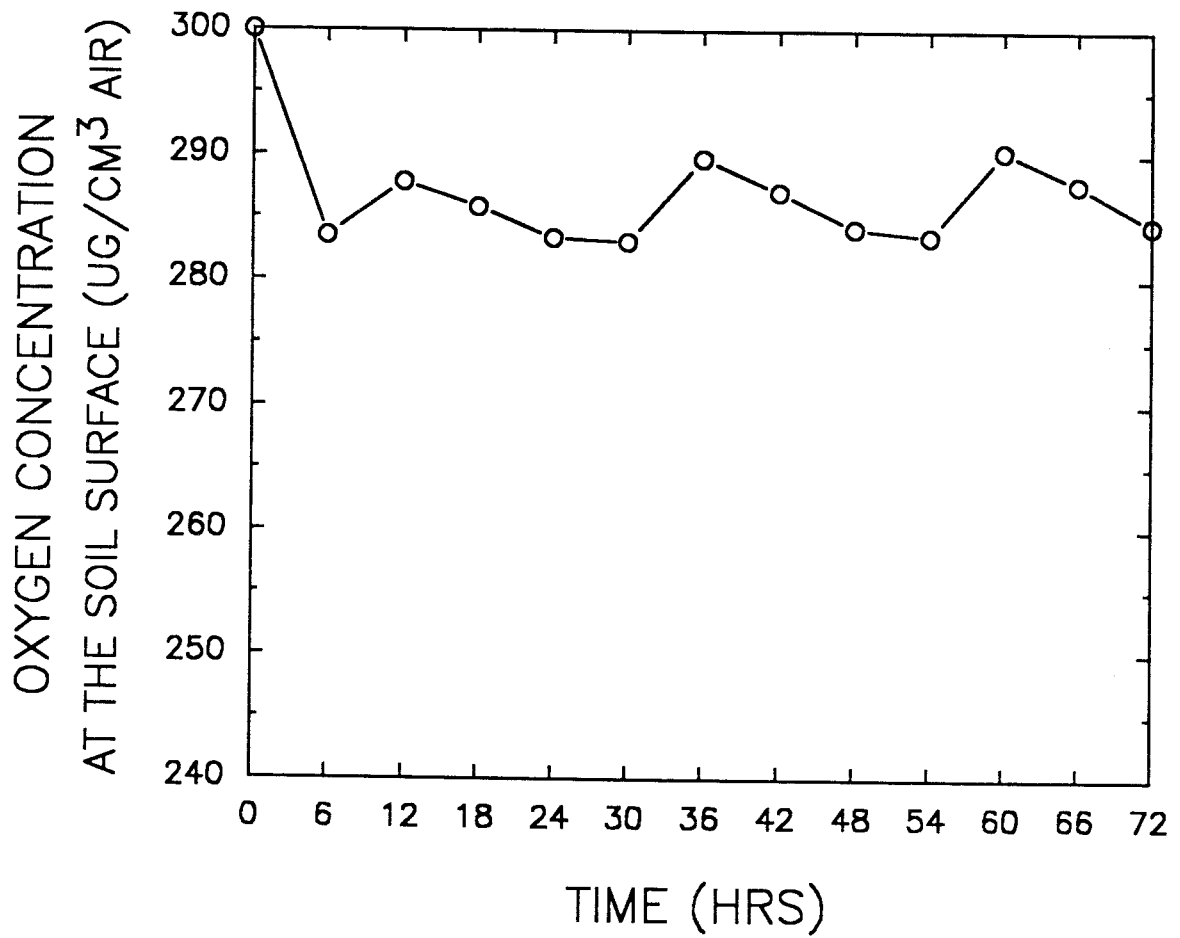


Figure 86. Oxygen concentration as a function of time at the soil surface from 0 to 72 hours.

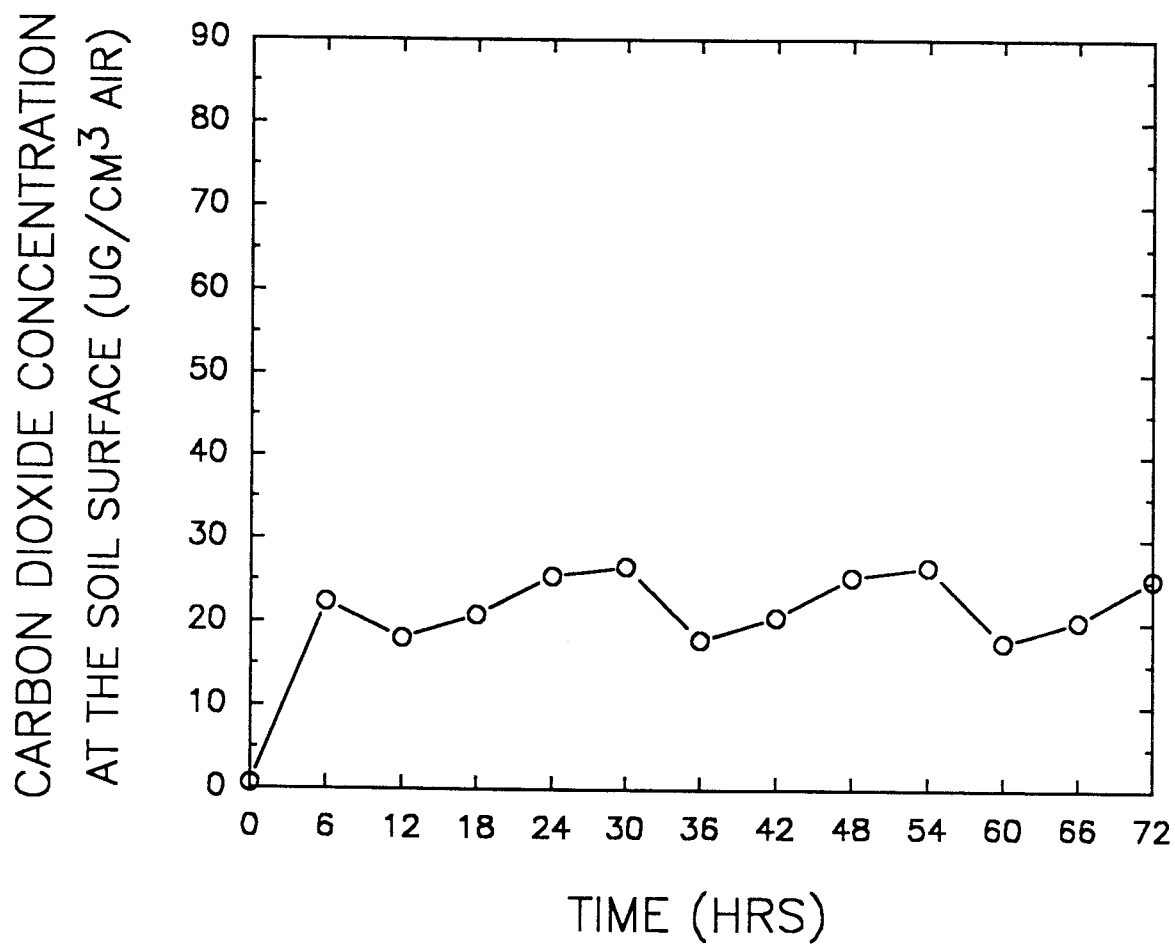


Figure 87. Carbon dioxide concentration as a function of time at the soil surface from 0 to 72 hours.

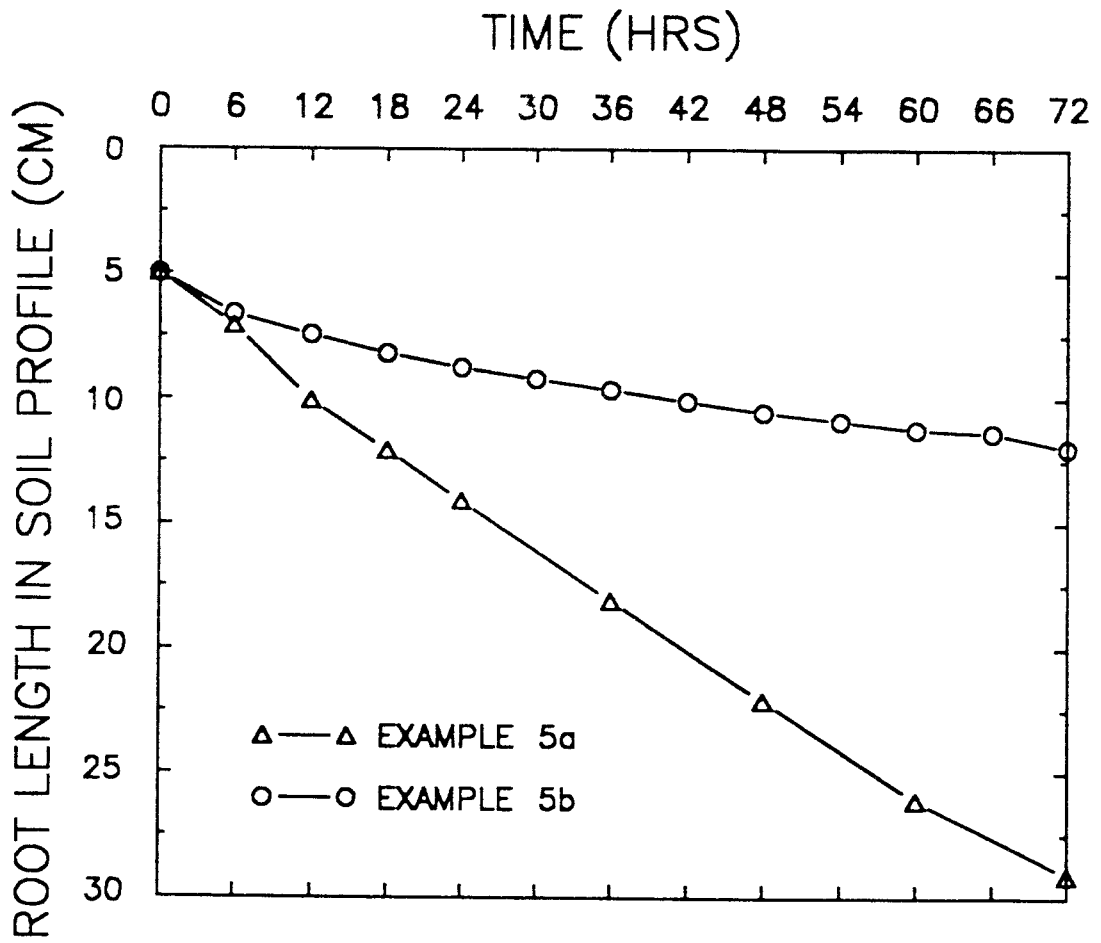


Figure 88. Root length as a function of time in the soil profile from 0 to 72 hours.

## SUMMARY AND CONCLUSIONS

Results of this Study

The dynamic exchange of oxygen and carbon dioxide between atmosphere and soil, as affected by climatic conditions, soil physical properties, and biological activities was studied, using a one-dimensional mathematical model. This model consists of four sets of non-linear partial differential field equations, which describe the time-dependent simultaneous transport of water, heat, oxygen, and carbon dioxide through the plant canopy and soil system.

Finite difference methods were used to find the approximate solutions for the four sets of non-linear partial differential field equations. The field equations for the transport of water and heat were approximated by using the implicit backward difference scheme. The field equations for the transport of oxygen and carbon dioxide were approximated by using the forward Euler-Lagrange time integrator explicit scheme. The computer program to simulate the mathematical model was written in Fortran code.

Examples were chosen to demonstrate applications of the mathematical model. Simultaneous transport of water, heat, oxygen, and carbon dioxide through Indio loam soil, during infiltration, redistribution, and evaporation periods was evaluated. The simultaneous transport of water, oxygen, and carbon dioxide through the compacted versus non-compacted soil during infiltration, redistribution, and evaporation periods was investigated. Diffusion

of oxygen and carbon dioxide within a crop canopy and soil system was examined. The effects of oxygen concentration and carbon dioxide concentration on the root elongation rate were evaluated. Effects of rate of oxygen consumption and carbon dioxide production by plant roots and soil microorganisms on the transport of oxygen and carbon dioxide was also estimated. Several different functions for the root elongation rate and the root oxygen consumption rates were used. Root elongation rate was chosen to depend on soil oxygen or carbon dioxide concentration, in addition to being depend on time. Root oxygen consumption rate was assumed to be a function of root age, in addition to being a function of oxygen or carbon dioxide concentration.

Input parameters for the simulations were obtained from several sources. Attempts were made to obtained realistic values for the input parameters.

Solutions obtained by solving the examples illustrate that the simultaneous transport of water, heat, oxygen, and carbon dioxide was well predicted by the model. The rate of diffusion of oxygen and carbon dioxide through the soil was strongly controlled by the climatic conditions, soil water content, and root respiration activities. Root growth below a compacted soil layer was restricted due to lower oxygen concentration. The plant canopy has decisive effects on the concentrations of oxygen and carbon dioxide at the soil surface, thereby affecting the diffusion of oxygen and carbon dioxide through the soil.

The transport of carbon dioxide behaving as ideal versus non-ideal gas through the soil was tested. Although differences of

carbon dioxide concentrations with ideal versus non-ideal behavior were detected, the small difference did not have a significant effect on the activities of roots and microorganisms (Nobel and Palta, 1989).

### Applications

The mathematical model may be applied to study the following problems:

(1) The model can be used to predict the rate of diffusion of oxygen and carbon dioxide through the plant canopy and soil system under different climatic conditions described by solar radiation, rainfall rate and duration, relative humidity, and air temperature, different soil physical properties such as soil water content, soil temperature, and compacted soil layer, and different biological activities such as photosynthesis and respiration activities of plant leaves, and respiration activities of roots and soil microorganisms.

(2) The model can be used to compare the concentrations of oxygen and carbon dioxide in the soil profile, calculated from the model, with the concentrations of oxygen and carbon dioxide required by plant roots to prevent deficiency of oxygen and excess of carbon dioxide in the root zone. Decisions about whether the soil aeration conditions need to be improved or not, can be based on the results. For example, if the deficiency of oxygen and excess of carbon dioxide was predicted by the model under given conditions, the soil aeration conditions can be changed by management practices such as tillage and drainage. This will help farmers to manipulate the gaseous exchange

between the atmosphere and soil to improve the yields of crops.

(3) The model can also be used to gain a better understanding of the dynamics of gaseous exchange between the atmosphere and soil for researchers who are interested in soil aeration problems.

### Advantages, Disadvantages, and Further

#### Development of the Model

The advantages, disadvantages, and further development of the model are discussed as follows.

(1) The model simulate the diffusion of oxygen and carbon dioxide through the plant canopy and soil system, as controlled by solar radiation, rainfall rate and duration, relative humidity, air temperature, soil water content, soil temperature, replacement of soil air by water due to soil wetting and replacement of soil water by air due to soil drying, photosynthesis and respiration activities of plant leaves, and respiration activities of roots and soil microorganisms. Also considered are the adsorption of oxygen and carbon dioxide by colloidal surfaces of soil particles and the dissolution of oxygen and carbon dioxide in soil water during the transport processes.

(2) The model does not include the mass flow of oxygen and carbon dioxide through soil. Although the diffusion of oxygen and carbon dioxide is the main mechanism for the transport of oxygen and carbon dioxide through soil (Wilson, et al., 1985), the mass flow mechanism should be included for purposes of accuracy in the further development of the model. The reason for not including the mass flow of oxygen

and carbon dioxide through the soil in the model was to avoid the model becoming too complicated.

(3) Entrapped air was assumed to be negligible. This is justified by a low rate of the infiltration of water to the soil, and a stable soil structure, i.e., no swelling and shrinking. In the natural soil, this is may not be true.

(4) The processes of replacement of soil air by water due to soil wetting and the replacement of soil water by air due to soil drying will bring the oxygen and carbon dioxide out of or into the soil. It is assumed that the volume of air being replaced by water during soil wetting equals to the volume of water being added to the soil. Similarly, it is assumed that the volume of water being replaced by air during soil drying equals to the volume of air entering the soil. These assumptions are valid when there is no entrapped air in the processes, the soil pores are continues, and connect to the atmosphere.

(5) It is assumed that there is no uptake of water by plant roots. This is done because our research focused on the transport of oxygen and carbon dioxide in the soil. However, the model can easily be modified to include the uptake of water by plant roots.

(6) The thermal diffusion of oxygen and carbon dioxide through soil caused by the soil temperature gradient was not considered. Few methods are available for modeling the thermal diffusion of gases through soil caused by the soil temperature gradient. More work is needed to find these solutions in the further development of the model. However, the diffusion coefficients of oxygen and carbon

dioxide were chosen to be a function of temperature as follows,

$$D = D_0 \left( \frac{T}{T_0} \right)^m, \quad (170)$$

where  $D$  is the diffusion coefficient of oxygen (or carbon dioxide) ( $\text{cm}^2 \text{hr}^{-1}$ ),  $T$  is temperature ( $^{\circ}\text{C}$ ),  $m$  is constant ( $m = 1.75$  for oxygen and  $m = 2$  for carbon dioxide), and  $D_0$  and  $T_0$  are diffusion coefficient of oxygen (or carbon dioxide) ( $\text{cm}^2 \text{hr}^{-1}$ ) and temperature ( $^{\circ}\text{C}$ ) at reference state, respectively. As is indicated in equation (170), the changes of soil temperature affect the diffusion coefficients of oxygen and carbon dioxide, thereby affecting the diffusion of oxygen and carbon dioxide through the soil.

(7) Sensitivity analysis of the model is needed. Results of such analysis could help to understand what parameters are important in governing the transport of oxygen and carbon dioxide through the soil.

## REFERENCES

- Alexander, M. 1961. Introduction to soil microbiology. John Wiley & Sons, Inc., New York. PP. 25-29.
- Birkle, D. E., J. Letey, L. H. Stolzy, and T. E. Szuszkiewicz. 1964. Measurement of oxygen diffusion rates with the platinum microelectrode. *Hilgardia* 35:555-556.
- Brady N. C. 1984. The nature and Properties of soils. Macmillan Publishing Company, New York. PP. 750.
- Bridge, B. J. and A. J. Rixon. 1976. Oxygen uptake and respiration quotient of field soil cores in relation to their air-filled pore space. *J. Soil Sci.* 27:279-286.
- Cheng, R. T., V. Casulli, and S. N. Milford. 1984. Eulerian-Lagrangian solution of the convection-dispersion equation in natural coordinates. *Water Resour. Res.* 20:944-952.
- Collin, M. and A. Rasmuson. 1988. A comparison of gas diffusion models for unsaturated porous media. *Soil Sci. Soc. Am. J.* 52:1559-1565.
- De Willigen, P. and M. Van Noordwijk, 1989. Model calculations on the relative importance of internal longitudinal diffusion for aeration of roots of non-wetland plants. *Plant and Soil.* 113:111-119.
- Devlin, R. M. and A. V. Barker. 1971. Photosynthesis. Van Nostrand Reinhold Company, New York. PP. 268-270.
- Dixon, W. J., and F. J. Massey Jr. 1983. Introduction to statistical analysis. McGraw-Hill book company, New York. PP. 59-63.
- Ghildyal, B. P. and R. P. Tripathi. 1987. Soil physics. John Wiley & Sons, New York. PP. 3-526.
- Glinski, J., and W. Stepniewski. 1985. Soil aeration and its role for plants. CRC Press, Inc. Boca Raton, Florida. PP. 229.
- Harvey, R. W., R. L. Smith, and L. George. 1984. Effect of organisms contamination upon microbial distributions and heterotrophic uptake in a Cape Cod, Mass. aquifer. *Appl. Environ. Microbiol.*, 48:1197-1202.
- Hiemenz, P. C. 1986. Principles of Colloid and Surface Chemistry. Marcel Dekker, Inc., New York and Basel. PP. 815

- Hillel, D. 1982. Introduction to soil physics. Academic press, Orlando. PP. 9-224.
- Kursar, T. A. 1989. Evaluation of soil respiration and soil CO<sub>2</sub> concentration in a lowland moist forest in Panama. Plant and Soil. 113:21-29.
- Lambers, H. and E. Steingrover. 1978. Efficiency of root respiration of a float-tolerant and a flood-intolerant Senecio species as affected by low oxygen tension. Physiol. Plant. 42:179-184.
- Lemon E. R. 1962. Soil aeration and plant root relations. I. Theory. Agronomy J. 54:167-170.
- Lemon E. R. and C. L. Wiegand. 1962. Soil aeration and plant root relations. II. Root Respiration. Agronomy J. 54:171-175.
- Levitt, J. 1969. Introduction to plant physiology. The C. V. Mosby Company, Saint Louis. PP. 157-159.
- Lewis, G. N. and M. Randall. 1961. Thermodynamics. McGraw-Hill Book Company, New York. PP. 723.
- Lindstrom, F. T. and W. T. Piver. 1985. A mathematical model of the transport and the fate of toxic chemicals in a simple aquifer. Tech. Rep. No. 52, Oregon State University, Department of Mathematics, Corvallis, Oregon.
- Lindstrom, F. T., L. Boersma, M. A. Barlaz, and F. Beck. 1989. Transport and fate of water and chemicals in laboratory scale, single layer aquifers. Volume 1. Mathematical model. Special report 845. Agricultural Experiment Station, Oregon State University, Corvallis, Oregon.
- Luxmoore, J. R., L. H. Stolzy, and J. Letey. 1970. Oxygen diffusion in the soil-plant system. I. A model. Agronomy J. 62:317-322.
- Marschner, H. 1986. Mineral nutrition of higher plants. Academic press, London, Orlando, New York. PP. 674.
- McCoy, E. L., L. Boersma, M. L. Unger, and S. Akrotanakul. 1984. Toward understanding soil water uptake by plant root. Soil Sci. 137:69-77.
- McIntyre, D. S. 1970. The platinum microelectrode method for soil aeration measurement. In "Advances in Agronomy," Vol. 22 Academic Press, New York. PP. 235-283.
- Mendoza, C. A. and E. D. Frind. 1990. Advective-Dispersive Transport of dense organic vapor in the unsaturated zone. I. Model development. Water Resour. Res. 26:379-387.

- Molz, F. J., M. A. Widdowson, and L. D. Benefield. 1986. Simulation of microbial growth dynamic coupled to nutrient and oxygen transport in porous media. *Water Resour. Res.* 22:1207-1216.
- Moore, W. J., 1983. *Basic physical chemistry*. Prentice-Hall, Inc., Englewood Cliffs, New Jersey. PP. 711.
- Mualem, Y. 1976. A new model for predicting the hydraulic conductivity of unsaturated porous media. *Water Resour. Res.* 12:513-522.
- Nobel, P. S. 1983. *Biophysical plant physiology and ecology*. W. H. Freeman and Company, San Francisco. PP. 608
- Nobel, P. S. and J. A. Palta. 1989. Soil O<sub>2</sub> and CO<sub>2</sub> effects on root respiration of cacti. *Plant and Soil.* 120:263-271.
- Oates, K., and S. A. Barber. 1987. Nutrient uptake: A microcomputer program to predict nutrient absorption from soil by roots. *J. Agron. Educ.* 16:65-68.
- Partington, J. R. 1949. *An advanced treatise on physical chemistry*. Vol. I. Longmans, London.
- Redmond, K. T. 1988. Hourly summarized weather statistics for Western Oregon. Department of Atmospheric Science, Climatic Research Institute, Oregon State University, Corvallis, Oregon 97331 (Personal communication).
- Skopp, J., 1985. Oxygen uptake and transport in soils: Analysis of the air-water interfacial area. *Soil Sci. Soc. Am. J.* 49:1327-1331.
- Solar Monitoring Lab. 1987. Pacific northwest solar radiation data. Solar energy center, Physics Dep., University of Oregon, Eugene, Oregon (Personal communication).
- Stolzy, L. H., and J. Letey. 1964. Characterizing soil oxygen conditions with a platinum microelectrode. *Adv. Agronomy J.* 16:249-279.
- Stumm, W and J. J. Morgan. 1981. *Aquatic chemistry*. An introduction emphasizing chemical equilibria in natural waters. A Wiley-interscience publication. John Wiley & Sons, New York. PP. 780.
- Thorstenson, D, C. and D. W. Pollock. 1989. Gas transport in unsaturated zones: Multicomponent systems and the adequacy of Fick's laws. *Water Resour. Res.* 25:477-507.

- Van Genuchten, M. Th. 1980. A close form equation for predicting the hydraulic conductivity of unsaturated soils. *Soil Sci. Soc. Am. J.* 44:892-898.
- Van Noordwijk, M. and P. DE Willigen. 1984. Mathematical methods on diffusion of oxygen to and within plant roots, with special emphasis on effects of soil-root contact. *Plant and Soil.* 77:233-241.
- Varga, R. S. 1962. *Matrix Iterative Analysis.* Prentice-Hall, Englewood Cliffs, N. J. PP. 322.
- Wallace, J. M. and P. V. Hobbs. 1977. *Atmospheric science, An introductory survey.* Academic press, Orlando. PP. 75.
- Weast, R. C. 1986. *Handbook of chemistry and physics.* CRC press, Boca Raton, Fla.
- Widdowson, M. A., F. J. Molz, and L. D. Benefield. 1988. A numerical transport model for oxygen- and nitrate-based respiration linked to substrate and nutrient availability in porous media. *Water Resour. Res.* 24:1553-1565.
- Wilson, G. V., B. R. Thiesse, and H. D. Scott. 1985. Relationships among oxygen flux, soil water tension, and aeration porosity in a drying soil profile. *Soil Sci.* 139:30-36.

## APPENDICES

## APPENDIX I

Definitions of Mathematical Symbols and UnitsFor Equations (61) Through (70)

Symbol	Meaning	Units
$\alpha_{\text{air}}$	Albedo of air	dimensionless
$\alpha_{\text{soil}}$	Albedo of soil surface	dimensionless
$\alpha_{\text{water}}$	Albedo of water surface	dimensionless
$\alpha_{\text{tort}}$	Tortuosity of the soil	dimensionless
$c_w$	Specific heat of water	cal g <sup>-1</sup> °C <sup>-1</sup>
$D_{\text{atm}}$	Molecular diffusion coefficient of water vapor in air	cm <sup>2</sup> hr <sup>-1</sup>
$D_{\text{wvmax}}$	Maximum value of the dispersion coefficient of water vapor in the boundary layer of the atmosphere	cm <sup>2</sup> hr <sup>-1</sup>
$D_{\text{atm}}^*$	Logistic representation of the boundary layer wind speed dependent coefficient of dispersion of water vapor	cm <sup>2</sup> hr <sup>-1</sup>
$e_{\text{H}_2\text{O}}^{\text{air}}(T_a)$	Saturated vapor pressure of the air	mm Hg
$\epsilon$	Soil porosity	cm <sup>3</sup> soil voids cm <sup>-3</sup> soil
$\epsilon_{\text{air}}$	Emissivity of the air above the soil	dimensionless
$\epsilon_o$	Porosity of the soil at the atmosphere-soil interface	cm <sup>3</sup> soil voids cm <sup>-3</sup> soil
$\epsilon_{\text{soil}}$	Emissivity of the soil	dimensionless
$\epsilon_{\text{water}}$	Emissivity of the water	dimensionless
$\sigma$	Stefan-Boltzman constant	cal hr <sup>-1</sup> cm <sup>-2</sup> °C <sup>-4</sup>

$\vec{H}_{ss}$	Transfer of heat by conduction through the soil particles	cal cm <sup>-2</sup> hr <sup>-1</sup>
$\vec{H}_{sl}$	Transfer of heat by conduction and convection in the liquid phase water	cal cm <sup>-2</sup> hr <sup>-1</sup>
$\vec{H}_{sv}$	Transfer of heat by conduction in the vapor phase water and by transport in the form of latent heat	cal cm <sup>-2</sup> hr <sup>-1</sup>
$h(\theta_0^*, T_0^*)$	Relative humidity at the atmosphere-soil interface	dimensionless
$\lambda_{air}$	Thermal conductivity of the air	cal cm <sup>-1</sup> hr <sup>-1</sup> °C <sup>-1</sup>
$\lambda_{amax}$	Maximum value of the effective thermal conductivity of the air	cal cm <sup>-1</sup> hr <sup>-1</sup> °C <sup>-1</sup>
$\lambda_{air}^*$	The effective thermal conductivity of the air at the boundary of atmosphere-soil interface	cal cm <sup>-1</sup> hr <sup>-1</sup> °C <sup>-1</sup>
$\theta_0^*$	Water content at the atmosphere-soil interface	cm <sup>3</sup> cm <sup>-3</sup>
$\rho_w$	Density of water	g cm <sup>-3</sup>
$\rho_{wv}^{sat}(T_a)$	Density of water vapor at saturation at temperature $T_a$	g cm <sup>-3</sup>
$\vec{q}_{heatin}$	Heat flux into the soil surface by rainwater	(cal cm <sup>-2</sup> hr <sup>-1</sup> )
$\vec{q}_{htevp}$	Heat flux out of the soil surface due to evaporation or heat flux into the soil surface due to condensation	(cal cm <sup>-2</sup> hr <sup>-1</sup> )
$\vec{q}_{htswr}$	Heat flux into the soil surface by short wave radiation	(cal cm <sup>-1</sup> hr <sup>-1</sup> )

$\vec{q}_{htssl}$	Heat flux through the soil surface via sensible heat	(cal cm <sup>-2</sup> hr <sup>-1</sup> )
$\vec{q}_{htlwra}$	Heat flux into the soil surface by long wave radiation	(cal cm <sup>-2</sup> hr <sup>-1</sup> )
$\vec{q}_{htlwrs}$	Heat flux out of the soil surface by long wave radiation	(cal cm <sup>-2</sup> hr <sup>-1</sup> )
$\vec{q}_{hs}$	Total heat flux into, or out of, the soil surface	(cal cm <sup>-2</sup> hr <sup>-1</sup> )
$T_{rw}$	Temperature of rain water	°C
$T_o^*$	Temperature at the atmosphere-soil interface	°C
WS	Wind speed	cm hr <sup>-1</sup>
$\delta z$	Thickness of boundary layer at the atmosphere-soil interface	cm
z	Thickness of air or depth of soil	cm

## APPENDIX II

Finite Difference Formulations for Approximating  
Four Field Equations

In order to solve field equations of water, heat, oxygen, and carbon dioxide, the following finite difference formulations were used:

$$(1) \quad \left. \frac{\partial \theta}{\partial z} \right|_{z_{i+1/2}} \approx \frac{\theta_{i+1} - \theta_i}{\Delta z_{i+1}}$$

$$(2) \quad \left. \frac{\partial \theta}{\partial z} \right|_{z_{i-1/2}} \approx \frac{\theta_i - \theta_{i-1}}{\Delta z_i}$$

$$(3) \quad \left. \frac{\partial T}{\partial z} \right|_{z_{i+1/2}} \approx \frac{T_{i+1} - T_i}{\Delta z_{i+1}}$$

$$(4) \quad \left. \frac{\partial T}{\partial z} \right|_{z_{i-1/2}} \approx \frac{T_i - T_{i-1}}{\Delta z_i}$$

$$(5) \quad \left. \frac{\partial P}{\partial z} \right|_{i, n} \approx \frac{2(P_{i+1/2, n} - P_{i-1/2, n})}{\Delta z_{i-1} + \Delta z_i}$$

$$(6) \quad \theta_{i+1/2} \approx \frac{\theta_{i+1} + \theta_i}{2}$$

$$(7) \quad \theta_{i-1/2} \approx \frac{\theta_i + \theta_{i-1}}{2}$$

$$(8) \quad T_{i+1/2} \approx \frac{T_{i+1} + T_i}{2}$$

$$(9) \quad T_{i-1/2} \approx \frac{T_i + T_{i-1}}{2}$$

$$(10) \quad \int_{t_n}^{t_{n+1}} g(t) dt = \Delta t g(t_{n+1})$$

$$(11) \quad \int_{z_{i-1/2}}^{z_{i+1/2}} g(z) dz = \frac{\Delta z_i + \Delta z_{i+1}}{2} g_k(z)$$

## APPENDIX III

Conversion of Units

Units of parameters of  $S_{mo}$  and  $S_{rt}$ , extracted from literatures, are different from the requirements of oxygen and carbon dioxide field equations (Equation (52) and (53)). Therefore, conversions of units are necessary. These are discussed in the following sections.

Conversion of Unit for the Rate of Oxygen Consumption by Roots ( $S_{rt}$ )

The unit of rate of oxygen consumption by roots is commonly expressed as  $\mu\text{g cm}^{-3}$  fresh roots  $\text{hr}^{-1}$  in the literatures. This unit needs to be converted to  $\mu\text{g cm}^{-3}$  air  $\text{hr}^{-1}$ , as was required by the unit used in the oxygen equation.

It was assumed that the average root volume is 3% of the total soil volume in this dissertation (Marschner, 1986). Therefore, the unit in  $\mu\text{g cm}^{-3}$  fresh roots  $\text{hr}^{-1}$  can be converted to  $\mu\text{g cm}^{-3}$  air  $\text{hr}^{-1}$  as following:

$$\frac{\mu\text{g}}{\text{cm}^3 \text{ fresh root} \cdot \text{hr}} = \frac{\mu\text{g}}{\text{cm}^3 \text{ fresh root} \cdot \text{hr}} \cdot \frac{0.03 \text{ cm}^3 \text{ fresh root} \cdot \text{hr}}{\text{cm}^3 \text{ soil}}$$

$$\cdot \frac{\text{cm}^3 \text{ soil}}{(\epsilon - \theta) \text{ cm}^3 \text{ air}}$$

$$= \frac{0.03 \mu\text{g}}{(\epsilon - \theta) \text{ cm}^3 \text{ air}},$$

where  $(\epsilon - \theta)$  is the volume of soil air ( $\text{cm}^3 \text{ air cm}^{-3} \text{ soil}$ ). The conversion was done in the computer program.

Conversion of Unit for the Rate of Oxygen Consumption by Microorganisms (Smo)

The unit of rate of oxygen consumption by soil microorganisms is expressed as  $\text{g colony}^{-1} \text{ hr}^{-1}$ . This unit needs to be converted to  $\mu\text{g cm}^{-3} \text{ air hr}^{-1}$ , as was required by the unit used in the oxygen field equation.

It was assumed that the population density of bacteria in the soil is  $6 \times 10^6$  bacterial  $\text{g}^{-1}$  soil, the bulk density of the soil is  $1.67 \text{ g soil cm}^{-3}$  soil, and density of bacterial in the colony is  $100$  bacterial  $\text{colony}^{-1}$  (Molz, et al., 1986). With the above assumptions, the unit in  $\text{g colony}^{-1} \text{ hr}^{-1}$  can be converted to  $\mu\text{g cm}^{-3} \text{ air hr}^{-1}$  as following:

$$\begin{aligned} \frac{\text{g oxygen}}{\text{colony} \cdot \text{hr}} &= \frac{\text{g oxygen}}{\text{colony} \cdot \text{hr}} \cdot \frac{6 \times 10^6 \text{ bacterial}}{\text{g soil}} \cdot \frac{1.67 \text{ g soil}}{\text{cm}^3 \text{ soil}} \\ &\cdot \frac{\text{colony}}{100 \text{ bacterial}} \cdot \frac{\text{cm}^3 \text{ soil}}{(\epsilon - \theta) \text{ cm}^3 \text{ air}} \\ &= \frac{1.002 \times 10^5 \text{ g oxygen}}{\text{cm}^3 \text{ air} \cdot \text{hr}} \end{aligned}$$

$$= \frac{0.1002 \mu\text{g oxygen}}{\text{cm}^3 \text{ air} \cdot \text{hr}} .$$

where  $(\epsilon - \theta)$  is the volume of soil air ( $\text{cm}^3 \text{ air cm}^{-3} \text{ soil}$ ). The conversion was done in the computer program.

## APPENDIX IV

Computer Program Information Flow and Program Listing

Figure 89 shows the general modular design and information flow for the computer program. This program was written in ANSCII Standard Fortran 77. Each module was compiled separately and then the resulting objective codes were linked together to create an executable code called MIXMAIN.EXE. Each module contains many helpful comments which make the codes more easily understand.

Module MIXMAIN.FOR is the main calling program. All the major Fortran variables were listed and categorized in common blocks named COMMON.ODC. As was shown on Figure 89, calls from MIXMAIN.FOR are in the following order:

- (1) MIXREAD. It reads in all the simulation input data;
- (2) MIXUNCS. It computes universal characterizing constants for a particular run;
- (3) MIXWRTO. It prints out all input parameters, calculated parameters, and initial field distributions;
- (4) MIXLREV. It decides when to begin or end the light cycle and rain cycle according to input parameters;
- (5) MIXING. It carries out the time integration for all four field equations;
- (6) MIXWATR. It estimates the water field equation;
- (7) MIXHEAT. It estimates the heat field equations;
- (8) MIXTHOM. It solves the tridiogal system of equations

- resulting from water and heat field equations;
- (9) MIXBNDY. It estimates the atmosphere-soil interface boundary conditions for water and heat field equations;
  - (10) MIXOXY. It estimates the oxygen field equations;
  - (11) MIXCBN. It estimates the carbon dioxide field equation;
  - (12) MIXCUM. It writes out all necessary simulation output results.

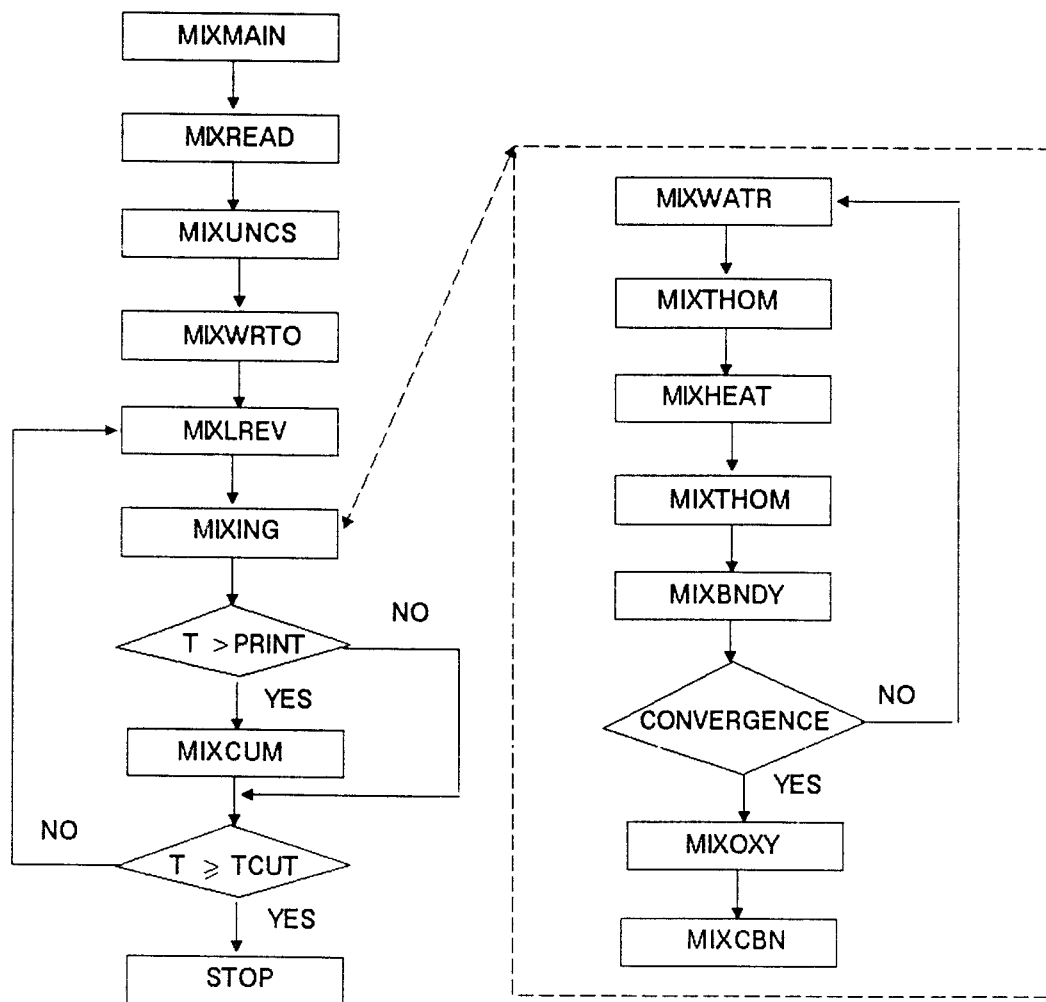


Figure 89. Basic computer program flow structures.

Program Listing

```

*MIXMAIN                               Last Revision: August 21, 1990
C                                       Source File:   MIXMAIN.FOR

      PROGRAM MIXMAIN
*****
* THIS PROGRAM SOLVES THE ONE-DIMENSIONAL MATHEMATICAL MODEL FOR *
* THE SIMULTANEOUS TRANSPORT OF WATER , HEAT, OXYGEN, AND CARBON *
* DIOXIDE THROUGH UNSATURATED SOIL. IT INCLUDES THE FOLLOWING *
* SUBROUTINES: *
* *
* (1) MIXMAIN.FOR. MAIN LISTING OF COMMON BLOCKS AND *
* THE CALLING PROGRAM; *
* (2) MIXREAD.FOR. INPUT ALL SYSTEM PARAMETERS, INITIALIZATION *
* VARIABLES, ETC.; *
* (3) MIXUNCS.FOR. CALCULATE ALL UNIVERSAL SYSTEM CONSTANTS FOR *
* THE RUN; *
* (4) MIXWRTO.FOR. WRITE OUT ALL SYSTEM PARAMETERS, *
* INITIALIZATION VARIABLES, AND CONSTANTS; *
* (5) MIXLREV.FOR. LIGHT OR RAIN EVENT CHECKING WATER AND HEAT *
* PARAMETER CALCULATIONS; *
* (6) MIXING.FOR. TIME INTEGRATION OF THE SYSTEM; *
* (7) MIXWATR.FOR. WATER SYSTEM SET UP; *
* (8) MIXHEAT.FOR. HEAT SYSTEM SET UP; *
* (9) MIXOXY.FOR. OXYGEN SYSTEM SET UP; *
* (10) MIXCBN.FOR. CARBON DIOXIDE SYSTEM SET UP; *
* (11) MIXBNDY.FOR. BOUNDARY INFORMATION DEFINED; *
* (12) MIXTHOM.FOR. SOLVE THE TRIDIAGONAL MATRIX; *
* (13) MIXCUM.FOR. WRITE OUT THE COMPUTATION RESULTS AND STORE *
* THE RESULTS FOR CONC. PROFILE PRINTING *
* NOTE! *
* I WISH TO EXPRESS THANKS TO DR. LINDSTROM FOR HIS WILLINGNESS *
* TO PROVIDE ME SOME OF HIS COMPUTER SUBROUTINES WHICH HAVE BEEN *
* MODIFIED AND USED IN THIS PROGRAM. *
* *
* I AM GRATEFUL TO MR. DAVID E. CAWLFIELD, A COMPUTER *
* SPECIALIST, FOR MAKING AN EFFICIENT CODING, FREQUENT INSIGHT, *
* HELP, AND DISCUSSION ON THE PROGRAM. *
* *****
      IMPLICIT NONE
      $include: 'common.ocd'
      DOUBLE PRECISION TOLD, PTIME
      common /local1/ told
      CHARACTER*20 OUTFILE, INPUT1, INPUT2, INPUT3, INPUT4, INPUT5,
      & P1RNFL, P2RNFL, RESOXC
      INTEGER IDAY, IHRS, IMIN
C..The following variables *really* are REALs . . .

```

```

REAL    START, TOOK, SECOND
C
C  UNITS 2-6 ARE USED FOR INPUT DATA;
C  UNITS 1, 7, 8, AND 9 ARE USED FOR OUTPUT.
C
1000 FORMAT(A)
2000 FORMAT(1X,A,1X,$)
WRITE(*,2000) 'Enter OUTFILE =>'
READ (*,1000) OUTFILE
WRITE(*,2000) 'Enter INFILE1 =>'
READ (*,1000) INPUT1
WRITE(*,2000) 'Enter INFILE2 =>'
READ (*,1000) INPUT2
WRITE(*,2000) 'Enter INFILE3 =>'
READ (*,1000) INPUT3
WRITE(*,2000) 'Enter INFILE4 =>'
READ (*,1000) INPUT4
WRITE(*,2000) 'Enter INFILE5 =>'
READ (*,1000) INPUT5
WRITE(*,2000) 'Enter P1RNFL =>'
READ (*,1000) P1RNFL
WRITE(*,2000) 'Enter P2RNFL =>'
READ (*,1000) P2RNFL
WRITE(*,2000) 'Enter RESOXC =>'
READ (*,1000) RESOXC
C
OPEN(UNIT=1, FILE=OUTFILE)
OPEN(UNIT=2, FILE=INPUT1)
OPEN(UNIT=3, FILE=INPUT2)
OPEN(UNIT=4, FILE=INPUT3)
OPEN(UNIT=5, FILE=INPUT4)
OPEN(UNIT=6, FILE=INPUT5)
OPEN(UNIT=7, FILE=P1RNFL)
OPEN(UNIT=8, FILE=P2RNFL)
OPEN(UNIT=9, FILE=RESOXC)
C
ILIVNT = 1
IRAVNT = 1
KNDX   = 0
LINDEX = 2
C
C  READ IN THE INPUT DATA
C
CALL OXREAD
WRITE(*,*) 'Data is now read in ...'
WRITE(*,*) 'Calculating porous medium properties ...'
CALL UNVCON
C

```

```

C  INITIALIZE TIME AND COUNTERS.
C
    T    = T0
    DT   = DT0
    TPRT = 0.0D0
    TOLD = T
C..Shave a little off of PTIME to account for round-off
    PTIME = PRIN(1) - 0.01D0*DT
    IEVENT(1) = 0
    IEVENT(2) = 0
    NCALLS = 0
    TNOW1 = 0.0D0
    T1     = 0.0D0
C
    WRITE(*,*) 'Writing out all input data and parameters.'
    CALL WRITOUT
C  WRITE THE TITLE FOR THE EVAPORATION PRINT OUT, ETC.
    WRITE(8,2010)
    2010 FORMAT(2X, 'TIME', 4X, 'WATER EVAP.', 4X, 'TEMP1', 4X,
    & 'TEMP5', 4X, 'TEMP10', 4X, 'TEMP20', 4X, 'TEMP50', 4X, 'SINFL')
C..Shave a little off TCUT to account for round-off
    TCUT = TCUT - 0.01D0*DT
    WRITE(*,*) 'Beginning system simulation ...'
    START = SECOND()
    2100 FORMAT(A, 1X, F11.4)
-----
C  MAIN LOOP:  SIMULATE SYSTEM OPERATION OVER TIME
C  REPEAT ...{Stmt 10}... UNTIL (T > TCUT)
C
100 CONTINUE
    TOLD = T
    DT   = DT0
    WRITE(*,2100) ' Time =', TOLD
    CALL LRAEV(TOLD)
C
    CALL INTGRL(TOLD)
C
    T    = TOLD + DT
    TPRT = TPRT + DT
C
    IF (TPRT .GE. PTIME .OR. KNDX .EQ. 1) THEN
        CALL WRITCMP
        TPRT = 0.0D0
        KNDX = 0
    ENDIF
C
200 IF (T .LE. TCUT) GO TO 100
C

```

```

C..Compute the *integration time* (startup is ignored). . .
  TOOK = SECOND() - START
  IDAY = TOOK / 86400.
  TOOK = MOD(TOOK, 86400.)
  IHRS = TOOK / 3600.
  TOOK = MOD(TOOK, 3600.)
  IMIN = TOOK / 60.
  WRITE(*,2200) IDAY, IHRS, IMIN
2200 FORMAT(//,1X,'Total integration time was ', I2.2, ' days, ',
  & I2.2, ' hours, and ', I2.2, ' minutes.')
999 STOP 'Normal Fortran Termination.'
  END

*SECOND   Time *function*                Last Revision: June 27, 1990
C..SP version                               Source File: FSECONS.FOR
  REAL FUNCTION SECOND()
  INTEGER*2 IH, IM, IS, IHU
  REAL      START, DAY
  SAVE     START, DAY

*****
* Returns the number of seconds and hundredths of seconds elapsed *
* since midnight.                               D. E. Cawlfeld, July '89. *
*****
  DATA START, DAY/ 2*0.0 /
  CALL GETTIM(IH, IM, IS, IHU)
  SECOND = 3600.*IH + 60.*IM + IS + 0.01*IHU
C..The addition of 1 second avoids a single precision round-off error
  IF (SECOND+DAY+1.0 .LT. START) DAY = DAY + 86400.
  SECOND = SECOND + DAY
  START = SECOND
  RETURN
  END

```

```

*MIXREAD                               Last Revision:  March 21, 1989
C                                       Source File:   MIXREAD.FOR
      SUBROUTINE OXREAD
C
C THIS SUBROUTIN READ IN ALL THE PARAMETERS, CONSTANTS, AND
C VALUES FOR SOLVING THE THREE FIELD EQUATIONS
C
      IMPLICIT DOUBLE PRECISION(A-H,O-Z)
      IMPLICIT INTEGER(I-N)
C
      $include:'common.ocd'
      INTEGER  I, J
C
C ENTER RUN CONTROL INFORMATION
C
      WRITE(*,*) 'Reading from file  CBOX1.DAT'
      READ(2,*) T0,TCUT,DT0,DT1
      READ(2,*) (PRTIN(I), I=1,16)
      READ(2,*) (NPRINT(I), I=1,20)
C
C READ IN STORAGE NODE INDICIES.
C
      READ(2,*) (NNSTRZ(I), I=1,25)
C
C READ IN NUMBER OF INTERNAL VERTICAL SOIL NODES.
C
      READ(2,*) NSLZM1
      NSLZZZ=NSLZM1+1
      NSLZP1 = NSLZZZ+1
C
C READ BOUNDARY LAYER THICKNESS AND DISTANCE BETWEEN NODES.
C
      READ(2,*) DELTAZ
      DO 18, I=1,NSLZZZ
         READ(2,*) DZ(I)
18 CONTINUE
C
C READ ALBEDO, EMISSIVITY, AND HEAT TRANSFER PARAMETERS.
C
      READ(2,*) ALBAIR,ALBWAT,ALBSOI
      READ(2,*) EMSAIR,EMSWAT,EMSSOI
      READ(2,*) LAMBHT
      READ(2,*) LAMSLD
      READ(2,*) SHTSAN,SHTSIL,SHTCLA,SHTWAT,SHTAIR
C
C READ IN SOIL PARTICLE DENSITY
C
      READ(2,*) RHOSND,RHOCLA,RHOSIL

```

```

C
C READ LIQUID WATER AND VAPOR PARAMETERS
C
C     READ(2,*) GAMTLI,BETATV
C     READ(2,*) NWVAIR
C     READ(2,*) (DWVAR(I),I=1,NWVAIR)
C     READ(2,*) RHOWAT,RHOAIR
C READ IN BOUNDARY LAYER WIND SPEED
C
C     READ(2,*) WS
C
C READ THE TEMPERATURE FIELD PARAMETERS
C
C INPUT FOURIER COEFFICIENTS FOR TEMP AND RHIN DRIVING FUNCTIONS
C NCFIMP = NUMBER OF TEMPERATURE COEFFICIENTS
C NCFFRH = NUMBER OF RELATIVE HUMIDITY COEFFICIENTS
C MIMP AND MRH IDENTIFY THE INDEX OF THE COEFFICIENTS
C
C READ IN THE NUMBER OF A AND B COEFFICIENTS FOR TEMP AND RHIN
C
C     READ(2,*) NCFIMP,NCFFRH
C
C READ IN THE TEMPERATURE COEFFICIENTS AND FREQUENCIES
C
C     DO 13, I = 1,NCFIMP
C         READ(2,*) ATEMP(I),BTEMP(I),OMEGTP(I)
13 CONTINUE
C
C READ IN THE RELATIVE HUMIDITY COEFFICIENTS AND ITS FOURIER
C FREQUENCY
C
C     DO 23, I = 1,NCFFRH
C         READ(2,*) ARHIN(I),BRHIN(I),OMGRHI(I)
23 CONTINUE
C
C READ IN THE CONSTANT TERMS
C
C     READ(2,*) TPINMU,RHINMU,TPWATI
C
C*****
C
C READ IN OXYGEN FIELD PARAMETERS
C
C     WRITE(*,*) 'Reading from file CBOX2.DAT'
C     READ(3,*) OMIGO2,OMGCO2,HO2,HCO2
C     READ(3,*) DO20,DCO20
C
C*****

```

```

C READ IN SOIL CHARACTERIZING PARAMETERS.
C
  WRITE(*,*) 'Reading from file CBOX3.DAT'
  READ(4,*) (THEAST(J),J=1,NSLZP1)
  READ(4,*) (TORT(J),J=1,NSLZP1)
  READ(4,*) (EPS(J),J=1,NSLZP1)
  READ(4,*) (PCTSAN(J),J=1,NSLZP1)
  READ(4,*) (PCTCLA(J),J=1,NSLZP1)
  READ(4,*) (PCTSIL(J),J=1,NSLZP1)
  READ(4,*) (ALPTH(J),J=1,NSLZP1)
  READ(4,*) (BETATH(J),J=1,NSLZP1)
  READ(4,*) (GAMCNS(J),J=1,NSLZP1)
  READ(4,*) (KTHSTS(J),J=1,NSLZP1)
  READ(4,*) (THIRES(J),J=1,NSLZP1)
  READ(4,*) (DALPTZ(J),J=1,NSLZP1)
  READ(4,*) (DBETAZ(J),J=1,NSLZP1)
  READ(4,*) (DTHPSZ(J),J=1,NSLZP1)
  READ(4,*) (DTHREZ(J),J=1,NSLZP1)
C
C*****
C READ INITIAL WATER, TEMPERATURE, AND OXYGEN CONCENTRATION VALUES.
C
  WRITE(*,*) 'Reading from file CBOX4.DAT'
  READ(5,*) THIAA,TEMPA
  DO 127, J=1,NSLZP1
    READ(5,*) THIAS(J),TEMPS(J)
  127 CONTINUE
C INCLUDE THE PLANT CANOPY PART
  DO 1001, J=1, NSLZP1+100
    CO2(J)=300.DO
    CCO2(J)=0.6134D0
  1001 CONTINUE
C
C*****
C READ IN UV, RAIN, AND SOLAR INTENSITY CHARACTERIZING PARAMETERS.
C
  WRITE(*,*) 'Reading from file CBOX5.DAT'
  DO 15, I=1,5
    READ(6,*) QRAIN(I),QSR(I)
  15 CONTINUE
C
C
C NLIEV AND NRAEV SHOULD BE THE DESIRED NUMBER OF
C LIGHT EVENTS + 1 AND NUMBER OF RAIN EVENTS + 1,
C RESPECTIVELY. THESE ADDED EVENT TIMES SHOULD BE
C SPECIFIED GREATER THAN TCUT TO MAKE THE PROGRAM
C RUN.
C

```

```
      READ(6,*) NLIEV,NRAEV
C
C READ IN THE LIGHT CYCLE AND RAIN CYCLE TIME EVENTS TIMES.
C
      DO 16, I=1,NLIEV
        READ(6,*) TLION(I),TLIOF(I)
16 CONTINUE
      DO 17, I=1,NRAEV
        READ(6,*) TRAON(I),TRAOF(I)
17 CONTINUE
C
      RETURN
      END
```

```

*MIXUNCS                               Last Revision:  March 21, 1989
C                                       Source File:   MIXUNCS.FOR
      SUBROUTINE UNVCON
C THIS SUBROUTINE COMPUTES THE SOIL PROPERTIES AND OTHER UNIVERSAL
C CONSTANTS
      IMPLICIT DOUBLE PRECISION(A-H,O-Z)
      IMPLICIT INTEGER(I-N)
C
$include: 'common.ocd'
      INTEGER I
C
C MISCELLANEOUS CONSTANTS
C
      GRAV = 1.271376D10
      R = 5.98104D13
      SIGMA = 4.896D-9
C
C CALCULATE NODAL POSITIONS.
C
      ZNODE(1)=0.0D0
      DO 30, I=1,NSLZZZ
          ZNODE(I+1) = ZNODE(I)+DZ(I)
30 CONTINUE
C
C MORE CALCULATED SOIL PROPERTIES.
C
      DO 50, I = 1,NSLZP1
          LAMSOL(I) = LAMSLD
          SHTSOL(I) = SHTSAN*PCTSAN(I)+SHTSIL*PCTSIL(I)+SHTCLA*PCTCLA(I)
          RHOSOL(I) = RHOSND*PCTSAN(I)+RHOSIL*PCTSIL(I)+RHOCLA*PCTCLA(I)
          RHOB(I) = RHOSOL(I)*(1.D0-EPS(I))
50 CONTINUE
C
C MISCELLANEOUS CONSTANTS
C
      DAIM = DWVAR(1)
      BETAVA = DWVAR(3)
C
      RETURN
      END

```

```

*MIXWRIO                               Last Revision: June 14, 1990
C                                       Source File:   MIXWRIO.FOR

      SUBROUTINE WRIOUT
C THIS SUBROUTINE WRITES OUT ALL SYSTEM PARAMETERS, INITIALIZATION
C SYSTEM VARIABLES, AND UNIVERSAL CONSTANTS
      IMPLICIT DOUBLE PRECISION(A-H,O-Z)
      IMPLICIT INTEGER(I-N)
C
C$include: 'common.ocd'
      INTEGER I
      IF(NPRINT(1).EQ.1) THEN
          GO TO 1000
      ENDIF
C
C      PRINT OUT RUN CONTROL INFORMATION.
C
      WRITE(1,5) T0,TCUT,DTO,DT1
5  FORMAT(20X,'RUN CONTROL INFORMATION.',/,
& 10X,'T0=' ,F10.4,2X,'TCUT=' ,F10.4,2X,'DTO=' ,F10.4,2X,'DT1=' ,
& F10.4,/)
      WRITE(1,6) (PRTIN(I),I=1,16)
6  FORMAT(10X,'PRTIN(I)=' ,5(1X,F10.4),/)
      WRITE(1,7) (NPRINT(I),I=1,20)
7  FORMAT(10X,'NPRINT(I)=' ,20I3,/)
      WRITE(1,15) (NNSTRZ(I),I=1,25)
15 FORMAT(10X,'NNSTRZ(I)=' ,25I3,/)
C
C      PRINT GEOMETRICAL PARAMETERS.
C
      WRITE(1,8)
8  FORMAT(10X,'LAYER, THICKNESS (CM) ,',
& ' NODAL POSITION (CM) .',/)
      DO 9, I=1,NSLZZZ
          WRITE(1,10) I,DZ(I),ZNODE(I)
10  FORMAT(10X,I4,2X,2(2X,E13.4))
9  CONTINUE
      WRITE(1,11) NSLZM1,ZNODE(NSLZP1)
11  FORMAT(1X,/,,'NUMBER OF INTERNAL SOIL NODES= ',I3,
&3X,'SOIL THICKNESS (CM)= ',F10.4,/)
      WRITE(1,19) DELTAZ
19  FORMAT(6X,'BOUNDARY LAYER THICKNESS=' ,F10.4,/)
      WRITE(1,43) RHOSND,RHOCLA,RHOSIL
43  FORMAT(1X,'RHOSND= ',E13.4,2X,'RHOCLA= ',E13.4,2X,
& 'RHOSIL=' ,E13.4,/)
      WRITE(1,44) ALBAIR,ALBWAT,ALBSOI
44  FORMAT(1X,'ALBAIR= ',E13.4,2X,'ALBWAT= ',E13.4,
& 2X,'ALBSOI= ',E13.4,/)
      WRITE(1,46) EMSAIR,EMSWAT,EMSSOI

```

```

46 FORMAT(1X,'EMSAIR= ',E13.4,2X,'EMSWAT= ',E13.4,
& 2X,'EMSSOI= ',E13.4,/)
WRITE(1,48) LAMBHT
48 FORMAT(1X,'LAMBHT= ',1X,E13.4,/)
WRITE(1,49) LAMSLD
49 FORMAT(1X,'LAMSLD =',E13.4,/)
WRITE(1,50) SHTSAN,SHTSIL,SHTCLA,SHTWAT,SHTAIR
50 FORMAT(1X,'SHTSAN= ',E13.4,2X,'SHTSIL= ',E13.4,2X,
& 'SHTCLA= ',E13.4,2X,'SHTWAT= ',E13.4,2X,
& 'SHTAIR= ',E13.4,/)
WRITE(1,51) GAMTLI,BETATV
51 FORMAT(1X,'GAMTLI= ',E13.4,2X,'BETATV= ',E13.4,/)
WRITE(1,52) (DWVAR(I),I=1,NWVAIR)
52 FORMAT(1X,'DWVAR(I)= ',3(1X,E13.4),/)
WRITE(1,53) RHOWAT,RHOAIR,WS
53 FORMAT(1X,'RHOWAT=',E13.4,2X,'RHOAIR=',E13.4,2X,
& 'WS = ',E13.4,/)
C
C PRINT OUT THE DRIVING FUNCTIONS PARAMETERS
C AND THE TIME EVENTS PARAMETERS.
C
WRITE(1,62)
62 FORMAT(/,10X,' DRIVING FUNCTION PARAMETERS. ')
WRITE(1,64)
64 FORMAT(//,3X,'FOURIER COEFFICIENTS',/)
WRITE(1,66) NCFIMP,NCFFRH
66 FORMAT(1X,'NCFIMP =',I3,' NCFFRH =',I3,/)
WRITE(1,68)
68 FORMAT(1X,///,' INDEX',3X,'ATEMP',8X,'BTEMP')
DO 54, I = 1,NCFIMP
WRITE(1,70) I,ATEMP(I),BTEMP(I)
70 FORMAT(1X,I3,2X,F10.6,2X,F10.6)
54 CONTINUE
WRITE(1,72)
72 FORMAT(1X,///,' INDEX',3X,'ARHIN',8X,'BRHIN')
DO 55, I = 1,NCFFRH
WRITE(1,700) I,ARHIN(I),BRHIN(I)
700 FORMAT(1X,I3,2X,F10.6,2X,F10.6)
55 CONTINUE
WRITE(1,74) TPINMU,RHINMU,TPWATI
74 FORMAT(1X,///,' TPINMU = ',F10.6,3X,'RHINMU = ',F10.6,
&3X,'TPWATI = ',F10.6)
WRITE(1,76)
76 FORMAT(//,1X,'INDEX',3X,'OMEGTP')
DO 56, I = 1,NCFIMP
WRITE(1,78) I,OMEGTP(I)
78 FORMAT(1X,I3,2X,F10.6)
56 CONTINUE

```

```

WRITE(1,80)
80 FORMAT(//,1X,'INDEX',3X,'OMGRHI')
DO 57, I = 1,NCFFRH
WRITE(1,788) I,OMGRHI(I)
788 FORMAT(1X,I3,2X,F10.6)
57 CONTINUE
WRITE(1,82)
82 FORMAT(1X,//,1X,'INDEX',3X,'QRAIN',7X,'QSR',/)
DO 83, I=1,5
WRITE(1,84) I,QRAIN(I),QSR(I)
84 FORMAT(1X,I4,2(1X,E13.4))
83 CONTINUE
C
WRITE(1,85)
85 FORMAT(1X,//,1X,'INDEX',4X,'TIME LIGHT ON',3X,
&'TIME LIGHT OFF',/)
DO 86, I=1,NLIEV
WRITE(1,87) I,TLION(I),TLIOF(I)
87 FORMAT(1X,I4,7X,E13.4,6X,E13.4)
86 CONTINUE
C
WRITE(1,88)
88 FORMAT(1X,//,1X,'INDEX',4X,'TIME RAIN ON',3X,'TIME RAIN OFF',/)
DO 89, I=1,NRAEV
WRITE(1,90) I,TRAON(I),TRAOF(I)
90 FORMAT(1X,I4,5X,E13.4,5X,E13.4)
89 CONTINUE
C
C PRINT OUT OXYGEN PARAMETERS
C
WRITE(1,400)
400 FORMAT(/,10X,'OXYGEN PARAMETERS',/)
WRITE(1,415) OMIGO2,OMGCO2
415 FORMAT(10X,'OMIGO2=',E11.4,2X,'OMIGCO2=',E11.4,2X,/)
WRITE(1,430) DO20,DCO20,HO2,HCO2
430 FORMAT(10X,'DO20=',E13.4,2X,'DCO20=',E13.4,2X,'HO2=',E13.4,
&2X,'HCO2=',E13.4,/)
C
C PRINT OUT INPUT WATER, TEMP., AND OXYGEN CONC.
C
WRITE(1,104)
104 FORMAT(1X,/,3X,'AIR R.H.',7X,'AIR TEMP.',3X,'TOP CAN.OXY. CONC.',
&3X,'TOP CAN. CAR. DIO. CONC.')
WRITE(1,105)
105 FORMAT(2X,'(PERCENT) (DEG. KELVIN) (UG/CM3 AIR)
&(UG/CM3 AIR)',/)
WRITE(1,106) THIAA,TEMPA,CO2(1),CO2(1)
106 FORMAT(2X,E13.4,5X,E13.4,3X,E13.4,3X,E13.4,/)

```

```

WRITE(1,107)
107 FORMAT(5X, 'INITIAL FIELD DISTRIBUTIONS',/)
WRITE(1,108)
108 FORMAT(1X, 'LAYER', 8X, 'WATER', 15X, 'TEMPERATURE', 9X, 'OXYGEN',
& 11X, 'CARBON DIOXIDE')
WRITE(1,410)
410 FORMAT(8X, '(CM3 WATER/CM-3 SOIL)', 1X, '(DEG. KELVIN)', 10X,
& '(UG/CM-3 SOIL AIR)')
DO 341, I=1, NSLZP1
WRITE(1,342) I, THTAS(I), TEMPS(I), CO2(I), CCO2(I)
342 FORMAT(2X, I3, 6X, E13.4, 10X, E13.4, 7X, E13.4, 5X, E13.4)
341 CONTINUE
C
C PRINTOUT UNIVERSAL CONSTANTS
C
WRITE(1,112)
112 FORMAT(/, 5X, ' UNIVERSAL CONSTANTS ')
WRITE(1,114) GRAV, R, SIGMA
114 FORMAT(/, ' GRAV = ', E13.4, 2X, 'R = ', E13.4, 2X, 'SIGMA = ', E13.4, /)
C
WRITE(1,200)
200 FORMAT(10X, 'TABLES OF SOIL PROPERTIES',/)
WRITE(1,206)
206 FORMAT(/, 10X, 'THTAST(I)',/)
WRITE(1,203) (THTAST(I), I=1, NSLZP1)
203 FORMAT(1X, 10(1X, E12.4))
WRITE(1,212)
212 FORMAT(/, 10X, 'TORT(I)',/)
WRITE(1,203) (TORT(I), I=1, NSLZP1)
WRITE(1,214)
214 FORMAT(/, 10X, 'EPS(I)',/)
WRITE(1,203) (EPS(I), I=1, NSLZP1)
WRITE(1,220)
220 FORMAT(/, 10X, 'PCTSAN(I)',/)
WRITE(1,203) (PCTSAN(I), I=1, NSLZP1)
WRITE(1,222)
222 FORMAT(/, 10X, 'PCTCLA(I)',/)
WRITE(1,203) (PCTCLA(I), I=1, NSLZP1)
WRITE(1,224)
224 FORMAT(/, 10X, 'PCTSIL(I)',/)
WRITE(1,203) (PCTSIL(I), I=1, NSLZP1)
WRITE(1,226)
226 FORMAT(/, 10X, 'RHOSOL(I)',/)
WRITE(1,203) (RHOSOL(I), I=1, NSLZP1)
WRITE(1,228)
228 FORMAT(/, 10X, 'RHOB(I)',/)
WRITE(1,203) (RHOB(I), I=1, NSLZP1)
WRITE(1,230)

```

```
230 FORMAT(/,10X,'SHISOL(I)',/)
    WRITE(1,203)(SHISOL(I),I=1,NSLZP1)
    WRITE(1,232)
232 FORMAT(/,10X,'LAMSOL(I)',/)
    WRITE(1,203)(LAMSOL(I),I=1,NSLZP1)
    WRITE(1,790)
790 FORMAT(/,10X,'ALPTH(I)',/)
    WRITE(1,203)(ALPTH(I),I=1,NSLZP1)
    WRITE(1,710)
710 FORMAT(/,10X,'BETATH(I)',/)
    WRITE(1,203)(BETATH(I),I=1,NSLZP1)
    WRITE(1,720)
720 FORMAT(/,10X,'GAMCNS(I)',/)
    WRITE(1,203)(GAMCNS(I),I=1,NSLZP1)
    WRITE(1,730)
730 FORMAT(/,10X,'KIHSTS(I)',/)
    WRITE(1,203)(KIHSTS(I),I=1,NSLZP1)
    WRITE(1,740)
740 FORMAT(/,10X,'THIRES(I)',/)
    WRITE(1,203)(THIRES(I),I=1,NSLZP1)
    WRITE(1,750)
750 FORMAT(/,10X,'DALPTZ(I)',/)
    WRITE(1,203)(DALPTZ(I),I=1,NSLZP1)
    WRITE(1,760)
760 FORMAT(/,10X,'DBETAZ(I)',/)
    WRITE(1,203)(DBETAZ(I),I=1,NSLZP1)
    WRITE(1,770)
770 FORMAT(/,10X,'DIHISZ(I)',/)
    WRITE(1,203)(DIHISZ(I),I=1,NSLZP1)
    WRITE(1,780)
780 FORMAT(/,10X,'DIHREZ(I)',/)
    WRITE(1,203)(DIHREZ(I),I=1,NSLZP1)
    WRITE(1,233)
233 FORMAT(/,5X,' OUTPUT DATA FOR DYNAMIC SYSTEM ',/)
C
1000 RETURN
    END
```

```

*MIXLREV                               Last Revision:  March 21, 1989
C                                       Source File:   MIXLREV.FOR
      SUBROUTINE IRAEV(TOLD)
C THIS SUBROUTINE CHECKS THE LIGHT AND RAIN CYCLES
      IMPLICIT DOUBLE PRECISION (A-H,O-Z)
      IMPLICIT INTEGER(I-N)
C
C$include: 'common.ocd'
      double precision told
      double precision tran2,tnow,tstar,ttest1,ttest2,ttest3,ttest4
      common /local2/  tran2,tnow,tstar,ttest1,ttest2,ttest3,ttest4
C
      TRAN2 = 1.0D-6
C
      TNOW = T
C
      TSTAR = TOLD+DT
C
      TTEST1 = DABS(TSTAR-TLION(ILIVNT))
      IF (TSTAR.LT.TLION(ILIVNT).AND.TTEST1.LT.TRAN2) GO TO 50
      IF (TSTAR.LT.TLION(ILIVNT)) GOTO 40
      IF (TOLD.LT.TLION(ILIVNT).AND.TSTAR.GE.TLION(ILIVNT)) GOTO 50
      IF (TOLD.GE.TLION(ILIVNT).AND.TSTAR.LT.TLIOF(ILIVNT)) GOTO 60
      IF (TOLD.LT.TLIOF(ILIVNT).AND.TSTAR.GE.TLIOF(ILIVNT)) GOTO 70
      TTEST4 = DABS(TSTAR-TLIOF(ILIVNT))
      IF (TSTAR.LT.TLIOF(ILIVNT).AND.TTEST4.LT.TRAN2) GO TO 70
      IF (TSTAR.GT.TLIOF(ILIVNT)) GOTO 80
      GO TO 150
C
      40 QSR(1) = 0.0D0
      IEVENT(1) = 0
      GO TO 150
C
      50 DT = TLION(ILIVNT)-TOLD
      IEVENT(1) = 0
      QSR(1)=0.0D0
      TSTAR=TOLD+DT
      KNDX = 1
      GO TO 150
C
      60 IEVENT(1)=1
C
      150 TTEST2 = DABS(TSTAR-TRAON(IRAVNT))
      IF (TSTAR.LT.TRAON(IRAVNT).AND.TTEST2.LT.TRAN2) GO TO 110
      IF (TSTAR.LT.TRAON(IRAVNT)) GOTO 100
      IF (TOLD.LT.TRAON(IRAVNT).AND.TSTAR.GE.TRAON(IRAVNT)) GOTO 110
      IF (TOLD.GE.TRAON(IRAVNT).AND.TSTAR.LT.TRAOF(IRAVNT)) GOTO 120
      IF (TOLD.LT.TRAOF(IRAVNT).AND.TSTAR.GE.TRAOF(IRAVNT)) GOTO 130

```

```
TTEST3 = DABS (TSTAR-TRAOF (IRAVNT))
IF (TSTAR.LT.TRAOF (IRAVNT) .AND. TTEST3 .LT. TRAN2) GO TO 130
IF (TSTAR.GT.TRAOF (IRAVNT)) GOTO 140
RETURN

C
100 QRAIN(1) = 0.0D0
    IEVENT(2) = 0
    RETURN

C
110 DT = TRAON (IRAVNT) -TOLD
    IEVENT(2) = 0
    QRAIN(1)=0.0D0
    KNDX = 1
    RETURN

C
120 IEVENT(2)=1
    QRAIN(1) = QRAIN(2)
    RETURN

C
130 DT = TRAOF (IRAVNT) -TOLD
    IEVENT(2) = 1
    QRAIN(1)=QRAIN(2)
    KNDX = 1
    RETURN

C
140 QRAIN(1) = 0.0D0
    IEVENT(2)=0
    IRAVNT = IRAVNT+1
    RETURN

C
70 DT = TLIOF (ILIVNT) -TOLD
   TSTAR=TOLD+DT
   IEVENT(1) = 1
   KNDX = 1
   GO TO 150

C
80 QSR(1) = 0.0D0
   IEVENT(1)=0
   ILIVNT = ILIVNT+1
   GO TO 150
END
```

```

*MIXING
C
SUBROUTINE INTGRL(TOLD)
C
C THIS SUBROUTINE DOES THE TIME INTEGRATION OF FILED EQUATIONS.
C THE TIME STEP FOR SOLVING WATER AND HEAT EQUATIONS (IMPLICIT METHOD)
C IS LARGER THAN THAT FOR SOLVING OXYGEN AND CARBON DIOXIDE (EXPLICIT
C METHOD).
C
C      IMPLICIT NONE
C
C $include: 'common.ocd'
C      DOUBLE PRECISION TOLD
C      INTEGER I, J, KITEST, ITRIP
C      DOUBLE PRECISION TOLRN1, TOLRN2, TNOW, TTEMPA, ATHOLD, ATHNEW,
C      & ATMOLD, ATMNEW, DELTH, DELTP, TCH, DTCH
C      common /local7/ tolrm1, tolrm2, tnow, ttempa, athold, athnew,
C      & atmold, atmnew, delth, deltp, tch, dtch
C
C      SYSTEM DRIVING VARIABLES
C
C      SECTION 1 COMPUTES THE TEMPERATURE AND RELATIVE HUMIDITY
C      OF THE AIR OVER THE SOIL SLAB AT EACH TIME STEP.
C      IT ASSUMES THAT THE AIR DATA HAS BEEN FOURIER ANALYZED.
C      THE CALCULATED VALUES ARE IN VARIABLES TMPAIN AND RHAIN.
C      TPINMU AND RHINMU ARE THE CONSTANT TERMS, READ IN AS INPUTS.
C      ATEMP AND ARHIN ARE THE A FOURIER COEFFICIENTS.
C      BTEMP AND BRHIN ARE THE B FOURIER COEFFICIENTS.
C      THE PROGRAM CAN ACCEPT UP TO 20 COEFFICIENTS.
C
C      TOLRN1 = 0.001D0
C      TOLRN2 = 0.01D0
C      TMPAIN = 0.D0
C      RHAIN = 0.D0
C      TNOW = TOLD
C      IF (NCFIMP .NE. 1) THEN
C          DO 11, I = 1, NCFIMP
C              TMPAIN = ATEMP(I) * DCOS(OMEGTP(I) * TNOW) + TMPAIN
C              TMPAIN = BTEMP(I) * DSIN(OMEGTP(I) * TNOW) + TMPAIN
11      CONTINUE
C      ENDIF
C      IF (NCFFRH .NE. 1) THEN
C          DO 13, I = 1, NCFFRH
C              RHAIN = ARHIN(I) * DCOS(OMGRHI(I) * TNOW) + RHAIN
C              RHAIN = BRHIN(I) * DSIN(OMGRHI(I) * TNOW) + RHAIN
13      CONTINUE
C      ENDIF
12 CONTINUE

```

Last Revision: August 21, 1990  
Source File: MIXING.FOR

```

TMPAIN = TMPAIN+TPINMU+273.0D0
RHAIN = RHAIN+RHINMU
C
C IF RAINING, AIR TEMP. IS REDUCED 50% AS COMPARED WITH NO RAIN
C
      IF (IEVENT(2) .EQ. 1) TMPAIN =(TMPAIN-273.0D0)*0.50D0+273.0D0
C
      TTEMPA = TMPAIN-273.0D0
      RSWVIN = 0.004928D0+0.0002581D0*TTEMPA +0.0000183D0*TTEMPA*TTEMPA
      IF (TMPAIN .GE. 295.5D0) RSWVIN=RSWVIN +
&  0.0000213D0*(TMPAIN-295.5D0)**2
      RSWVIN=RSWVIN/1000.D0
      RHOWVA = RSWVIN*RHAIN
      INFLTR = QRAIN(1)
      IF (IEVENT(2) .EQ. 1) RHAIN = 1.D0
      IF (IEVENT(1) .EQ. 1) GO TO 15
      QSR(1) = 0.0D0
      TNOW1 = 0.0D0
      GO TO 16
15 TNOW1 = TNOW1+DT
C THE GAUSSIAN DISTRIBUTION FUNCTION IS USED TO FIT THE RADIATION
C DATA
      IF(IEVENT(2).EQ.1) GO TO 17
C QSR(1) IS SOLAR RADIATION
C QSR(2), QSR(3), QSR(4) ARE THE COEFFICIENTS IN GUASSIAN FUNCTION
C QSR(5) IS THE REDUCTION FACTOR OF RADIATION DUE TO THE RAIN
      QSR(1) = QSR(2)*DEXP((-0.5D0)*(((TNOW1-QSR(3))/QSR(4))**2))
      GO TO 16
17 QSR(1) =QSR(2)*QSR(5)*DEXP((-0.5D0)*(((TNOW1-QSR(3))/QSR(4))**2))
16 TEMPA = TMPAIN
      THTAA = RHAIN
C
C SECTION 2: INITIALIZATION OR UPDATE OF FIELD VARIABLES.
C
      DO 21, J=1,NSLZP1
          THINNEW(J)=IHTAS(J)
          THIOLD(J)=IHTAS(J)
          TMPNEW(J)=TEMPS(J)
          TMPOLD(J)=TEMPS(J)
21 CONTINUE
      DO 22, J=1, NSLZP1+100
          CLDO2(J)=CO2(J)
          CLDCO2(J)=CCO2(J)
22 CONTINUE
C
C SECTION 3: BEGIN MASTER ITERATION LOOP FOR THE HEAT AND WATER FIELDS.
C
      KITEST=0

```

```
100 CONTINUE
    WRITE(*,1) ' .'
    1 FORMAT(A,\)
C
C SUB SECTION 3A: CALL TO SUBROUTINE MOISTR.
C
    CALL MOISTR(KITEST)
C
C SUB SECTION 3B: CALL TO SUBROUTINE THOMAS
C
    SET UP THE "KNOWN VECTOR" FOR
    THE THOMAS SYSTEM SOLVER.
C
    DO 26, J=2,NSLZZZ
        YDUM(J)=YTH(J)
26 CONTINUE
C
    CALL THOMAS
C
    REDEFINITION OF WATER VARIABLES.
C
    DO 31, J=2,NSLZZZ
        THINNEW(J)=XDUM(J)
31 CONTINUE
C
C SUB SECTION 3C: CALL TO SUBROUTINE HEAT.
C
    CALL HEAT(KITEST)
C
C SUB SECTION 3D: CALL TO SUBROUTINE THOMAS.
C
    SET UP THE "KNOWN VECTOR" FOR
    THE THOMAS SYSTEM SOLVER.
C
    DO 36, J=2,NSLZZZ
        YDUM(J)=YTP(J)
36 CONTINUE
C
    CALL THOMAS
C
    REDEFINITION OF HEAT VARIABLES.
C
    DO 41, J=2,NSLZZZ
        TMPNEW(J)=XDUM(J)
41 CONTINUE
C
C SUB SECTION 3E: CALL TO SUBROUTINE BOUNDRY.
C
```

```

        IF(NPRINT(5).EQ.1) GO TO 42
        CALL BOUNDRY
42 CONTINUE
C
C SUB SECTION 3F: TEST FOR CONVERGENCE.
C
        DO 46, J=2,NSLZZZ
            ATHOLD=DABS (THTOLD(J) )
            ATHNEW=DABS (THINNEW(J) )
            ATMOLD=DABS (TMPOLD(J) )
            ATMNEW=DABS (TMPNEW(J) )
            DELTH=DABS (ATHNEW-ATHOLD)
            DELTP=DABS (ATMNEW-ATMOLD)
            IF(DELTH.GE.TOLRN1) GO TO 50
            IF(DELTP.GE.TOLRN2) GO TO 50
46 CONTINUE
C
C CONVERGENCE HAS BEEN ACHIEVED.
C
        DO 56, J=1,NSLZP1
            THTOLD(J)=THTAS(J)
            TMPOLD(J)=TEMPS(J)
            THTAS(J)=THINNEW(J)
            TEMPS(J)=TMPNEW(J)
56 CONTINUE
C
        IF(NPRINT(13).EQ.1) GO TO 60
        WRITE(1,61) KITEST
61 FORMAT(1X, 'CONVERGENCE IN ',I2, ' LOOPS',/)
60 CONTINUE
C
        GO TO 200
C
50 KITEST=KITEST+1
        IF(KITEST.GE.61) GO TO 250
C
C UPDATE ITERATIVE FIELD VARIABLES.
C
        DO 66, J=1,NSLZP1
            THTOLD(J)=THINNEW(J)
            TMPOLD(J)=TMPNEW(J)
66 CONTINUE
C
        GO TO 100
C
250 WRITE(*,67)
67 FORMAT(5X, '*** WARNING: FAILURE TO CONVERGE IN 60 LOOPS ***',/)
C

```

```
200 CONTINUE
C
C SUB SECTION 3G: CALL TO SUBROUTINE MIXOXY.
C
      ITRIP=0
      TCH=0.0D0
C T1 IS USED TO CALCULATE THE ROOT LENGTH.
C T IS FOR LARGE STEP USING IN WATER AND HEAT
C T1 IS FOR SMALL STEP USING IN OXYGEN AND CARBON DIOXIDE
300 T1=T1+DT1
      CALL MIXOXY
C
C SUBSECTION 3H: CALL TO SUBROUTINE THOMAS.
C
      CALL MIXCBN
C
C UPDATE THE VARIABLES
C
      DO 350, J=1,NSLZP1+100 !FROM TOP CANOPY TO LOWER SOIL BND.
          CLDO2(J)=CO2(J)
          CLDCO2(J)=CCO2(J)
350 CONTINUE
C
C CHECK TIME FOR MATCHING THE TIME STEP FOR WATER AND HEAT (DT).
C IF THE TIME TCH SMALLER THAN DT, NEED ITERATION FOR O2 AND CO2.
C DTCH IS FOR AVOIDING MORE ITERATION.
      DTCH=DT - 0.01D0*DT1
      TCH=TCH+DT1
      ITRIP=ITRIP+1
      WRITE(*,600) ITRIP,T1
600 FORMAT(2X, ' ITRIP=',I2,' T1=',F10.6)
      IF(TCH .LE. DTCH) THEN
          GO TO 300
      ENDIF
      RETURN
      END
```

```

*MIXWATR                               Last Revision:  March 21, 1989
C                                       Source File:   OXYWATR.FOR
      SUBROUTINE MOISTR(KITEST)
C
C THIS SUBROUTINE SOLVES THE WATER FIELD EQUATION
      IMPLICIT DOUBLE PRECISION(A-H,O-Z)
      IMPLICIT INTEGER(I-N)
C
C $include: 'common.oed'
      INTEGER KITEST, J
      REAL*8 SMHEAT(NX), TTMP1, ARG3, DATCON, THTBAR, DTHLQB,
&  EMIHTB, RHOWVB, RELHMB, DTHVPB, DTPLQB, DTPVPB, XKONTB,
&  PPSIZB, DPSIZB, EPSB, COEF0, CON4, CON5, CON6
      common /local3/smheat, ttmpl, arg3, datcon, thtbar, dthlqb,
&  emthtb, rhowvb, relhmb, dthvpb, dtplqb, dtpvpb, xkontb,
&  ppsizb, dpsizb, epsb, coef0
C
      DOUBLE PRECISION RATIO1, ARG1, POWR1, COEF1,
&  ARG2, PART1, PART2, PART3, PART4, PART5
C
C
C
C MOST OF THE SYSTEM TRANSPORT AND TRANSFER COEFFICIENTS
C ARE CALCULATED IN THIS SECTION.  FOR EXAMPLE, THE
C WATER POTENTIAL FUNCTION, WATER CONDUCTIVITY,
C ETC.
C
C CALCULATE THE WATER POTENTIAL, CONDUCTIVITY, DIFFUSIVITY ETC.
C FUNCTIONS
C
C INITIALIZE THE PARAMETERS NEEDED FOR KOZENY FUNCTION
C
C CALCULATE THE DIHTZ FOR THE PPSIZ
C TOP BOUNDARY NODE.
C
      DIHTZ(1)=(THTOLD(2)-THTOLD(1))/DZ(1)
C
C MIDDLE NODES.
C
      DO 15, J=2,NSLZZZ
          CON4=-DZ(J)/(DZ(J-1)*(DZ(J-1)+DZ(J)))
          CON5=1.0D0/DZ(J-1)-1.0D0/DZ(J)
          CON6=DZ(J-1)/(DZ(J)*(DZ(J-1)+DZ(J)))
          DIHTZ(J)=CON4*THTOLD(J-1)+CON5*THTOLD(J)+CON6*THTOLD(J+1)
15 CONTINUE
C
C BOTTOM BOUNDARY NODE.
C

```

```

DIHTZ (NSLZP1)=(THTOLD(NSLZP1)-THTOLD(NSLZZZ))/DZ(NSLZZZ)
C
C
DO 20, J=1,NSLZP1
C
  IF (THTOLD(J) .LE. THTRES(J)) THEN
    PSI(J) = 1.D20
    PRINT *, 'OOPS CASE 1'
  ELSE IF (THTOLD(J) .GE. THTAST(J)) THEN
    PSI(J) = 0.D0
    THTOLD(J) = THTAST(J)
    PRINT *, 'OOPS CASE 2'
  ELSE
    RATIO1=(THTAST(J)-THIRES(J))/(THTOLD(J)-THIRES(J))
    ARG1=RATIO1**BETATH(J)
    PSI(J)= -ALPTH(J)*(ARG1-1.0D0)
  ENDIF
  POWR1=BETATH(J)-1.0D0
  COEF1=ALPTH(J)*BETATH(J)*(THTAST(J)-THIRES(J))
  COEF1=COEF1/((THTOLD(J)-THIRES(J))**2)
  PPSITH(J)=COEF1*RATIO1**POWR1
  IF (THTOLD(J) .LE. THTRES(J)) THEN
    KONHS(J) = 1.D-25
  ELSE IF (THTOLD(J) .GE. THTAST(J)) THEN
    KONHS(J) = KTHSTS(J)
  ELSE
    ARG2 = (1.0D0/RATIO1)**GAMCNS(J)
    KONHS(J) = ARG2*KTHSTS(J)
  ENDIF
C
  PART1=PPSITH(J)*DIHTZ(J)
  PART2=(1.0D0-(RATIO1)**BETATH(J))*DALPTZ(J)
  PART3=-ALPTH(J)*DLOG(RATIO1)*((RATIO1)**BETATH(J))*DBETAZ(J)
  PART4=-ALPTH(J)*BETATH(J)*((RATIO1)**BETATH(J))
  PART4=(PART4/(THTAST(J)-THIRES(J)))*DIHTSZ(J)
  PART5=(-ALPTH(J)*BETATH(J))/((THTOLD(J)-THIRES(J))**2)
  PART5=PART5*(RATIO1)**POWR1*DTHREZ(J)
  PPSIZ(J)=PART1+PART2+PART3+PART4+PART5
C
  TIMP1=IMPOLD(J)-273.0D0
  RHOWVX(J)=0.004928D0+0.0002581D0*TIMP1+0.0000183D0*TIMP1*TIMP1
  IF (IMPOLD(J) .GE. 295.5D0) RHOWVX(J)=RHOWVX(J)+0.0000213D0*(
&  IMPOLD(J)-295.5D0)*(IMPOLD(J)-295.5D0)
  RHOWVX(J)=RHOWVX(J)/1000.0D0
  ARG3=GRAV*PSI(J)/(R*IMPOLD(J))
C
  RELHUM(J)=DEXP(ARG3)
C

```

```

LVAP(J)=595.88D0-0.547D0*(TMPOLD(J)-273.0D0)
C
DTHLQS(J)=KONIHS(J)*PPSIH(J)
C
DTPLQS(J)=KONIHS(J)*GAMILI*PSI(J)
C
DATCON=DAIM*TORT(J)
DPSIZ(J)=DATCON*GRAV/(R*TMPOLD(J))
DTHVPS(J)=DPSIZ(J)*PPSIH(J)
C
DTPVPS(J)=ARG3*(GAMILI-1.D0/TMPOLD(J))
DTPVPS(J)=DTPVPS(J)+BETATV/RHOWWX(J)
DTPVPS(J)=DTPVPS(J)*DATCON
C
20 CONTINUE
C
C THE COEFFICIENT FUNCTIONS IN WATER EQUATION ARE DEFINED.
C
DO 30, J=1,NSLZP1
C
PMO(J)=RHOWAT+(EPS(J)-THTOLD(J))*RHOWWX(J)*RELHUM(J)/THTOLD(J)
30 CONTINUE
C
DO 31, J=1,NSLZZZ
C
THTBAR=(THTOLD(J+1)+THTOLD(J))/2.D0
DTHLQB=(DTHLQS(J+1)+DTHLQS(J))/2.D0
EMIHTB=((EPS(J+1)-THTOLD(J+1))+(EPS(J)-THTOLD(J)))/2.D0
RHOWVB=(RHOWWX(J+1)+RHOWWX(J))/2.D0
RELHMB=(RELHUM(J+1)+RELHUM(J))/2.D0
DTHVPB=(DTHVPS(J+1)+DTHVPS(J))/2.D0
DTPLQB=(DTPLQS(J+1)+DTPLQS(J))/2.D0
DTPVPB=(DTPVPS(J+1)+DTPVPS(J))/2.D0
XKONTB=(KONIHS(J+1)+KONIHS(J))/2.D0
PPSIZB=(PPSIZ(J+1)+PPSIZ(J))/2.D0
DPSIZB=(DPSIZ(J+1)+DPSIZ(J))/2.D0
EPSB=(EPS(J+1)+EPS(J))/2.D0
C
PM2(J)=RHOWAT*THTBAR*DTHLQB+EMIHTB*RHOWVB*RELHMB*DTHVPB
PM3(J)=RHOWAT*THTBAR*DTPLQB+EMIHTB*RHOWVB*RELHMB*DTPVPB
PM4(J)=RHOWAT*XKONTB*(1.D0-PPSIZB)+RHOWVB*RELHMB*DPSIZB*PPSIZB
PM5(J)=EPSB*RHOWVB*RELHMB*DPSIZB*PPSIZB
C
31 CONTINUE
C
DO 40, J=2,NSLZZZ
COEF0=2.D0*DT/(DZ(J)+DZ(J-1))
C

```

```

C      DEFINE MATRIX ELEMENTS FOR WATER AND HEAT MATRICES
C
      ADT1(J)=-COEF0*(PM2(J-1)/DZ(J-1)+PM4(J-1)/2.DO)
      ADT2(J)=PM0(J)+COEF0*(PM2(J-1)/DZ(J-1)+PM2(J)/DZ(J)+ PM4(J)/2.
&      DO-PM4(J-1)/2.DO)
      ADT3(J)=-COEF0*(PM2(J)/DZ(J)-PM4(J)/2.DO)
      DTB1M2(J)=-COEF0*PM3(J-1)/DZ(J-1)
      DTB2M2(J)=COEF0*(PM3(J-1)/DZ(J-1)+PM3(J)/DZ(J))
      DTB3M2(J)=-COEF0*PM3(J)/DZ(J)
C
40 CONTINUE
C
C      CALCULATE THE "KNOWN" VECTORS
C
      IF (KITEST.EQ.0) THEN
        DO 60, J=2,NSLZZZ
          SUMAM1(J)=THTAS(J)*RHOWAT+(EPS(J)-THTAS(J))*RHOWVX(J)*
&          RELHUM(J)
60      CONTINUE
      ENDIF
C
C      SUM THE CONTRIBUTIONS FROM THE HEAT FIELD TERMS FOR ALL J.
C
      DO 70, J=2,NSLZZZ
        SMHEAT(J)=DTB1M2(J)*IMPOLD(J-1) +DTB2M2(J)*IMPOLD(J)+DTB3M2(J)*
&        IMPOLD(J+1)
70 CONTINUE
C
C CALCULATE THE TOP AND BOTTOM VECTORS
C TOP NODE
C
      COEF0=2.DO*DT/(DZ(1)+DZ(2))
      YTH(2)=SUMAM1(2)-SMHEAT(2)-ADT1(2)*THTOLD(1)
&      -COEF0*(PM5(1)-PM5(2))
C BOTTOM NODE
      COEF0=2.DO*DT/(DZ(NSLZM1)+DZ(NSLZZZ))
      YTH(NSLZZZ)=SUMAM1(NSLZZZ)-SMHEAT(NSLZZZ)
&      -ADT3(NSLZZZ)*THTOLD(NSLZP1)
&      -COEF0*(PM5(NSLZM1)-PM5(NSLZZZ))
C
      DO 90, J=3,NSLZM1
C
C CALCULATE THE MIDDLE VECTORS
C
      COEF0=2.DO*DT/(DZ(J-1)+DZ(J))
      YTH(J)=SUMAM1(J)-SMHEAT(J) -COEF0*(PM5(J-1)-PM5(J))
C
90 CONTINUE

```

C

RETURN  
END

```

*MIXHEAT                               Last Revision: August 21, 1990
C                                       Source File:   MIXHEAT.FOR
      SUBROUTINE HEAT(KITEST)
C THIS SUBROUTIN SOLVES THE HEAT FIELD EQUATIONS
      IMPLICIT NONE
C
$include:'common.ooc'
      INTEGER KITEST, J
      DOUBLE PRECISION LAMWAB,LAMAIB,LVAPB,LAMSOB
      DOUBLE PRECISION SMMOIS(NX)
      DOUBLE PRECISION TTTIMP, EMIHT, THTBAR, TMPBAR, DTHLQB,
& EMIHTB, RHOWVB, RELHMB, DTHVPB, DTPLQB, DTPVPB,
& XKONTB, PPSIZB, DPSIZB, EPSB, FACTOB, COEF0
      DOUBLE PRECISION AVE, DUM1, DUM2, HALF
      PARAMETER (HALF = 0.5D0)
      common /local4/ tttimp, emtht, thtbar, tmpbar, dthlqb,
& emthtb, rhowvb, relhmb, dthvpb, dtplqb, dtpvpb,
& xkontb, ppsizb, dpsizb, epsb, factob, coef0
C
C..The following is a STATEMENT FUNCTION . . .
C
      AVE(DUM1, DUM2) = HALF * (DUM1 + DUM2)
C
C CALCULATE THE CORRECTION FACTOR,LAMWAT,LAMAIR
C
      DO 400, J=1, NSLZP1
      IF (THTOLD(J) .EQ. 0) THEN
          FACTOR(J) = 1.0D0
      ELSE IF ((THTOLD(J)-0.2868D0) .LT. 0) THEN
          FACTOR(J)=1.1325D0-4.62304D0*THTOLD(J) +
& 47.5762D0*THTOLD(J)**2
      ELSE
          FACTOR(J)=1.1325D0-4.62304D0*THTOLD(J) +
& 47.5762D0*THTOLD(J)**2 - 20.0921D0*(THTOLD(J)-0.2868D0)-
& 47.4759D0*(THTOLD(J)-0.2868D0)**2
      ENDIF
C
      TTTIMP = TMPOLD(J)-273.0D0
      LAMWAT(J) = (1.32D0+5.59D0*0.001D0*TTTIMP-
& 2.63D0*0.00001D0*TTTIMP**2)*3.6D0
      LAMAIR(J)=(0.0566D0+0.000153D0*TTTIMP)*3.6D0
400 CONTINUE
C
C THE COEFFICIENT FUNCTIONS ARE DEFINED.
C
      DO 30, J=1,NSLZP1
C
      EMIHT=EPS(J)-THTOLD(J)

```

```

      PH0(J)=(1.D0-EPS(J))*SHTSOL(J)*RHOSOL(J) +
&      EMIHT*SHTAIR*RHOAIR+THTOLD(J)*SHIWAT*RHOWAT
C
      30 CONTINUE
C..Most of the following are averaged by function AVE . . .
      DO 31, J = 1, NSLZZZ
C
      THTBAR = AVE(THTOLD(J+1),THTOLD(J))
      TMPBAR = AVE(TMPOLD(J+1),TMPOLD(J))
      DTHLQB = AVE(DTHLQS(J+1),DTHLQS(J))
      EMIHTB = AVE((EPS(J+1)-THTOLD(J+1)), (EPS(J)-THTOLD(J)))
      RHOWVB = AVE(RHOWVX(J+1),RHOWVX(J))
      RELHMB = AVE(RELHUM(J+1),RELHUM(J))
      DIHVPS = AVE(DIHVPS(J+1),DIHVPS(J))
      DTPLQB = AVE(DTPLQS(J+1),DTPLQS(J))
      DTPVPB = AVE(DTPVPS(J+1),DTPVPS(J))
      XKONTB = AVE(KONTHS(J+1),KONTHS(J))
      PPSIZB = AVE(PPSIZ(J+1),PPSIZ(J))
      DPSIZB = AVE(DPSIZ(J+1),DPSIZ(J))
      EPSB   = AVE(EPS(J+1),EPS(J))
      LVAPB  = AVE(LVAP(J+1),LVAP(J))
      LAMSOB = AVE(LAMSOL(J+1),LAMSOL(J))
      FACTOB = AVE(FACTOR(J+1),FACTOR(J))
      LAMWAB = AVE(LAMWAT(J+1),LAMWAT(J))
      LAMAIB = AVE(LAMAIR(J+1),LAMAIR(J))
C
      PH2(J)=THTBAR*SHIWAT*RHOWAT*TMPBAR*DTHLQB +
&      EMIHTB*RHOWVB*RELHMB*LVAPB*DIHVPS
      PH3(J)=(1.D0-EPSB)*LAMSOB*FACTOB+THTBAR*(LAMWAB+SHIWAT*RHOWAT
&      *TMPBAR*DTPLQB)+EMIHTB*(LAMAIB+RHOWVB*RELHMB*LVAPB*DTPVPB)
      PH4(J)=SHIWAT*RHOWAT*THTBAR*(1.D0-PPSIZB)*XKONTB
      PH5(J)=EMIHTB*RHOWVB*RELHMB*LVAPB*PPSIZB*DPSIZB
      31 CONTINUE
C
      DO 40, J=2,NSLZZZ
      COEF0 = 2.D0*DT / (DZ(J-1)+DZ(J))
C
C      DEFINE MATRIX ELEMENTS FOR WATER AND HEAT MATRICES
C
      ADT1(J) = -COEF0*(PH3(J-1)/DZ(J-1)+PH4(J-1)/2.D0)
      ADT2(J) =  PH0(J)+COEF0*(PH3(J-1)/DZ(J-1)+PH3(J)/DZ(J) +
&      PH4(J)/2.D0-PH4(J-1)/2.D0)
      ADT3(J)  = -COEF0*(PH3(J)/DZ(J)-PH4(J)/2.D0)
      DTB1H1(J) = -COEF0*PH2(J-1)/DZ(J-1)
      DTB2H1(J) =  COEF0*(PH2(J-1)/DZ(J-1)+PH2(J)/DZ(J))
      DTB3H1(J) = -COEF0*PH2(J)/DZ(J)
C
      40 CONTINUE

```

```

C
C CALCULATE THE "KNOWN" VECTORS.
C
  IF (KITEST.EQ.0) THEN
    DO 60, J=2,NSLZZZ
      SUMAH1(J)=( (1.DO-EPS(J)) *SHTSOL(J) *RHOSOL(J)+SHTAIR*RHOAIR
&      *(EPS(J)-IHTAS(J))+RHOWAT*SHTWAT*IHTAS(J) ) *TEMPS(J)
60  CONTINUE
    ENDIF
C
C SUM THE CONTRIBUTIONS FROM THE WATER FIELD TERMS FOR ALL J.
C
  DO 70, J=2,NSLZZZ
    SMMOIS(J) = DTB1H1(J) *THINEW(J-1) +
&    DTB2H1(J) *THINEW(J)+DTB3H1(J) *THINEW(J+1)
70 CONTINUE
C
C CALCULATE THE TOP AND BOTTOM VECTORS
C TOP NODE
  COEFO = 2.DO*DT/(DZ(1)+DZ(2))
  YTP(2) = SUMAH1(2)-SMMOIS(2)-ADT1(2) *IMPOLD(1)
&  -COEFO*(PH5(1)-PH5(2))
C BOTTOM NODE
  COEFO = 2.DO*DT/(DZ(NSLZM1)+DZ(NSLZZZ))
  YTP(NSLZZZ) = SUMAH1(NSLZZZ)-SMMOIS(NSLZZZ)
&  -ADT3(NSLZZZ) *IMPOLD(NSLZP1)
&  -COEFO*(PH5(NSLZM1)-PH5(NSLZZZ))
C
  DO 90, J=3,NSLZM1
C
C CALCULATE THE MIDDLE VETORS
C
  COEFO = 2.DO*DT / (DZ(J-1)+DZ(J))
  YTP(J) = SUMAH1(J)-SMMOIS(J) -COEFO*(PH5(J-1)-PH5(J))
C
90 CONTINUE
C
  RETURN
  END

```

```

*THOMAS                               Last Revision:  March 21, 1989
C                                       Source File:   OXYTHOM.FOR
      SUBROUTINE THOMAS
C
C 3-POINT COMPUTATIONAL MOLECULE FOR THE TRIDIAGONAL SYSTEM.
C
      IMPLICIT DOUBLE PRECISION(A-H,O-Z)
      IMPLICIT INTEGER(I-N)
C
C $include: 'common.ocd'
      INTEGER  J, NSLZM2
      DOUBLE PRECISION CTEMP(NX), DTEMP(NX), DENOM
      common /local6/  ctemp, dtemp, denom
C
      CTEMP(2)=ADT3(2)/ADT2(2)
      DTEMP(2)=YDUM(2)/ADT2(2)
      DO 10, J=3,NSLZZZ
          DENOM=ADT2(J)-ADT1(J)*CTEMP(J-1)
          CTEMP(J)=ADT3(J)/DENOM
          DTEMP(J)=(YDUM(J)-ADT1(J)*DTEMP(J-1))/DENOM
10 CONTINUE
C
      XDUM(NSLZZZ)=DTEMP(NSLZZZ)
C
      NSLZM2=NSLZM1-1
C
      DO 20, J=1,NSLZM2
          XDUM(NSLZZZ-J)=DTEMP(NSLZZZ-J)-CTEMP(NSLZZZ-J)*XDUM(NSLZP1-J)
20 CONTINUE
C
      RETURN
      END

```

```

*MIXBNDY                               Last Revision: August 21, 1990
C                                       Source File:   MIXBNDY.FOR
      SUBROUTINE BOUNDRY
C THIS SUBROUTINE SIMULATES THE AIR-SOIL SURFACE INTERFACE DYNAMIC
C BOUNDARY CONDITIONS ON THE HEAT AND WATER FIELDS
      IMPLICIT NONE
C
C$include: 'common.ooc'
      INTEGER K
      DOUBLE PRECISION LAMAX,LAMIN
      DOUBLE PRECISION GXYZ1, GXYZ2
      DIMENSION GXYZ1(3),GXYZ2(3)
      DOUBLE PRECISION T0OLD, TH0OLD, T0OLD0, TH0LD0, DTH0, DTO0,
& OODXTH, OODXT0, CON2, DWVMAX, CON5, CON51, CON52, ARGW0,
& TTEMPA, DROWV0, DATCON, CON0, CON00, CON1, GRDTH0, GRADT0,
& GRADTA, GRADH0, CON3, CON4, CON7, CON8, CON10, CON11, CON12,
& DROVSA, DSTAIR, VAPRES, GP1TH0, GP1T0, GP2TH0, GP2T0,
& XNUMTH, XNUMT0, DENOM, QUOTTH, QUOTT0
      common /local5/ t0old, th0old, t0old0, th0ld0, dth0, dto0,
& oodxth, oodxt0, con2, dwvmax, con5, con51, con52, argw0,
& ttempa, drowv0, datcon, con0, con00, con1, grdth0, gradt0,
& gradta, gradh0, con3, con4, con7, con8, con10, con11, con12,
& drovsa, dstair, vapres, gp1th0, gp1t0, gp2th0, gp2t0,
& xnumth, xnumt0, denom, quotth, quott0
C
      DOUBLE PRECISION RATIO0, ARG0, POWR0, COEF0,
& PART1, PART2, PART3, PART4, PART5, ARG30
C
C
C INITIALIZATION
C
      T0OLD = TMPNEW(1)
      TH0OLD = THINew(1)
      T0OLD0 = T0OLD
      TH0LD0 = TH0OLD
C
      DTH0 = 0.0001D0
      DTO0 = 0.001D0
      OODXTH = 1.D0/DTH0
      OODXT0 = 1.D0/DTO0
C
      CON2 = DEXP(-BETAVA*WS)
      DWVMAX = DWVAR(2)
      CON2 = DAIM*DWVMAX/(DAIM+(DWVMAX-DAIM)*CON2)
C
      LAMAX = LAMAIR(1)
      LAMIN = LAMAIR(1)
      CON5 = DEXP(-LAMBHT*WS)

```

```

CON51 = LAMIN*LAMAX
CON52 = LAMIN+(LAMAX-LAMIN)*CON5
CON5  = CON51/CON52
C
C BEGIN VARIABLE UPDATE LOOP.
      C
DO 70, K = 1, 3
  IF      (K .EQ. 1) THEN
  ELSE IF (K .EQ. 2) THEN
    THOOLD = THOLDO+DIHO
    TOOLD  = TOOLDO
  ELSE IF (K .EQ. 3) THEN
    THOOLD = THOLDO
    TOOLD  = TOOLDO+DTOO
  ELSE
    PRINT *, 'Illegal K in IF'
    STOP 72
  ENDIF
  LVAP(1) = 595.88D0-0.547D0*(TOOLD-273.0D0)
C
C INITIALIZE THE KOZENY FUNCTION PARAMERS, ETC.
C
      DIHTZ(1) = (THINNEW(2)-THOOLD)/DZ(1)
C
  IF (THOOLD .LE. THITRES(1)) THEN
    PSI(1) = 1.D20
    PRINT *, 'OOPS CASE 1 (BNDY) '
  ELSE IF (THOOLD .GE. THITAST(1)) THEN
    PSI(1) = 0.D0
    THOOLD = THITAST(1)
    PRINT *, 'OOPS CASE 2 (BNDY) '
  ELSE
    RATIO0 = (THITAST(1)-THITRES(1))/(THOOLD-THITRES(1))
    ARG0   = RATIO0**BETATH(1)
    PSI(1) = -ALPTH(1)*(ARG0-1.0D0)
  ENDIF
  POWRO = BETATH(1)-1.0D0
  COEFO = ALPTH(1)*BETATH(1)*(THITAST(1)-THITRES(1))
  COEFO = COEFO/((THOOLD-THITRES(1))**2)
  PPSITH(1) = COEFO*RATIO0**POWRO
  IF (THOOLD .LE. THITRES(1)) THEN
    KONTHS(1) = 1.D-25
  ELSE IF (THOOLD .GE. THITAST(1)) THEN
    KONTHS(1) = KIHSTS(1)
  ELSE
    ARG30 = (1.0D0/RATIO0)**GAMCNS(1)
    KONTHS(1) = ARG30*KIHSTS(1)
  ENDIF

```

```

C
PART1 = PPSITH(1)*DIHTZ(1)
PART2 = (1.0D0-(RATIO0)**BETATH(1))*DALPTZ(1)
PART3 = -ALPTH(1)*DLOG(RATIO0)*((RATIO0)**BETATH(1))*DBETAZ(1)
PART4 = -ALPTH(1)*BETATH(1)*((RATIO0)**BETATH(1))
PART4 = (PART4/(THTAST(1)-THIRES(1)))*DIHTSZ(1)
PART5 = (-ALPTH(1)*BETATH(1))/((THOOLD-THIRES(1))**2)
PART5 = PART5*(RATIO0)**POWR0*DIHREZ(1)
PPSIZ(1) = PART1+PART2+PART3+PART4+PART5

C
C
ARGW0 = (PSI(1)*GRAV)/(R*TOOLD)
RELHUM(1) = DEXP(ARGW0)
DPSIZ(1) = DATM*TORT(1)*GRAV/(R*TOOLD)

C
TTEMPA = TOOLD-273.0D0
RHOWVX(1) = 0.004928D0+0.0002581D0*TTEMPA +
& 0.0000183D0*TTEMPA*TTEMPA
IF (TOOLD .GE. 295.5D0) RHOWVX(1) = RHOWVX(1) +
& 0.0000213D0*(TOOLD-295.5D0)**2
RHOWVX(1) = RHOWVX(1)/1000.0D0

C
DROWVO = 0.0002581D0+0.0000366D0*TTEMPA
IF (TOOLD .GT. 295.5D0) DROWVO= DROWVO +
& 0.0000426D0*(TOOLD-295.5D0)
DROWVO = DROWVO/1000.0D0

C
DIHLQS(1) = KONIHS(1)*PPSITH(1)
DATCON = DATM*TORT(1)
DIHVPS(1) = DATCON*GRAV*PPSITH(1)/(R*TOOLD)
DIPLQS(1) = KONIHS(1)*GAMILI*PSI(1)
DIPVPS(1) = ARGW0*(GAMILI-1.0D0/TOOLD)
DIPVPS(1) = DIPVPS(1)+DROWVO/RHOWVX(1)
DIPVPS(1) = DIPVPS(1)*DATCON
CON0 = SHIWAT*TOOLD
CON00 = SHIWAT*TPWATI
CON1 = RHOWAT*THOOLD
GRDIHO = (THINEW(2)-THOOLD)/DZ(1)
GRADTO = (TMPNEW(2)-TOOLD)/DZ(1)
GRADTA = (TOOLD-TEMPA)/DELTAZ
GRADHO = (RELHUM(1)-HTTAA)/DELTAZ
CON3 = (EPS(1)-THOOLD)*RHOWVX(1)*RELHUM(1)
CON4 = EMSSOI*(1.0D0-EPS(1))+EMSWAT*THOOLD +
& EMSAIR*(EPS(1)-THOOLD)
CON4 = CON4*SIGMA*TOOLD**4
CON7 = ALBSOI*(1.0D0-EPS(1))+THOOLD*ALBWAT +
& ALBAIR*(EPS(1)-THOOLD)
CON7 = (1.0D0-CON7)*QSR(1)

```

```

CON8 = KONTHS(1)*(1.D0-PPSIZ(1))
C
IF (THOOLD .EQ. 0.D0) THEN
  FACTOR(1) = 1.0D0
ELSE IF ((THOOLD-0.2868D0) .LT. 0) THEN
  FACTOR(1) = 1.1325D0-4.62304D0*THOOLD+47.5762D0*THOOLD**2
ELSE
  FACTOR(1) = 1.1325D0-4.62304D0*THOOLD+47.5762D0*THOOLD**2 -
&    20.0921D0*(THOOLD-0.2868D0)-47.4759D0*(THOOLD-0.2868D0)**2
ENDIF
LAMWAT(1) = (1.32D0+5.59D0*0.001D0*(T0OLD-273.0D0) -
&    2.63D0*0.00001D0 *(T0OLD-273.0D0)**2)*3.6D0
LAMAIR(1) = (0.0566D0+0.000153D0*(T0OLD-273.0D0))*3.6D0
CON10 = (1.D0-EPS(1))*LAMSOL(1)*FACTOR(1)
CON11 = THOOLD*(LAMWAT(1)+CON0*RHOWAT*DTPLQS(1))
CON12 = (EPS(1)-THOOLD)*LAMAIR(1)+CON3*LVAP(1)*DTPVPS(1)
C
TTEMPA = TEMPA-273.0D0
RHOVSA = 0.004928D0 + 0.0002581D0*TTEMPA +
&    0.0000183D0*TTEMPA*TTEMPA
IF (TEMPA .GE. 295.5D0) RHOVSA = RHOVSA +
&    0.0000213D0*(TEMPA-295.5D0)**2
RHOVSA = RHOVSA/1000.0D0
C
DROVSA = .0002581D0+.0000366D0*TTEMPA
IF (TEMPA .GE. 295.5D0) DROVSA = DROVSA +
&    .0000426D0*(TEMPA-295.5D0)
DROVSA = DROVSA/1000.0D0
C
QEVAPE = -CON2*(DROVSA*THTAA*GRADTA+RHOVSA*GRADH0)
QHTSSL = -CON5*GRADTA
QHTESL = LVAP(1)*QEVAPE
C
ESTAIR = 4.66894D0+0.24594D0*(TEMPA-273.0D0) +
&    0.02764D0*(TEMPA-273.0D0)**2
IF (TEMPA .GE. 295.5D0) ESTAIR = ESTAIR +
&    0.02018D0*(TEMPA-295.5D0)**2
C
DSTAIR = 0.24594D0+0.05528D0*TTEMPA
IF (TEMPA .GE. 295.5D0) DSTAIR = DSTAIR +
&    0.04036D0*(TEMPA-295.5D0)
C
VAPRES = SIGMA*EMSAIR*(.605D0+.048D0*DSQRT(ESTAIR))
C
GXYZ1(K) = (CON1*CON0*DTHLQS(1) + CON3*LVAP(1)*DTHVPS(1)) *
&    (-GRDTH0)+CON1*CON0*CON8
GXYZ1(K) = GXYZ1(K)+CON3*LVAP(1)*DPSIZ(1)*(-PPSIZ(1))
GXYZ1(K) = GXYZ1(K)+(CON10+CON11+CON12)*(-GRADT0)

```

```

GXYZ1(K) = GXYZ1(K) -RHOWAT*CON00*INFLTR
GXYZ1(K) = GXYZ1(K) -QHTESL-QHTSSL-CON7+ CON4-VAPRES*TEMPA**4
C
GXYZ2(K) = (CON1*DTHLQS(1)+CON3*DTHVPS(1)) * (-GRDTH0)+CON1*CON8
GXYZ2(K)=GXYZ2(K) -CON3*DPSIZ(1)*PPSIZ(1) +
&      (CON1*DTPLOS(1)+CON3*DTPVPS(1)) * (-GRADT0)
C
C PRINT THE SOIL SURFACE INFILTRATION RATE
C
      IF (K .EQ. 3) THEN
          SINFL=GXYZ2(K)
      ENDIF
C
      GXYZ2(K) = GXYZ2(K) -RHOWAT*INFLTR-QEVAP
C
70 CONTINUE
C
      TH0OLD = TH0LD0
      T0OLD  = T0OLD0
C
      GP1TH0 = OODXTH*(GXYZ1(2)-GXYZ1(1))
      GP1T0  = OODXT0*(GXYZ1(3)-GXYZ1(1))
C
      GP2TH0 = OODXTH*(GXYZ2(2)-GXYZ2(1))
      GP2T0  = OODXT0*(GXYZ2(3)-GXYZ2(1))
C
      XNUMTH = -GXYZ1(1)*GP2T0+GXYZ2(1)*GP1T0
      XNUMT0 = -GXYZ2(1)*GP1TH0+GXYZ1(1)*GP2TH0
C
      DENOM  = GP1TH0*GP2T0-GP1T0*GP2TH0
C
      QUOTTH = XNUMTH/DENOM
      QUOTT0 = XNUMT0/DENOM
C
200 FORMAT(5X,10(1X,E10.4))
      IF (NPRINT(11) .NE. 1) THEN
          WRITE(1,200) TH0OLD,T0OLD,GXYZ1(1),GXYZ2(1),GP1TH0,GP1T0,
&      GP2TH0,GP2T0
          WRITE(1,200) XNUMTH,XNUMT0,DENOM,QUOTTH,QUOTT0
      ENDIF
C
300 TMPNEW(1) = TMPNEW(1) + QUOTT0
      THNEW(1)  = THNEW(1)  + QUOTTH
C
      TMPOLD(1) = T0OLD
      THTOLD(1) = TH0OLD
C
      GRADTA = (TMPNEW(1)-TEMPA)/DELTAZ

```

```

QEVAP = -CON2*(DROVSA*THATA*GRADTA+RHOVSA*GRADH0)
QHTSSL = -CON5*GRADTA
QHTESL = LVAP(1)*QEVAP

```

C

C SET UP SOME HEAT FLUX PARAMETERS FOR PRINT OUT

C

```

QHRAIN = RHOWAT*SHIWAT*(TPWATI-273.0D0)*INFLTR
QHSWR = ALBSOI*(1.0D0-EPS(1)) + THINEW(1)*ALBWAT +
& ALBAIR*(EPS(1)-THINEW(1))
QHSWR = (1.0D0 - QHSWR)*QSR(1)
QHLWRO = EMSSOI*(1.0D0-EPS(1))+ EMSWAT*THINEW(1) +
& EMSAIR*(EPS(1)-THINEW(1))
QHLWRO = -QHLWRO*SIGMA*(TMPNEW(1)-273.0D0)**4
QHLWRI = SIGMA*EMSAIR*(.605D0+.048D0*DSQRT(ESTAIR))
QHLWRI = QHLWRI*(TEMPA-273.0D0)**4
HNET = QHRAIN+QHSWR+QHLWRO+QHLWRI+QHTSSL+QHTESL
RETURN
END

```



```

      DZA(JJ)=DZ(J)
      ANODE(JJ)=ZNODE(J)
500 CONTINUE
      DO 10, J=1,NUNODE
C
C CALCULATE OXYGEN AND CARBON DIOXIDE DIFFUSION COEFFICIENTS WHICH
C ARE FUNCTIONS OF TEMP. AND WATER CONTENT
C 1. DIFFUSION COEFF. WITHIN THE PLANT CANNOPY. J=101 IS AT SOIL
C SURFACE
      IF (J .LT. 101) THEN
          DO2(J)=DO20*(TMPAIN/273.0D0)**1.75D0
          DCO2(J)=DCO20*(TMPAIN/273.0D0)**2
      ELSE IF (J .GE. 101) THEN
C 2. DIFFUSION COEFF. IN SOIL
          DO2(J)=DO20*(QMPOLD(J)/273.0D0)**1.75D0
          DO2(J)=DO2(J)*((1.0D0-QHTOLD(J)/QEPS(J))**2) *(QEPS(J)-
& QHTOLD(J))**(2*0.7D0)
C
          DCO2(J)=DCO20*(QMPOLD(J)/273.0D0)**2
          DCO2(J)=DCO2(J)*((1.0D0-QHTOLD(J)/QEPS(J))**2) *(QEPS(J)-
& QHTOLD(J))**(2*0.7D0)
          ENDIF
10 CONTINUE
C
C CALCULATE BIOLOGICAL ACTIVITIES WITHIN PLANT CANOPY AND THROUGH SOIL
C 1. WITHIN PLANT CANOPY
C CHECK THE DAY TIME
      NDAY=INT(T)/24
      TDAY=T-24.D0*NDAY
      DO 400, J=1, 80
          PHO2(J)=0.D0
          RESO2(J)=0.D0
          IF((TDAY .GE. 6.D0) .AND. (TDAY .LE. 18.D0)) THEN
              PHO2(J)=0.7273D0*PHCO2(J)
          ENDIF
          RESO2(J)=0.7273D0*RESCO2(J)
400 CONTINUE
C 2. CALCULATE ROOT LENGTH
      IF(T .EQ. 0D0) THEN
          PRTLNG=5.D0
      ENDIF
C ROOT GROWTH RATE IS FUNCTION OF TIME AND CO2 CONC. AT ROOT TIP
      URTLNG=0.4D0*DT1
C a. PLUS 2 BELOW IS DUE TO LAYER NUMBER NOT EQUAL TO DEPTH
      ITIP=NINT(PRTLNG)+102
C b. FRACTION OF ROOT GROWTH RATE AS FUNCTION OF ROOT TIP CO2 CON.
      FACT1=1.0D0/(1.0D0+200.D0*EXP(0.2*(CLDCO2(ITIP)-50.D0)))
      RTLENG=URTLNG*FACT1 + PRTLNG

```

```

      PRTLNG=RTLENG
      CSINK=0.0D0
      DO 20, J=101, NUNODE
C   CALCULATE SINK RATE OF OXYGEN BY ROOTS
      SRT(J) = 0.D0
C   CHECK ROOT LENGTH TO MATCH WITH THE NODE POSITION
      IF((RTLENG .GE. ANODE(J)) .OR. (ABS(ANODE(J)-RTLENG) .LE. 0.
&     5D0)) THEN
      SRT(J)=10.0D0/(1.0D0+2000.D0*EXP(0.3*(CLDCO2(J)-50.D0)))
C   FRACTION OF GROWTH RATE AS FUNCTION OF DISTANCE FROM TIP
      RNODE(J)=ABS(RTLENG - ANODE(J))
      FACT2=0.9D0*EXP(-0.15*RNODE(J))+0.1D0
      SRT(J)=SRT(J)*FACT2
      ENDIF
C
C   CALCULATE SINK RATE OF OXYGEN BY MICROORGANISMS
C
      SMO(J) = 0.D0
      IF(ANODE(J) .LE. 20.04D0) THEN
      GMASIN=1.4D0
      U0=0.18D0
      EMC=1.4D-4
      SBSTRA=2.0D0
      CKSB=120.0D0
      CKO=150.0D0
      A0=0.042D0
      SKO=0.77D0
      DIVID1=SBSTRA/(CKSB+SBSTRA)
      DIVID2=CLDO2(J)/(CKO+CLDO2(J))
      SMO(J)=GMASIN*U0*EMC*DIVID1*DIVID2+A0*SKO*EMC*DIVID2
C
C   CONVERT UG /COLONY HR TO UG/CM3 SOIL AIR HR
C
      SMO(J)=1.002D5*SMO(J)
      ENDIF
C
C   USE Q10 VALUE OF 2 FOR TEMPERATURE CHANGE (25oC IS REFERENCE)
C   Q10=2 MEANS DECREASE 10oC REDUCED 50% OF RESPIRATION
C
      GSINK(J)=SRT(J)+SMO(J)
CCC     IF(QMPOLD(J) .EQ. 298.0D0) THEN
      TSINK(J)=GSINK(J)
CCC     ELSE IF (QMPOLD(J) .LT. 298.0D0) THEN
CCC       TSINK(J)=GSINK(J)-GSINK(J)*(298.0D0-QMPOLD(J))*0.05D0
CCC     ELSE IF (QMPOLD(J) .GT. 298.0D0) THEN
CCC       TSINK(J)=GSINK(J)+GSINK(J)*(QMPOLD(J)-298.0D0)*0.05D0
CCC     ENDIF
C

```

```

C CSINK IS CUMULATIVE SINK FOR PRINT OUT
C
      CSINK=CSINK+TSINK(J)
C
      SINK(J)=DT1*TSINK(J)
C
20 CONTINUE
C
C CALCULATE ALL COEFFICIENTS AND CONCENTRATION
C
C TOP NODE IS CHANGING WITH TIME.
C
      CO2(1)=300.D0
C
C INTERIOR NODE
      DO 30, J=2,NUNODE-1
        IF(J .LT. 101) THEN
          COEFF1=1.0
          COEFF3=1.0
          PC1=1.D0
          BPC1=1.D0
          REPLE(J)=0.D0
        ELSE IF (J .GE. 101) THEN
          REPLE(J)=(QHTAS(J)-QHTOLD(J))/DT1
          COEFF1=(QEPS(J)-QHTAS(J))+QHTAS(J)*HO2+(1.D0-QEPS(J))*
& OMIGO2
          COEFF3=(QEPS(J)-QHTOLD(J))+QHTOLD(J)*HO2+(1.D0-QEPS(J))*
& OMIGO2
          PC1=((QEPS(J+1)-QHTOLD(J+1))+QEPS(J)-QHTOLD(J))*0.5D0
          BPC1=((QEPS(J)-QHTOLD(J))+QEPS(J-1)-QHTOLD(J-1))*0.5D0
        ENDIF
        COEFF2=2.0D0*DT1/(DZA(J-1)+DZA(J))
        CON4=(CLDO2(J+1)-CLDO2(J))/DZA(J)
        BCON4=(CLDO2(J)-CLDO2(J-1))/DZA(J-1)
        DC1=(DO2(J+1)+DO2(J))*0.5D0
        CON1=LOG(FUGO2(J+1))-LOG(FUGO2(J))
        CON2=CLDO2(J+1)-CLDO2(J)
        CON3=(CLDO2(J+1)+CLDO2(J))*0.5D0
        BDC1=(DO2(J)+DO2(J-1))*0.5D0
        BCON1=LOG(FUGO2(J))-LOG(FUGO2(J-1))
        BCON2=CLDO2(J)-CLDO2(J-1)
        BCON3=(CLDO2(J)+CLDO2(J-1))*0.5D0
C
C CALCULATE THE CONCENTRATION
C
      IF (CON2 .EQ. 0.0D0) THEN
        FTERM1=1.0D0
      ELSE

```

```

      FTERM1=CON3*(CON1/CON2)+1.0D0
    ENDIF
    FTERM2=PC1*DC1*FTERM1*CON4
    IF (BCON2 .EQ. 0.0D0) THEN
      STERM1=1.0D0
    ELSE
      STERM1=BCON3*(BCON1/BCON2)+1.0D0
    ENDIF
    STERM2=BPC1*BDC1*STERM1*BCON4
  C
    IF( J .LT. 101) THEN
      IF((TDAY .GE. 6.D0) .AND. (TDAY .LE. 18.D0)) THEN
        CO2(J) = (1.0D0/COEFF1)*(COEFF3*CLD02(J) + COEFF2*(
&      FTERM2-STERM2) + PHO2(J)*DT1 - RESO2(J)*DT1)
      ELSE IF((TDAY .LT. 6.D0) .OR. (TDAY .GT. 18.D0)) THEN
        CO2(J) = (1.0D0/COEFF1)*(COEFF3*CLD02(J) + COEFF2*(
&      FTERM2-STERM2) - RESO2(J)*DT1)
      ENDIF
      ELSE IF(J .GE. 101) THEN
        CO2(J) = (1.0D0/COEFF1)*(COEFF3*CLD02(J) + COEFF2*(FTERM2-
&      STERM2) - SINK(J) - DT1*REPLE(J)*CLD02(J))
      ENDIF
    30 CONTINUE
  C
  C BOTTOM NODE
  C SECOND TYPE BOUNDARY CONDITION IS USED FOR CLD02(NSLZP1)
  C NO DIFFUSION OCCURS AT THIS BOUNDARY LAYER.
  C
    CLD02(NSLZP1)=CLD02(NSLZZZ)
  C
    RETURN
  END

```

```

*MIXCBN
C
SUBROUTINE MIXCBN
C
C THIS SUBROUTIN SOLVES CO2 TRANSPORT THROUGH SOIL FOR CARBON DIOXIDE
C SPECIES. THE EXPLICITT METHOD HAS BEEN USED. A SECOND TYPE
C BOUNDARY CONDITION IS USED FOR BOTTOM BOUNDARY CONDITION
C
IMPLICIT NONE
C
$include:'common.oocd'
INTEGER J, JJ, NUNODE, NDAY
DOUBLE PRECISION
& COEFF1, COEFF2, COEFF3, PC1, DC1, CON1, CON2,
& CON3, CON4, BPC1, BDC1,
& BCON1, BCON2, BCON3, BCON4,
& FTERM1, FTERM2, STERM1, STERM2, DZA, TDAY,
& QHTAS, QHTOLD, QMPOLD, QEPS, FUGCO2, FACT6, FACT7
DIMENSION QHTAS(253), QHTOLD(253),
& QEPS(253), FUGCO2(253), QMPOLD(253), DZA(253)
C
NUNODE = NSLZP1+100
IF (T .EQ. 0.D0) THEN
DO 450, J = 1, NUNODE
FUGCO2(J) = 1.D0
QHTAS(J) = 0.D0
QHTOLD(J) = 0.D0
QEPS(J) = 0.D0
QMPOLD(J) = 0.D0
PHCO2(J) = 0.D0
RESCO2(J) = 0.D0
IF (J .LT. 101) THEN
DZA(J) = 1.0D0
ENDIF
450 CONTINUE
ENDIF
C
C REARRANGE THE WATER, POROSITY ARRAYS
C
DO 500, J = 1, NSLZP1
JJ = J+100
QHTAS(JJ) = QHTAS(J)
QHTOLD(JJ) = QHTOLD(J)
QEPS(JJ) = QEPS(J)
QMPOLD(JJ) = QMPOLD(J)
DZA(JJ) = DZA(J)
500 CONTINUE

```

Last Revision: August 21, 1990

Source File: MIXCBN.FOR

```

C
C CALCULATE BIO. ACTIVITIES WITHIN PLANT CANOPY AND THROUGH SOIL
C 1. WITHIN PLANT CANOPY.
C CHECK THE DAY TIME
  NDAY = INT(T)/24
  TDAY = T - 24.DO*NDAY
  DO 400, J = 1, 80
    PHCO2(J) = 0.DO
    RESCO2(J) = 0.DO
    IF((TDAY .GE. 6.DO) .AND. (TDAY .LE. 18.DO)) THEN
      PHCO2(J) = 585.7142853-265*TDAY+41.041667*TDAY**2 -
&      2.5*TDAY**3 + 0.0520833*TDAY**4
      FACT6 = 1.DO/(1.DO+200.DO*(EXP(-0.5*(CLDCO2(J)-0.2))))
      PHCO2(J) = PHCO2(J)*FACT6
    ENDIF
    RESCO2(J) = 6.171945707-2.7183258*TDAY+0.885168*TDAY**2 -
&      0.064325*TDAY**3+0.00134*TDAY**4
    FACT7 = 1.DO/(1.DO+100*(EXP(-0.04*(CLDO2(J)-50))))
C REDUCE RESP. RATE BY TIMES 0.3
  RESCO2(J) = FACT7*RESCO2(J)*0.3DO
  400 CONTINUE
C
C 2. CALCULATE THE SOURCE IN SOIL
C ASSUMING R.Q.(RESPIRATORY QUOTIENT) VALUE EQUAL TO UNITY
C
  CSOURC = 0.0DO
  DO 20, J = 101, NUNODE
    SOUSRT(J) = (44.0DO*SRT(J))/32.0DO
    SOUSMO(J) = (44.0DO*SMT(J))/32.0DO
C
C USE Q10 VALUE OF 2 FOR TEMPERATURE CHANGE (25oC IS REFERENCE)
C Q10=2 MEANS DECREASE 10oC REDUCED 50% OF RESPIRATION
C
  GSOURC(J) = SOUSRT(J)+SOUSMO(J)
CCC  IF(QMPOLD(J) .EQ. 298.0DO) THEN
    TSOURC(J) = GSOURC(J)
CCC  ELSE IF (QMPOLD(J) .LT. 298.0DO) THEN
CCC    TSOURC(J) = GSOURC(J)-GSOURC(J) *
CCC    (298.0DO-QMPOLD(J))*0.05DO
CCC  &
CCC  ELSE IF (QMPOLD(J) .GT. 298.0DO) THEN
CCC    TSOURC(J) = GSOURC(J)+GSOURC(J) *
CCC    (QMPOLD(J)-298.0DO)*0.05DO
CCC  &
CCC  ENDIF
C
C CSOURC IS CUMULATIVE SOURCE FOR PRINT OUT
C
  CSOURC = CSOURC+TSOURC(J)
C

```

```

        SOURC(J) = DT1*TSOURC(J)
C
C 20 CONTINUE
C
C CALCULATE ALL COEFFICIENTS AND CONCENTRATIONS
C
C TOP NODE IS CONSTANT AND EQUAL TO ATMOSPHERE CON.
C
        CCCO2(1) = 0.6134D0
C
C INTERIOR NODE
C
        DO 30, J = 2, NUNODE-1
          IF(J .LT. 101) THEN
            COEFF1 = 1.0
            COEFF3 = 1.0
            PC1 = 1.D0
            BPC1 = 1.D0
          ELSE IF (J .GE. 101) THEN
            COEFF1 = (QEPS(J)-QHTAS(J))+QHTAS(J)*HCO2 +
&                (1.D0-QEPS(J))*OMGCO2
            COEFF3 = (QEPS(J)-QHTOLD(J))+QHTOLD(J)*HCO2 +
&                (1.D0-QEPS(J))*OMGCO2
            PC1 = ((QEPS(J+1)-QHTOLD(J+1))+ (QEPS(J)-QHTOLD(J)))*0.5D0
            BPC1 = ((QEPS(J)-QHTOLD(J))+ (QEPS(J-1)-QHTOLD(J-1)))*0.5D0
          ENDIF
          COEFF2 = 2.0D0*DT1/(DZA(J-1)+DZA(J))
          CON4 = (CLDCO2(J+1)-CLDCO2(J))/DZA(J)
          BCON4 = (CLDCO2(J)-CLDCO2(J-1))/DZA(J-1)
          DC1 = (DCO2(J+1)+DCO2(J))*0.5D0
          CON1 = LOG(FUGCO2(J+1))-LOG(FUGCO2(J))
          CON2 = CLDCO2(J+1)-CLDCO2(J)
          CON3 = (CLDCO2(J+1)+CLDCO2(J))*0.5D0
          BDC1 = (DCO2(J)+DCO2(J-1))*0.5D0
          BCON1 = LOG(FUGCO2(J))-LOG(FUGCO2(J-1))
          BCON2 = CLDCO2(J)-CLDCO2(J-1)
          BCON3 = (CLDCO2(J)+CLDCO2(J-1))*0.5D0
C
C CALCULATE THE CONCENTRATION
C
          IF(CON2 .EQ. 0.0D0) THEN
            FTERM1 = 1.0D0
          ELSE
            FTERM1 = CON3*(CON1/CON2)+1.0D0
          ENDIF
          FTERM2 = PC1*DC1*FTERM1*CON4
          IF (BCON2 .EQ. 0.0D0) THEN
            STERM1 = 1.0D0

```

```

ELSE
  STERM1 = BCON3*(BCON1/BCON2)+1.0D0
ENDIF
STERM2 = BPC1*BDC1*STERM1*BCON4
C
IF (J .LT. 101) THEN
  IF ((TDAY .GE. 6.D0) .AND. (TDAY .LE. 18.D0)) THEN
    CCO2(J) = (1.0D0/COEFF1)*( COEFF3*CLDCO2(J) +
&      COEFF2*(FTERM2-STERM2) - PHCO2(J)*DT1 + RESCO2(J)*DT1)
  ELSE IF ((TDAY .LT. 6.D0) .OR. (TDAY .GT. 18.D0)) THEN
    CCO2(J) = (1.0D0/COEFF1)*( COEFF3*CLDCO2(J) +
&      COEFF2*(FTERM2-STERM2) + RESCO2(J)*DT1)
  ENDIF
  ELSE IF (J .GE. 101) THEN
    CCO2(J) = (1.0D0/COEFF1) *
&      ( COEFF3*CLDCO2(J) + COEFF2*(FTERM2-STERM2) +
&      SOURC(J) - DT1*REPLE(J)*CLDCO2(J) )
  ENDIF
30 CONTINUE
C
C BOTTOM NODE
C SECOND TYPE BOUNDARY CONDITION IS USED FOR CLD02(NSLZP1)
C NO DIFFUSION OCCURS AT THIS BOUNDARY LAYER.
C
CLDCO2(NSLZP1) = CLDCO2(NSLZZZ)
RETURN
END

```



```

C
  WRITE(1,16) IEVENT(1),IEVENT(2)
16 FORMAT(/,10X,'IEVENT(1)=' ,I2,5X,'IEVENT(2)=' ,I2,/)
C
40 FORMAT(10X, A, E10.4)
  WRITE(1,40) 'RELATIVE HUMIDITY OF THE OUTER BOUNDARY LAYER AIR=',
& THIAA
  WRITE(1,40) 'RELATIVE HUMIDITY AT THE SOIL SURFACE=', RELHUM(1)
  WRITE(1,40) 'SATURATED WATER VAPOR DENSITY IN AIR=', RHOVSA
  WRITE(1,40) 'SATURATED WATER VAPOR DENSITY AT AIR-SOIL INTERFACE=',
& RHOWVX(1)
  WRITE(1,40) 'EVAPORATIVE(-) OR CONDENSIVE(+) FLUX=', QEVAP
  WRITE(1,40) 'AIR TEMP. AT OUTER BOUNDARY LAYER EDGE=', TEMPA
  WRITE(1,40) 'SURFACE INFILTRATION RATE(CM/HR)=' , INFLTR
  IF (INFLTR .GT. 0.0) THEN
    WRITE(1,40) 'TEMP. RAIN WATER=', TPWATI
  ENDIF
  WRITE(1,40) 'SOLAR RADIATION=', QSR(1)
  WRITE(1,40) 'EVAPORATIVE(-) OR CONDENSIVE(+) HEAT TRANSFER=',
& QHTESL
  WRITE(1,40) 'SENSIBLE HEAT TRANSFER=', QHTSSL
  WRITE(1,40) 'TRANSFER OF HEAT OF RAIN WATER INTO SOIL=', QHRAIN
  WRITE(1,40) 'SHORT WAVE RADIATION INTO SOIL=', QHSWR
  WRITE(1,40) 'LONG WAVE RADIATION OUT OF SOIL=', QHLWRO
  WRITE(1,40) 'LONG WAVE RADIATION INTO SOIL=', QHLWRI
  WRITE(1,40) 'TOP OXYGEN CONC.(MICROGM/CUBIC CM AIR)=' , CO2(1)
  WRITE(1,40) 'TOP CAR. DIOXIDE CONC.(MICROGM/CUBIC CM AIR)=' ,
& COO2(1)
  WRITE(1,40) 'ROOT LENGTH=' , RTLENG
C
C WRITE OUT WATER EVAP, TEMP.,SURFACE INF. ETC. FOR FIGURES
C
  WRITE(8,175) TIMEST(NCALLS),QEVAP,TEMPS(1),TEMPS(7),TEMPS(12),
& TEMPS(22),TEMPS(52),SINFL
C
175 FORMAT(2X,8(E10.4))
151 FORMAT(5X,'TIMEST=' ,E10.4)
160 FORMAT(3X,'LAYER',4X,'NODE POSITION',4X,'WATER',9X,'TEMP',
& 10X,'OXYGEN',5X,'CARBON DIO',6X,'SRT',11X,'SMO')
161 FORMAT(12X,'( CM )',10X, '(CM3/CM3 SOIL)',2X,'(K)',9X,
& '(UG/CM3 SOIL AIR)',12X,'UG /CM3 /HR')
1160 FORMAT(3X,'LAYER',4X,'OXYGEN',5X,
& 'CARBON DIO',8X,'PHO2',10X,'PHCO2',9X,'RESO2',8X,'RESCO2')
1161 FORMAT(12X, '(UG/CM3 SOIL AIR)',22X,'UG /CM3 /HR')
152 FORMAT(2X,I3,4X,E12.4,2X,E12.4,2X,E12.4,2X,E12.4,2X,E12.4,
& 2X,E12.4,2X,E12.4)
1152 FORMAT(2X,I3,4X,E12.4,2X,E12.4,2X,E12.4,2X,E12.4,
& 2X,E12.4,2X,E12.4)

```

```
C
C STORE THE TEMPERATURE, WATER, OXYGEN, CARBON DIOXIDE ,
C AND SINK PROFILES
C
    CHECK = PRFIN(LINDEX)
    IF (T .GE. CHECK) THEN
150   WRITE(7,151) TIMEST(NCALLS)
      WRITE(9,151) TIMEST(NCALLS)
      WRITE(7,160)
      WRITE(7,161)
      WRITE(9,1160)
      WRITE(9,1161)
      DO 153, J = 1, NSLZP1
        JS = J+100
        WRITE(7,152) J,ZNODE(J),THIAS(J),TEMPS(J),
&          CO2(JS),COO2(JS),SRT(JS),SMO(JS)
153   CONTINUE
      DO 1153, J=1,100
        WRITE(9,1152) J,CO2(J),COO2(J),PHO2(J),PHCO2(J),
&          RESO2(J),RESCO2(J)
1153  CONTINUE
      LINDEX=LINDEX+1
    ENDIF
C
200 RETURN
    END
```

\*COMMONS

Last Revision: JUNE 13, 1989

C

Source File: COMMON.OCD

INTEGER NX, NY  
 PARAMETER (NX=153)  
 PARAMETER (NY=253)

C

DOUBLE PRECISION WS  
 COMMON/AIMSOL/ WS  
 DOUBLE PRECISION ALBSOI, ALBAIR, ALEWAT  
 COMMON/ALBEDO/ ALBSOI, ALBAIR, ALEWAT  
 DOUBLE PRECISION KONTHS  
 COMMON/CONDCT/ KONTHS (NX)  
 DOUBLE PRECISION GRAV, R, SIGMA  
 COMMON/CONST1/ GRAV, R, SIGMA  
 INTEGER IEVENT, ILIVNT, IRVNT, LINDEX, KNDX, NCALLS  
 COMMON/COUNT1/ IEVENT (2), ILIVNT, IRVNT, LINDEX,  
 & KNDX, NCALLS  
 DOUBLE PRECISION RHOAIR, RHOWAT, RHOSOL, RHOB  
 COMMON/DENSI1/ RHOAIR, RHOWAT, RHOSOL (NX), RHOB (NX)  
 DOUBLE PRECISION RHOSND, RHOSIL, RHOCLA  
 COMMON/DENSI2/ RHOSND, RHOSIL, RHOCLA  
 DOUBLE PRECISION RSWVIN, RHOVSA  
 COMMON/DENSI3/ RSWVIN, RHOVSA  
 DOUBLE PRECISION QRAIN, QSR, INFLTR, SINFL  
 COMMON/DRVFT1/ QRAIN (5), QSR (5), INFLTR, SINFL  
 INTEGER NLIEV, NRAEV  
 DOUBLE PRECISION TLION, TLIOF, TRAON, TRAOF  
 COMMON/EVNTS1/ NLIEV, NRAEV, TLION (60), TLIOF (60), TRAON (60),  
 & TRAOF (60)  
 DOUBLE PRECISION TNOW1, TNOW2  
 COMMON/EVNTS2/ TNOW1, TNOW2  
 DOUBLE PRECISION QEVAP, QHTESL, QHTSSL, QMCV1S  
 COMMON/FLOWS1/ QEVAP, QHTESL, QHTSSL, QMCV1S  
 DOUBLE PRECISION QHRAIN, QHSWR, QHLWRO, QHLWRI, HNET  
 COMMON/FLOWS2/ QHRAIN, QHSWR, QHLWRO, QHLWRI, HNET  
 DOUBLE PRECISION ATEMP, BTEMP, ARHIN, BRHIN, TPINMU, RHINMU  
 COMMON/FOURC1/ ATEMP (20), BTEMP (20), ARHIN (20), BRHIN (20),  
 & TPINMU, RHINMU  
 INTEGER NCFIMP, NCFFRH  
 DOUBLE PRECISION OMEGTP, OMGRHI  
 COMMON/FOURC2/ OMEGTP (20), OMGRHI (20), NCFIMP, NCFFRH  
 DOUBLE PRECISION DZ  
 COMMON/GEOM1 / DZ (NX)  
 DOUBLE PRECISION ZMNODE, ZNODE, DELTAZ, RNODE  
 COMMON/GEOM2 / ZMNODE (NX), ZNODE (NX), DELTAZ, RNODE (NY)  
 DOUBLE PRECISION LVAP  
 COMMON/HEAT1 / LVAP (NX)  
 DOUBLE PRECISION SHISOL

```

COMMON/HEAT2 /      SHTSOL(NX)
DOUBLE PRECISION   SHTSAN, SHTSIL, SHTCLA, SHTAIR, SHIWAT
COMMON/HEAT3 /      SHTSAN, SHTSIL, SHTCLA, SHTAIR, SHIWAT
DOUBLE PRECISION   LAMBHT, LAMSLD, LAMWAT, LAMSOL, LAMAIR
COMMON/HEAT4 /      LAMBHT, LAMSLD, LAMWAT(NX), LAMSOL(NX),
&      LAMAIR(NX)
DOUBLE PRECISION   TMPAIN, TPWATI
COMMON/HEAT5 /      TMPAIN, TPWATI
DOUBLE PRECISION   EMSWAT, EMSAIR, EMSSOI
COMMON/HEAT7 /      EMSWAT, EMSAIR, EMSSOI
DOUBLE PRECISION   PH0, PH2, PH3, PH4, PH5
COMMON/HEAT8 /      PH0(NX), PH2(NX), PH3(NX), PH4(NX), PH5(NX)
DOUBLE PRECISION   DTB1H1, DTB2H1, DTB3H1
COMMON/HEAT9 /      DTB1H1(NX), DTB2H1(NX), DTB3H1(NX)
DOUBLE PRECISION   HSTORE, HFLUX
COMMON/HEAT10/     HSTORE, HFLUX
INTEGER            NSLZM1, NSLZZZ, NSLZP1
COMMON/INDEX1/     NSLZM1, NSLZZZ, NSLZP1
INTEGER            NPRINT, NNSTRZ
COMMON/INDEX2/     NPRINT(20), NNSTRZ(30)
DOUBLE PRECISION   PSI, PPSITH, DPSIZ, PPSIZ
COMMON/MOSTR1/     PSI(NX), PPSITH(NX), DPSIZ(NX), PPSIZ(NX)
DOUBLE PRECISION   DTHLQS, DTPLQS, DTHTZ
COMMON/MOSTR2/     DTHLQS(NX), DTPLQS(NX), DTHTZ(NX)
DOUBLE PRECISION   PM0, PM2, PM3, PM4, PM5
COMMON/MOSTR3/     PM0(NX), PM2(NX), PM3(NX), PM4(NX), PM5(NX)
DOUBLE PRECISION   DTB1M2, DTB2M2, DTB3M2
COMMON/MOSTR4/     DTB1M2(NX), DTB2M2(NX), DTB3M2(NX)
DOUBLE PRECISION   DO2, DO20, DCO2, DCO20
COMMON/OXYCAR1 /   DO2(NY), DO20, DCO2(NY), DCO20
DOUBLE PRECISION   OMIGO2, OMGCO2, PHO2, PHCO2
COMMON/OXYCAR2 /   OMIGO2, OMGCO2, PHO2(NY), PHCO2(NY)
DOUBLE PRECISION   SMO, SRT, SOUSMO, SOUSRT, RTLENG
COMMON/OXYCAR3 /   SMO(NY), SRT(NY), SOUSMO(NY), SOUSRT(NY), RTLENG
DOUBLE PRECISION   HO2, HCO2, OXYDIF, CABDIF, RESO2, RESCO2
COMMON/OXYCAR4 /   HO2, HCO2, OXYDIF, CABDIF, RESO2(NY), RESCO2(NY)
DOUBLE PRECISION   SINK, GSINK, TSINK, CSINK
COMMON/OXYCAR5 /   SINK(NY), GSINK(NY), TSINK(NY), CSINK
DOUBLE PRECISION   SOURC, GSOURC, TSOURC, CSOURC
COMMON/OXYCAR6 /   SOURC(NY), GSOURC(NY), TSOURC(NY), CSOURC
DOUBLE PRECISION   PPSIZ
COMMON/OXYCAR7 /   PPSIZ(NX)
DOUBLE PRECISION   CLDO2, CLDCO2, CO2, CCO2
COMMON/OXYCAR8 /   CLDO2(NY), CLDCO2(NY), CO2(NY), CCO2(NY)
DOUBLE PRECISION   T0, TCUT, DT0, DT1, DT, PRFIN, T, TPRT, T1
COMMON/RUNCT1/     T0, TCUT, DT0, DT1, DT, PRFIN(20), T, TPRT, T1
DOUBLE PRECISION   THTOLD, TMPOLD, THINew, TMPNEW
COMMON/STATV1/     THTOLD(NX), TMPOLD(NX), THINew(NX), TMPNEW(NX)

```

DOUBLE PRECISION	THTAA, TEMPA, CAT
COMMON/STATV3/	THTAA, TEMPA, CAT
DOUBLE PRECISION	THTAS, TEMPS
COMMON/STATV4/	THTAS (NX) , TEMPS (NX)
DOUBLE PRECISION	THTAST
COMMON/SOIL8 /	THTAST (NX)
DOUBLE PRECISION	THTRES
COMMON/SOIL9 /	THTRES (NX)
DOUBLE PRECISION	KIHSTS
COMMON/SOIL10/	KIHSTS (NX)
DOUBLE PRECISION	TORT
COMMON/SOIL14/	TORT (NX)
DOUBLE PRECISION	EPS
COMMON/SOIL16/	EPS (NX)
DOUBLE PRECISION	PCTSAN
COMMON/SOIL23/	PCTSAN (NX)
DOUBLE PRECISION	PCTCLA
COMMON/SOIL24/	PCTCLA (NX)
DOUBLE PRECISION	PCTSIL
COMMON/SOIL25/	PCTSIL (NX)
DOUBLE PRECISION	GAMTLI
COMMON/SOIL32/	GAMTLI
DOUBLE PRECISION	ALPTH
COMMON/SOIL33/	ALPTH (NX)
DOUBLE PRECISION	BETATH
COMMON/SOIL34/	BETATH (NX)
DOUBLE PRECISION	GAMCNS
COMMON/SOIL35/	GAMCNS (NX)
DOUBLE PRECISION	DALPTZ
COMMON/SOIL36/	DALPTZ (NX)
DOUBLE PRECISION	DBETAZ
COMMON/SOIL37/	DBETAZ (NX)
DOUBLE PRECISION	DIHTSZ
COMMON/SOIL38/	DIHTSZ (NX)
DOUBLE PRECISION	DITHREZ
COMMON/SOIL39/	DITHREZ (NX)
DOUBLE PRECISION	FACTOR
COMMON/THERM /	FACTOR (NX)
DOUBLE PRECISION	ADT1, ADT2, ADT3
COMMON/THOMS1/	ADT1 (NX) , ADT2 (NX) , ADT3 (NX)
DOUBLE PRECISION	XDUM, YDUM
COMMON/THOMS2/	XDUM (NX) , YDUM (NX)
DOUBLE PRECISION	YTH, YTP, YCH
COMMON/THOMS3/	YTH (NX) , YTP (NX) , YCH (NX)
DOUBLE PRECISION	SUMAM1, SUMAH1
COMMON/SUMDUM/	SUMAM1 (NX) , SUMAH1 (NX)
DOUBLE PRECISION	TIMEST
COMMON/SUMAR4/	TIMEST (250)

```
DOUBLE PRECISION  EH2OVP, ESTAIR, RHAIN
COMMON/VAPOR1/    EH2OVP, ESTAIR, RHAIN
DOUBLE PRECISION  DTHVPS, DTPVPS
COMMON/VAPOR2/    DTHVPS (NX) , DTPVPS (NX)
INTEGER           NWVAIR
DOUBLE PRECISION  BETATV, BETAVA, DATM, DWVAR
COMMON/VAPOR3/    BETATV, BETAVA, DATM, DWVAR(10) , NWVAIR
DOUBLE PRECISION  RELHUM, RHOWVX
COMMON/VAPOR4/    RELHUM(NX) , RHOWVX(NX)
DOUBLE PRECISION  RHOWVA
COMMON/VAPOR5/    RHOWVA
DOUBLE PRECISION  VLZZ, REPLE
COMMON/VELCT1/    VLZZ (NX) , REPLE (NY)
```